Brushless DC permanent magnet micro-wind generator modeling and optimization over long-term wind-speed cycle operation

Andreea-Adriana Laczko

N° d'ordre : 313

CENTRALE LILLE

THÈSE

présentée en vue
d'obtenir le grade de

DOCTEUR

en

Spécialité : Génie électrique

par

Andreea Adriana **LACZKO (ZAHARIA)**

DOCTORAT DELIVRE CONJOINTEMENT PAR CENTRALE LILLE ET L'UNIVERSITÉ TECHNIQUE DE CLUJ-NAPOCA (UTC-N), ROUMANIE DANS LE CADRE D'UNE COTUTELLE INTERNATIONALE DE THESE

Titre de la thèse :

Optimisation du dimensionnement et de la commande sur cycle de fonctionnement d'un générateur à aimants permanents et auto-commutation pour applications micro-éoliennes

Thèse soutenue le 15 décembre 2016 devant le jury d'examen :

Président	**Radu MUNTEANU,** *Professeur, UTC-N, Roumanie*
Rapporteur	**Mohamed GABSI,** *Professeur, Ecole Normale Supérieure de Cachan, France*
Rapporteur	**Maria IMECS,** *Professeur, UTC-N, Roumanie*
Co-directeurs de thèse	**Stéphane BRISSET,** *Maître de conférences, HDR, L2EP – Centrale Lille, France*
	Mircea M. RADULESCU, *Professeur, UTC-N, Roumanie*
Membre	**Frédéric GILLON,** *Maître de conférences, HDR, L2EP – Centrale Lille, France*

Thèse préparée dans le Laboratoire L2EP – Centrale Lille
École Doctorale SPI 072

Content

Notations and Definitions

General acronyms

BDFRM	Brushless doubly fed reluctance machine
BLDCPM	Brushless DC permanent magnet
CIG	Cage induction generator
DFIG	Doubly fed induction generator
EMF	Electromotive force
FE	Finite element
IGBT	Insulated gate bipolar transistor
MOSFET	Metal–oxide–semiconductor field-effect transistor
MPPT	Maximum power point tracking
PMSG	Permanent magnet synchronous generator
PWM	Pulse width modulation
$\mu WECS$	Micro-wind energy conversion system

Micro-wind turbine notations

T_{wt} :	Active torque provided by the turbine [N.m]
ρ_{air} :	Air density [kg/m3]
v_n :	Base/nominal wind speed [m/s]
v_{in} :	Cut-in wind speed [m/s]
v_{max} :	Cut-off wind speed [m/s]
f_{wt} :	Friction coefficient (N.m/rad)
C_p :	Power coefficient of the turbine
R_{wt} :	Radius of the turbine rotor blades [m]
J :	Rotor inertia [kg.m2]
λ :	Tip speed ratio coefficient
v_w :	Wind speed [m/s]

Generator notations

g :	Air gap thickness [mm]
$\hat{B}_{ry}$:	Amplitude of the magnetic flux density in the generator's rotor yoke [T]
$\hat{B}_{pm}$:	Amplitude of the magnetic flux density in the permanent magnets [T]
$\hat{B}_{th}$:	Amplitude of the magnetic induction in the stator tooth [T]
e_{ph} :	Back-EMF voltage [V]

k_e :	Back-EMF voltage coefficient
P_b :	Base or nominal power of the generator [W]
D_s :	Bore diameter [mm]
k_r :	Copper filling coefficient
P_j :	Copper losses [W]
ρ_{co} :	Copper resistivity at 0° C [Ω·m]
δ_{dens} :	Current density in the conductors [A/mm^2]
d_{co} :	Density of the copper [kg/m3]
d_{pm} :	Density of the permanent magnets [kg/m3]
d_{sy}, d_{ry} :	Density of the stator and rotor yokes [kg/m3]
d_{th} :	Density of the stator teeth [kg/m3]
h_{th} :	Depth of the main stator tooth [mm]
k_{eddy} :	Eddy current loss coefficient obtained from manufacturer data
f_{ele} :	Fundamental frequency of the machine [Hz]
k_{hys} :	Hysteresis loss coefficient obtained from manufacturer data
P_{Fe_eddy} :	Iron (eddy) losses [W]
P_{Fe_hys} :	Iron (hysteresis) losses [W]
k_{st} :	Laminated filling factor
k_{lk} :	Leakage coefficient
L_m :	Magnetic length of the machine [mm]
L_m :	Magnetic length of the machine [mm]
$\hat{P}_{mech}$:	Mechanical losses [W]
M :	Mutual phase inductance [H]
v_n :	Neutral voltage [V]
p :	Number of generator pole-pairs
N_s :	Number of slots
$\hat{P}_{em}$:	Peak electromagnetic power [W]
$\hat{T}_{em}$:	Peak electromagnetic torque [Nm]
$\hat{I}$:	Peak phase current [A]
$\hat{B}_g$:	Peak value of the magnetic flux density in the air gap [T]
$\hat{B}_{sy}$:	Peak value of the magnetic induction in the generator's stator yoke [T]
$\hat{E}$:	Phase back-EMF peak voltage [V]
i_{ph} :	Phase current [A]

R_{ph} :	Phase resistance [ohm]
L_{ph} :	Phase self-inductance [H]
v_{ph} :	Phase to neutral voltage [V]
r_{rs} :	Ratio between the length of the rotor on the one of the stator
μ_r :	Relative magnetic permeability
B_r :	Remnant induction of the magnets [T]
Ω :	Rotational mechanical speed of the turbine/generator [rad/s]
a, b, c :	Stator phase windings notation
R_s :	Stator radius [mm]
L_{ths} :	The medium length of a half turn [mm]
α_{pm}, α_{co} :	Thermal coefficients of the permanent magnets and copper
h_{c_int} :	Thickness of the intermediate pole shoe [mm]
h_c :	Thickness of the main pole shoe [mm]
h_{pm} :	Thickness of the permanent magnet [mm]
h_{ry} :	Thickness of the rotor yoke [mm]
h_{sy} :	Thickness of the stator yoke [mm]
z :	Total number of conductors carrying current
α_{int} :	Widening of the intermediate stator tooth [rad]
α :	Widening of the main stator tooth [rad]
β :	Widening of the permanent magnet [rad]
l_{th_int} :	Width of the intermediate stator tooth [mm]
l_{th} :	Width of the main stator tooth [mm]

Power electronic converter notations

V_{CE} :	Collector-emitter voltage of the IGBT [V]
T_{comm} :	Commutation time of the machine [s]
P_{cond_IGBT} :	Conduction losses in the IGBTs [W]
V_{dc} :	DC bus voltage [V]
t_f :	Falling transit time [s]
V_F :	Forward ON-voltage in the diode [V]
f_{mod} :	Modulation factor ($0 < \mathrm{f_{mod}} < 1$)
I_{n_IGBT} :	Nominal current of the IGBT [A]
V_n :	Nominal voltage available in the machine [V]

V_{CE0} :	ON-state, zero current collector-emitter voltage [V], obtained from the manufacturer datasheet
t_r :	Rising transit time [s]
P_{diode} :	Switching and commutation losses in the diodes [W]
f_{sw} :	Switching frequency [Hz]
P_{sw_IGBT} :	Switching losses in the IGBTs [W]
$I_{CC(test)}$:	Test current [A]
$V_{CC(test)}$:	Test voltage [V]
I_{F_AVG} :	The average forward current of the diode during phase commutation [A]
I_{C_RMS} :	The current during the 120◦ switch conduction period [A]
E_{OFF} :	Turn-off switching losses [J]
E_{ON} :	Turn-on switching losses [J]

Notations for the optimization methodology

GA	Genetic algorithm
OF	Optimization function
SAb	Semi-analytical model with barycenter method
SU	Surrogate model

General Introduction

The work conducted for the developing of this thesis was realized based on a joint supervision (co-tutelle) between The Technical University of Cluj-Napoca, Romania and Ecole Centrale de Lille, France.

The design of stand-alone μWECS for residential use represents the core of the present study. It is concerned with three-phase star-connected BLDCPM generator, having outer rotor with Nd-Fe-B surface-mounted PMs, and concentrated stator-armature windings with quasi-trapezoidal stator-phase back-EMF voltages. The BLDCPM generator is direct-driven by horizontal-axis low-speed micro-wind turbine. Generator-side three-phase full-bridge AC/DC power electronic converter (rectifier) is considered for controlling the output DC-bus constant voltage.

Due to the variable wind speed, many fluctuations occur in the power and frequency of the BLDCPM generator, compelling its design for large speed-range operation.

Hence, the thesis work aims at determining the optimal design parameters of the BLDCPM generator ensuring minimum power losses of μWECS over long-term wind-speed cycle operation, and thereby maximizing the extracted wind power and increasing the efficiency of the overall system.

In advance to the optimization, an adapted simulation model needs to be developed in terms of results accuracy and simulation time. Therefore, it is necessary to determine the modeling level, as well as the design variables of each component of the system. As the optimization appeals to an algorithm for the design process, the number of model evaluations can be fairly important. The more design variables and constraints, the higher the model evaluation count. As a result, reduction of the simulation time, as well as integration and exploitation of the available data from the wind-speed profile for determining the total power losses of considered μWECS are of main concern.

It is now possible to provide an overview of the aims set for this thesis, which are to (i) analyze and develop a simulation model of the wind system, as well as (ii) determining and developing a reduction method for the wind speed profile based on which (iii) the power losses in the system can be calculated and (iv) included in the optimization approaches in view of their minimization while determining the optimum geometrical and electrical parameters of the BLDCPM generator.

The thesis content is structured on six chapters. A brief description of each chapter is given herewith.

Chapter 1 outlines first the small wind turbine market and industry, and then describes the main features of present μWECS topologies. The final part of the chapter approaches the BLDCPM generator-based μWECS for further study throughout the thesis.

In **chapter 2** the basic models of μWECS components, i.e. micro-wind turbine, BLDCPM generator and associated AC/DC power converter, are developed. Three models are proposed for the BLDCPM generator, namely analytical model, semi-analytical model and finite element-based model. Comparative model simulations are carried out, mainly in terms of simulation time and results accuracy in order to adopt the most suitable model for determination of generator parameters.

Chapter 3 is concerned with the analysis of the wind-speed profile employed in the μWECS design, as well as with the techniques that can be used for reduction of its simulation time and amount of data. For this, three reduction methods are studied, one that deals with the average wind speed of the cycle, the second based on statistical distribution of the wind speed data and finally the barycenter method. This chapter also approaches the calculation of losses using the proposed method of wind speed cycle simplification corroborated by simulations of the micro-wind energy conversion system operating under long-term and reduced wind speed cycle. A sensitivity analysis of the wind turbine performance points is also conducted in order to observe how some output quantities of the μWECS are affected by their variation.

In **chapter 4** design optimization of the BLDCPM generator-based micro-wind turbine system is carried out entailing the description of the objective function and design variables. In order to achieve feasible solution, several constraints have to be analyzed on the inputs and outputs of the model, resulting in a constrained mono-objective optimization which relies on the genetic algorithm (GA) for its resolution. Two optimization approaches are proposed: one single-level approach that employs the semi-analytical model into optimization and another two-level approach based on the analytical model and an iteratively correction strategy. At the end, the results obtained with both approaches are provided and discussed.

Chapter 5 reports on the hardware and software components of the experimental set-up used and on the practical operational results obtained for the three-phase outer rotor BLDCPM machine prototype.

In the **last part,** general conclusions of the thesis are drawn and some suggestions for future work in the same area are given.

Chapter 1

Brushless DC Permanent Magnet Generator for Micro-Wind Turbine Applications

1.1 Introduction

Worldwide focus has been directed for the past decades towards the advancement in the clean energy technologies as a counteraction to the fossil fuels dependency and nuclear technologies. Among the alternative energy production solutions, the *wind energy* has been the fastest-growing source of renewable energy contributing to the modern distributed electric power generation. Therefore, researchers have been prompted to develop optimized wind energy conversion systems in terms of design and components, such as wind turbines, electric generators, power electronic converters and their controls.

Since mechanical power of wind turbines strongly depends on the rotor area and on the cube of wind speed and since only 59.3% of the total wind power can be harvested, according to Bet'z law [1], it was ascertained that high-power wind turbines can produce more electric energy. Due to this fact, an exponential increase over the last two decades has been noted in the size of commercial wind turbines, as well as in their installed capacity across the world, as shown in *fig. 1.1*. The wind power capacity installed worldwide is expected to reach 500 GW by the end of 2016 [2].

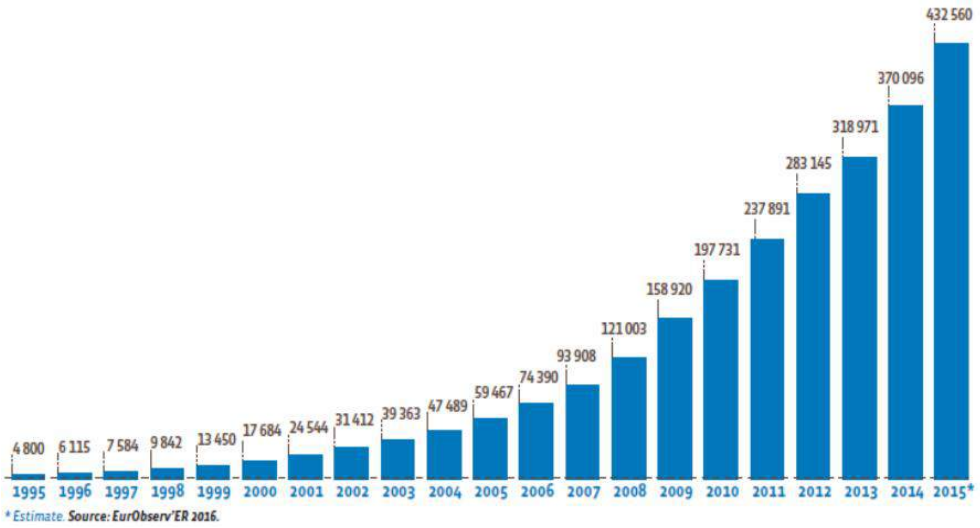

Fig. 1.1. Total cumulative wind power capacity installed worldwide since 1995 (MW) [2]

This development of the wind markets and nevertheless of all renewable energy markets is motivated by the environmental issues emerged over the last years, like air pollution and

climate changes due to CO_2 emissions, as well as for the financial incentives policy support of various national governments for promoting the use of local manufacturing and by impelling utilities to purchase renewable energy. Nowadays, the wind energy systems can strongly compete to the conventional sources of electricity (coal, nuclear, gas, etc.) as they are one of the least cost renewable energy resource for new power generation [3].

As against the large-scale high-power wind turbine manufacturing, the small wind turbine market was formerly neglected. However, for the past years, the small wind-turbine capacity installed worldwide has shown an annual growth rate of 19 – 35 %. Subsequently, the small wind turbine market is estimated with a steady growth rate of 20 % from 2015 to 2020, so that its industry is forecasted to reach a cumulative installed capacity of close to 3 GW by 2020 [4].

The International Electrotechnical Commission (IEC) standard IEC 61400-2 defines the small-scale wind turbine as having a rotor swept area of less than 200 m^2, leading to a rated power up to 50 kW delivered at a voltage below 1 kV AC or 1,5 kV DC. As a sub-category of small wind turbines, the *micro-wind turbine* has a rated power from 1 kW to 7 kW, and rotor swept area of less than 40 m^2.

1.2 Micro-wind energy conversion systems

The micro-wind energy conversion system (μWECS) generates electricity by converting the kinetic energy from the wind into electrical energy. The micro-wind turbine, which is the main mechanical component of the μWECS, captures the energy from the moving wind by means of rotor blades and transfers it to the generator.

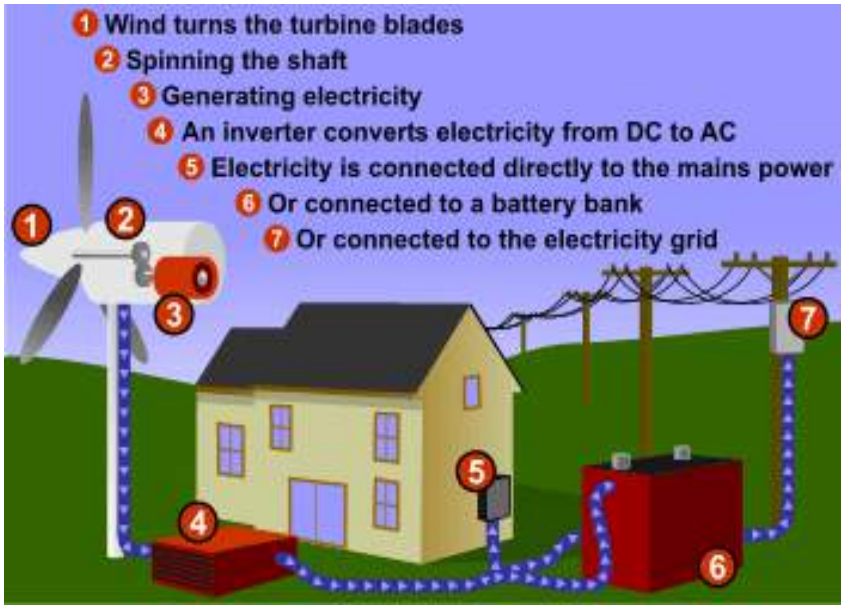

Fig. 1.2. Pictorial representation of a micro-wind energy conversion system (μWECS) [5]

The generator shaft is driven by the micro-wind turbine to generate electric power and the mechanical coupling between them can be achieved directly or by means of a gear device. Finally, the generated electrical energy can be stored into batteries or used to power isolated loads distributed by an electrical grid (*fig. 1.2*). Several additional components are needed depending on the connection method, i.e. a DC/AC converter and a step up/down transformer unit for the utility /household grid connection and/or a DC/DC power converter for the battery bank charging [5].

The components of a μWECS can be categorized according to the power that they produce or convert in two major classes, i.e. (i) *mechanical*, represented by the turbine assembly and (ii) *electrical*, defined by the electric generator and power electronic converter(s). For an efficient and reliable conversion of the wind energy into electric energy a third component category is emerged related to the control systems of both mechanical and electrical components. For improved efficiency of the μWECS different combinations and designs of the above components can be encountered, resulting into several μWECS configurations that have been developed and which are further described below.

A simple classification of the micro-wind turbines can be made in terms of their rotor-axis orientation, leading to two main structures, i.e. of horizontal axis and of vertical axis (*fig. 1.3*). Various comparative studies can be found in the technical literature [1], [6] revealing the merits and drawbacks of each structure, which are synthetized in Table 1.1.

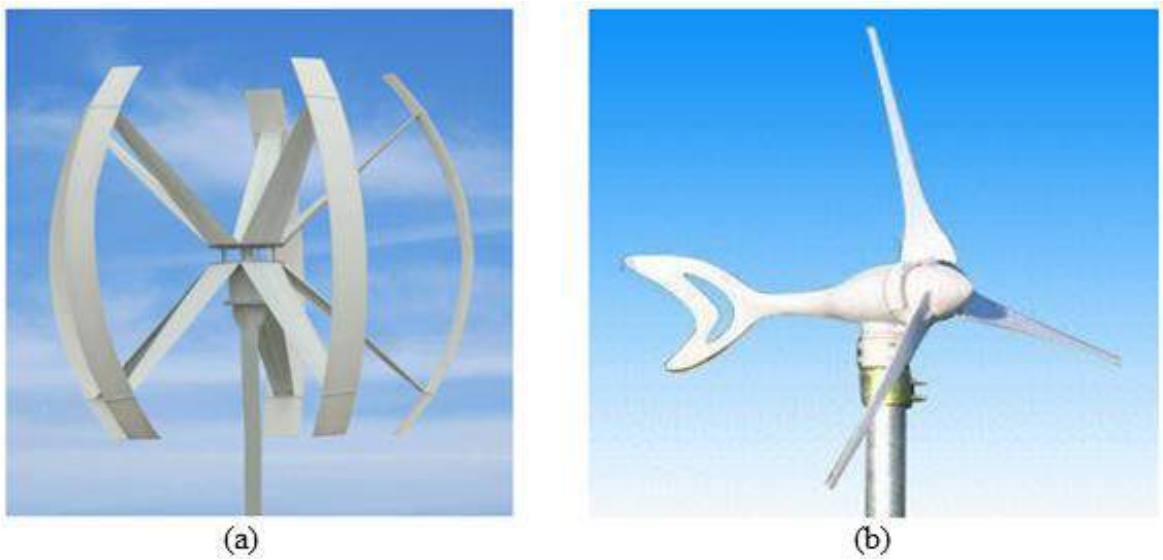

Fig. 1.3. Micro-wind turbine structure with (a) horizontal-axis and (b) vertical-axis orientation, respectively [7]

Table 1.1 Advantages and disadvantages of horizontal-axis and vertical-axis micro-wind turbines [1]

	Advantages	***Disadvantages***
Horizontal-axis micro-wind turbine	• Higher wind energy conversion efficiency • Access to stronger wind due to high tower • Power regulation by stall and pitch angle control at high wind speeds	• Higher installation cost, stronger tower to supply heavy weight of nacelle • Longer cable from the top of tower to ground • Orientation required (yaw control)
Vertical-axis micro-wind turbine	• Lower installation cost and easier maintenance due to the ground-level gearbox and generator • Operation independent of wind direction • Suitable for rooftops (stronger wind without need of tower)	• Lower wind energy conversion efficiency • Higher torque fluctuations and prone to mechanical vibrations • Limited options for power regulation at high wind speeds

However, as specified in [1], the main classification criterion of μWECS topologies is represented by the drive train configuration. A brief schematic representation based on this criterion is given in *fig. 1.4*, followed by a description of several μWECS topologies that have been developed over the recent years.

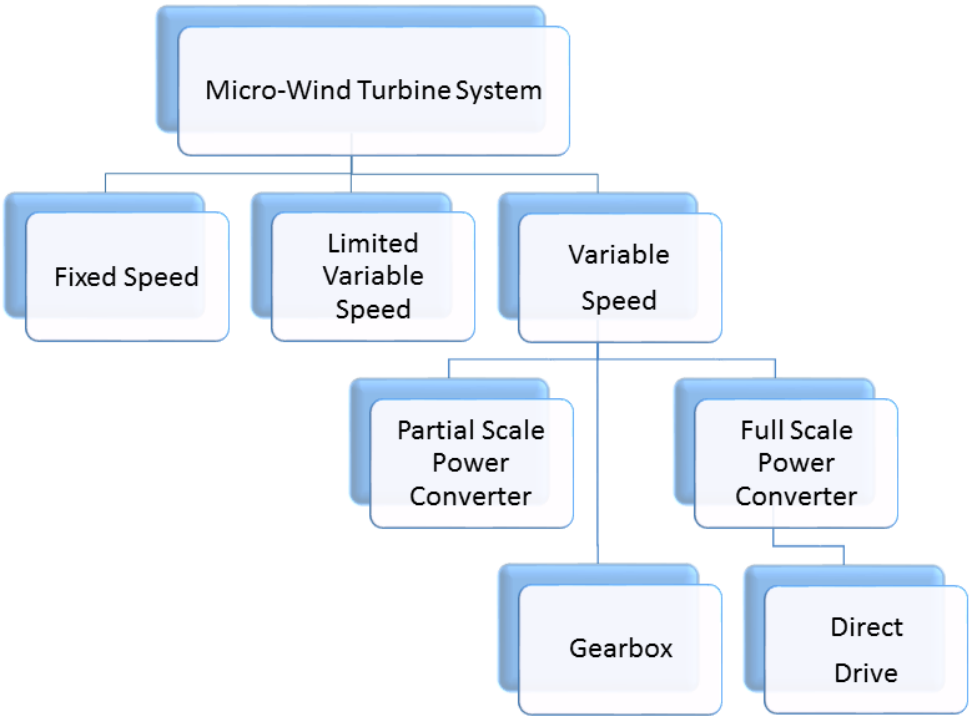

Fig. 1.4. Classification of micro-wind turbine systems based on drive train topology

A. Fixed speed drive train topology

The fixed-speed topology was the first one developed for the micro-wind turbine systems (*fig. 1.5*). It consists of a multiple-stage gearbox coupled to a cage induction generator (CIG) without any power converter unit, but equipped with a capacitor bank for reactive power compensation and connected to the grid by means of a transformer. Even if it presents easy implementation and relatively low manufacturing cost, the inability to control even the narrow speed range at which it was designed for operation, resulting into lower wind energy conversion efficiency and high mechanical stresses on the system, has turned the attention to the semi-variable and variable speed micro-wind turbine systems. [8].

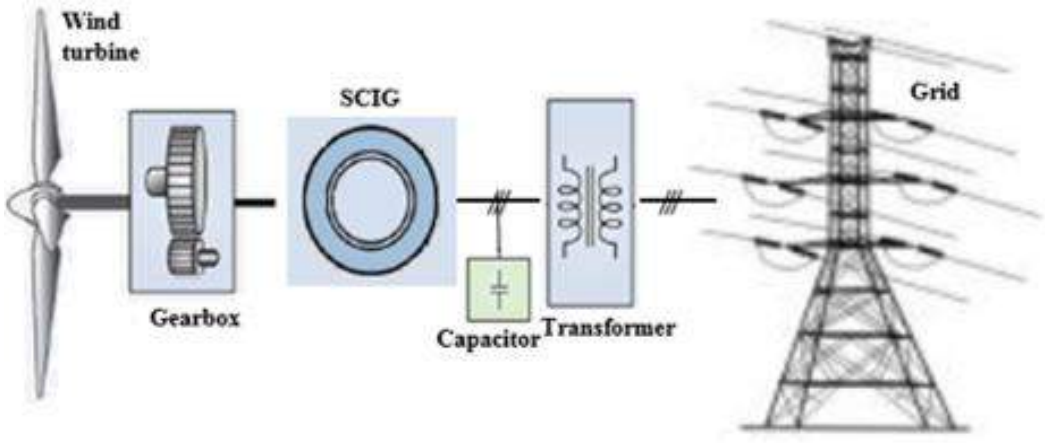

Fig. 1.5. Fixed-speed micro-wind turbine system topology based on cage induction generator

B. Variable speed drive train topology

Under variable-speed operation the energy conversion efficiency increases and the mechanical stress and maintenance requirements reduce, leading to a higher life cycle of the micro-wind turbine. Controlling and maximizing the wind power extraction becomes possible under variable-speed operation by employing pitch regulation and maximum power point tracking (MPPT) control. The micro-wind turbine systems that fall into this category can use partial-scale or full scale power electronic converters when connected to the utility grid. Although the additional power converter losses and the higher manufacturing costs that characterize these topologies, they still remain dominant on the micro-wind turbine market.

- **Variable speed partial scale power converter class**

This class exploits mainly the *doubly-fed induction generator* (DFIG), being based on a direct connection of the stator terminals to the power grid, whilst the rotor has an intermediate

coupling with a back-to-back power converter allowing a bidirectional power flow in the rotor circuit, as shown in *fig. 1.6*. The high overall efficiency as well as the increased dynamic performances prompt the DFIG topology as the prevailing technology in today's micro-wind industry [8].

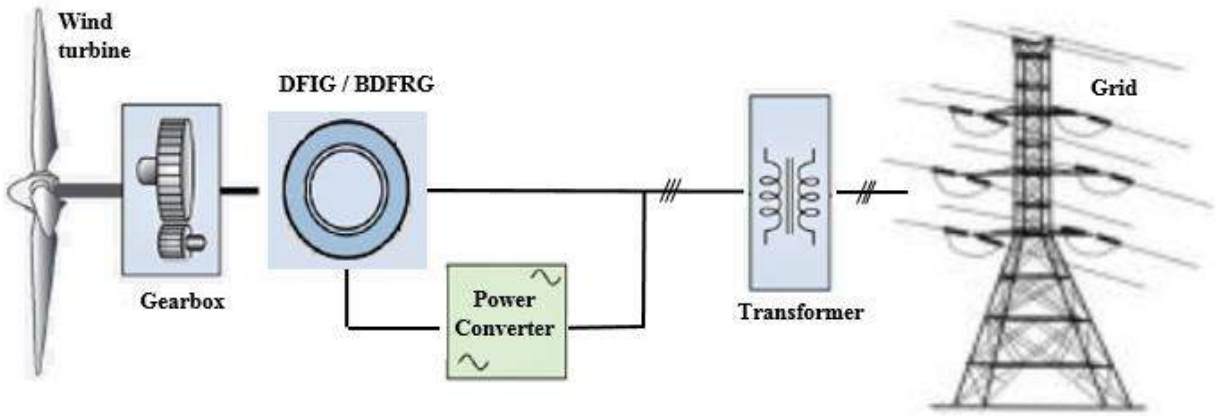

Fig. 1.6. Variable-speed micro- wind turbine system based on DFIG and partial-scale power converter

More recent studies [9] also include in this class the *brushless doubly-fed reluctance generator* (BDFRG) that shows promising performances in terms of cost and efficiency. However, the lack of a well-defined electromagnetic design procedure makes it an arguable solution for the micro-wind energy conversion system.

- **Variable speed full scale power converter class**

By employing a full scale power converter increased performances can be obtained. This topology is used either in direct-drive or in geared configuration. Removing the gearbox from the wind turbine improves reliability, but brings about higher cost and weight. A gearbox system was formerly considered less expensive than a direct-drive one due to cost savings in case of high-speed generators [10] but in the last years considerable progress has been made towards the weight and cost reduction of the direct-drive micro-wind systems. The generators employed in this drive train topology are the cage-rotor and wound-rotor induction generators, as well as the permanent- magnet synchronous generator (PMSG). Since it represents a low-speed brushless machine, the PMSG has become well-suited for direct-drive micro-wind applications (*fig. 1.7*) [8].

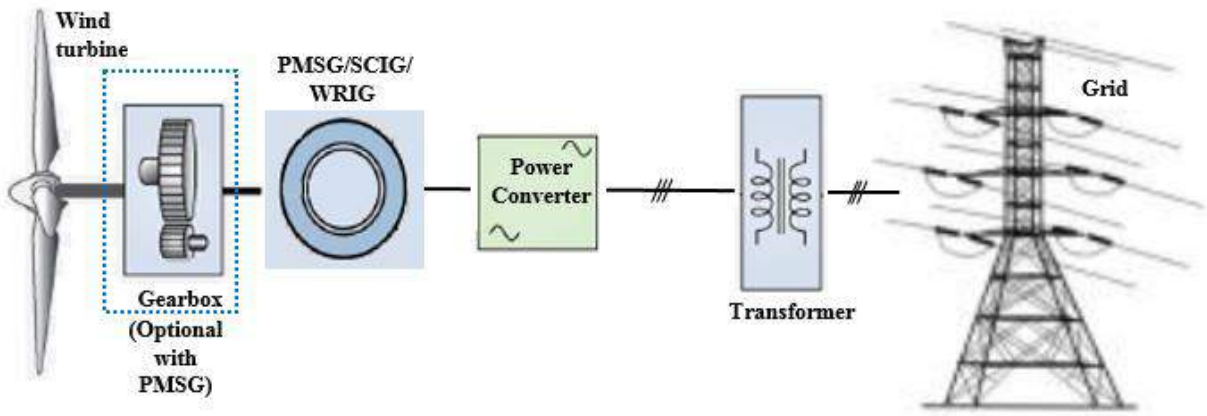

Fig. 1.7. Variable-speed micro-wind turbine system with full scale power converter

C. Power electronic converters for micro-wind turbine systems

The power electronic converters associated to the micro-wind turbine systems are intended to match the micro-wind turbine characteristics with the grid-connection or stand-alone (off-grid) requirements. They incorporate IGBT or MOSFET power devices, which are usually controlled through pulse-width-modulated (PWM) signals and if used in a back-to-back combination a bidirectional power flow is possible in the micro-wind turbine system, from the generator to the utility grid and inversely. Different power converter topologies that can be used in back-to-back combination are presented in *fig. 1.8*. The complexity and increased cost of power converters with more than three levels, i.e. multi-level converters, do not justify their use in the micro-wind turbine systems.

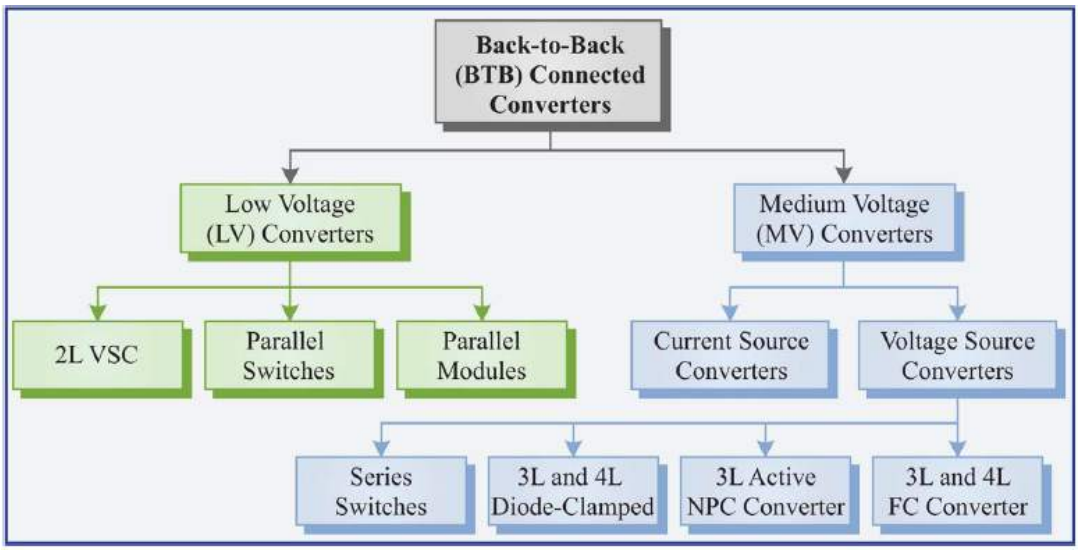

Fig. 1.8 Classification of back-to-back power electronic converters (VSC: voltage source converter, NPC: neutral-point clamped, FC: flying capacitor, 2L: two-level, 3L: three-level, 4L: four-level) [8]

Passive or unidirectional power converter topology has also been proposed in the technical literature [11], [12]. The passive solution comprises a diode rectifier for the generator side and a voltage-source inverter for the grid side as presented in *fig. 1.9*, being well-suited for the variable-speed micro-wind turbine systems. A DC/DC converter (dashed red line in *fig. 1.9*) has to be considered as DC-link for maximizing the power delivered by the micro-wind turbine.

Certainly, a more complex power converter design comes with improved performances but with higher cost of the overall system. As there is no such thing as a perfect system, in the end only the compromises are the solution for achieving a good balance between cost and performances.

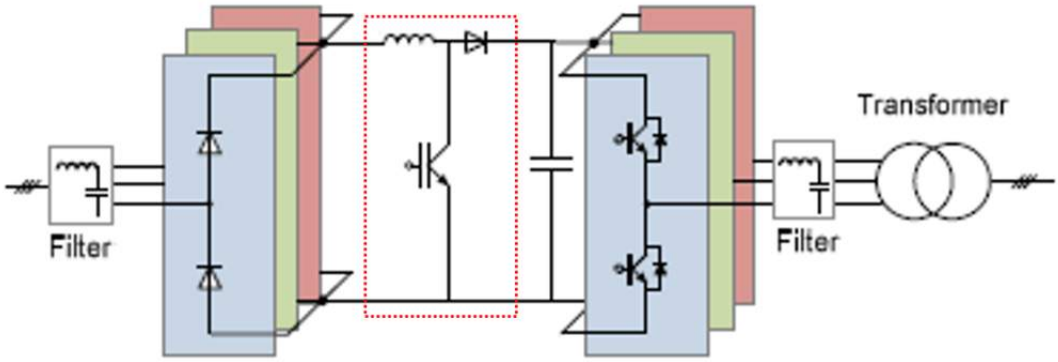

Fig. 1.9. Full-scale unidirectional power converter topology [12]

The grid-connected μWECS offers the possibility of absorbing electric energy from the grid when the micro-wind turbine does not produce enough energy to supply the load, as well as conducting to the grid the extra energy for reduction in the utility bill. In spite of that, due to wind speed variations, reflected in the quality of the active power of the micro-wind turbine system, grid connection of μWECS is not always the preferred solution as the frequency and voltage will continuously change.

An alternative solution to grid connection is represented by the stand-alone micro-wind turbine systems, which require batteries for energy storage and later use of the excess energy. Stand-alone (off-grid) μWECS operate properly with deep-cycle batteries as they can charge and discharge heaps of times compared to the automotive batteries who have a short-life in deep-cycling operations [13], [14]. Additional components need to be added such as charging controller to prevent the overcharge of the batteries, as well as large storage battery bank to cover all the electrical needs during idle periods of the stand-alone micro-wind turbine system.

However, if the average annual wind speed is rather low the stand-alone micro-wind turbine system may not be enough for residential use. For that reason, hybrid micro-power

generation systems are more appropriate, by combining the micro-wind turbine with other renewable energy sources such as photovoltaic or micro-hydro technologies.

1.3 Description of the micro-wind energy conversion system under study

Multiple aspects have to be taken into consideration in choosing a micro-wind energy conversion system (μWECS) in accordance with prescribed specifications and desired performances, some of them being listed below:

- Micro-wind turbine structure and features (tip speed ratio, power coefficient)
- Drive train design
- Operating wind speeds
- Type of electric generator and associated power electronic converter
- Control methods
- Manufacturing and maintenance cost

Several of the above specifications are going to be discussed in this subchapter, specifically those related to the mechanical and electrical components of the system. The architecture of the μWECS to be studied is outlined in *fig.1.10*, where the micro-wind turbine, the electric generator, the generator-side AC/DC power converter (rectifier) and the DC bus are represented. It is assumed that the DC-bus is connected to battery-bank and provided with constant-voltage control.

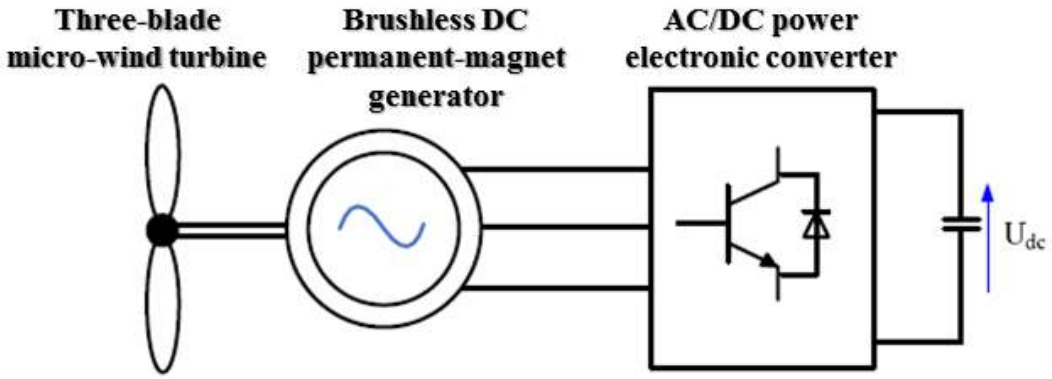

Fig. 1.10 Micro-wind energy conversion system (μWECS) under study

This structure can be considered as a good example of a complex μWECS as it incorporates subsystems belonging to different physical domains such as aerodynamic, mechanic and electric with strong interference between each other, imposing to consider in the design process the overall system, rather than its components separately. Therefore, the

approach based on design optimization, which represents the objective of this thesis, is justified and perhaps even necessary for achieving competitive performances.

The **variable-speed horizontal-axis three-bladed micro-wind turbine** topology is considered for further study. The choice is justified by the advantages that the horizontal axis configuration provides for the variable speed operation, i.e. reduced mechanical stress on the generator shaft, direct control of air-gap torque, possibility for separate control of active and reactive powers and up to 15% more power generation than the fixed speed turbines [15] .

A direct drive configuration is preferred for the studied micro-wind turbine system as it is a less expensive and less complex solution, more favored for the small wind turbines based residential use applications, being characterized with low rotational speed and high torque, lower maintenance and improved reliability [16], [17].

The **three-phase brushless DC permanent-magnet (BLDCPM) generator** with surface-mounted PM outer rotor and concentrated stator-phase windings producing trapezoidal EMFs is considered for this study as the electrical generator suited for micro-wind turbine applications. The BLDCPM generator consists in a simple construction, based on armature windings on the stator and permanent magnets on the rotor. The lack of brushes in its configuration yields several benefits for this topology as improved efficiency, better reliability, longer life with less maintenance, higher power density and higher torque to weight ratio [18].

Typically the BLDCPM generator stator is built of steel stacked laminations for star-connected phase windings arrangement. The number of slots in the stator is chosen depending on rotor poles, phase number and winding configuration. As for the BLDCPM generator rotor different possible configurations are possible, e.g. inner or outer rotor topology, surface-mounted, buried or inserted rotor-PM arrangement. As reported in [19] and [20] the outer-rotor topology provides a viable solution for small-scale and gearless wind turbine applications. Among PM materials, rare-earth alloys, like Nd-Fe-B, have been used, as they lead to higher air-gap magnetic flux density and higher electromagnetic torque, at smaller rotor size.

The operation principle of the BLDCPM is based on the attraction and repulsion between the stator and rotor magnetic poles. As the rotor shaft of the BLDCPM generator is driven in motion by the micro-wind turbine, the constant excitation field, provided by the permanent magnets on the rotor, induces dynamic back-EMFs in stator-armature phase windings. This stator-phase back-EMF voltage is proportional to the magnetic field strength and has quasi-trapezoidal shape due to the non-sinusoidal distribution of the air-gap magnetic flux density in respect of the rotor position. In practice this waveform is not quite trapezoidal as several factors intervene, such as manufacturing, leakage flux, material saturation, etc.

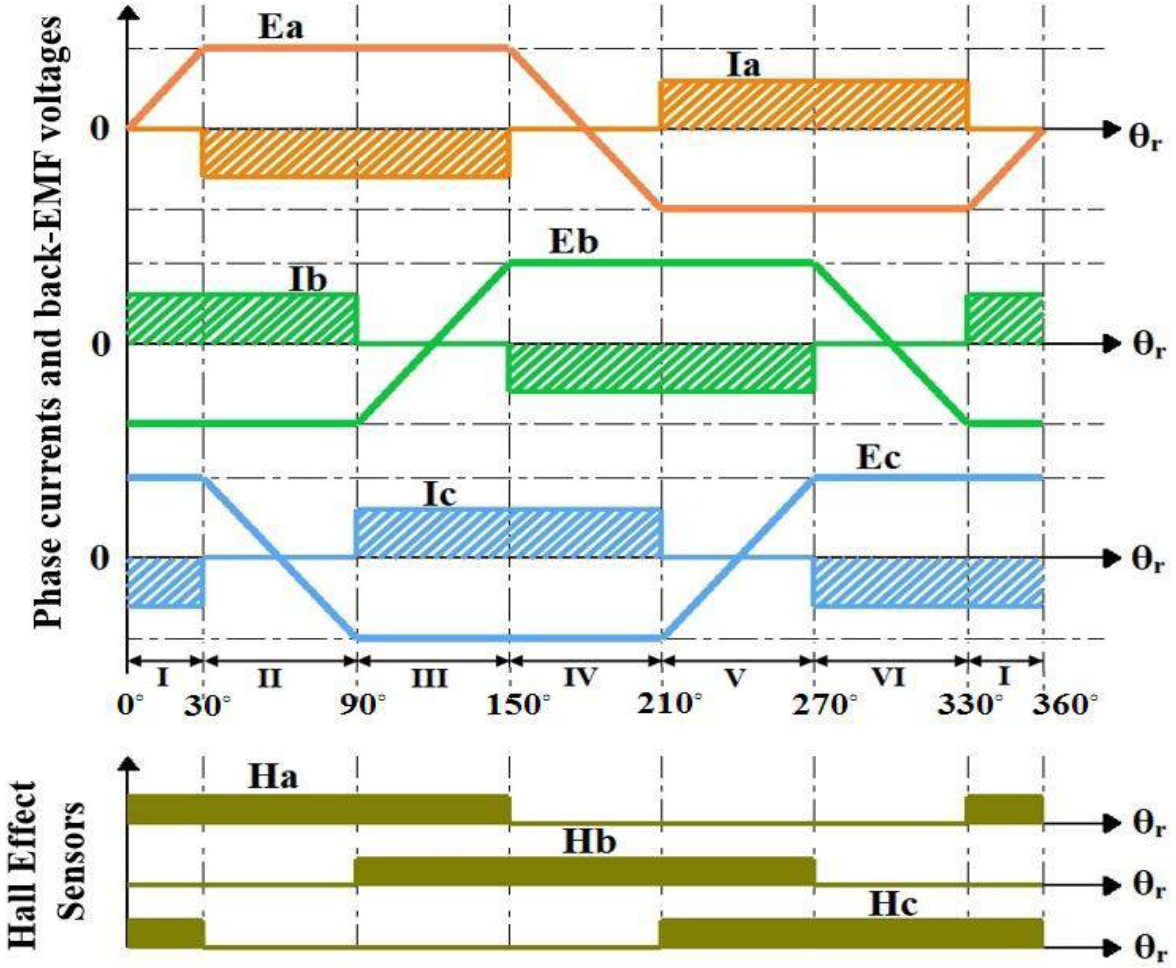

Fig. 1.11 Idealized waveforms of the stator-phase back-EMF voltages and currents with respect to Hall-effect rotor-position sensor waveforms

When a load is connected to the stator terminals of the BLDCPM generator, dynamically-induced three-phase electric current flows in the common circuit of stator-phase windings and electrical load. The rotor position relative to the stator-phase windings is essential to the generator, as it determines the direction and the sign of the stator-phase back-EMF and current, hence the electronic commutation of the BLDCPM generator. The sensing of the rotor position can be done with rotary encoders or by means of Hall-effect sensors placed in appropriate positions in order to synchronize the current flow in the stator-phase windings with the instantaneous rotor position (*fig. 1.11*).

The signal provided by each Hall sensor changes every 60° electrical degrees, therefore only six steps are needed to complete an electrical cycle, during which only two out of three phases are conducting for 120° electrical degrees. The quasi-rectangular three-phase stator-armature currents are controlled to be in phase with the quasi-trapezoidal stator-phase back-EMF voltages, thus producing unidirectional constant electromagnetic torque. However, the ideal constant electromagnetic torque cannot be achieved in practice due to cogging torque and

torque ripple phenomena. Cogging (or detent) torque is present even for zero-current in the stator-phase windings, while the torque ripple is mainly due to the stator-phase current commutations occurring every 60° electrical degrees.

The **power electronic converter associated to BLDCPM generator** is represented by the conventional three-phase full-bridge rectifier with six commutation power electronic devices with anti-parallel mounted diodes, as shown in *fig. 1.12*. The basic electronic control of the stator-phase currents is usually done by pulse width modulated (PWM) signals applied to the rectifier power electronic devices (IGBTs) in accordance with the switching pattern, which relies on the information provided by the Hall-effect rotor-position sensors. The information from the sensors allows the division of an electrical cycle into six states/sectors of 60° electrical degrees. Each sector, in its turn consists of (i) *a commutation interval*, during whom all three phases are active because of the remaining freewheeling current in the phase just switched-off and (ii) *a conduction interval* with only two phases energized according to the operating states of the PWM rectifier.

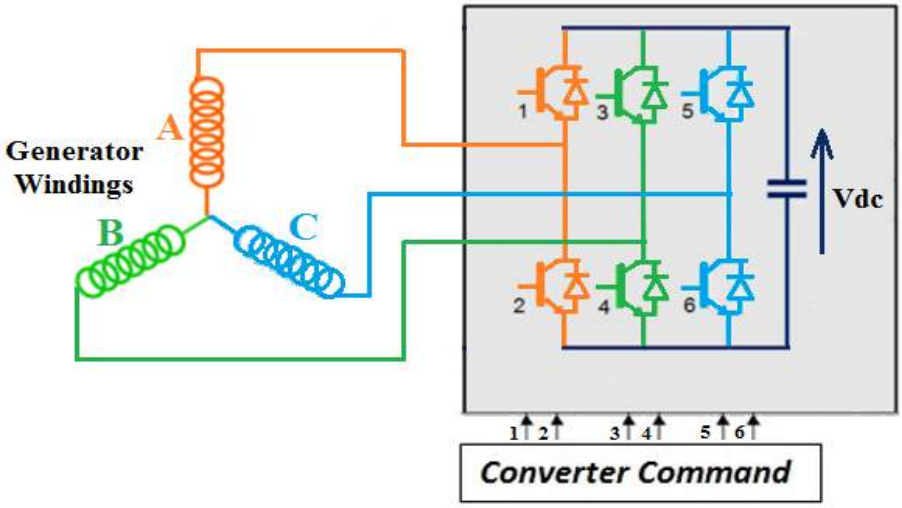

Fig. 1.12. Three-phase star-connected BLDCPM generator with associated active rectifier

1.4 Conclusions

After a short introduction into the context of the present wind market and worldwide installed capacity, a simple presentation of the micro-wind turbine system topologies is introduced. This classification allows an easy passage to the description of the micro-wind energy conversion system to be studied. The configuration is represented by the variable-speed horizontal-axis three-bladed micro-wind turbine, three-phase brushless DC permanent magnet generator and the three-phase full-bridge electronic power converter. Analysis provided for each component allows to establish the following steps for investigation:

- The modeling of the wind energy system and the variables to be considered for each component
- The physical constraints of the system that should be integrated for the design of the generator
- The methods, assumptions and simplifications that need to be done to reduce the simulation and optimization time

Selected references

[1] Lang Y., Zargari N., Kouro S. Wu B., *Power conversion and control of wind energy systems*.: John Wiley & Sons, 2011.

[2] Wind Energy Barometer, "EUROBSERV'ER," 2016.

[3] Renewable Energy Policy Network for the 21st Century, "Renewables 2015 Global Status Report," 2015.

[4] World Wind Energy Association, "Small wind world report 2016,".

[5] Exploring Green Technology. [Online]. http://exploringgreentechnology.com

[6] K., Dincer I., Naterer G. F. Pop, "Energy and exergy efficiency comparison of horizontal and vertical axis wind turbines," *Renewable Energy*, 2010.

[7] Newmeil Industry and International Trading (Suzhou) Co., Ltd. [Online]. http://www.newmeilwindturbine.com/

[8] B. Wu, P.C. Sen, S. Kouro, M. Narimani V. Yaramasu, "High-power wind energy conversion systems: State-of-the-art and emerging technologies," *Proceedings of the IEEE*, vol. 103, no. 5, pp. 740-788, December 2015.

[9] Tiago Staudt, *Brushless doubly-fed reluctance machine modeling, design and optimization, PhD Thesis*., 2015.

[10] and Zhe Chen Li H., "Overview of different wind generator systems and their comparisons," *Renewable Power Generation, IET 2.2*, pp. 123-138., 2008.

[11] Dinavahi V., & Knight A. M. Baroudi J. A., "A review of power converter topologies for wind generators," *Renewable Energy*, pp. 2369-2385, 2007.

[12] Liserre M., & Ma K. Blaabjerg F., "Power electronics converters for wind turbine systems," *IEEE Transactions on Industry Applications*, pp. 708-71, 2012.

[13] Østergaard J. Divya K. C., "Battery energy storage technology for power systems—An overview," *Electric Power Systems Research*, 2009.

[14] Teodorescu R., Rasmussen C. N., Rodriguez P., & Vikelgaard H. Świerczyński M., "Overview of the energy storage systems for wind power integration enhancement," *IEEE International Symposium on Industrial Electronics*, 2010.

[15] Xie Y., & Tan Z. Cao W., "Wind turbine generator technologies," in *ADVANCES IN WIND*.: INTECH Open Access Publisher, 2012.

[16] Ferreira J. A., Jensen B. B., Abrahamsen A. B., Atallah K., McMahon R. A. Polinder H., "Trends in wind turbine generator systems," *IEEE Journal of Emerging and Selected Topics in Power Electronics*, 2013.

[17] Polikarpova M., Roytta P., Alexandrova J., Pyrhonen J., Nerg J.,Backman J. Semken R. S., "Direct-drive permanent magnet generators for high-power wind turbines: Benefits and limiting factors," *IET Renewable Power Generation*, 2012.

[18] G.H. Rim R. Krishnan, "Modeling, simulation, and analysis of variable-speed constant frequency power conversion scheme with a permanent magnet brushless DC generator," *IEEE Transactions on Industrial Electronics*, pp. 291-296, 1990.

[19] Yeadon A. Yeadon W., *Handbook of small electric motors*.: McGraw Hill Professional, 2001.

[20] Ocak C. Tarımer İ., "Performance comparision of internal and external rotor structured wind generators mounted from same permanent magnets on same geometry," *Elektronika ir Elektrotechnika*, pp. 65-70, 2015.

Chapter 2

Modeling and Simulation of the BLDCPM Generator-Based Micro-Wind Energy Conversion System in View of Its Optimization

2.1 Introduction

Establishing the right level of modeling which allows the resolving (by means of optimization) of the pursued objective in a manner somewhat fast represents a challenge for the modeling process. Also, the number of simulations necessary in the design stage plus the pursued accuracy of the outputs are determinant factors. Therefore the aim of this chapter is to present the design of the components associated to the micro-wind energy conversion system in order to be able to:

- Calculate the power losses in each component (*Chapter 3*), whose minimization over a long-term wind speed profile will be attempted
- Determine which of the components parameters need to be considered in the formulation of the optimization problem (*Chapter 4*)

In the last part a simulation process of the overall system will be conducted to conclude which of the three proposed models can be a viable solution in terms of precision and simulation time for the future design optimization process.

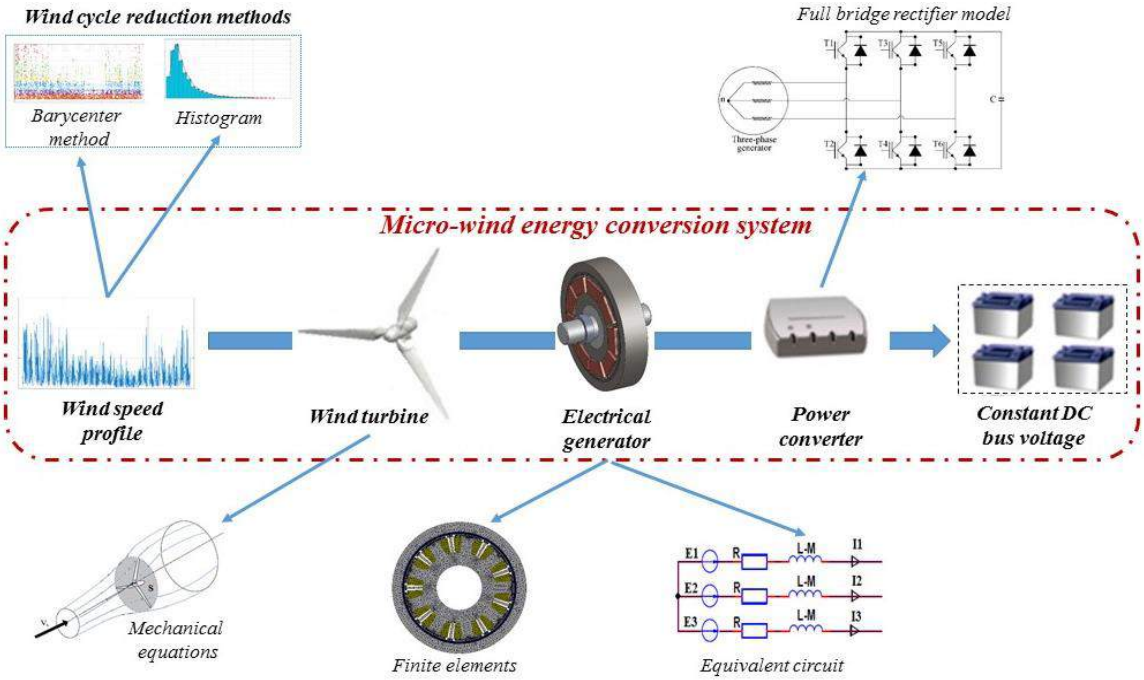

Fig. 2.1. Retained architecture of the micro-wind energy conversion system

The architecture of the μWECS is depicted in *fig. 2.1* and it consists of the following models that were developed and analyzed in this thesis:

- The long-term wind speed profile which will be examined in the third part of the thesis in view of its reduction
- The three-bladed horizontal axis wind turbine that provides the assessment of the available power in the wind speed helping to establish the speed and torque limits of the generator
- The brushless DC permanent magnet generator and rectifier assembly: an analytical, a semi-analytical and a numerical model are investigated based on the machine's dimensions
- The DC bus which is considered to have a constant voltage

2.2 Modeling description of the μWECS components

2.2.1 Micro-wind turbine model

The mechanical power that the wind turbine can produce may be expressed as [1]:

$$P_{wt} = 0.5\rho_{air}\pi R_{wt}^2 C_p(\lambda) v_w^3 \tag{2.1}$$

where

ρ_{air} : Air density [kg/m^3]

R_{wt} : Radius of the turbine rotor blades [m]

C_p : Power coefficient of the turbine

λ : Tip speed ratio coefficient

v_w : Wind speed [m/s]

The power coefficient from the equation is an important parameter as it provides an idea about how many of the kinetic energy from the air mass can be converted into mechanical energy by the wind turbine. According to Betz's law [1] this conversion rate cannot be higher than *0.59* and in practice is even less because of the mechanical imperfections. This coefficient can be calculated through interpolation [2] based on *(2.2)* as a function of tip speed ratio (*fig. 2.2*), while the latter can be defined as in *(2.3).*

$$C_p(\lambda) = -3.98 \cdot 10^{-8} \cdot \lambda^7 - 4.21 \cdot 10^{-6} \cdot \lambda^6 + 2.1 \cdot 10^{-4} \cdot \lambda^5 - 3.1 \cdot 10^{-3} \cdot \lambda^4 + 1.64 \cdot 10^{-2} \cdot \lambda^3 - 0.0176 \cdot \lambda^2 + 0.0174 \cdot \lambda - 1.93 \cdot 10^{-3} \tag{2.2}$$

$$\lambda = \frac{\Omega R_{wt}}{v_w} \tag{2.3}$$

with

Ω : Rotational mechanical speed of the turbine/generator [rad/s]

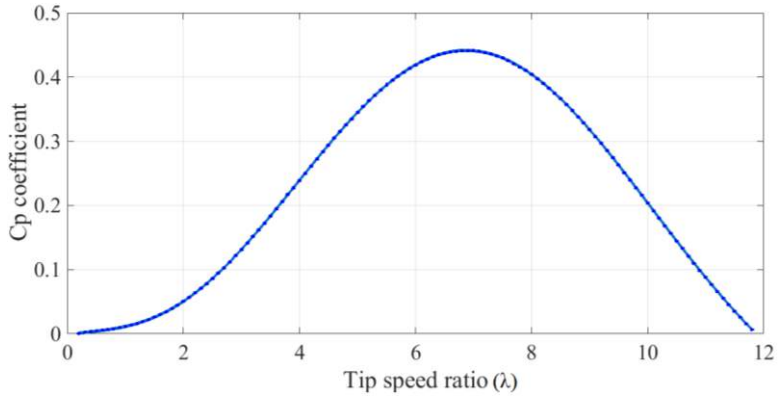

Fig. 2.2. Wind turbine power coefficient as a function of tip speed ratio

From *fig. 2.2* it can be observed that the optimum value of the power coefficient is $C_{p\_max} = 0.441$ at an optimum tip speed ratio of $\lambda_{opt} = 6.9$.

Based on the above, the power characteristics of the turbine as a function of rotational speed have the waveforms as depicted in *fig. 2.3.* It can be noticed that the optimal power extraction varies with the changing of the wind speed.

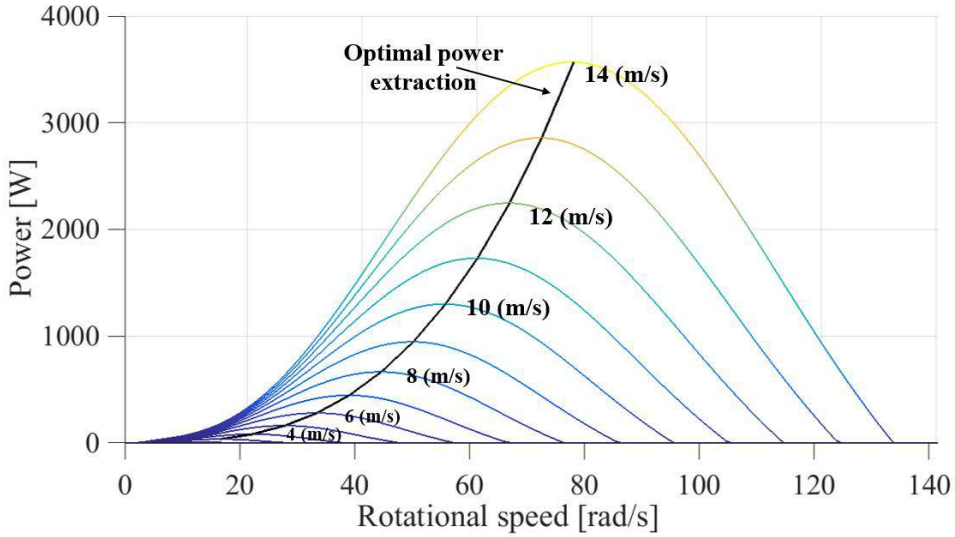

Fig. 2.3. Power characteristics of a micro-wind turbine for several wind speeds

The operation areas of the wind turbine can be classified based on the wind speed, resulting into three main regions: low-speed, MPPT (maximum power point tracking) control and high speed, as presented in *fig. 2.4.* The wind turbine starts the operation at a cut-in wind

speed which denotes the level at which the turbine captures enough power to overcome its power losses. Further on, it continues the process of optimum power extraction until the base wind speed value is reached which corresponds to the level at which the generator also achieves its nominal power. A MPPT strategy is therefore adopted in this region, which corresponds at an operation at C_{p_max} and λ_{opt}. For wind speeds outrunning the rated value, the turbine is kept to function at its nominal power by means of different control techniques, such as pitch/stall systems or power limitation strategies [3]. When the highest wind speed (represented by the cut-off speed) at which the turbine is allowed to operate is reached the turbine ceases power generation through its shut-down, for mechanical damage protection.

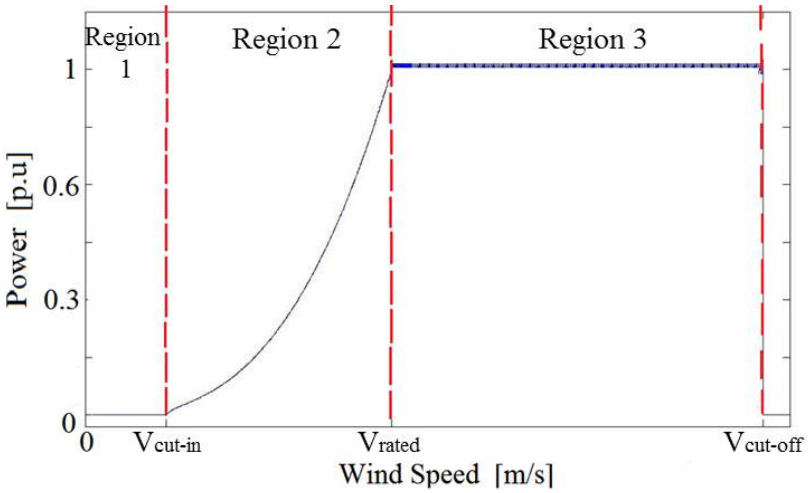

Fig. 2.4. Operation regions of a micro-wind turbine

2.2.2 Modeling of the generator-rectifier assembly

As the simulation time is of great importance for the optimization process, models with high accuracy can evolve it into a time-consuming process, especially when considering optimization over a long-term wind speed cycle for the minimization or maximization of different quantities. For this, three modeling simulation levels of the generator will be analyzed throughout this section to establish the suitable one that can be used in the design optimization process of the micro-wind energy conversion system [4]. All of them depend on the sizing characteristics of the generator which will be determined beforehand and will work as a background function for each of the simulation model during the optimization.

2.2.2.1 Dimensional features of the BLDCPM generator

The geometrical equations examined for the design of the BLDCPM generator are based on the descriptions provided in [5], [6] and based on the sizing model presented in [7].

These equations, given in ***Appendix 2.A***, are found on the geometrical quantities listed in *table 2.1* and presented in *fig. 2.5*, making possible to determine the dimensional and electrical parameters required by the simulation models.

Table 2.1. Main geometric parameters of the BLDCPM generator

R_s :	Stator radius [mm]
L_m :	Magnetic length of the machine [mm]
g :	Air gap thickness [mm]
l_{th} :	Width of the main stator tooth [mm]
l_{th_int} :	Width of the intermediate stator tooth [mm]
h_{th} :	Depth of the main stator tooth [mm]
h_{pm} :	Thickness of the permanent magnet [mm]
h_{sy} :	Thickness of the stator yoke [mm]
h_{ry} :	Thickness of the rotor yoke [mm]
h_c :	Thickness of the main pole shoe [mm]
h_{c_int} :	Thickness of the intermediate pole shoe [mm]
α :	Widening of the main stator tooth
α_{int} :	Widening of the intermediate stator tooth
β :	Widening of the permanent magnet

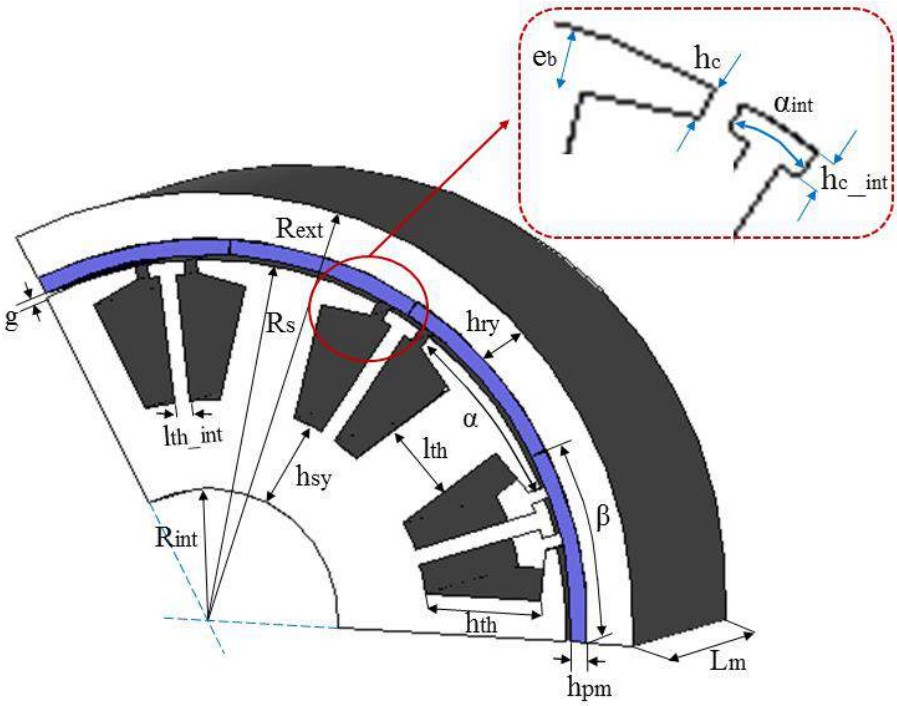

Fig. 2.5. Geometric model of the BLDCPM generator

Given the fact that some of the sizing equations recline on several input parameters (which are fixed and will not be considered to be optimized) related to the material properties, few assumptions have to be considered when performing the calculations:

- The slot copper filling coefficient is set to $k_r = 0.5$
- The stator's laminated filling factor is considered $k_{st} = 0.95$
- The remnant induction of the magnets is chosen $B_r = 1$ [T] whereas their relative magnetic permeability is equal to $\mu_r = 1.05$
- The shape of the magnetic induction in the air gap is considered ideal

2.2.2.2 Analytical simulation model

The analytical simulation model is a static one based on the sizing and circuit equations of the machine written by considering only the amplitude of the involved quantities. As it computes only peak or mean values its best feature resides in the fast simulation time (as it will be seen in the simulation *subchapter 2.3*), whereas its inability to predict some phenomena in the currents and torque waveforms represents its main disadvantage.

Several assumptions are made for this model in order to simply its construction.

First of all, knowing that for a wye connection two phases are energized simultaneously and the back EMF is proportional to the rotational speed of the generator, at constant operation its amplitude is sufficient to be taken into account for the calculation of the generator's phase current and electromagnetic torque:

$$\hat{E} = k_e \Omega \tag{2.4}$$

$$\hat{I} = \frac{\hat{P}_{em}}{2\hat{E}} \tag{2.5}$$

$$\hat{T}_{em} = 2k_e\hat{I} \tag{2.6}$$

where

$\hat{E}$: Phase back-EMF peak voltage [V]

k_e : Back-EMF voltage coefficient

$\hat{I}$: Peak phase current [A]

$\hat{P}_{em}$: Peak electromagnetic power [W]

$\hat{T}_{em}$: Peak electromagnetic torque [Nm]

Secondly, as the generator is of direct-driven type, it is assumed that its rotational speed can be determined from the tip speed ratio equation *(2.3)*, whereas its developed electromagnetic power is assumed to derive from *(2.1)* considering the optimum power extraction from the wind speed:

$$\Omega = \frac{\lambda_{opt} v_w}{R_{wt}} \tag{2.7}$$

$$\hat{P}_{em} = \begin{cases} 0, & v_w < v_{in}, v_w \geq v_{max} \\ \frac{\pi}{2} \rho_{air} R_{wt}^5 \frac{C_{p\_opt}}{\lambda_{opt}^3} \Omega^3 - \hat{P}_{mech}, & v_{in} \leq v_w \leq v_b \\ P_b - \hat{P}_{mech}, & v_b < v_w < v_{max} \end{cases} \tag{2.8}$$

with

P_b : Base or nominal power of the generator [W]

$\hat{P}_{mech}$: Mechanical losses [W]

v_{in} : Cut-in wind speed [m/s]

v_b : Base/rated wind speed [m/s]

v_{max} : Cut-off wind speed [m/s]

As final remarks, the implementation of the above equations is done in Matlab programming environment and no control is implemented for this model as the commutation of the phases is not explicitly taken into consideration.

2.2.2.3 Semi-analytical simulation model

In order to assess for the dynamic properties of the generator, which have a great impact upon the quality of the electrical energy generated, a second simulation model is investigated, i.e. the time-based semi-analytical model. Its description relies on three parts: the first one introduces the electrical equations upon which the modeling of the generator is realized whilst the second and the third parts reveal the control and associated power converter model.

A) Electrical equations

The analysis of the three-phase generator is based on a couple of hypothesis such as:

- The materials saturation effect is not accounted for
- The resistances and inductances of the three-stator phase windings are considered identical and constant

- The trapezoidal back-EMF voltage shape is presumed ideal and identical in all phases

Based on the above, the phase voltage of the three-phase star-connected BLDCPM generator with isolated neutral point stator windings results as follows [8]:

$$v_{ph}(t) = R_{ph} i_{ph}(t) + (L_{ph} - M)\frac{di_{ph}(t)}{dt} + e_{ph}(t) + v_n(t) \tag{2.9}$$

$$v_n(t) = \frac{1}{3}\left(\sum v_{abc}(t) - \sum e_{abc}(t)\right) \tag{2.10}$$

$$i_a(t) + i_b(t) + i_c(t) = 0 \tag{2.11}$$

with

v_{ph} : Phase to neutral voltage [V]

R_{ph} : Phase resistance [ohm]

i_{ph} : Phase current [A]

L_{ph}: Phase self-inductance [H]

M : Mutual phase inductance [H]

e_{ph} : Back-EMF voltage [V]

v_n : Neutral voltage [V]

a, b, c : Stator phase windings notation

The trapezoidal back-EMF voltages of the generator depend on the rotor position θ_r to be determined and knowing that each of the phase presents a 120° electrical degree shift from the others, the expression for each phase can be found as:

$$e_a(\theta_r) = \begin{cases} \left(\frac{6}{\pi}\hat{E}\right)\theta_r, & 0 < \theta_r < {}^{\pi}/_{6} \\ \hat{E}, & {}^{\pi}/_{6} < \theta_r < {}^{5\pi}/_{6} \\ -\left(\frac{6}{\pi}\hat{E}\right)\theta_r + 6\hat{E}, & {}^{5\pi}/_{6} < \theta_r < {}^{7\pi}/_{6} \\ -\hat{E}, & {}^{7\pi}/_{6} < \theta_r < {}^{11\pi}/_{6} \\ \left(\frac{6}{\pi}\hat{E}\right)\theta_r - 12\hat{E}, & {}^{11\pi}/_{6} < \theta_r < 2\pi \end{cases} \quad e_b(\theta_r) = \begin{cases} -\hat{E}, & 0 < \theta_r < {}^{\pi}/_{2} \\ \left(\frac{6}{\pi}\hat{E}\right)\theta_r - 4\hat{E}, & {}^{\pi}/_{2} < \theta_r < {}^{5\pi}/_{6} \\ \hat{E}, & {}^{5\pi}/_{6} < \theta_r < {}^{9\pi}/_{6} \\ \left(\frac{6}{\pi}\hat{E}\right)\theta_r + 12\hat{E}, & {}^{9\pi}/_{6} < \theta_r < {}^{11\pi}/_{6} \\ -\hat{E}, & {}^{11\pi}/_{6} < \theta_r < 2\pi \end{cases}$$

$$e_c(\theta_r) = \begin{cases} \hat{E}, & 0 < \theta_r < {}^{\pi}/_{6} \\ -\left(\frac{6}{\pi}\hat{E}\right)\theta_r + 2\hat{E}, & {}^{\pi}/_{6} < \theta_r < {}^{\pi}/_{2} \\ -\hat{E}, & {}^{\pi}/_{2} < \theta_r < {}^{7\pi}/_{6} \\ \left(\frac{6}{\pi}\hat{E}\right)\theta_r - 8\hat{E}, & {}^{7\pi}/_{6} < \theta_r < {}^{9\pi}/_{6} \\ \hat{E}, & {}^{9\pi}/_{6} < \theta_r < 2\pi \end{cases} \tag{2.12}$$

From these, the electromagnetic power and torque developed by the generator can be computed based on:

$$P_{em}(t) = e_a(t)i_a(t) + e_b(t)i_b(t) + e_c(t)i_c(t) \tag{2.13}$$

$$T_{em}(t) = \frac{1}{\Omega(t)} P_{em}(t) \tag{2.14}$$

For the electro-mechanical connection part between the wind turbine and the machine, using the generator convention, equation *(2.15)* introduces the dynamic behavior of the assembly. However, such a relation is not required if a constant rotor-speed operation (steady-state) is employed, since the above equations can be resolved directly for currents and electromagnetic torque.

$$T_{wt}(t) - T_{em}(t) - f_{wt}\Omega(t) = J\frac{d\Omega(t)}{dt} \tag{2.15}$$

where

T_{wt} : Active torque provided by the turbine [N.m]

J : Rotor inertia [kg.m^2]

f_{wt} : Friction coefficient (N.m/rad), equal to 0.025.

This friction coefficient, which depends on the rotor shape and on the rotational speed, helps in approximating the mechanical losses caused by the rotation of the rotor, based on the value information provided in [2].

B) Control loops

A schematic representation of the semi-analytical model implemented in Matlab/Simulink environment is depicted in *fig. 2.6*. As observed, a power outer-loop and a hysteresis current control strategies are implemented to assure that the generator is able to develop power equal to the active one harvested by the turbine from the wind.

The error signal between a reference power and the power delivered by the generator is processed with the help of a PI controller whose proportional and integral coefficients are determined by means of trial and error method. The output of this regulation helps in determining the phase reference currents based on the $120° -$ switching pattern of the generator, which is dependent on the rotor's angular position as exemplified in *table 2.2*.

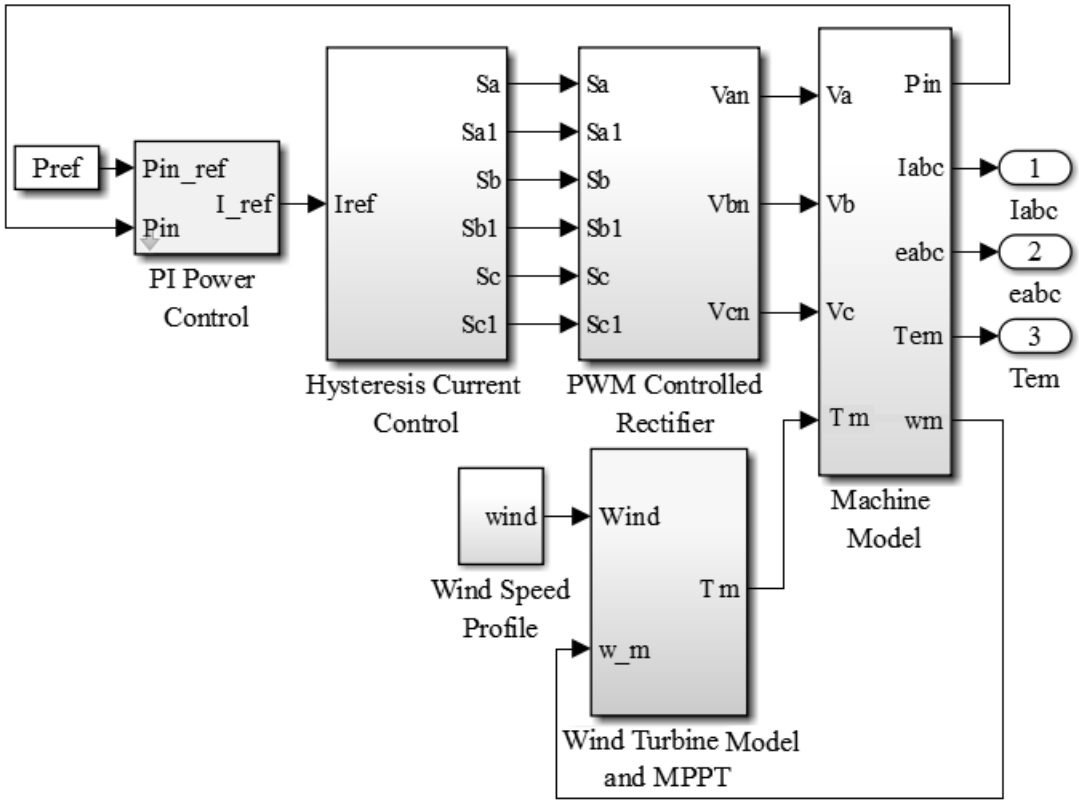

Fig. 2.6. Semi-analytical simulation model scheme in Matlab/Simulink environment

Table 2.2. Reference phase currents vs. rotor position

Sector	$\boldsymbol{\theta_r}$	$\boldsymbol{I_{a\_ref}}$	$\boldsymbol{I_{b\_ref}}$	$\boldsymbol{I_{c\_ref}}$
1	$330° - 30°$	0	$-I_{ref}$	I_{ref}
2	$30° - 90°$	I_{ref}	$-I_{ref}$	0
3	$90° - 150°$	I_{ref}	0	$-I_{ref}$
4	$150° - 210°$	0	I_{ref}	$-I_{ref}$
5	$210° - 270°$	$-I_{ref}$	I_{ref}	0
6	$270° - 330°$	$-I_{ref}$	0	I_{ref}

The hysteresis current control scheme, based on adjusting the armature windings currents to track the reference ones, is used afterwards to obtain the PWM driving signals of the rectifier's power devices. This hysteresis controller maintains the phase currents between an imposed band (*fig. 2.7-c*) by transmitting, through ON (1) and OFF (0) signals, to the power devices when to open and when to close. This hysteresis band can be estimated based on [9]:

$$\Delta i = \frac{V_{dc}}{L} \frac{1}{\frac{1}{t_r} + \frac{1}{t_f}} \tag{2.16}$$

where

t_r : Rising transit time

t_f : Falling transit time

If the two transit times are assumed equal for the IGBT-rectifier switching period T_R (with $T_R = 1/f_R$ and$f_R = f_{IGBT}$) then *(2.16)* becomes [9]:

$$\Delta i = \frac{V_{dc}}{2Lf_R} \tag{2.17}$$

C) Generator-side power electronic converter

The $120° -$ commutation pattern allows the division of an electrical cycle of $360°$ into six operating states or sectors of $60°$, corresponding to the position information provided by the Hall sensors mounted on the stator or determined with the help of a rotary encoder. Each of these sectors, in their turn, consist of a commutation and a conduction interval, whose operation features are going to be emphasized by an exemplification on only one sector as for the others the same principle applies.

As exemplified in *fig. 2.7-a*, the conduction interval corresponds to the normal flow (red line) of the current through the two stator windings and then via the two equivalent power devices of the rectifier, i.e. the lower-side transistor *T2* for *a-phase* and upper-side transistor *T5* for *c-phase,* while no current exists in the third phase. As the two transistors are ON-state, the currents in the phases increase up to a certain point where they are limited by the hysteresis current regulation. This means that the genuine current of *c-phase* is compared to its rectangular reference current by means of a hysteresis comparator. The task of this comparator is to determine the phase current to follow the reference one, by alternating its flow direction based on the signals provided to the transistors and diodes and thus maintaining it between imposed bands. As shown in *fig. 2.7-c* when the current in *c-phase* reaches the upper limit $i_{c\_ref} + \Delta i/2$ the output of the hysteresis comparator signals the upper transistor *T5* to turn off, allowing the current to decrease slowly through the lower diode *D6* until the lower limit $i_{c\_ref} - \Delta i/2$ is attained, at which point the *T5* transistor starts to operate again. This chopping operation of the phase current repeats until the end of the considered sector, which represents also the beginning of the commutation interval. The same regulation principle is applied for each of the other phases as well.

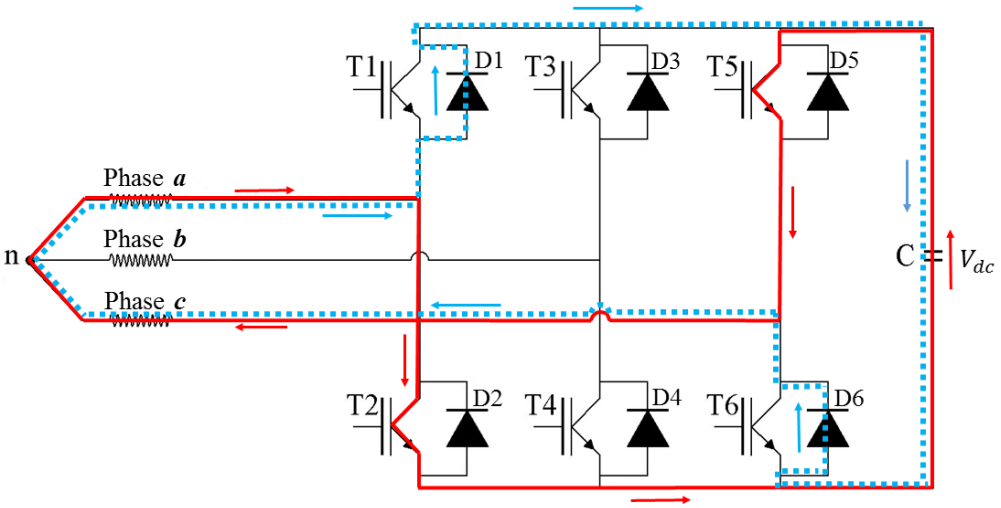

A) Conduction interval

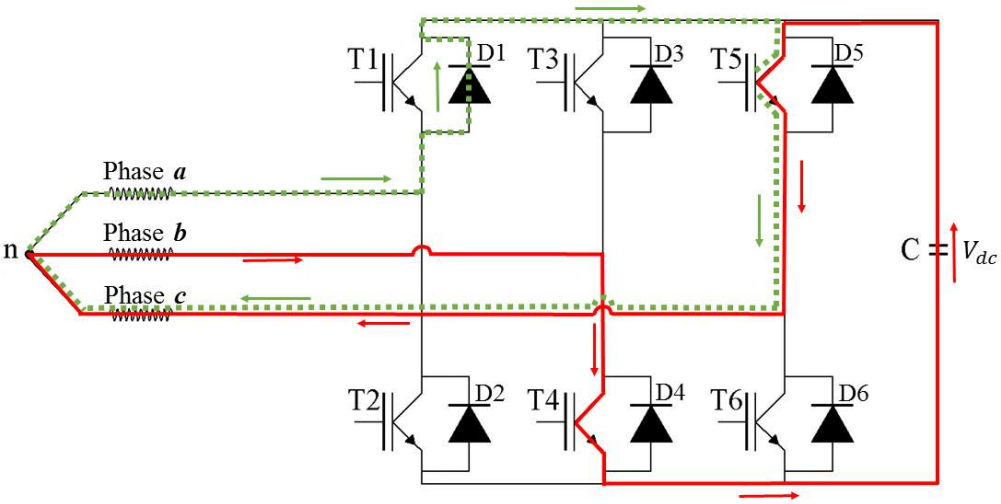

B) Commutation interval

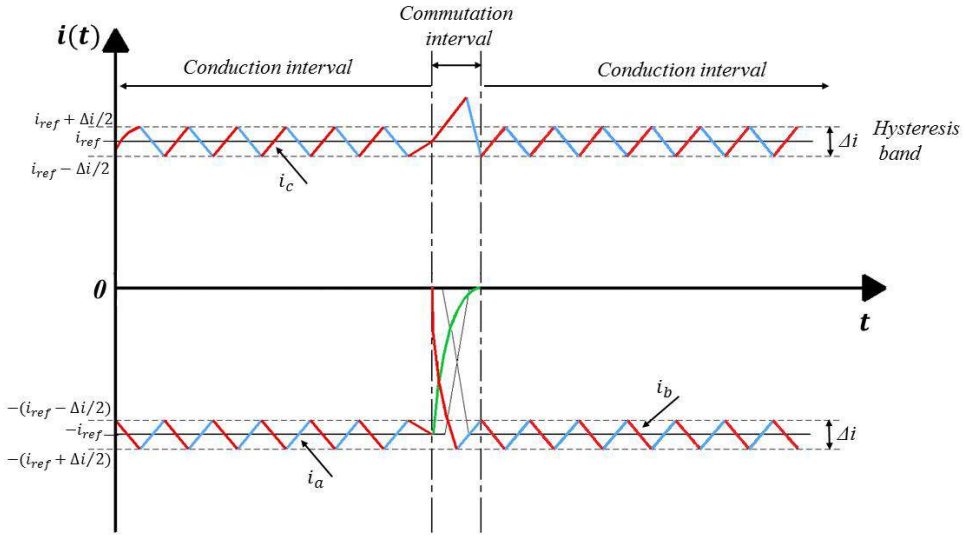

C) Hysteresis current regulation

Fig. 2.7. Equivalent circuit and current path corresponding to one of the six operation states (sectors) of the generator-side three-phase PWM rectifier

The passage from a conduction operation sector to another is accomplished by interchanging the generator's phases, also known as the commutation interval (*fig. 2.7-b*) when the current flows through all the three stator windings. Two distinct current paths can be observed during this interval:

- The main current path (red line) is through the corresponding two series connected phase windings of the sector under consideration and via their equivalent power devices, e.g. *b-phase* and *c-phase* windings with their corresponding *T4*, respectively *T5* transistors
- The second path of the current (green dotted line) is the one through *c-phase* winding with *T5* turned on and through a-phase winding via the fly-back diode *D1*. This current flow is due to the existence for a short period of time of a freewheeling current in the phase just switched off (*a-phase* winding), hence the moment of its disappearance denotes the end of the commutation and the beginning of the normal operation of the sector in cause.

However, the existence of the second path of the current appears only in the cases when the value of the DC bus voltage (V_{dc}) fulfills one of the following inequalities:

$$V_{dc} < 4\hat{E} \;\; or \;\; V_{dc} > 4\hat{E} \tag{2.18}$$

As a result a peak in the current's waveform appears during the switching of the phases as it can be seen in *fig. 2.6-c*. This situation can be explained by the fact that the decaying of the current in the switched off phase (*a-phase* winding) is done in a slower manner than the rising of the current in the ongoing phase (*b-phase* winding), hence the altered current waveform of the third phase (*c-phase* winding). The amplitude of the peak is strongly influenced by the DC voltage and as it will be seen after the simulations in *section 2.3* it produces a proportional oscillation in the torque's waveform as well.

Nevertheless, based on the driving signals the voltages of the output terminals of the BLDCPM micro-wind generator can be determined in accordance to the operation interval of the controlled PWM rectifier for each of the six sectors as in [10].

2.2.2.4 Finite element-based numerical model

As neither the analytical nor the semi-analytical models do not take into consideration the non-linear materials characteristics and the complex geometry of the machine a third model is investigated and that is the finite element (FE)-based numerical model. The advantage in using this model is its high precision, but unfortunately it is well known for its

huge evaluation time making it a displeasing strategy to be considered in optimization. Nevertheless, it can be used outside the optimization loop as a validation model in order to refine the obtained results. Another good feature of the numerical model is that it gives the possibility to validate some physical quantities such as flux densities, inductances etc.

The FE-discretized cross-sectional model of the BLDCPM generator (*fig. 2.8*) was created based on the dimensional parameters of a reference machine and subjected to numerical field analysis by means of JMAG Designer software [11]. Several steps need to be followed for creating the model in JMAG, i.e. to create the geometry, set the materials in each part of the generator, to create the winding configuration, set the conditions, generate the mesh, model the electrical circuit; this is time-consuming and also difficult. Therefore, a link has been created between JMAG Designer and Matlab through a script file based Visual Basic language which facilitates the automatic configuration of the generator design and associated electric circuit in a short period of time, allowing also to modify the input specifications, to implement the conditions, to perform a transient analysis upon the model and to save the results in Excel files, which can be easily visualized afterwards in Matlab software. The interface created with Matlab is a text file, each line containing a value for the considered input data.

The script for the operation at load conditions of the reference machine in JMAG Designer is provided in ***Appendix 2.B***. It was meant as a general script, there forth it can be used to analyze other topologies for this type of machine with outer rotor configuration, by simply changing the geometrical dimensions.

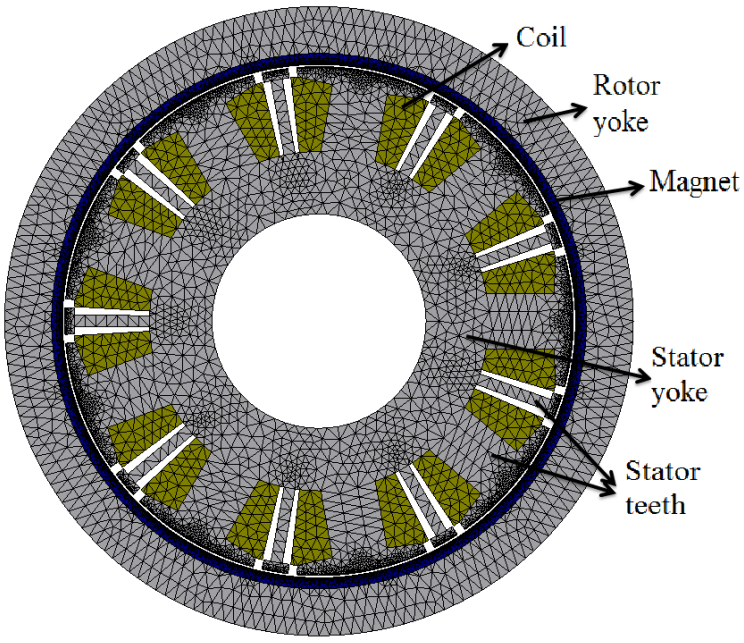

Fig. 2.8. FE-discretized 2D cross-sectional model of the reference BLDCPM machine

For the FE analysis a full 2D view of the generator was considered, but by applying symmetry and boundary conditions a reduction in its modelling is possible which helps in further reducing the simulation time necessary for one mechanical cycle investigation.

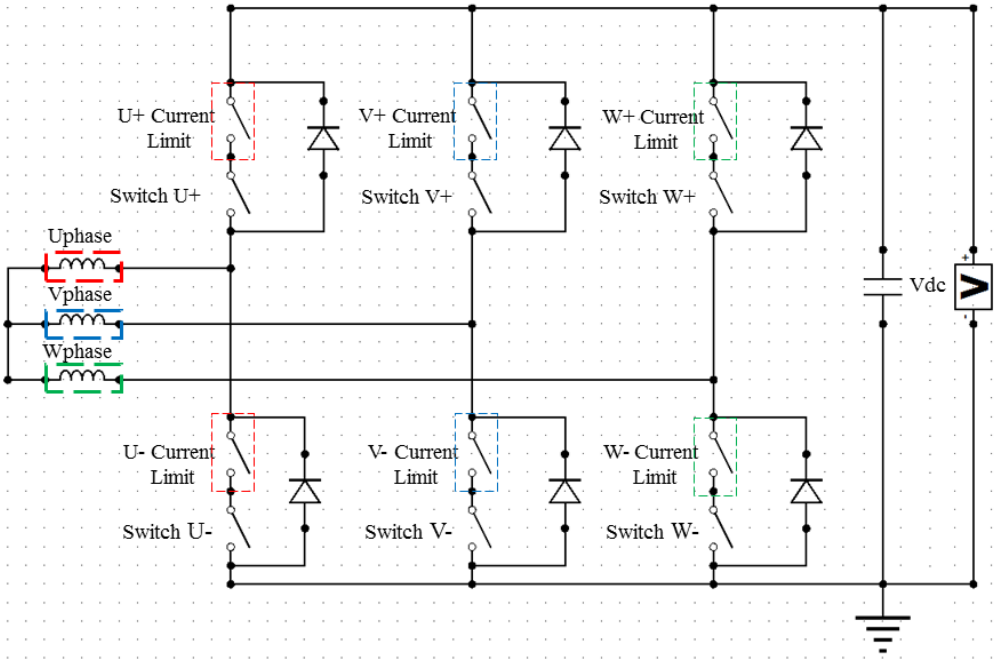

Fig. 2.9. Electric circuit of the FE 2D model

The electrical circuit considered for this model resembles the one from *fig. 2.9*, consisting also of hysteresis limitation switches for each of the phase current.

The active materials used for the machine parts are summarized in *table 2.3*, while their properties can be found by means of data sheets insured by the industries.

Table 2.3. Active materials used in the FE-modeling of the BLDCPM machine

Part	**Material data**
Stator core	JFE Steel: 50JN400
Rotor core	JFE Steel: 50JN400
Permanent magnet	Reversible NdFeB Radial Pattern (Circular Direction)
Winding	Copper

The accuracy of the FE-model is given by the mesh discretization of the model and by the number of divisions. In the construction of the mesh the element size of the air region is set to 1 mm and the element size for the parts is set to 4 mm. A transient analysis is used since the electromagnetic torque and rotor-speed are time-variant and a number of steps and divisions of 1200 and 600 respectively. The analysis of just one mechanical cycle is sufficient

to observe the behavior of several parameters of the machine that are going to be presented in *section 2.3.*

2.3 Simulations of the micro-wind turbine system over base point operation

To evaluate the simulation models presented above, a reference machine is considered, whose characteristics are presented in *table 2.4*, corresponding to the outer-rotor BLDCPM machine studied in [7].

Table 2.4. Parameters of the reference BLDCPM machine

Parameter	Value
Bore diameter D_s	189 [mm]
Airgap g	0.8 [mm]
Magnetic length of the machine L_m	45 [mm]
Width of the main stator tooth l_{th}	20.617 [mm]
Width of the intermediate stator tooth l_{th_int}	4.123 [mm]
Depth of the main stator tooth h_{th}	24.934 [mm]
Thickness of the permanent magnet h_{pm}	4.091 [mm]
Thickness of the stator yoke h_{sy}	23.194 [mm]
Thickness of the rotor yoke h_{ry}	17.413 [mm]
Thickness of the main pole shoe h_c	3.467 [mm]
Thickness of the intermediate pole shoe h_{c_int}	3.591 [mm]
Number of pole pairs p	6
Number of slots N_s	9
Current density δ_{dens}	3 [A/mm^2]
Phase resistance R_{ph}	0.036 [Ω]
Phase inductance L_{ph}	1.353 [mH]
Base electromagnetic torque T_{em}	20 [Nm]
DC bus voltage V_{dc}	120 [V]

A more detailed view of the flux densities along with the flux lines in the reference machine obtained after a FE simulation are presented in *fig.2.10.* It is noticeable that the path of the flux lines is through the airgap, slots and stator yoke to close through the rotor yoke of the machine. The contour plot of the flux densities indicates that the highest flux appears in the stator tooth when in aligned position with the surface mounted permanent magnets on the rotor.

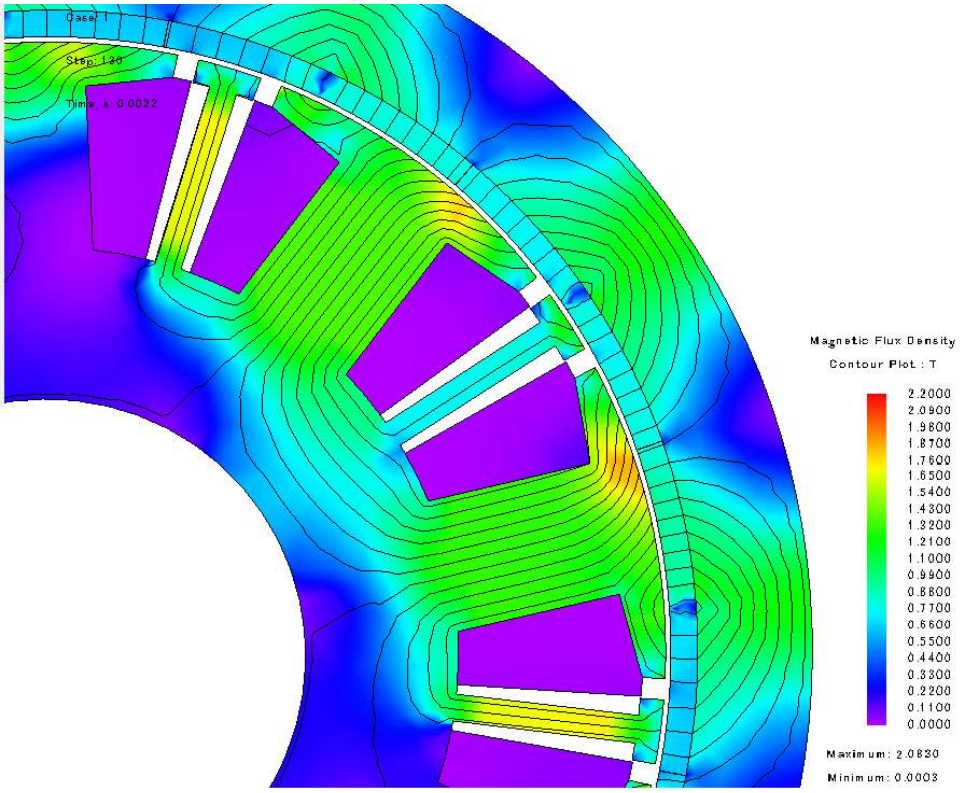

Fig. 2.10. Magnetic flux-line distribution and flux density results of FEanalysis

In order to analyze some parameters the analytical, semi-analytical and FE models were simulated for the base operating point, which corresponds to the rated speed of 490 [rpm], equivalent to a 9.3 [m/s] wind speed. To be noted that the simulations of the semi-analytical and FE models are considered dynamic in their nature (even if performed at steady state) due to the fact that they analyze the behavior of the machine during one electrical/mechanical cycle operation.

The waveforms of the back-EMF voltages are presented in *fig. 2.11* for the semi-analytical and FE models. As a note for the electromagnetic parameters presented throughout this subchapter, because the analytical model is not time dependent, the instant values obtained with this model will only be listed in *table 2.5* for comparison to the values obtained with the other two models.

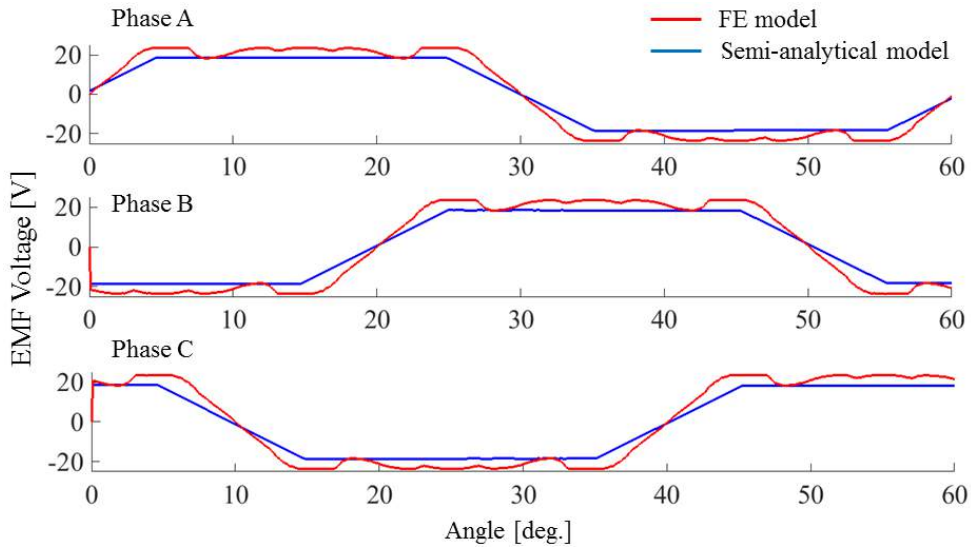

Fig. 2.11. Comparative FE-computed and semi-analytically-modeled back-EMF waveforms of the BLDCPM reference machine

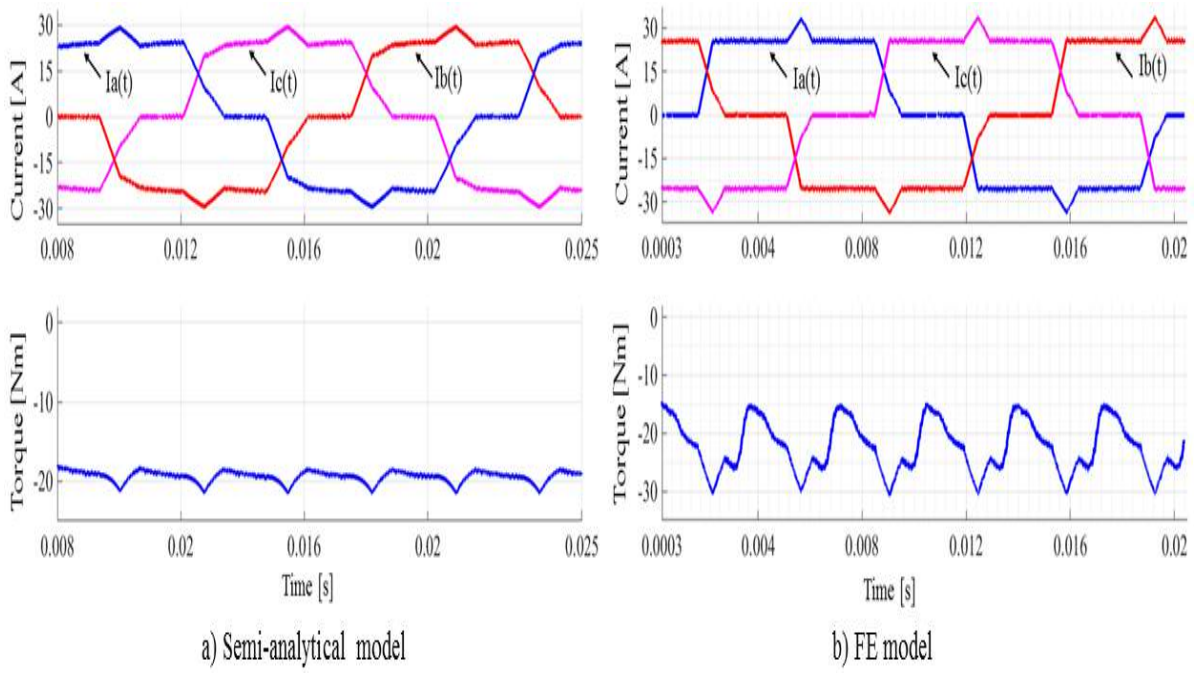

Fig. 2.12. FE-computed and semi-analytically obtained three-phase stator-current and electromagnetic torque waveforms of the BLDCPM reference machine

The stator-winding phase-current and electromagnetic torque waveforms are presented in *fig. 2.12 (a, b)*, obtained for the DC-bus voltage $V_{dc} = 60\,V$.

As it can be seen from *fig. 2.12*, a peak in the current waveforms appears if the V_{dc} voltage is less than four times the amplitude of the back-EMF, as in equation *(2.15)*. Moreover, this causes also an additional pulsation of the electromagnetic torque, proportional to the current ripple, each time the phases commute. Basically, each quantity (electromagnetic

torque and power, copper loss, rectifier conduction and switching losses) that relies on the phase currents for its calculation presents this oscillation into its waveform. How it can be remarked, the amplitude of the oscillations are smaller for the semi-analytical model compared to the FE one. This is justified by the fact that neither the cogging torque that results from the interaction of the magnet with the slotted stator nor the magnetic saturation are considered in the modeling phase of the generator. Also, because of the PI power control the response time of the system is slower, meaning that the currents and torque cannot reach their nominal values instantly as those of the FE-based model.

To better observe the differences between the models at that low DC-bus voltage simulation, an average torque error between the (i) numerical and analytical models (orange rhomb) and (ii) numerical and semi-analytical models (red circle), as well as a maximum current error obtained likewise are represented in *fig. 2.13* alongside the CPU computation time, for the base operating point.

The values for these electromagnetic parameters of the machine are also compared in *table 2.5* for the three models (analytical, semi-analytical and FE), by indicating the simulation time for each of the models as well.

Table 2.5. Results comparison between the models of the BLDCPM machine for the Vdc = 60 V

Parameter	**BLDCPM Machine models**		
	Analytical(1)	**Semi-analytical**	**Numerical**
a-Phase Back-EMF voltage e_a [V] (2)	20.38	20.39	23.71
Electromagnetic torque T_{em} [N.m] (3)	19.49	20.4	21.63
Electromagnetic torque ripple ΔT_{em} [N.m] (4)	0	3.38	15.67
a-Phase current I_a [A] (2)	24.54	29.42	33
a-Phase current overrun ΔI_a [A]	0	5.2	9
Simulation time	8e-5 [s]	3 [s]	≈ 1 [h] 30 [min]

(1) Instant value

(2) Maximum value over period operation

(3) Average value over one period operation

(4) Calculated as $\Delta T_{em} = max(T_{em}) - min(T_{em})$

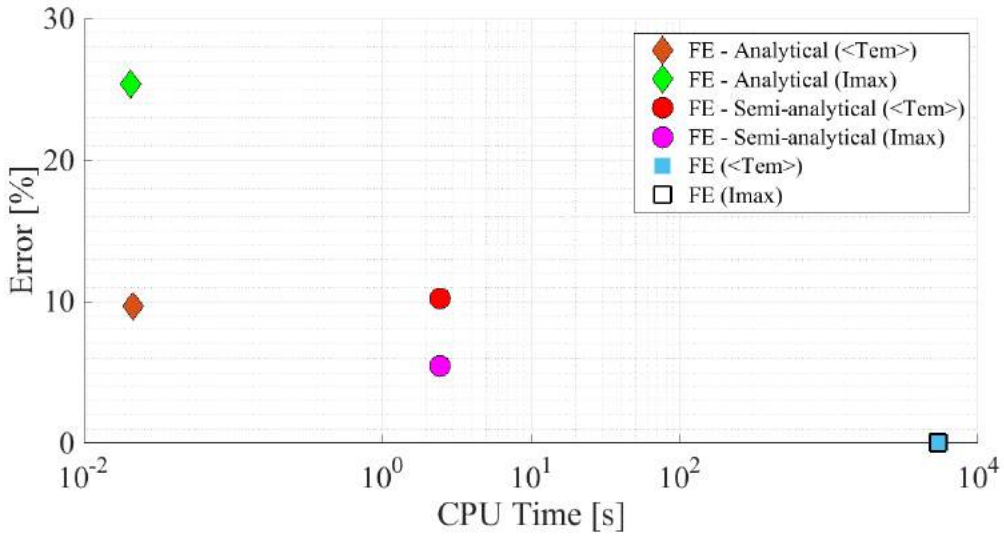

Fig. 2.13. Errors for average electromagnetic torque and maximum current in FE-based, semi-analytical, analytical models vs. CPU time in logarithmic scale

As it can be seen the CPU time necessary for one FE simulation of one operating speed is fairly high, therefore it seems more appropriate for the design optimization process to use the analytical or the semi-analytical models as they perform faster, given also the fact that during the optimization the model is going to be evaluated for hundreds or thousands of simulations. On the contrary, coupling the FE model to the optimization may be done in the final design stage when only a couple of parameters could be optimized for a refined solution that gives the best results to the desired application.

2.4 Conclusions

In this chapter the components of the μWECS have been detailed. Three simulation models for the BLDCPM generator-rectifier assembly, i.e. analytical, semi-analytical and numerical models, have been proposed and investigated. All of them rely on the sizing parameters of the machine, which can be determined based on the equations provided in *Appendix 2.A*.

To make a choice, some simulations were effected at the base operating point with the values of a reference machine, which helped to determine the accuracy and the required simulation time for each of the models. The numerical model, based on a transient magnetic field analysis by taking into account the rotor motion, the electromagnetic nonlinearities, the geometry of the machine, etc. reveals high precision, but its huge evaluation time makes it a non-viable solution for the optimization.

On the other hand, the time-dependent semi-analytical model, faster in computation time, neglects some of the electromagnetic properties of the machine, but demonstrates its ability to detect the phenomena that appears in the waveforms of several quantities during the commutation and conduction periods of the rectifier.

Lastly, the time-based characteristics of the semi-analytical model have been discharged and reshaped for faster usage, resulting into the analytical model. As this one gives only average or peak values of the electromagnetic parameters, it has the advantage of being the fastest and yet the roughest of the models.

These latter two models seem to be the appropriate solution for the optimization process and their accuracy quite acceptable, although a significant difference can be observed between them and the FE-based model, hence, a correction coefficient should be calculated and applied to the outputs of these models.

Before passing to the design optimization of the BLDCPM generator, it is necessary to search which of the above models performs faster and better when considering a long-term wind-speed profile. Since the analytical model is fast in computation time, it is assumed that it will be able to calculate the power losses over the entire wind-speed profile in a short period of time. However, as it will be seen in the next chapter, this principle does not apply for the semi-analytical model, which implies the need for analyzing several methods that can help in reducing the wind-speed profile and integrating it in the calculation procedure of the μWECS. This enquire will be done by the upcoming chapter.

Selected references

[1] G. L. Johnson, *Wind energy systems*, Electronic edition ed., 2001.

[2] A. Jaafar, B. Sareni, X. Roboam, J. Belhadj M. Belouda, "Design methodologies for sizing a battery bank devoted to a stand-alone and electronically passive wind turbine system," *Renewable and Sustainable Energy Reviews, Elsevier*, vol. 60, pp. 144-154, 2016.

[3] T. Ackermann, *Wind power in power systems*, Wiley ed., 2005.

[4] **Andreea Adriana Laczko (Zaharia)**, S. Brisset and M.M. Radulescu, "Modeling approaches to brushless DC permanent-magnet generator for use in micro-wind turbine applications," *International Conference on Electrical Machines ICEM 2016, IEEE*, 2016.

[5] J. R., & Miller, T. J. E. Hendershot, *Design of brushless permanent-magnet motors*,

Magna Physics Pub. ed., 1994.

[6] Jacek F. Gieras, *Permanent magnet motor technology, design and applications (third edition)*, Taylor and Francis Group ed., 2010.

[7] S. Brisset, Brochet P., "Analytical model for the optimal design of a brushless DC wheel motor," *COMPEL-The international journal for computation and mathematics in electrical and electronic engineering*, vol. 24, no. 3, pp. 829-848, 2005.

[8] T.-H. Kim, M. Ehsani H.-W. Lee, "Practical control for improving power density and efficiency of the BLDC generator," *IEEE transactions on power electronics*, vol. 20, no. 1, pp. 192-199, 2005.

[9] Ciprian Simon, *ANALYSIS AND CONTROL OF THE FAULT-TOLERANT OPERATION OF SMALL ELECTRONICALLY-COMMUTATED MOTORS.*: PhD Thesis, 2010.

[10] **A. A., Zaharia**, M. V., Radulescu, M. M., & Brisset, S. Laczko, "Modeling and simulation of a brushless DC permanent-magnet generator-based wind energy conversion system," *Ecological Vehicles and Renewable Energies (EVER), 2015 Tenth International Conference on (pp. 1-7). IEEE.*, 2015.

[11] JMAG - Simulation Technology for Electromechanical Design. [Online]. https://www.jmag-international.com/

[12] T. J. E., Hendershot, J. R. Miller, *Design of brushless permanent-magnet machines*, Motor Design Books, Ed., 2010.

Appendix 2.A

Sizing Model of the BLDCPM Generator

In order to describe the sizing equations of the BLDCPM generator, based on the work of [7], [12] the geometric model of the machine presented in *fig. 2.4* of *chapter 2* is taken again.

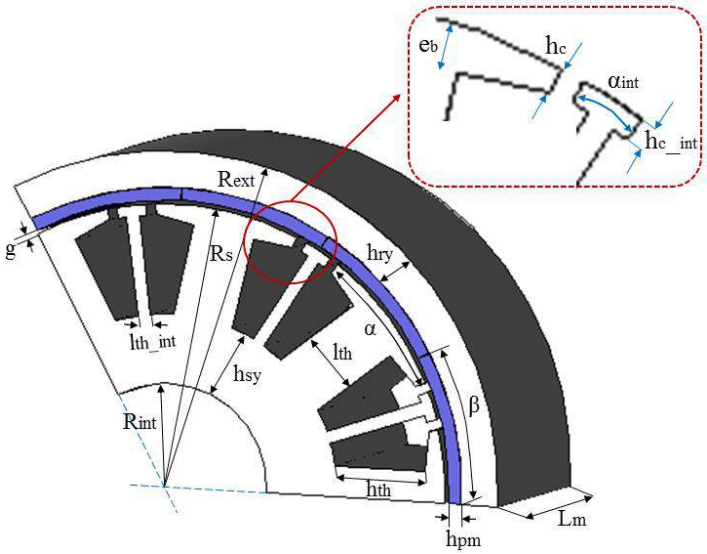

Fig. A.1 Geometric model of the BLDCPM generator

The bore radius R_s of the stator helps in resolving the several geometric relations that characterize the generator. Starting from the assumption that the flux linkage of one coil versus the rotor position presents a linear variation, the expression for the amplitude of the back-EMF has the following form [7]:

$$\hat{E}_{ph} = \frac{z}{4}\hat{B}_g 2R_s L_m \Omega \tag{A.1}$$

where

z : Total number of conductors carrying current

$\hat{B}_g$: Peak value of the magnetic flux density in the air gap [T]

L_m : Magnetic length of the machine [mm]

The amplitude of the back-EMF phase voltage can also be estimated as in *(A.2)* with the help of the DC bus voltage V_{dc} and k_v coefficient, the latter one representing the ratio between the half of the DC bus voltage and the back-EMF one at base speed operation:

$$\hat{E}_{ph} = \frac{V_{dc}}{2k_v} \tag{A.2}$$

For a generator with radial magnetic induction in the air gap and magnets, presuming a constant air gap thickness, it can be assumed that the magnetic induction in the air gap presents an ideal waveform as in *fig. A.2*. This makes possible to define the opening of the main (α) and intermediate (α_{int}) stator tooth and the width of the magnets (β) so that the flux to be maximum:

$$\alpha = \frac{\pi}{p}, \qquad \alpha_{int} = \frac{\alpha}{5}, \qquad \beta = \frac{\pi}{p} \tag{A.3}$$

with

p : Number of generator pole-pairs

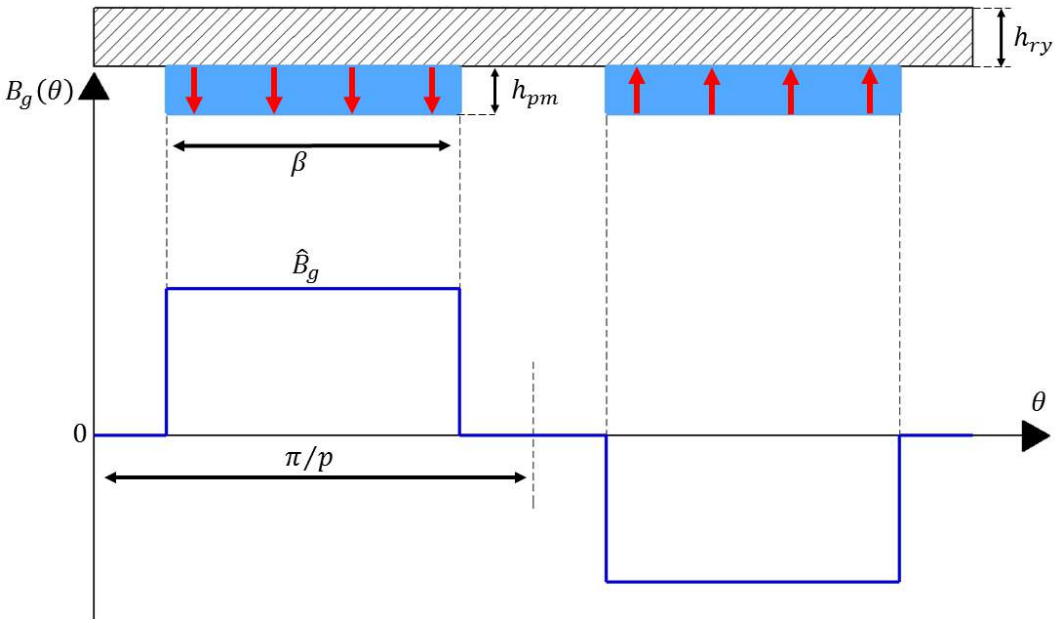

Fig. A.2 Ideal waveform of the magnetic induction in the air gap

From the above and based on the flux conservation between a magnet and the main stator tooth, the peak value of the magnetic flux density in the magnet can be calculated as:

$$\hat{B}_{pm} = \frac{\hat{B}_g \alpha R_s}{\beta (R_s + g) r_{rs} k_{lk}} \tag{A.4}$$

where

g : Air gap thickness [mm]

r_{rs} : Ratio between the length of the rotor on the one of the stator $(1 < r_{rs} \leq 1.2)$

k_{lk} : Leakage coefficient set to 0.8

Further on, the dimensions of the generator can be determined based on the following relations:

- The width of the main (l_{th}) and intermediate $\left(l_{th\_int}\right)$ stator tooth:

$$l_{th} = \frac{\hat{B}_g}{\hat{B}_{th}} \alpha R_s \tag{A.5}$$

$$l_{th\_int} = \frac{\hat{B}_g}{\hat{B}_{th}} \alpha_{int} R_s \tag{A.6}$$

with

$\hat{B}_{th}$: Amplitude of the magnetic induction in the stator tooth [T]

- The thickness of the main pole shoe:

$$e_b = \left[\frac{\hat{B}_g}{\hat{B}_{th}}\left(\frac{\alpha}{2} - \sin^{-1}\left(\frac{l_{th}}{2R_s}\right)\right)R_s\right] + R_s\left[1 - \cos\left(\sin^{-1}\left(\frac{l_{th}}{2R_s}\right)\right)\right] \tag{A.7}$$

- The number of stator slots (N_s):

$$N_s = \frac{3}{2}p \tag{A.8}$$

- The depth of the main stator tooth (h_{th}) from the slot area:

$$A_{slot} = h_{th}[2\pi(R_s - e_b) - \pi h_{th} - N_s l_{th}] \tag{A.9}$$

$$A_{slot} k_r = \frac{3}{2} z \frac{\hat{I}}{\delta} \tag{A.10}$$

with

δ: Current density in the conductors [A/mm^2]

k_r : Slot filling coefficient: set to 0.5

- The thickness of the main (h_c) and intermediate $\left(h_{c\_int}\right)$ stator pole shoes:

$$h_c = \frac{e_b}{\cos(\alpha/2)} - R_s\left(\frac{1}{\cos(\alpha/2)} - 1\right) \tag{A.11}$$

$$h_{c\_int} = R_s[1 - \cos(\alpha_{int}/2)] + h_c \cos(\alpha_{int}/2) \tag{A.12}$$

- The thickness of the stator $\left(h_{sy}\right)$ and rotor $\left(h_{ry}\right)$ yokes:

$$h_{sy} = \frac{1}{2}\frac{\hat{B}_{th}}{\hat{B}_{sy}} l_{th} \tag{A.13}$$

$$h_{ry} = \frac{1}{2}\frac{\hat{B}_{pm}}{\hat{B}_{ry}} \beta(R_s + g) \tag{A.14}$$

where

$\hat{B}_{sy}$: Peak value of the magnetic induction in the generator's stator yoke [T]

$\hat{B}_{ry}$: Amplitude of the magnetic flux density in the generator's rotor yoke [T]

$\hat{B}_{pm}$: Amplitude of the magnetic flux density in the permanent magnets [T]

- The exterior (D_{ext}) and interior (D_{int}) diameters:

$$D_{int} = 2R_s - 2\left(e_b + h_{th} + h_{sy}\right) \tag{A.15}$$

$$D_{ext} = 2R_s + 2\left(g + h_{pm} + h_{ry}\right) \tag{A.16}$$

with

h_{pm} : Thickness of the generator's permanent magnets [mm]

A simple iterative thermal model, build on the assumption that the temperature in the permanent magnets is equal to the one in the stator copper coils $\left(T_{pm} = T_{co}\right)$ helps in determining the thickness of the permanent magnet (based on a simplified equation of the Ampere's law at no-load operation) and to determine the phase resistance of the generator:

$$\frac{1}{\mu_{pm}}\left[\hat{B}_{pm} - B_r\left(1 + \alpha_{pm}T_{pm}\right)\right]h_{pm} + \hat{B}_g g = 0 \tag{A.17}$$

$$R_{ph} = \rho_{co}(1 + \alpha_{co}T_{co})\frac{z}{2}L_{ths}\frac{\delta}{\hat{I}} \tag{A.18}$$

where

μ_{pm} : Relative permeability

B_r : Remnant induction of the permanent magnets at $0^\circ C$ [T]

α_{pm}, α_{co} : Thermal coefficients of the permanent magnets and copper respectively

ρ_{co} : Copper resistivity at $0^\circ C$ [Ω·m]

An important parameter in the design stage of the generator is represented by the maximum current that the stator windings can support, above which the corresponding high value of the magnetic flux density in the magnets can cause their demagnetization and which can be obtained based on the following equality:

$$\frac{1}{\mu_0\mu_{pm}}\left[B_c - B_r\left(1 + \alpha_{pm}T_{pm}\right)\right]h_{pm} + \frac{zI_{max}}{4p} + \frac{B_c}{\mu_0}\frac{\beta}{\alpha}\left(1 + \frac{2g}{2R_s}\right)r_s k_{lk} g = 0 \tag{A.19}$$

Another electromagnetic parameter required in the simulation models is the phase inductance which can be computed from the radial flux that crosses the air gap (ψ_g) and from the fluxes in the slots (ψ_s) and in the pole shoe(ψ_{ps}):

$$L_{ph} = \frac{3}{2}\psi_g + 2(\psi_s + \psi_{ps}) \tag{A.20}$$

After the dimensional characteristics of the generator are determined, it is possible to calculate the mass of each of its components:

- The mass of the stator is composed of three parts: yoke (M_{sy}), teeth (M_{th}) and copper windings (M_{co})

$$M_{sy} = d_{sy}\pi h_{sy}\left[2(R_s - e_b - h_{th}) - h_{sy}\right]L_m \tag{A.21}$$

$$M_{th} = d_{th}N_s\left[(l_{th} + l_{th\_int})h_{th} + \left(\alpha\frac{e_b + h_c}{2} + \alpha_{int}\frac{h_{c\_int} + h_c}{2}\right)R_s\right]L_m \tag{A.22}$$

$$M_{co} = d_{co}\frac{3}{2}z\frac{\hat{I}}{\delta}L_{ths} \tag{A.23}$$

- The mass of the permanent magnets is:

$$M_{pm} = d_{pm}p\beta h_{pm}\left[h_{pm} + 2(R_s + g)\right]L_m r_{rs} \tag{A.24}$$

- The mass of the rotor can be calculated as:

$$M_{ry} = d_{ry}\pi h_{ry}\left[h_{ry} + 2(R_s + e_b + h_{pm})\right]L_m r_{rs} \tag{A.25}$$

where

d_{sy}, d_{ry} : Density of the stator and rotor yokes [kg/m^3]

d_{th} : Density of the stator teeth [kg/m^3]

d_{co} : Density of the copper [kg/m^3]

d_{pm} : Density of the permanent magnets [kg/m^3]

L_{ths} : The medium length of a half turn [mm]

Finally, the total mass of the generator results as:

$$M_{g\_tot} = M_{sy} + M_{th} + M_{co} + M_{pm} + M_{ry} \tag{A.26}$$

Appendix 2.B

VBScript for the Pre- and Post-Processing in JMAG Designer of the BLDCPM Generator

```
' JMAG-Designer Script
'Created by ZAHARIA ANDREEA 21.03.2016
Set designer = CreateObject("designer.Application.140")
Set designerstarter = CreateObject ("designerstarter.InstanceManager")
Set objFSO = CreateObject("Scripting.FileSystemObject")
Const ForReading = 1
Set objFile = objFSO.OpenTextFile("F:\ANDREEA_ASUS\DOCTORAT\MatlabJmag\BLDC_inputs.txt",
ForReading)
strContents = objFile.ReadAll
Execute strContents
'================================================
'          drawing and simulation of complete machine in 2D
'------------------------------------------------
'  Dist_coils - distance between coil and interior pole shoe (mm)
'    DistMag - distance between magnets (mm)
'    D_Shaft - shaft diameter (mm)
'   D_extStat - stator diameter
'       JugS - stator yoke height (mm)
'         wS - main stator tooth length (mm)
'         hc - main stator tooth width sole (mm)
'         hd - stator tooth height (mm)
'         Ns - no. of slots
'   arc_talpa - arc opening of the main stator pole shoe (rad)
'     alfa_i - arc opening of the intermediate stator pole shoe(rad)
'         li - intermediate stator tooth length (mm)
'         Nr - no. of magnets
'         hi - intermediate stator tooth width
'    D_intMag - magnet interior diameter (mm)
'    D_extMag - magnet exterior diameter (mm)
'     D_extR - exterior diameter of the rotor (mm)
'         Lm - magnetic length of the machine (mm)
'     turn_ph - number of turns per phase
'        Rph - phase resistance (ohm)
'      speed - machine rated speed (rpm)
'       Iref - rated current (A)
'     deltai - hysteresis band
'        Vdc - Vdc voltage (V)
'   size_part - size of mesh in machine parts
'    size_gap - size of mesh in machine air-gap
'   RadialDiv - radial divisions in mesh properties
'     CircDiv - circumferential divisions in mesh properties
'  no_paralel - number of processor to be used
' case1_steps - number of steps
'   case1_div - number of divisions in simulation
'    MaxIter - maximum no. of iterations
'================================================================
'          INPUTS - CONSTANT VARIABLES
'----------------------------------------------------------------------------------------------------------------------
---- m=3'no. of phases : arc_talpa=(2*pi)/Nr  : alfa_i=arc_talpa/5
'================================================================
'          RELATIONS NEEDED IN THE SCRIPT
'================================================================
'Stator
```

```
maxArcOpenStat = (2*pi)/Ns : R_Shaft = D_Shaft/2 : R_ShaftJug = R_Shaft+JugS : R_extStat = D_extStat/2
R_ShaftJugPol = R_ShaftJug+hd : R_extStatTalp = R_extStat-hc : ArcCoilOpen =
(maxArcOpenStat/2)*Dist_coils
LatPolMicInt1 = (li)/R_ShaftJug : h_polMic = R_extStat-R_ShaftJug-hi
'%%%%%%%%%%%%%%%%%%%%%%%%%%%%%%%%%%%%%%%%%%%%%%%%%%%%%%%%%%%%%%%%%%%%%%%%%%%%
'Magnet
maxArcOpenMag = (2*pi)/(Nr) : R_intMag = D_intMag/2 : R_extMag = D_extMag/2
ArcOpenMag = maxArcOpenMag
'%%%%%%%%%%%%%%%%%%%%%%%%%%%%%%%%%%%%%%%%%%%%%%%%%%%%%%%%%%%%%%%%%%%%%%%%%%%%
'Rotor
R_extR = D_extR/2 : ArcOpenRot = (2*pi)/(Nr)
'%%%%%%%%%%%%%%%%%%%%%%%%%%%%%%%%%%%%%%%%%%%%%%%%%%%%%%%%%%%%%%%%%%%%%%%%%%%%
'For coils and magnets set part
U_dw1=Ns+2: U_dw2=2*U_dw1 : U_up1=U_dw1+3
V_up1=Ns+1: V_up2=V_up1+5 : V_dw1=V_up1+3: V_dw2=V_dw1+V_up1
W_up1=Ns+3: W_up2=W_up1+4 : W_dw1=W_up1+Ns
Mup=Ns*3+1 : Mdw=Mup+1
'%%%%%%%%%%%%%%%%%%%%%%%%%%%%%%%%%%%%%%%%%%%%%%%%%%%%%%%%%%%%%%%%%%%%%%%%%%%%
'Starting study
study="Transient2D" : name_study="Transient_load"
'Set materials
mat_stator="50JN400" : mat_rotor="50JN400" : mat_coil="Copper" : mat_PM="Reversible/NdFeB_Br=1.0(T)"
'%%%%%%%%%%%%%%%%%%%%%%%%%%%%%%%%%%%%%%%%%%%%%%%%%%%%%%%%%%%%%%%%%%%%%%%%%%%%
'Material properties
eddy_stator=0 : lamination_stator=1 : stator_factor=98 : flag_stator=0 : saturation_stator=100
eddy_rotor=0 : lamination_rotor=1 : rotor_factor=98 : flag_rotor=0  : saturation_rotor=100
eddy_PM=0 : temp_PM=0 : pattern_PM="RadialCircular" : orientation_PMup=0 : orientation_PMdw=0
use_ironLoss=1 : calc_type_ironLoss=2
'%%%%%%%%%%%%%%%%%%%%%%%%%%%%%%%%%%%%%%%%%%%%%%%%%%%%%%%%%%%%%%%%%%%%%%%%%%%%
'Conditions
angle = 0 : axis_speed =0 :  axis_torque=0
'Iron loss condition
frequency_type=1
base_freq=((Nr/2)*speed*(pi/30))/(2*pi)
'Circuit load  %%RECTIFIER%%
on_state=1 : off_state=0
'for U-
u1=0 : u2=30*(2/Nr) : u3=u2+0.001 : u4=u2+120*(2/Nr) : u5=u4+0.001 : u6=360*(2/Nr)
'for U+
u7=0 : u8=210*(2/Nr) : u9=u8+0.001 : u10=u8+120*(2/Nr) : u11=u10+0.001 : u12=360*(2/Nr)
'for V-
v1=0 : v2=30*(2/Nr) : v3=v2+0.001 : v4=270*(2/Nr) : v5=v4+0.001 : v6=360*(2/Nr)
'for V+
v7=0 : v8=90*(2/Nr) : v9=v8+0.001 : v10=v8+120*(2/Nr) : v11=v10+0.001 : v12=360*(2/Nr)
'for W-
w1=0 : w2=150*(2/Nr) : w3=w2+0.001 : w4=w2+120*(2/Nr) : w5=w4+0.001 : w6=360*(2/Nr)
'for W+
w7=0 : w8=90*(2/Nr) : w9=w8+0.001 : w10=330*(2/Nr) : w11=w10+0.001 : w12=360*(2/Nr)
'Hysterezis
hyst_type=2 : Imax=Iref+(deltai/2) : Imin=Iref-(deltai/2)
'Study case set-up
Case1_description = "Study of an outer rotor BLDCPM generator geometry "
paralel=1 : case1_step_type=1 : case1_end_point=((60/speed)*(360/Nr))/360
'=================================================================
'                    START GEOMETRY
'=================================================================
Set app = designer
Call app.NewProject("Optimizare")
Call app.SaveAs("C:/Users/azaharia/Desktop/Deschide_Jmag/script complet/BLDC_script_draw.jproj")
Call app.LaunchGeometryEditor()
```

```
'====================================================================
'                    CREATE STATOR
'====================================================================
Set geomApp = app.CreateGeometryEditor()
Set ref1 = geomApp.GetDocument().GetAssembly().GetItem("XY_PLANE")
Set ref2 = geomApp.GetDocument().CreateReferenceFromItem(ref1)
Call geomApp.GetDocument().GetAssembly().CreateSketch(ref2)
Call geomApp.GetDocument().GetAssembly().GetItem("Sketch").OpenSketch()
Call geomApp.GetDocument().GetAssembly().GetItem("Sketch").CreateVertex(0, 0)

'Stator – shaft - circle
x_Shaft = R_Shaft*cos(maxArcOpenStat)
y_Shaft = R_Shaft*sin(maxArcOpenStat)
Call geomApp.GetDocument().GetAssembly().GetItem("Sketch").CreateArc(0, 0, R_Shaft, 0, x_Shaft, y_Shaft)
'Stator - inferior yoke - circle
Jug_anglePctInf = (wS/2)/R_ShaftJug
arcPolJug = (maxArcOpenStat-((wS)/R_ShaftJug)-LatPolMicInt1)/2
Jug_anglePctSup1 = Jug_anglePctInf+arcPolJug
x_JugInf = R_ShaftJug*cos(Jug_anglePctInf)
y_JugInf = R_ShaftJug*sin(Jug_anglePctInf)
x_JugSup = R_ShaftJug*cos(Jug_anglePctSup1)
y_JugSup = R_ShaftJug*sin(Jug_anglePctSup1)
Call geomApp.GetDocument().GetAssembly().GetItem("Sketch").CreateArc(0, 0, x_JugInf, y_JugInf,
x_JugSup, y_JugSup)
'Stator - superior yoke - circle
Jug_anglePctSup2 = Jug_anglePctInf+arcPolJug+LatPolMicInt1
Jug_anglePctSup = maxArcOpenStat-((wS/2)/R_ShaftJug)
x_JugInf1 = R_ShaftJug*cos(Jug_anglePctSup2)
y_JugInf1 = R_ShaftJug*sin(Jug_anglePctSup2)
x_JugSup1 = R_ShaftJug*cos(Jug_anglePctSup)
y_JugSup1 = R_ShaftJug*sin(Jug_anglePctSup)
Call geomApp.GetDocument().GetAssembly().GetItem("Sketch").CreateArc(0, 0, x_JugInf1, y_JugInf1,
x_JugSup1, y_JugSup1)
'Stator - inferior main pole shoe - circle
x_talp1Sup = R_extStat*cos(arc_talpa/2)
y_talp1Sup = R_extStat*sin(arc_talpa/2)
Call geomApp.GetDocument().GetAssembly().GetItem("Sketch").CreateArc(0, 0, R_extStat, 0, x_talp1Sup,
y_talp1Sup)
'Stator - superior main pole shoe - circle
ArcTalpPctInf = maxArcOpenStat-(arc_talpa/2)
x_talp2Inf = R_extStat*cos(ArcTalpPctInf)
y_talp2Inf = R_extStat*sin(ArcTalpPctInf)
x_talp2Sup = R_extStat*cos(maxArcOpenStat)
y_talp2Sup = R_extStat*sin(maxArcOpenStat)
Call geomApp.GetDocument().GetAssembly().GetItem("Sketch").CreateArc(0, 0, x_talp2Inf, y_talp2Inf,
x_talp2Sup, y_talp2Sup)
'Stator - intermediate tooth - circle
descArcTalpMic = (maxArcOpenStat-arc_talpa-alfa_i)/2
ArcTalpMic1 = (arc_talpa/2)+descArcTalpMic
ArcTalpMic2 = (arc_talpa/2)+descArcTalpMic+alfa_i
x_talp2InfPolMic = R_extStat*cos(ArcTalpMic1)
y_talp2InfPolMic = R_extStat*sin(ArcTalpMic1)
x_talp2SupPolMic = R_extStat*cos(ArcTalpMic2)
y_talp2SupPolMic = R_extStat*sin(ArcTalpMic2)
Call geomApp.GetDocument().GetAssembly().GetItem("Sketch").CreateArc(0, 0, x_talp2InfPolMic,
y_talp2InfPolMic, x_talp2SupPolMic, y_talp2SupPolMic)
'Stator - inferior pole shoe -inferior line
Call geomApp.GetDocument().GetAssembly().GetItem("Sketch").CreateLine(R_Shaft, 0, R_extStat, 0)
'Stator – inferior pole shoe – superior line
ArcTalpPol = (wS/2)/(R_ShaftJugPol)
x_TalpPol1End = R_ShaftJugPol*cos(ArcTalpPol)
```

```
y_TalpPol1End = R_ShaftJugPol*sin(ArcTalpPol)
Call geomApp.GetDocument().GetAssembly().GetItem("Sketch").CreateLine(x_JugInf, y_JugInf,
x_TalpPol1End, y_TalpPol1End)
'Stator – inferior pole – sole – superior line
x_talp1LineSup = R_extStatTalp*cos(arc_talpa/2)
y_talp1LineSup = R_extStatTalp*sin(arc_talpa/2)
Call geomApp.GetDocument().GetAssembly().GetItem("Sketch").CreateLine(x_talp1LineSup, y_talp1LineSup,
x_talp1Sup, y_talp1Sup)
'Stator – inferior pole – sole – inferior line
Call geomApp.GetDocument().GetAssembly().GetItem("Sketch").CreateLine(x_talp1LineSup, y_talp1LineSup,
x_TalpPol1End, y_TalpPol1End)
'Stator – superior pole – superior line
Call geomApp.GetDocument().GetAssembly().GetItem("Sketch").CreateLine(x_Shaft, y_Shaft, x_talp2Sup,
y_talp2Sup)
'Stator – superior pole – superior line
ArcTalpPol2 = maxArcOpenStat-((wS/2)/R_ShaftJugPol)
x_TalpPol2End = R_ShaftJugPol*cos(ArcTalpPol2)
y_TalpPol2End = R_ShaftJugPol*sin(ArcTalpPol2)
Call geomApp.GetDocument().GetAssembly().GetItem("Sketch").CreateLine(x_JugSup1, y_JugSup1,
x_TalpPol2End, y_TalpPol2End)
'Stator – superior pole – sole – inferior line
ArcTalpPctInf2 = maxArcOpenStat-(arc_talpa/2)
x_talp2InfEnd = R_extStatTalp*cos(ArcTalpPctInf2)
y_talp2InfEnd = R_extStatTalp*sin(ArcTalpPctInf2)
Call geomApp.GetDocument().GetAssembly().GetItem("Sketch").CreateLine(x_talp2Inf, y_talp2Inf,
x_talp2InfEnd, y_talp2InfEnd)
'Stator – superior pole – sole – superior line
Call geomApp.GetDocument().GetAssembly().GetItem("Sketch").CreateLine(x_TalpPol2End, y_TalpPol2End,
x_talp2InfEnd, y_talp2InfEnd)
' Stator – intermediate pole – inferior line
AcrcPolMic = (alfa_i-((li)/R_ShaftJugPol))/2
AcrcInfPolMic = ArcTalpMic1+AcrcPolMic
x_PolMicInfEnd = (R_ShaftJug+h_polMic)*cos(AcrcInfPolMic)
y_PolMicInfEnd = (R_ShaftJug+h_polMic)*sin(AcrcInfPolMic)
Call geomApp.GetDocument().GetAssembly().GetItem("Sketch").CreateLine(x_JugSup, y_JugSup,
x_PolMicInfEnd, y_PolMicInfEnd)
' Stator – intermediate pole – superior line
AcrcSupPolMic = AcrcInfPolMic+((li)/R_ShaftJugPol)
x_PolMicSupEnd = (R_ShaftJug+h_polMic)*cos(AcrcSupPolMic)
y_PolMicSupEnd = (R_ShaftJug+h_polMic)*sin(AcrcSupPolMic)
Call geomApp.GetDocument().GetAssembly().GetItem("Sketch").CreateLine(x_JugInf1, y_JugInf1,
x_PolMicSupEnd, y_PolMicSupEnd)
' Stator – intermediate pole – sole – inferior line
x_PolMicInfTalpEnd = (R_extStat-hi)*cos(ArcTalpMic1)
y_PolMicInfTalpEnd = (R_extStat-hi)*sin(ArcTalpMic1)
Call geomApp.GetDocument().GetAssembly().GetItem("Sketch").CreateLine(x_talp2InfPolMic,
y_talp2InfPolMic, x_PolMicInfTalpEnd, y_PolMicInfTalpEnd)
' Stator – intermediate pole – sole – superior line
x_PolMicSupTalpEnd = (R_extStat-hi)*cos(ArcTalpMic2)
y_PolMicSupTalpEnd = (R_extStat-hi)*sin(ArcTalpMic2)
Call geomApp.GetDocument().GetAssembly().GetItem("Sketch").CreateLine(x_talp2SupPolMic,
y_talp2SupPolMic, x_PolMicSupTalpEnd, y_PolMicSupTalpEnd)
' Stator – intermediate pole – sole- inferior line from yoke
Call geomApp.GetDocument().GetAssembly().GetItem("Sketch").CreateLine(x_PolMicInfEnd,
y_PolMicInfEnd, x_PolMicInfTalpEnd, y_PolMicInfTalpEnd)
' Stator – intermediate pole – sole – superior line from yoke
Call geomApp.GetDocument().GetAssembly().GetItem("Sketch").CreateLine(x_PolMicSupEnd,
y_PolMicSupEnd, x_PolMicSupTalpEnd, y_PolMicSupTalpEnd)
'Select rectangle
Call geomApp.View().SelectByRectangleWorldPos(-10, -10, 0, D_extStat, D_extStat, 0, 0)
'Create region
```

```
Call geomApp.GetDocument().GetAssembly().GetItem("Sketch").CreateRegions()
Call geomApp.GetDocument().GetAssembly().GetItem("Sketch").CreateRegionRadialPattern()
Call geomApp.GetDocument().GetAssembly().GetItem("Sketch").GetItem("Region Radial
Pattern").SetProperty("Merge", 1)
Set ref1 = geomApp.GetDocument().GetAssembly().GetItem("Sketch").GetItem("Vertex")
Set ref2 = geomApp.GetDocument().CreateReferenceFromItem(ref1)
Call geomApp.GetDocument().GetAssembly().GetItem("Sketch").GetItem("Region Radial
Pattern").SetPropertyByReference("Center", ref2)
ReDim refarray(0)
refarray(0) = "faceregion(TRegionItem47)"
Call geomApp.GetDocument().GetAssembly().GetItem("Sketch").GetItem("Region Radial
Pattern").SetProperty("Region", refarray)
Call geomApp.GetDocument().GetAssembly().GetItem("Sketch").GetItem("Region Radial
Pattern").SetProperty("Angle", (360/Ns))
Call geomApp.GetDocument().GetAssembly().GetItem("Sketch").GetItem("Region Radial
Pattern").SetProperty("Instance", Ns)
Call geomApp.GetDocument().GetAssembly().GetItem("Sketch").SetProperty("Name", "Stator core")
Call geomApp.GetDocument().GetAssembly().GetItem("Stator core").SetProperty("Color", "darkgreen")
Call geomApp.GetDocument().GetAssembly().GetItem("Stator core").CloseSketch()
'=====================================================================
'                    END STATOR
'=====================================================================
'=====================================================================
'                    CREATE COILS
'=====================================================================
Set geomApp = app.CreateGeometryEditor()
Set ref1 = geomApp.GetDocument().GetAssembly().GetItem("XY_PLANE")
Set ref2 = geomApp.GetDocument().CreateReferenceFromItem(ref1)
Call geomApp.GetDocument().GetAssembly().CreateSketch(ref2)
Call geomApp.GetDocument().GetAssembly().GetItem("Sketch.2").OpenSketch()
Call geomApp.GetDocument().GetAssembly().GetItem("Sketch.2").CreateVertex(0, 0)
'Coil 1 – yoke - circle
x_coil1End = R_ShaftJug*cos(ArcCoilOpen)
y_coil1End = R_ShaftJug*sin(ArcCoilOpen)
Call geomApp.GetDocument().GetAssembly().GetItem("Sketch.2").CreateArc(0, 0, x_JugInf, y_JugInf,
x_coil1End, y_coil1End)
'Coil 2 – yoke - circle
Arc_coil2End = ArcCoilOpen+(maxArcOpenStat-ArcCoilOpen*2)
x_coil2End = R_ShaftJug*cos(Arc_coil2End)
y_coil2End = R_ShaftJug*sin(Arc_coil2End)
Call geomApp.GetDocument().GetAssembly().GetItem("Sketch.2").CreateArc(0, 0, x_coil2End, y_coil2End,
x_JugSup1, y_JugSup1)
'Coil 1 – inferior line
Call geomApp.GetDocument().GetAssembly().GetItem("Sketch.2").CreateLine(x_JugInf, y_JugInf,
x_TalpPol1End, y_TalpPol1End)
'Coil 1 – superior line
x_coil1LineSup = R_extStatTalp*cos(ArcCoilOpen)
y_coil1LineSup = R_extStatTalp*sin(ArcCoilOpen)
Call geomApp.GetDocument().GetAssembly().GetItem("Sketch.2").CreateLine(x_coil1End, y_coil1End,
x_coil1LineSup, y_coil1LineSup)
'Coil 1 – sole – inferior line
Call geomApp.GetDocument().GetAssembly().GetItem("Sketch.2").CreateLine(x_talp1LineSup,
y_talp1LineSup, x_TalpPol1End, y_TalpPol1End)
'Coil 1 – sole – superior line
Call geomApp.GetDocument().GetAssembly().GetItem("Sketch.2").CreateLine(x_talp1LineSup,
y_talp1LineSup, x_coil1LineSup, y_coil1LineSup)
'Coil 2 – superior line
Call geomApp.GetDocument().GetAssembly().GetItem("Sketch.2").CreateLine(x_JugSup1, y_JugSup1,
x_TalpPol2End, y_TalpPol2End)
'Coil 2 – inferior line
x_coil2LineInf = R_extStatTalp*cos(Arc_coil2End)
```

```
y_coil2LineInf = R_extStatTalp*sin(Arc_coil2End)
Call geomApp.GetDocument().GetAssembly().GetItem("Sketch.2").CreateLine(x_coil2End, y_coil2End,
x_coil2LineInf, y_coil2LineInf)
'Coil 2 – sole – superior line
Call geomApp.GetDocument().GetAssembly().GetItem("Sketch.2").CreateLine(x_TalpPol2End,
y_TalpPol2End, x_talp2InfEnd, y_talp2InfEnd)
'Coil 2 – sole – inferior line
Call geomApp.GetDocument().GetAssembly().GetItem("Sketch.2").CreateLine(x_coil2LineInf, y_coil2LineInf,
x_talp2InfEnd, y_talp2InfEnd)
'Select rectangle
Call geomApp.View().SelectByRectangleWorldPos(-10, -10, 0, D_extStat, D_extStat, 0, 0)
'Create region
Call geomApp.GetDocument().GetAssembly().GetItem("Sketch.2").CreateRegions()
Call geomApp.GetDocument().GetAssembly().GetItem("Sketch.2").CreateRegionRadialPattern()
Set ref1 = geomApp.GetDocument().GetAssembly().GetItem("Sketch.2").GetItem("Vertex")
Set ref2 = geomApp.GetDocument().CreateReferenceFromItem(ref1)
Call geomApp.GetDocument().GetAssembly().GetItem("Sketch.2").GetItem("Region Radial
Pattern").SetPropertyByReference("Center", ref2)
ReDim refarray(1)
refarray(0) = "faceregion(TRegionItem71)"
refarray(1) = "faceregion(TRegionItem72)"
Call geomApp.GetDocument().GetAssembly().GetItem("Sketch.2").GetItem("Region Radial
Pattern").SetProperty("Region", refarray)
Call geomApp.GetDocument().GetAssembly().GetItem("Sketch.2").GetItem("Region Radial
Pattern").SetProperty("Angle", (360/Ns))
Call geomApp.GetDocument().GetAssembly().GetItem("Sketch.2").GetItem("Region Radial
Pattern").SetProperty("Instance", Ns)
Call geomApp.GetDocument().GetAssembly().GetItem("Sketch.2").SetProperty("Name", "Coil")
Call geomApp.GetDocument().GetAssembly().GetItem("Coil").SetProperty("Color", "gray")
Call geomApp.GetDocument().GetAssembly().GetItem("Coil").CloseSketch()
'====================================================================
'                    END COIL
'====================================================================
'====================================================================
'                    CREATE MAGNET
'====================================================================
Set geomApp = app.CreateGeometryEditor()
Set ref1 = geomApp.GetDocument().GetAssembly().GetItem("XY_PLANE")
Set ref2 = geomApp.GetDocument().CreateReferenceFromItem(ref1)
Call geomApp.GetDocument().GetAssembly().CreateSketch(ref2)
Call geomApp.GetDocument().GetAssembly().GetItem("Sketch.3").OpenSketch()
Call geomApp.GetDocument().GetAssembly().GetItem("Sketch.3").CreateVertex(0, 0)
'Magnet 1 – interior circle
distMag1Int = (DistMag/2)/R_intMag 'unghiul in rad de despartire
ArcOpenMag1Int = ArcOpenMag-distMag1Int
x_Mag1Int = R_intMag*cos(ArcOpenMag1Int)
y_Mag1Int = R_intMag*sin(ArcOpenMag1Int)
Call geomApp.GetDocument().GetAssembly().GetItem("Sketch.3").CreateArc(0, 0, R_intMag, 0, x_Mag1Int,
y_Mag1Int)
'Magnet 1 – exterior circle
distMag1Ext = (DistMag/2)/R_extMag 'unghiul in rad de despartire
ArcOpenMag1Ext = ArcOpenMag-distMag1Ext
x_Mag1Ext = R_extMag*cos(ArcOpenMag1Ext)
y_Mag1Ext = R_extMag*sin(ArcOpenMag1Ext)
Call geomApp.GetDocument().GetAssembly().GetItem("Sketch.3").CreateArc(0, 0, R_extMag, 0, x_Mag1Ext,
y_Mag1Ext)
'Magnet 1 – inferior line
Call geomApp.GetDocument().GetAssembly().GetItem("Sketch.3").CreateLine(R_intMag, 0, R_extMag, 0)
'Magnet 1 – superior line
Call geomApp.GetDocument().GetAssembly().GetItem("Sketch.3").CreateLine(x_Mag1Int, y_Mag1Int,
x_Mag1Ext, y_Mag1Ext)
```

```
'Select rectangle
Call geomApp.View().SelectByRectangleWorldPos(-10, -10, 0, D_extMag, D_extMag, 0, 0)
'Create region
Call geomApp.GetDocument().GetAssembly().GetItem("Sketch.3").CreateRegions()
Call geomApp.GetDocument().GetAssembly().GetItem("Sketch.3").CreateRegionRadialPattern()
Set ref1 = geomApp.GetDocument().GetAssembly().GetItem("Sketch.3").GetItem("Vertex")
Set ref2 = geomApp.GetDocument().CreateReferenceFromItem(ref1)
Call geomApp.GetDocument().GetAssembly().GetItem("Sketch.3").GetItem("Region Radial
Pattern").SetPropertyByReference("Center", ref2)
ReDim refarray(0)
refarray(0) = "faceregion(TRegionItem84)"
Call geomApp.GetDocument().GetAssembly().GetItem("Sketch.3").GetItem("Region Radial
Pattern").SetProperty("Region", refarray)
Call geomApp.GetDocument().GetAssembly().GetItem("Sketch.3").GetItem("Region Radial
Pattern").SetProperty("Angle", (360/Nr))
Call geomApp.GetDocument().GetAssembly().GetItem("Sketch.3").GetItem("Region Radial
Pattern").SetProperty("Instance", Nr)
' End sketch and change name and color
Call geomApp.GetDocument().GetAssembly().GetItem("Sketch.3").SetProperty("Name", "Magnet")
Call geomApp.GetDocument().GetAssembly().GetItem("Magnet").SetProperty("Color", "cyan")
Call geomApp.GetDocument().GetAssembly().GetItem("Magnet").CloseSketch()
'======================================================================
'                        END MAGNET
'======================================================================
'======================================================================
'                        CREATE ROTOR
'======================================================================
Set geomApp = app.CreateGeometryEditor()
Set ref1 = geomApp.GetDocument().GetAssembly().GetItem("XY_PLANE")
Set ref2 = geomApp.GetDocument().CreateReferenceFromItem(ref1)
Call geomApp.GetDocument().GetAssembly().CreateSketch(ref2)
Call geomApp.GetDocument().GetAssembly().GetItem("Sketch.4").OpenSketch()
Call geomApp.GetDocument().GetAssembly().GetItem("Sketch.4").CreateVertex(0, 0)
'Rotor – interior circle
x_RotInt = R_extMag*cos(ArcOpenRot)
y_RotInt = R_extMag*sin(ArcOpenRot)
Call geomApp.GetDocument().GetAssembly().GetItem("Sketch.4").CreateArc(0, 0, R_extMag, 0, x_RotInt,
y_RotInt)
'Rotor – exterior circle
x_RotExt = R_extR*cos(ArcOpenRot)
y_RotExt = R_extR*sin(ArcOpenRot)
Call geomApp.GetDocument().GetAssembly().GetItem("Sketch.4").CreateArc(0, 0, R_extR, 0, x_RotExt,
y_RotExt)
'Rotor – inferior line
Call geomApp.GetDocument().GetAssembly().GetItem("Sketch.4").CreateLine(R_extMag, 0, R_extR, 0)
'Rotor – superior line
Call geomApp.GetDocument().GetAssembly().GetItem("Sketch.4").CreateLine(x_RotInt, y_RotInt, x_RotExt,
y_RotExt)
'Select rectangle
Call geomApp.View().SelectByRectangleWorldPos(-10, -10, 0, D_extR, D_extR, 0, 0)
'Create region
Call geomApp.GetDocument().GetAssembly().GetItem("Sketch.4").CreateRegions()
Call geomApp.GetDocument().GetAssembly().GetItem("Sketch.4").CreateRegionRadialPattern()
Call geomApp.GetDocument().GetAssembly().GetItem("Sketch.4").GetItem("Region Radial
Pattern").SetProperty("Merge", 1)
Set ref1 = geomApp.GetDocument().GetAssembly().GetItem("Sketch.4").GetItem("Vertex")
Set ref2 = geomApp.GetDocument().CreateReferenceFromItem(ref1)
Call geomApp.GetDocument().GetAssembly().GetItem("Sketch.4").GetItem("Region Radial
Pattern").SetPropertyByReference("Center", ref2)
ReDim refarray(0)
refarray(0) = "faceregion(TRegionItem96)"
```

```
Call geomApp.GetDocument().GetAssembly().GetItem("Sketch.4").GetItem("Region Radial
Pattern").SetProperty("Region", refarray)
Call geomApp.GetDocument().GetAssembly().GetItem("Sketch.4").GetItem("Region Radial
Pattern").SetProperty("Angle", (360/Nr))
Call geomApp.GetDocument().GetAssembly().GetItem("Sketch.4").GetItem("Region Radial
Pattern").SetProperty("Instance", Nr)
' End sketch and change name and color
Call geomApp.GetDocument().GetAssembly().GetItem("Sketch.4").SetProperty("Name", "Rotor core")
Call geomApp.GetDocument().GetAssembly().GetItem("Rotor core").SetProperty("Color", "blue")
Call geomApp.GetDocument().GetAssembly().GetItem("Rotor core").CloseSketch()
'=====================================================================
'                       END ROTOR
'=====================================================================
'=====================================================================
'                       IMPORT GEOMETRY
'=====================================================================
'Import geometry
Call app.ImportDataFromGeometryEditor()
Call geomApp.GetDocument().SaveModeL(0)
Call geomApp.Quit()
'=====================================================================
'                       ADD PART NAME
'=====================================================================
Set app = designer
Call app.GetModel(0).SetName("BLDC_script_draw")
'=====================================================================
'                       SET COILS
'=====================================================================
'Dim i
For i = 1 to (((2*Ns)/3)+2)
  If i <= (((2*Ns)/3)+2-(Ns/3)) Then
    Do
      Select Case i
        Case 1,2
          If i = 2 Then
            Call app.GetModel(0).SetPartName("Coil", "Coil U Dw")
          Else
            Call app.GetModel(0).SetPartName("Coil", "Coil V Up")
          End If
        Case Else
          Call app.GetModel(0).SetPartName("Coil", "Coil W Up")
          Call app.GetModel(0).SetPartName("Coil", "Coil U Up")
          If i = (((2*Ns)/3)+2-(Ns/3)) Then
            Exit Do
          Else
            Call app.GetModel(0).SetPartName("Coil", "Coil V Up")
          End If
      End Select
    Exit Do
  Loop
  Else
    Call app.GetModel(0).SetPartName("Coil", "Coil V Dw")
    Call app.GetModel(0).SetPartName("Coil", "Coil W Dw")
    If i < (((2*Ns)/3)+2) Then
      Call app.GetModel(0).SetPartName("Coil", "Coil U Dw")
    End If
  End If
Next
'=====================================================================
Call app.GetModel(0).GetGroupList().CreateGroup("Coil U Dw")
For i = 1 to Ns/3
```

```
  Select Case i
  Case 1
    Call app.GetModel(0).GetGroupList().AddPartToGroup("Coil U Dw",U_dw1)
  Case Else
    Call app.GetModel(0).GetGroupList().AddPartToGroup("Coil U Dw",U_dw2)
    U_dw2=U_dw2+3
  End Select
Next
Call app.GetModel(0).GetGroupList().CreateGroup("Coil U Up")
For i = 1 to Ns/3
  Call app.GetModel(0).GetGroupList().AddPartToGroup("Coil U Up",U_up1)
  U_up1=U_up1+3
Next
Call app.GetModel(0).GetGroupList().CreateGroup("Coil V Up")
For i = 1 to Ns/3
  Select Case i
  Case 1
    Call app.GetModel(0).GetGroupList().AddPartToGroup("Coil V Up",V_up1)
  Case Else
    Call app.GetModel(0).GetGroupList().AddPartToGroup("Coil V Up",V_up2)
    V_up2=V_up2+3
  End Select
Next
Call app.GetModel(0).GetGroupList().CreateGroup("Coil V Dw")
For i = 1 to Ns/3
  Select Case i
  Case 1
    Call app.GetModel(0).GetGroupList().AddPartToGroup("Coil V Dw",V_dw1)
  Case Else
    Call app.GetModel(0).GetGroupList().AddPartToGroup("Coil V Dw",V_dw2)
    V_dw2=V_dw2+3
  End Select
Next
Call app.GetModel(0).GetGroupList().CreateGroup("Coil W Up")
For i = 1 to Ns/3
  Select Case i
  Case 1
    Call app.GetModel(0).GetGroupList().AddPartToGroup("Coil W Up",W_up1)
  Case Else
    Call app.GetModel(0).GetGroupList().AddPartToGroup("Coil W Up",W_up2)
    W_up2=W_up2+3
  End Select
Next
Call app.GetModel(0).GetGroupList().CreateGroup("Coil W Dw")
For i = 1 to Ns/3
  Call app.GetModel(0).GetGroupList().AddPartToGroup("Coil W Dw",W_dw1)
  W_dw1=W_dw1+3
Next
'=================================================================
'                    SET MAGNETS
'=================================================================
For i = 1 to Nr
  If (i mod 2 = 0) Then
    Call app.GetModel(0).SetPartName("Magnet", "Magnet Dw")
  Else
    Call app.GetModel(0).SetPartName("Magnet", "Magnet Up")
  End If
Next
'=================================================================
Call app.GetModel(0).GetGroupList().CreateGroup("Magnet Up")
For i = 1 to Nr/2
```

```
  Call app.GetModel(0).GetGroupList().AddPartToGroup("Magnet Up",Mup)
  Mup=Mup+2
Next
Call app.GetModel(0).GetGroupList().CreateGroup("Magnet Dw")
For i = 1 to Nr/2
  Call app.GetModel(0).GetGroupList().AddPartToGroup("Magnet Dw",Mdw)
  Mdw=Mdw+2
Next

'========================================================================
'                        SELECT STUDY
'========================================================================
Call app.GetModel(0).CreateStudy(study, name_study)
Call app.SetCurrentStudy(0)
'========================================================================
'                        SET MATERIALS
'========================================================================
'STATOR
Call app.GetModel(0).GetStudy(0).SetMaterialByName("Stator core", mat_stator)
Call app.GetModel(0).GetStudy(0).GetMaterial("Stator core").SetValue("EddyCurrent", eddy_stator)
Call app.GetModel(0).GetStudy(0).GetMaterial("Stator core").SetValue("Laminated", lamination_stator)
Call app.GetModel(0).GetStudy(0).GetMaterial("Stator core").SetValue("LaminationFactor", stator_factor)
Call app.GetModel(0).GetStudy(0).GetMaterial("Stator core").SetValue("SetInsulationFlag", flag_stator)
Call app.GetModel(0).GetStudy(0).GetMaterial("Stator core").SetValue("MagnetizationCorrection",
saturation_stator)
Call app.GetModel(0).GetStudy(0).GetMaterial("Rotor core").SetValue("UseIronLoss", use_ironLoss)
Call app.GetModel(0).GetStudy(0).GetMaterial("Rotor core").SetValue("CalcType", calc_type_ironLoss)
Call app.GetModel(0).GetStudy(0).GetMaterial("Rotor core").SetDirectionXYZ(1, 0, 0)
Call app.GetModel(0).GetStudy(0).GetMaterial("Rotor core").SetOriginXYZ(0, 0, 0)
'ROTOR
Call app.GetModel(0).GetStudy(0).SetMaterialByName("Rotor core", mat_rotor)
Call app.GetModel(0).GetStudy(0).GetMaterial("Rotor core").SetValue("EddyCurrent", eddy_rotor)
Call app.GetModel(0).GetStudy(0).GetMaterial("Rotor core").SetValue("Laminated", lamination_rotor)
Call app.GetModel(0).GetStudy(0).GetMaterial("Rotor core").SetValue("LaminationFactor", rotor_factor)
Call app.GetModel(0).GetStudy(0).GetMaterial("Rotor core").SetValue("SetInsulationFlag", flag_rotor)
Call app.GetModel(0).GetStudy(0).GetMaterial("Rotor core").SetValue("MagnetizationCorrection",
saturation_rotor)
Call app.GetModel(0).GetStudy(0).GetMaterial("Rotor core").SetValue("UseIronLoss", use_ironLoss)
Call app.GetModel(0).GetStudy(0).GetMaterial("Rotor core").SetValue("CalcType", calc_type_ironLoss)
Call app.GetModel(0).GetStudy(0).GetMaterial("Rotor core").SetDirectionXYZ(1, 0, 0)
Call app.GetModel(0).GetStudy(0).GetMaterial("Rotor core").SetOriginXYZ(0, 0, 0)
'MAGNET
Call app.GetModel(0).GetStudy(0).SetMaterialByName("Magnet Up", mat_PM)
Call app.GetModel(0).GetStudy(0).GetMaterial("Magnet Up").SetValue("EddyCurrent", eddy_PM)
Call app.GetModel(0).GetStudy(0).GetMaterial("Magnet Up").SetValue("TemperatureType", temp_PM)
Call app.GetModel(0).GetStudy(0).GetMaterial("Magnet Up").SetDirectionXYZ(1, 0, 0)
Call app.GetModel(0).GetStudy(0).GetMaterial("Magnet Up").SetOrientation(orientation_PMup)
Call app.GetModel(0).GetStudy(0).GetMaterial("Magnet Up").SetOriginXYZ(0, 0, 0)
Call app.GetModel(0).GetStudy(0).GetMaterial("Magnet Up").SetPattern(pattern_PM)
Call app.GetModel(0).GetStudy(0).GetMaterial("Magnet Up").SetValue("Poles", Nr)
Call app.GetModel(0).GetStudy(0).SetMaterialByName("Magnet Dw", mat_PM)
Call app.GetModel(0).GetStudy(0).GetMaterial("Magnet Dw").SetValue("EddyCurrent", eddy_PM)
Call app.GetModel(0).GetStudy(0).GetMaterial("Magnet Dw").SetValue("TemperatureType", temp_PM)
Call app.GetModel(0).GetStudy(0).GetMaterial("Magnet Dw").SetDirectionXYZ(1, 0, 0)
Call app.GetModel(0).GetStudy(0).GetMaterial("Magnet Dw").SetOrientation(orientation_PMdw)
Call app.GetModel(0).GetStudy(0).GetMaterial("Magnet Dw").SetOriginXYZ(0, 0, 0)
Call app.GetModel(0).GetStudy(0).GetMaterial("Magnet Dw").SetPattern(pattern_PM)
Call app.GetModel(0).GetStudy(0).GetMaterial("Magnet Dw").SetValue("Poles", Nr)
'COILS
Call app.GetModel(0).GetStudy(0).SetMaterialByName("Coil U Up", mat_coil)
Call app.GetModel(0).GetStudy(0).SetMaterialByName("Coil U Dw", mat_coil)
```

```
Call app.GetModel(0).GetStudy(0).SetMaterialByName("Coil V Up", mat_coil)
Call app.GetModel(0).GetStudy(0).SetMaterialByName("Coil V Dw", mat_coil)
Call app.GetModel(0).GetStudy(0).SetMaterialByName("Coil W Up", mat_coil)
Call app.GetModel(0).GetStudy(0).SetMaterialByName("Coil W Dw", mat_coil)
'========================================================================
'                        SET CONDITIONS
'========================================================================
'Load circuit
Call app.GetModel(0).GetStudy(0).CreateCircuit()
Call
app.GetModel(0).GetStudy(0).LoadCircuit("F:\ANDREEA_ASUS\DOCTORAT\MatlabJmag\circuit\circuit_loa
d_
voltage.jcir")
Call app.SetCurrentStudy(0)
Call app.GetModel(0).GetStudy(0).GetCircuit().GetComponent("Uphase").SetValue("Turn", turn_ph)
Call app.GetModel(0).GetStudy(0).GetCircuit().GetComponent("Uphase").SetValue("Resistance", Rph)
Call app.GetModel(0).GetStudy(0).GetCircuit().GetComponent("Uphase").SetValue("LeakageInductance", 0)
Call app.GetModel(0).GetStudy(0).GetCircuit().GetComponent("Vphase").SetValue("Turn", turn_ph)
Call app.GetModel(0).GetStudy(0).GetCircuit().GetComponent("Vphase").SetValue("Resistance", Rph)
Call app.GetModel(0).GetStudy(0).GetCircuit().GetComponent("Vphase").SetValue("LeakageInductance", 0)
Call app.GetModel(0).GetStudy(0).GetCircuit().GetComponent("Wphase").SetValue("Turn", turn_ph)
Call app.GetModel(0).GetStudy(0).GetCircuit().GetComponent("Wphase").SetValue("Resistance", Rph)
Call app.GetModel(0).GetStudy(0).GetCircuit().GetComponent("Wphase").SetValue("LeakageInductance", 0)
'Set commutation sequence for:
'Switch U-
Call app.GetDataManager().GetDataSet(2).SetName("Switch_U-")
ReDim refarray(5,1)
refarray(0,0) = u1
refarray(0,1) = off_state
refarray(1,0) = u2
refarray(1,1) = off_state
refarray(2,0) = u3
refarray(2,1) = on_state
refarray(3,0) = u4
refarray(3,1) = on_state
refarray(4,0) = u5
refarray(4,1) = off_state
refarray(5,0) = u6
refarray(5,1) = off_state
Call app.GetDataManager().GetDataSet("Switch_U-").SetTable(refarray)
Call app.GetModel(0).GetStudy(0).GetCircuit().GetComponent("U-CurrentLimit").SetValue("XType", 13)
Call app.GetModel(0).GetStudy(0).GetCircuit().GetComponent("U-CurrentLimit").SetValue("Period", 0)
Call app.GetModel(0).GetStudy(0).GetCircuit().GetComponent("U-CurrentLimit").SetValue("t1", 0)
Call app.GetModel(0).GetStudy(0).GetCircuit().GetComponent("U-CurrentLimit").SetValue("t2", 0)
Call app.GetModel(0).GetStudy(0).GetCircuit().GetComponent("U-CurrentLimit").SetValue("CurrentMax",
hyst_type)
Call app.GetModel(0).GetStudy(0).GetCircuit().GetComponent("U-CurrentLimit").SetValue("CurrentMax",
Imax)
Call app.GetModel(0).GetStudy(0).GetCircuit().GetComponent("U-CurrentLimit").SetValue("CurrentMin",
hyst_type)
Call app.GetModel(0).GetStudy(0).GetCircuit().GetComponent("U-CurrentLimit").SetValue("CurrentMin",
Imin)
'Switch U+
Call app.GetDataManager().GetDataSet(10).SetName("Switch_U+")
ReDim refarray(5,1)
refarray(0,0) = u7
refarray(0,1) = off_state
refarray(1,0) = u8
refarray(1,1) = off_state
refarray(2,0) = u9
refarray(2,1) = on_state
```

```
refarray(3,0) = u10
refarray(3,1) = on_state
refarray(4,0) = u11
refarray(4,1) = off_state
refarray(5,0) = u12
refarray(5,1) = off_state
Call app.GetDataManager().GetDataSet("Switch_U+").SetTable(refarray)
Call app.GetModel(0).GetStudy(0).GetCircuit().GetComponent("U+CurrentLimit").SetValue("XType", 13)
Call app.GetModel(0).GetStudy(0).GetCircuit().GetComponent("U+CurrentLimit").SetValue("Period", 0)
Call app.GetModel(0).GetStudy(0).GetCircuit().GetComponent("U+CurrentLimit").SetValue("t1", 0)
Call app.GetModel(0).GetStudy(0).GetCircuit().GetComponent("U+CurrentLimit").SetValue("t2", 0)
Call app.GetModel(0).GetStudy(0).GetCircuit().GetComponent("U+CurrentLimit").SetValue("CurrentMax",
hyst_type)
Call app.GetModel(0).GetStudy(0).GetCircuit().GetComponent("U+CurrentLimit").SetValue("CurrentMax",
Imax)
Call app.GetModel(0).GetStudy(0).GetCircuit().GetComponent("U+CurrentLimit").SetValue("CurrentMin",
hyst_type)
Call app.GetModel(0).GetStudy(0).GetCircuit().GetComponent("U+CurrentLimit").SetValue("CurrentMin",
Imin)
'Switch V-
Call app.GetDataManager().GetDataSet(4).SetName("Switch_V-")
ReDim refarray(5,1)
refarray(0,0) = v1
refarray(0,1) = on_state
refarray(1,0) = v2
refarray(1,1) = on_state
refarray(2,0) = v3
refarray(2,1) = off_state
refarray(3,0) = v4
refarray(3,1) = off_state
refarray(4,0) = v5
refarray(4,1) = on_state
refarray(5,0) = v6
refarray(5,1) = on_state
Call app.GetDataManager().GetDataSet("Switch_V-").SetTable(refarray)
Call app.GetModel(0).GetStudy(0).GetCircuit().GetComponent("V-CurrentLimit").SetValue("XType", 13)
Call app.GetModel(0).GetStudy(0).GetCircuit().GetComponent("V-CurrentLimit").SetValue("Period", 0)
Call app.GetModel(0).GetStudy(0).GetCircuit().GetComponent("V-CurrentLimit").SetValue("t1", 0)
Call app.GetModel(0).GetStudy(0).GetCircuit().GetComponent("V-CurrentLimit").SetValue("t2", 0)
Call app.GetModel(0).GetStudy(0).GetCircuit().GetComponent("V-CurrentLimit").SetValue("CurrentMax",
hyst_type)
Call app.GetModel(0).GetStudy(0).GetCircuit().GetComponent("V-CurrentLimit").SetValue("CurrentMax",
Imax)
Call app.GetModel(0).GetStudy(0).GetCircuit().GetComponent("V-CurrentLimit").SetValue("CurrentMin",
hyst_type)
Call app.GetModel(0).GetStudy(0).GetCircuit().GetComponent("V-CurrentLimit").SetValue("CurrentMin",
Imin)
'Switch V+
Call app.GetDataManager().GetDataSet(8).SetName("Switch_V+")
ReDim refarray(5,1)
refarray(0,0) = v7
refarray(0,1) = off_state
refarray(1,0) = v8
refarray(1,1) = off_state
refarray(2,0) = v9
refarray(2,1) = on_state
refarray(3,0) = v10
refarray(3,1) = on_state
refarray(4,0) = v11
refarray(4,1) = off_state
refarray(5,0) = v12
```

```
refarray(5,1) = off_state
Call app.GetDataManager().GetDataSet("Switch_V+").SetTable(refarray)
Call app.GetModel(0).GetStudy(0).GetCircuit().GetComponent("V+CurrentLimit").SetValue("XType", 13)
Call app.GetModel(0).GetStudy(0).GetCircuit().GetComponent("V+CurrentLimit").SetValue("Period", 0)
Call app.GetModel(0).GetStudy(0).GetCircuit().GetComponent("V+CurrentLimit").SetValue("t1", 0)
Call app.GetModel(0).GetStudy(0).GetCircuit().GetComponent("V+CurrentLimit").SetValue("t2", 0)
Call app.GetModel(0).GetStudy(0).GetCircuit().GetComponent("V+CurrentLimit").SetValue("CurrentMax",
hyst_type)
Call app.GetModel(0).GetStudy(0).GetCircuit().GetComponent("V+CurrentLimit").SetValue("CurrentMax",
Imax)
Call app.GetModel(0).GetStudy(0).GetCircuit().GetComponent("V+CurrentLimit").SetValue("CurrentMin",
hyst_type)
Call app.GetModel(0).GetStudy(0).GetCircuit().GetComponent("V+CurrentLimit").SetValue("CurrentMin",
Imin)
'Switch W-
Call app.GetDataManager().GetDataSet(5).SetName("Switch_W-")
ReDim refarray(5,1)
refarray(0,0) = w1
refarray(0,1) = off_state
refarray(1,0) = w2
refarray(1,1) = off_state
refarray(2,0) = w3
refarray(2,1) = on_state
refarray(3,0) = w4
refarray(3,1) = on_state
refarray(4,0) = w5
refarray(4,1) = off_state
refarray(5,0) = w6
refarray(5,1) = off_state
Call app.GetDataManager().GetDataSet("Switch_W-").SetTable(refarray)
Call app.GetModel(0).GetStudy(0).GetCircuit().GetComponent("W-CurrentLimit").SetValue("XType", 13)
Call app.GetModel(0).GetStudy(0).GetCircuit().GetComponent("W-CurrentLimit").SetValue("Period", 0)
Call app.GetModel(0).GetStudy(0).GetCircuit().GetComponent("W-CurrentLimit").SetValue("t1", 0)
Call app.GetModel(0).GetStudy(0).GetCircuit().GetComponent("W-CurrentLimit").SetValue("t2", 0)
Call app.GetModel(0).GetStudy(0).GetCircuit().GetComponent("W-CurrentLimit").SetValue("CurrentMax",
hyst_type)
Call app.GetModel(0).GetStudy(0).GetCircuit().GetComponent("W-CurrentLimit").SetValue("CurrentMax",
Imax)
Call app.GetModel(0).GetStudy(0).GetCircuit().GetComponent("W-CurrentLimit").SetValue("CurrentMin",
hyst_type)
Call app.GetModel(0).GetStudy(0).GetCircuit().GetComponent("W-CurrentLimit").SetValue("CurrentMin",
Imin)
'Switch W+
Call app.GetDataManager().GetDataSet(6).SetName("Switch_W+")
ReDim refarray(5,1)
refarray(0,0) = w7
refarray(0,1) = on_state
refarray(1,0) = w8
refarray(1,1) = on_state
refarray(2,0) = w9
refarray(2,1) = off_state
refarray(3,0) = w10
refarray(3,1) = off_state
refarray(4,0) = w11
refarray(4,1) = on_state
refarray(5,0) = w12
refarray(5,1) = on_state
Call app.GetDataManager().GetDataSet("Switch_W+").SetTable(refarray)
Call app.GetModel(0).GetStudy(0).GetCircuit().GetComponent("W+CurrentLimit").SetValue("XType", 13)
Call app.GetModel(0).GetStudy(0).GetCircuit().GetComponent("W+CurrentLimit").SetValue("Period", 0)
Call app.GetModel(0).GetStudy(0).GetCircuit().GetComponent("W+CurrentLimit").SetValue("t1", 0)
```

```
Call app.GetModel(0).GetStudy(0).GetCircuit().GetComponent("W+CurrentLimit").SetValue("t2", 0)
Call app.GetModel(0).GetStudy(0).GetCircuit().GetComponent("W+CurrentLimit").SetValue("CurrentMax",
hyst_type)
Call app.GetModel(0).GetStudy(0).GetCircuit().GetComponent("W+CurrentLimit").SetValue("CurrentMax",
Imax)
Call app.GetModel(0).GetStudy(0).GetCircuit().GetComponent("W+CurrentLimit").SetValue("CurrentMin",
hyst_type)
Call app.GetModel(0).GetStudy(0).GetCircuit().GetComponent("W+CurrentLimit").SetValue("CurrentMin",
Imin)
'Set Vdc voltage
Set func = app.FunctionFactory().Constant(Vdc)
Call app.GetModel(0).GetStudy(0).GetCircuit().GetComponent("Vdc").SetFunction(func)
'Coils condition for:
'U-phase
Call app.GetModel(0).GetStudy(0).CreateCondition("FEMCoil", "U_phase")
Call app.GetModel(0).GetStudy(0).GetCondition(0).SetLink("Uphase")
Call app.GetModel(0).GetStudy(0).GetCondition(0).GetSubCondition(0).SetName("Group 1")
Call app.GetModel(0).GetStudy(0).GetCondition(0).GetSubCondition(0).ClearParts()
Set sel = app.GetModel(0).GetStudy(0).GetCondition(0).GetSubCondition(0).GetSelection()
Call sel.SelectPart("Coil U Up")
Call app.GetModel(0).GetStudy(0).GetCondition(0).GetSubCondition(0).AddSelected(sel)
Call app.GetModel(0).GetStudy(0).GetCondition(0).CreateSubCondition("FEMCoilData", "Group 2")
Call app.GetModel(0).GetStudy(0).GetCondition(0).GetSubCondition(1).SetValue("Direction2D", 1)
Call app.GetModel(0).GetStudy(0).GetCondition(0).GetSubCondition(1).ClearParts()
Set sel = app.GetModel(0).GetStudy(0).GetCondition(0).GetSubCondition(1).GetSelection()
Call sel.SelectPart("Coil U Dw")
Call app.GetModel(0).GetStudy(0).GetCondition(0).GetSubCondition(1).AddSelected(sel)
'V-phase
Call app.GetModel(0).GetStudy(0).CreateCondition("FEMCoil", "V_phase")
Call app.GetModel(0).GetStudy(0).GetCondition(1).SetLink("Vphase")
Call app.GetModel(0).GetStudy(0).GetCondition(1).GetSubCondition(0).SetName("Group 1")
Call app.GetModel(0).GetStudy(0).GetCondition(1).GetSubCondition(0).ClearParts()
Set sel = app.GetModel(0).GetStudy(0).GetCondition(1).GetSubCondition(0).GetSelection()
Call sel.SelectPart("Coil V Up")
Call app.GetModel(0).GetStudy(0).GetCondition(1).GetSubCondition(0).AddSelected(sel)
Call app.GetModel(0).GetStudy(0).GetCondition(1).CreateSubCondition("FEMCoilData", "Group 2")
Call app.GetModel(0).GetStudy(0).GetCondition(1).GetSubCondition(1).SetValue("Direction2D", 1)
Call app.GetModel(0).GetStudy(0).GetCondition(1).GetSubCondition(1).ClearParts()
Set sel = app.GetModel(0).GetStudy(0).GetCondition(1).GetSubCondition(1).GetSelection()
Call sel.SelectPart("Coil V Dw")
Call app.GetModel(0).GetStudy(0).GetCondition(1).GetSubCondition(1).AddSelected(sel)
'W-phase
Call app.GetModel(0).GetStudy(0).CreateCondition("FEMCoil", "W_phase")
Call app.GetModel(0).GetStudy(0).GetCondition(2).SetLink("Wphase")
Call app.GetModel(0).GetStudy(0).GetCondition(2).GetSubCondition(0).SetName("Group 1")
Call app.GetModel(0).GetStudy(0).GetCondition(2).GetSubCondition(0).ClearParts()
Set sel = app.GetModel(0).GetStudy(0).GetCondition(2).GetSubCondition(0).GetSelection()
Call sel.SelectPart("Coil W Up")
Call app.GetModel(0).GetStudy(0).GetCondition(2).GetSubCondition(0).AddSelected(sel)
Call app.GetModel(0).GetStudy(0).GetCondition(2).CreateSubCondition("FEMCoilData", "Group 2")
Call app.GetModel(0).GetStudy(0).GetCondition(2).GetSubCondition(1).SetValue("Direction2D", 1)
Call app.GetModel(0).GetStudy(0).GetCondition(2).GetSubCondition(1).ClearParts()
Set sel = app.GetModel(0).GetStudy(0).GetCondition(2).GetSubCondition(1).GetSelection()
Call sel.SelectPart("Coil W Dw")
Call app.GetModel(0).GetStudy(0).GetCondition(2).GetSubCondition(1).AddSelected(sel)
'Motion condition
Call app.GetModel(0).GetStudy(0).CreateCondition("RotationMotion", "Speed_cond")
Call app.GetModel(0).GetStudy(0).GetCondition(3).SetValue("AngularVelocity", speed)
Call app.GetModel(0).GetStudy(0).GetCondition(3).SetValue("InitialRotationAngle", angle)
Call app.GetModel(0).GetStudy(0).GetCondition(3).SetValue("Axis2D", axis_speed)
Call app.GetModel(0).GetStudy(0).GetCondition(3).ClearParts()
```

```
Set sel = app.GetModel(0).GetStudy(0).GetCondition(3).GetSelection()
Call sel.SelectPart("Rotor core")
Call sel.SelectPart("Magnet Up")
Call sel.SelectPart("Magnet Dw")
Call app.GetModel(0).GetStudy(0).GetCondition(3).AddSelected(sel)
'Torque condition
Call app.GetModel(0).GetStudy(0).CreateCondition("Torque", "Torque_cond")
Call app.GetModel(0).GetStudy(0).GetCondition(4).SetValue("Axis2D", axis_torque)
Call app.GetModel(0).GetStudy(0).GetCondition(4).ClearParts()
Set sel = app.GetModel(0).GetStudy(0).GetCondition(4).GetSelection()
Call sel.SelectPart("Rotor core")
Call sel.SelectPart("Magnet Up")
Call sel.SelectPart("Magnet Dw")
Call app.GetModel(0).GetStudy(0).GetCondition(4).AddSelected(sel)
'Iron loss calculation condition
Call app.GetModel(0).GetStudy(0).CreateCondition("Ironloss", "Iron_loss")
If frequency_type=1 Then
  Call app.GetModel(0).GetStudy(0).GetCondition(6).SetValue("BasicFrequencyType", frequency_type)
  Call app.GetModel(0).GetStudy(0).GetCondition(6).SetValue("Poles", Nr)
  Call app.GetModel(0).GetStudy(0).GetCondition(6).SetValue("RevolutionSpeed", speed)
Else
  Call app.GetModel(0).GetStudy(0).GetCondition(6).SetValue("BasicFrequencyType", frequency_type)
  Call app.GetModel(0).GetStudy(0).GetCondition(6).SetValue("BasicFrequency", base_freq)
End If
Call app.GetModel(0).GetStudy(0).GetCondition(6).SetValue("JouleLossCalcType", 3)
Call app.GetModel(0).GetStudy(0).GetCondition(6).SetValue("Cyclicity", 0)
Call app.GetModel(0).GetStudy(0).GetCondition(6).SetValue("LaminationThickness", 0.5)
Call app.GetModel(0).GetStudy(0).GetCondition(6).SetValue("LaminationLossNumDivision", 5)
'=============================================================
'                      MESH SETUP
'=============================================================
'Add size control ( element part)
Call app.GetModel(0).GetStudy(0).GetMeshControl().CreateCondition("Part", "Part_cond")
Call app.GetModel(0).GetStudy(0).GetMeshControl().GetCondition(0).SetValue("Size", size_part)
Call app.GetModel(0).GetStudy(0).GetMeshControl().GetCondition(0).ClearParts()
Set sel = app.GetModel(0).GetStudy(0).GetMeshControl().GetCondition(0).GetSelection()
Call sel.SelectPart("Stator core")
Call sel.SelectPart("Rotor core")
Call sel.SelectPart("Magnet Up")
Call sel.SelectPart("Magnet Dw")
Call sel.SelectPart("Coil U Up")
Call sel.SelectPart("Coil U Dw")
Call sel.SelectPart("Coil V Up")
Call sel.SelectPart("Coil V Dw")
Call sel.SelectPart("Coil W Up")
Call sel.SelectPart("Coil W Dw")
Call app.GetModel(0).GetStudy(0).GetMeshControl().GetCondition(0).AddSelected(sel)
'Add size control ( air gap)
linii_stator=20 : linii_coil=10 : linii_magnet=4
polmic1=6 : polmic2=39 : polmic3_1=61 : polmic3_2=63 : polmic3_3=59
polmare1=5 : polmare2=27 : polmare3_1=49 : polmare3_2=51 : polmare3_3=47
tot_stator=Ns*linii_stator : tot_coil=Ns*linii_coil : tot_magnet=Nr*linii_magnet
pm1=tot_stator+tot_coil+1
pm1_1=pm1+2 : pm1_2=pm1+4
Call app.GetModel(0).GetStudy(0).GetMeshControl().CreateCondition("Edge", "Gap")
Call app.GetModel(0).GetStudy(0).GetMeshControl().GetCondition(1).SetValue("Size", size_gap)
Call app.GetModel(0).GetStudy(0).GetMeshControl().GetCondition(1).ClearParts()
Set sel = app.GetModel(0).GetStudy(0).GetMeshControl().GetCondition(1).GetSelection()
'% Edges intermediate and main stator teeth %
For i=1 to Ns
  Select Case i
```

```
    Case 1,2
    If i=2 Then
      Call sel.SelectEdge(polmic2)
      Call sel.SelectEdge(polmare2)
      polmic3=polmic2+linii_stator
      polmare3=polmare2+linii_stator
    End If
    Call sel.SelectEdge(polmic1)
    Call sel.SelectEdge(polmare1)
    Case 3
    If (Ns=6) Or (Ns=9) Then
      Call sel.SelectEdge(polmic3_1)
      Call sel.SelectEdge(polmare3_1)
      polmic4=polmic3_1+linii_stator
      polmare4=polmare3_1+linii_stator
    Else
      If (Ns=12) Then
        Call sel.SelectEdge(polmic3_2)
        Call sel.SelectEdge(polmare3_2)
        polmic4=polmic3_2+linii_stator
        polmare4=polmare3_2+linii_stator
      Else
        Call sel.SelectEdge(polmic3)
        Call sel.SelectEdge(polmare3)
        polmic4=polmic3+linii_stator
        polmare4=polmare3+linii_stator
      End If
    End If
    Case Else
    Call sel.SelectEdge(polmic4)
    Call sel.SelectEdge(polmare4)
    polmic4=polmic4+linii_stator
    polmare4=polmare4+linii_stator
  End Select
Next
'% Edges magnets %
For i=1 to Nr
  Select Case i
    Case 1
    If (Ns=6) Or (Ns=9) Then
      Call sel.SelectEdge(pm1_1)
      pm2=pm1_1+linii_magnet+1
    Else
      If (Ns=12) Then
        Call sel.SelectEdge(pm1_2)
        pm2=pm1_2+linii_magnet+1
      Else
      Call sel.SelectEdge(pm1)
      pm2=pm1+linii_magnet+1
      End If
    End If
    Case Else
    Call sel.SelectEdge(pm2)
    pm2=pm2+linii_magnet
  End Select
Next
Call app.GetModel(0).GetStudy(0).GetMeshControl().GetCondition(1).AddSelected(sel)
'Set mesh properties
Call app.GetModel(0).GetStudy(0).GetMeshControl().SetValue("MeshType", 1)
Call app.GetModel(0).GetStudy(0).GetMeshControl().SetValue("RadialDivision", RadialDiv)
Call app.GetModel(0).GetStudy(0).GetMeshControl().SetValue("CircumferentialDivision", CircDiv)
```

```
ReDim refarray(0,1)
refarray(0,0) = 1
refarray(0,1) = 0
Call app.GetModel(0).GetStudy(0).GetMeshControl().GetTable("SlideTable").SetTable(refarray)
Call app.GetModel(0).GetStudy(0).GetMeshControl().SetValue("2dMeshingMethod", 2)
Call app.GetModel(0).GetStudy(0).GetMeshControl().SetValue("AirRegionScale", 1.25)
Call app.GetModel(0).GetStudy(0).CreateMesh()
Call app.View().ShowMesh()
'========================================================================
'                    STUDY CASE SETUP 'LOAD'
'========================================================================
'Pre-processing
Call app.GetModel(0).GetStudy(0).SetDescription(Case1_description)
Call app.GetModel(0).GetStudy(0).GetStudyProperties().SetValue("ModelThickness", Lm)
Call app.GetModel(0).GetStudy(0).GetStudyProperties().SetValue("NonlinearMaxIteration", MaxIter)
Call app.GetModel(0).GetStudy(0).GetStudyProperties().SetValue("UseMultiCPU", paralel)
Call app.GetModel(0).GetStudy(0).GetStudyProperties().SetValue("MultiCPU", no_paralel)
Call app.GetModel(0).GetStudy(0).GetStep().SetValue("Step", case1_steps)
Call app.GetModel(0).GetStudy(0).GetStep().SetValue("StepType", case1_step_type)
Call app.GetModel(0).GetStudy(0).GetStep().SetValue("EndPoint", case1_end_point)
Call app.GetModel(0).GetStudy(0).GetStep().SetValue("StepDivision", case1_div)
Call app.View().SetCurrentCase(1)
Call app.GetModel(0).GetStudy(0).Run()
'Post-processing
Call app.SetCurrentStudy(0)
Call app.GetModel(0).GetStudy(0).CreateContour("flux density")
Call app.GetModel(0).GetStudy(0).GetContour(0).SetResultType("MagneticFluxDensity", "")
Call app.GetModel(0).GetStudy(0).GetContour(0).SetResultCoordinate("Global Rectangular")
Call app.View().SetContourView(true)
Call app.SetCurrentStudy(0)
Call app.GetModel(0).GetStudy(0).CreateFluxLine("flux line")
Call app.GetModel(0).GetStudy(0).GetFluxLine(0).SetResultType("VectorPotential", "")
Call app.GetModel(0).GetStudy(0).GetFluxLine(0).SetNormal(0, 0, 1)
Call app.View().SetFluxLineView(true)
'========================================================================
'                    SAVE RESULTS
'========================================================================
Call app.SetCurrentStudy(0)
Set tables = app.GetModel(0).GetStudy(0).GetResultTable()
Call tables.SetXYZComponent("Absolute")
Call tables.WriteAllTables("F:\ANDREEA_ASUS\DOCTORAT/MatlabJmag/Rezultate_load.csv", "Time")
'========================================================================
'                    DELETE MODEL
'========================================================================
Call app.DeleteModel(0)
objFile.Close
```

Chapter 3

Long-Term Wind-Speed Profile Modeling and Simulation for the Micro-Wind Energy Conversion System

3.1 Wind-speed profile

As the micro-wind turbine power changes with the cube of the wind speed, its expression emphasizes the important impact that the wind speed has upon the μWECS. Typically a wind speed profile consists of a large set of data measurements, which for this thesis represent the mean value taken over one hour of wind measurements, every hour for one year, resulting into 8759 measurements that describe the wind behavior (*fig. 3.1)*.

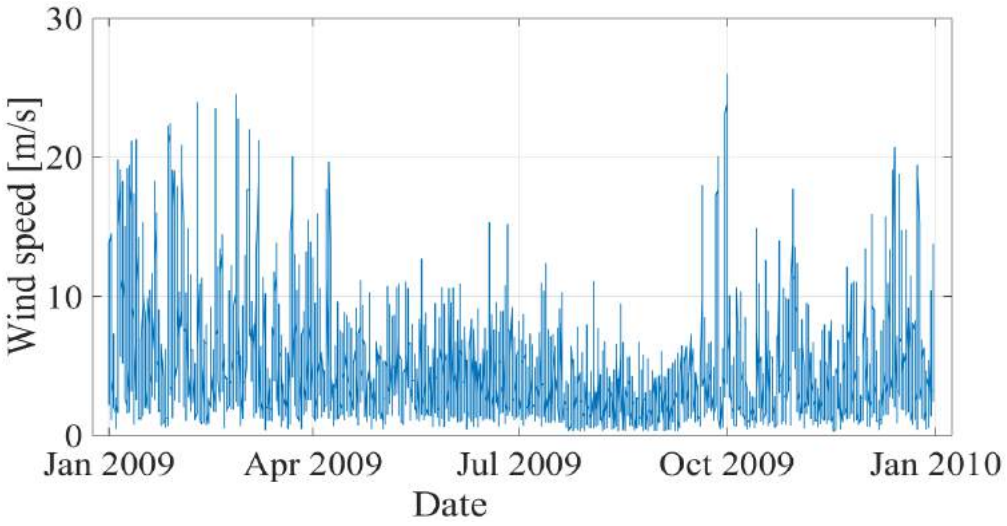

Fig. 3.1. Long-term wind speed profile representation

For evaluating the efficiency of the entire system, simulations over this type of long wind-speed cycle are necessary. This approach however is undesirable in the context of design optimization due to the fact that the simulation of the system repeats itself based on the variation domain of the design variables. Thus, the time needed to find the optimal sizing solution of the system is influenced by the duration of the wind profile. In respect to this, it could be concluded that a shorter wind profile, yet still pertinent for the objective of the design process, would represent a good alternative. Hence, in this chapter analyses are conducted, as well as presentation of methods that could be used for its reduction in order to find a solution to handle the simulation time of the wind energy system over this long-term wind-speed profile. In the last part of this chapter some simulation results obtained with the analytical and semi-analytical models over long-term and reduced wind-speed profile are also provided.

3.1.1 Methods for simplifying the long-term wind-speed profile

Classically, the design of a micro-wind generator is often done for the base operating point, corresponding to the base power or torque of the micro-wind turbine. At this point the generator can operate extensively without any damage. However, the difficulty is in searching for a certain wind speed of the wind-speed profile for which the design should be achieved and then used to calculate μWECS power losses.

To solve this problem three methods are investigated with the purpose of simplifying the long-term wind-speed profile:

A) The average wind speed

The first approach is to reduce the wind profile to a single operating point, i.e. the nominal/rated wind speed of the wind turbine. A method [1] is to consider this point equal to the average wind speed in the wind-speed profile, whose value may be determined by applying the following expression:

$$v_{rated} = \frac{\sum_{i=1}^{8759}(v_{w_i} t_i)}{\sum_{i=1}^{8759} t_i} \tag{3.1}$$

Further on the mechanical power extracted by the micro-wind turbine can be calculated, under the assumption of a MPPT strategy and considering for this study that the turbine does not operate for wind speeds $v_w < v_{in} = 2\ m/s$ or $v_w > v_{max} = 20\ m/s$, as well that it can function at the nominal power $P_{wt\_limit}(v_{rated})$, given by the average wind speed determined above, until the maximum wind speed is reached. *Fig. 3.2* represents the wind power that can be transmitted to the generator for each hour during the wind-speed cycle.

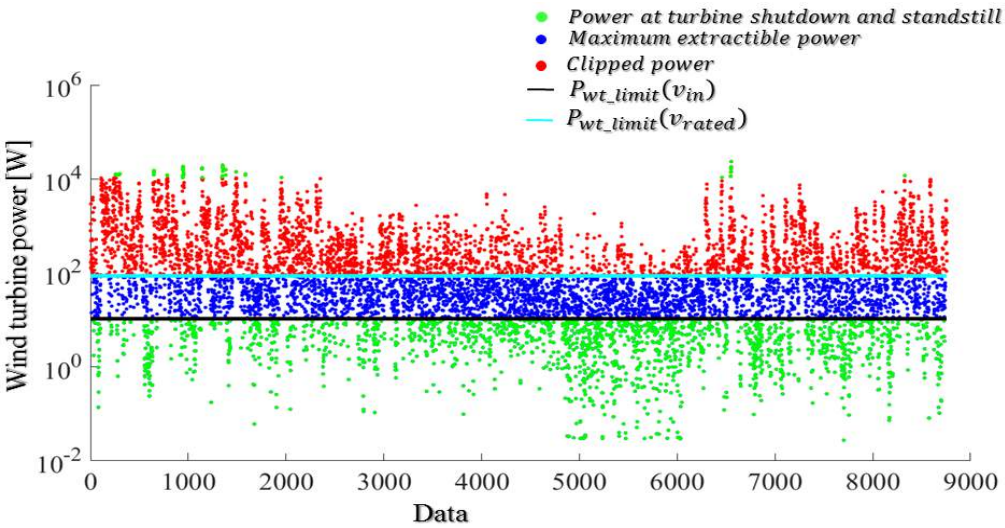

Fig. 3.2. Micro-wind turbine power over a wind-cycle operation in logarithmic scale

- An analysis on the operating time, starting from *fig. 3.2* and based on the assumptions stated earlier, denotes that the micro-wind turbine is unusable (zero power) for 22% of the time (1918 hours) over a wind cycle of 8759 hours. Likewise, the turbine operates under the MPPT strategy (maximum extractible power region represented with blue dots in *fig. 3.2*) for 38% (3337 hours) of the cycle, while 40% (3504 hours) of the time is limited (clipped power region represented with red dots in *fig. 3.2*) to function at the nominal power $P_{wt\_limit}(v_{rated})$.
- As shown in *fig.3.3*, another analysis compares the extracted energy by the wind turbine for the different operation modes with the total energy that could be extracted if only the MPPT was to be used. It appears that only 0.13% of the extracted energy cannot be retrieved due to wind speeds lower than 2m/s, when the turbine is at standstill. For the maximum power region only 3.45% is captured by the turbine, while 96.17% of the total extractible power is represented by the clipped power region. A low percentage of only 0.25% is owed to the shutdown of the turbine, but in this case because of wind speeds higher than $20\ m/s$.

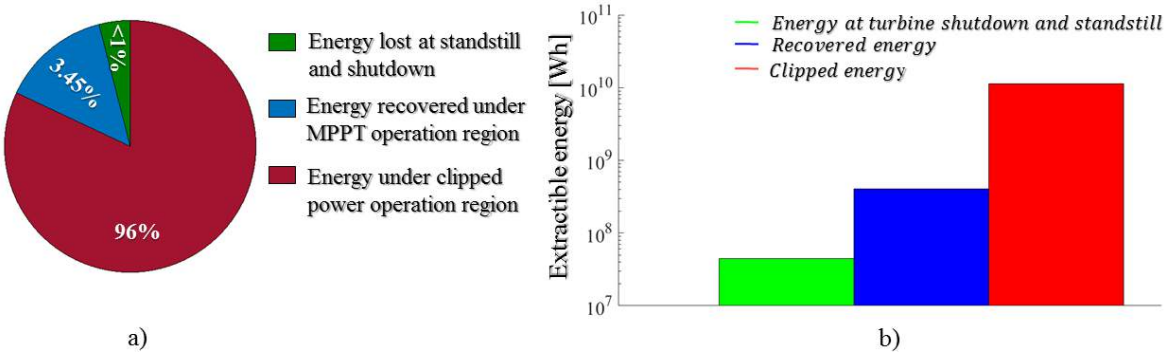

Fig. 3.3. Extractible energy by the micro-wind turbine, a) energy rate and b) energy distribution for different operation modes of the micro-wind turbine

B) The statistical distribution method based on histogram approach

The statistical distribution based on histogram approach can help to characterize the long-term wind-speed profile in terms of occurrences and help to reduce it into fewer operating points. On this basis, the wind data distribution can be discretized into *N* number of intervals/bins, evenly distributed, as illustrated in *fig.3.4*.

The discretization factor Δn chosen for the statistical distribution representation in *fig. 3.4* is 1m/s and the number of intervals is set to be equal to the maximum wind speed in the cycle. Each interval is associated to a mean wind speed value of the set of operating points

located in it and to a total number of points comprised within. *Fig. 3.5* summarizes the process employed for the generation of the new wind speed signal, whose duration and length will be given by $N \cdot \Delta n$.

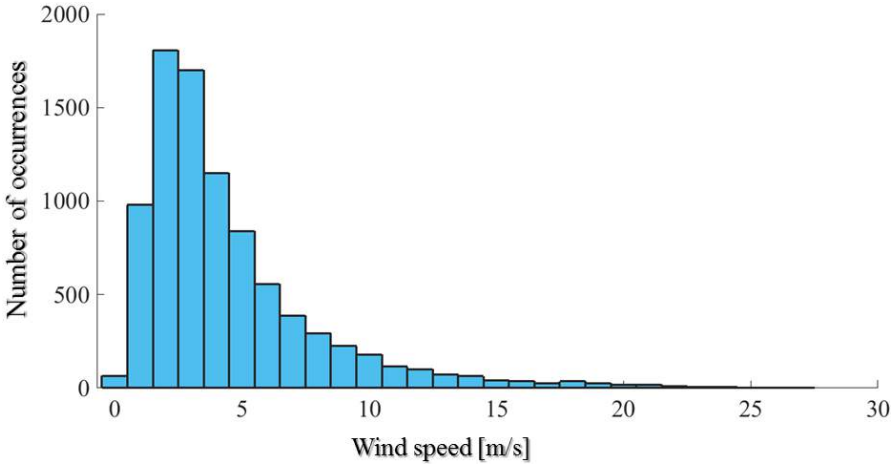

Fig. 3.4. Statistical distribution of the wind speed profile

An important aspect regarding this method is that it is quite sensitive to discretization. A high number of intervals will give better accuracy, but they can also lead to an increased simulation time, which can be detrimental in an optimization process. Another fact to be added is that, for simplification, the turbulence phenomena is not considered in the generation process of the new wind signal.

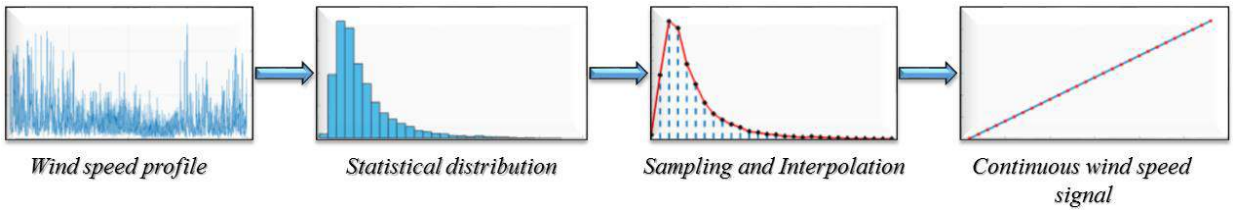

Fig. 3.5. Process of wind speed-profile simplification based on statistical distribution

Having determined the new wind speed operating points and their number of occurrences it is possible forwards to employ this signal in the simulation of the wind energy system for the calculation of the total power losses and compare them afterwards with the ones obtained after a complete cycle simulation, investigation that will be presented in *section 3.1.3*.

C) Barycenter method

The third method explored for simplifying the wind cycle is based on the barycenter method, which allows to reduce both the simulation time and the wind data that will be

considered for the design of the generator. A description of this method was reported in [2], where it was used to reduce the torque and speed driving cycles in the design optimization of an axial flux traction motor. This barycenter method is adapted to the wind energy system [3] for processing the large amount of wind-speed data. In order to reduce the cycle and in consequence the computation time, the totality of operating points within the wind-speed cycle are replaced with a low number of regions as illustrated in *fig. 3.6* with different colors, each region being represented by a barycenter and its corresponding parameters given by *equation (3.2)*. These parameters are further used for the losses calculation of each region *r*.

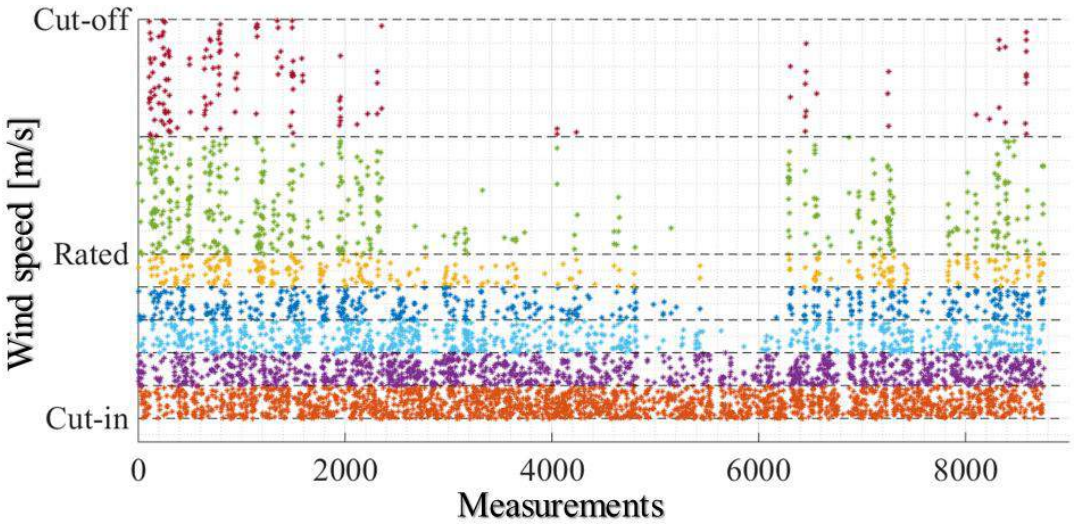

Fig. 3.6 Division example of the long-term wind-speed profile into a chosen number of regions

$$Bary_r = \begin{cases} \langle v_w \rangle_r , & mean\ wind\ speed \\ \langle v_w^2 \rangle_r , & mean\ square\ wind\ speed \\ \langle v_w^4 \rangle_r , & mean\ wind\ speed\ of\ 4th\ power \\ N_r , & number\ of\ points\ in\ the\ region\ r \end{cases} \tag{3.2}$$

3.1.2 Barycenter method applied to the computation of µWECS power losses over the long-term wind-speed cycle

The expressions for the power losses are based on the equations provided in [3], [4], [5] and reformulated afterwards in connection to the barycenter method in order to calculate them for each region as follows:

- ***Mechanical losses*** (P_{mech}) due to friction phenomena:

$$P_{mech,r} = f_{wt}\ \Omega_r^2\ N_r \frac{\langle v_w^2 \rangle_r}{\langle v_w \rangle_r^2} \tag{3.3}$$

with

f_{wt} : Friction coefficient (N.m/rad)

- ***Copper losses*** (P_j) caused by the currents in the stator windings:

$$P_{j,r} = 3RI_{RMS,r}^2 N_r \frac{\langle v_w^4 \rangle_r}{\langle v_w \rangle_r^4} \tag{3.4}$$

- The ***iron losses*** can be decomposed into three distinct parts: the hysteresis losses (P_{Fe_hys}), the losses caused by the eddy currents (P_{Fe_eddy}) and the excess losses, which are not included into this study.

$$P_{Fe\_hys,r} = k_{hys} \frac{N_p}{2\pi} \left(\hat{B}_{th}^{\alpha} + \hat{B}_{sy}^{\alpha}\right) \Omega_r N_r \frac{\langle v_w \rangle_r}{\langle v_w \rangle_r} \tag{3.5}$$

$$P_{Fe\_eddy,r} = k_{eddy} \frac{N_p^2}{\pi^3} \left(\hat{B}_{th}^2 + \hat{B}_{sy}^2\right) \Omega_r^2 N_r \frac{\langle v_w^2 \rangle_r}{\langle v_w \rangle_r^2} \tag{3.6}$$

where

k_{hys} : Hysteresis loss coefficient obtained from manufacturer data

k_{eddy} : Eddy current loss coefficient obtained from manufacturer data

- The considered three-phase power converter can exhibit ***conduction*** (P_{cond_IGBT}) and ***switching*** (P_{sw_IGBT}) ***losses*** in its IGBT devices as well as ***losses in*** their anti-parallel ***diodes***:

$$P_{cond\_IGBT,r} = 6\left[\frac{1}{3} f_{mod} \left(\frac{V_{CE} - V_{CE0}}{I_{n\_IGBT}}\right) I_{C\_RMS,r}^2 N_r \frac{\langle v_w^4 \rangle_r}{\langle v_w \rangle_r^4} + \frac{1}{3} f_{mod} V_{CE0} I_{RMS,r} N_r \frac{\langle v_w^2 \rangle_r}{\langle v_w \rangle_r^2}\right] \tag{3.7}$$

$$P_{sw\_IGBT,r} = 6\left[\frac{1}{3}(E_{ON} + E_{OFF}) \frac{V_n}{V_{CC(test)} I_{CC(test)}} I_{C\_pk,r} f_{sw} N_r \frac{\langle v_w^2 \rangle_r}{\langle v_w \rangle_r^2}\right] \tag{3.8}$$

$$P_{diode,r} = 6\left[\frac{1}{3}(1 - f_{mod}) V_F I_{C\_RMS,r} N_r \frac{\langle v_w^2 \rangle_r}{\langle v_w \rangle_r^2}\right] + 6V_F T_{comm} f_{ele} I_{F\_AVG,r} N_r \frac{\langle v_w^2 \rangle_r}{\langle v_w \rangle_r^2} \tag{3.9}$$

$$I_{C\_RMS} = I_{RMS} \quad , \quad I_{C\_pk} = I_{RMS} + 10\% I_{RMS} \quad , \quad I_{F\_AVG} = I_{C\_pk}/2 \tag{3.10}$$

where

f_{mod} : Modulation factor ($0 < f_{mod} < 1$)

V_{CE} : Collector-emitter voltage of the IGBT [V]

V_{CE0} : ON-state, zero current collector-emitter voltage [V], obtained from the manufacturer datasheet

I_{n_IGBT} : Nominal current of the IGBT [A]

I_{C_RMS} : The current during the 120° switch conduction period [A]

E_{ON} : Turn-on switching losses [J]

E_{OFF} : Turn-off switching losses [J]

V_n : Nominal voltage available in the machine [V]

$V_{CC(test)}$: Test voltage [V]

$I_{CC(test)}$: Test current [A]

f_{sw} : Switching frequency [Hz]

V_F : Forward ON-voltage in the diode [V]

T_{comm} : Commutation time of the machine [s]

f_{ele} : Fundamental frequency of the machine [Hz]

I_{F_AVG} : The average forward current of the diode during phase commutation [A]

A more detailed explanation on the entire process of how these losses equations are determined can be found in ***Appendix 3.A.***

To validate the method, at the first step the losses of the wind energy system were calculated for all points of the wind cycle by using the semi-analytical model and the totality of each loss was obtained through their addition. The second step was to compute the losses with the help of the same semi-analytical model by applying the barycenter method and the relations *(3.3)-(3.9)*, considering several number of regions. A relative error was then calculated between the values obtained at the first step and those from the second step and presented in *fig. 3.7* with and without taking into account the ratio of the barycenter parameters. Practically, the lack of ratio in the power losses expressions denotes that their calculation is done with the help of the statistical distribution by means of histogram approach. The curves in the figures show that the usage of the barycenter ratio allows to achieve a small error faster and with fewer regions.

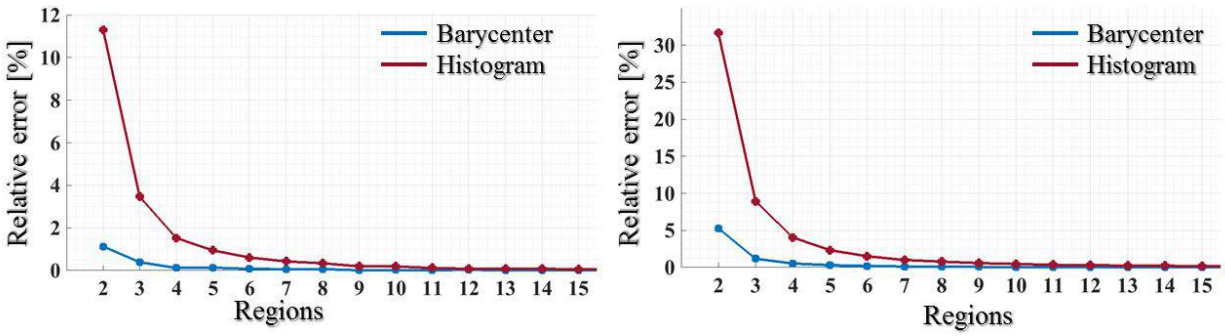

a) Mechanical loss b) Copper loss

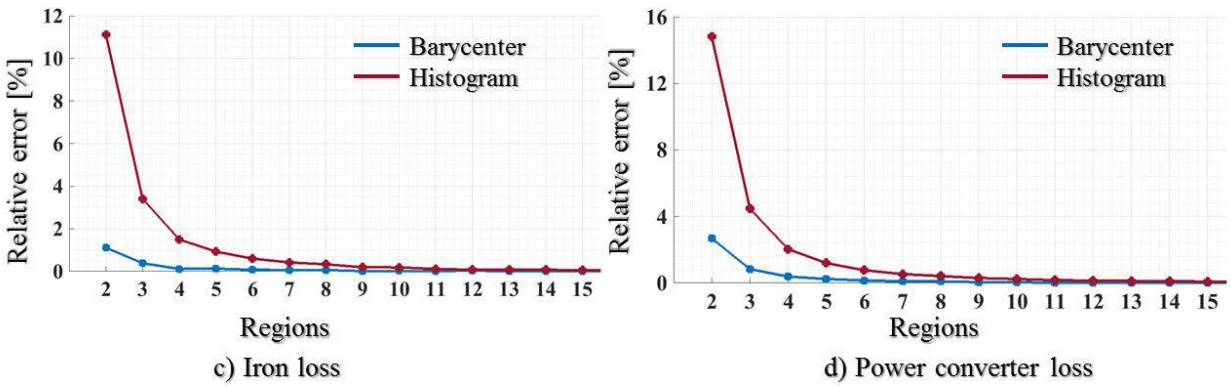

Fig. 3.7. Percentage errors between different total power losses of the wind energy system based reference BLDCPM generator

3.2 Simulations of µWECS operating over long-term wind-speed cycle

The µWECS discussed in *chapter 2* is implemented in Matlab, for the analytical model and in Matlab/Simulink for the semi-analytical model. The model simulations are performed with the BLDCPM generator parameters listed in *table 2.4* and on the micro-wind turbine performance points previously discussed, i.e. $v_{in} = 2\,m/s$, $v_n = 9.3\,m/s$ and $v_{max} = 20\,m/$, but now for a larger range of operating points. These simulations offer more details on how the losses and the efficiency of the overall wind energy system assembly are affected by these performance points. Furthermore, they also provide an insight of which of the two types of simulation models to be used in the optimization process as well as a comparison between several of their output quantities.

3.2.1 Simulations of analytical and semi-analytical models under long-term and reduced wind-speed cycle operation

In order to see how the performance points of the wind turbine affect the outputs of the wind energy system, several simulations are performed with the semi-analytical model under complete cycle operation. These factors along with their variation domain and number of considered levels, are presented in *table 3.1*.

For a full factorial design [7] with three factors and five levels the number of test conditions and results/responses is $N_{cond} = 5^3 = 125$, while setting the variation domain of the factors between [-1,1]. The test condition matrix and the response vector for this specific design resemble to those presented in equations *(3.11)* and *(3.12)*.

Table 3.1 Variation domain of the wind turbine performance factors

Level	Cut-in wind speed (v_{in})	Rated wind speed (v_n)	Cut-off wind speed (v_{max})
1 (-1)	1	7	18
2 (-0.5)	1.75	8	19
3 (0)	2.5	9	20
4 (0.5)	3.25	10	21
5 (1)	4	11	22

$$Test\ matrix = \begin{bmatrix} \overbrace{-1}^{v_{in}} & \overbrace{-1}^{v_n} & \overbrace{-1}^{v_{max}} \\ -0.5 & -1 & -1 \\ \vdots & \vdots & \vdots \\ 0.5 & 1 & 1 \\ 1 & 1 & 1 \end{bmatrix} \tag{3.11}$$

$$Results = \begin{bmatrix} P_{in\_total_1} & P_{losses\_total_1} & P_{out\_total_1} & \eta_{sys_1} \\ P_{in\_total_2} & P_{losses\_total_2} & P_{out\_total_2} & \eta_{sys_2} \\ \vdots & \vdots & \vdots & \vdots \\ P_{in\_total_{124}} & P_{losses\_total_{124}} & P_{out\_total_{124}} & \eta_{sys_{124}} \\ P_{in\_total_{125}} & P_{loses\_total_{125}} & P_{out\_total_{125}} & \eta_{sys_{125}} \end{bmatrix} \tag{3.12}$$

The general average of each result is calculated based on *(3.13)*, while the effect of each factor at a certain level can be found with the help of *(3.14)* [8]:

$$AVG = \left[\frac{1}{N_{cond}} \sum_{i=1}^{N_{cond}} P_{in\_total_i} \quad \frac{1}{N_{cond}} \sum_{i=1}^{N_{cond}} P_{losses\_total_i} \quad \frac{1}{N_{cond}} \sum_{i=1}^{N_{cond}} \eta_{sys_i} \right] \tag{3.13}$$

$$E_{factor_j} = (Average\ of\ the\ responses\ when\ factor\ is\ at\ level\ j) - AVG \tag{3.14}$$

The outputs of the system retained for presentation are the total power that can be extracted by the wind turbine $\left(\sum_{i=1}^{8759} P_{in_i}\right)$, the total power losses $\left(\sum_{i=1}^{8759} P_{losses_i}\right)$ over the long-term wind profile (composed of mechanical, Joule, iron and power converter losses), as well as the total output power $\left(\sum_{i=1}^{8759} P_{out_i}\right)$ and the overall efficiency of the wind energy system $\left(\eta_{sys} = \frac{\sum_{i=1}^{8759} P_{out_i}}{\sum_{i=1}^{8759} P_{in_i}}\right)$, which is the result of the ratio between the total useful power delivered by the wind energy system and the total power extracted by the wind turbine. These results are represented in *figs. 3.8-3.11* alongside their general average value.

It can be noticed that all responses are affected, some more and other less, by the variation of the wind turbine performance factors. The input power of the wind system and

therefore the losses and the output power decrease as the cut-in speed of the turbine increases. This is due to the fact that as depicted in the histogram figure (*fig. 3.4*), the large amount of wind speed data is situated between 0 and 5 m/s.

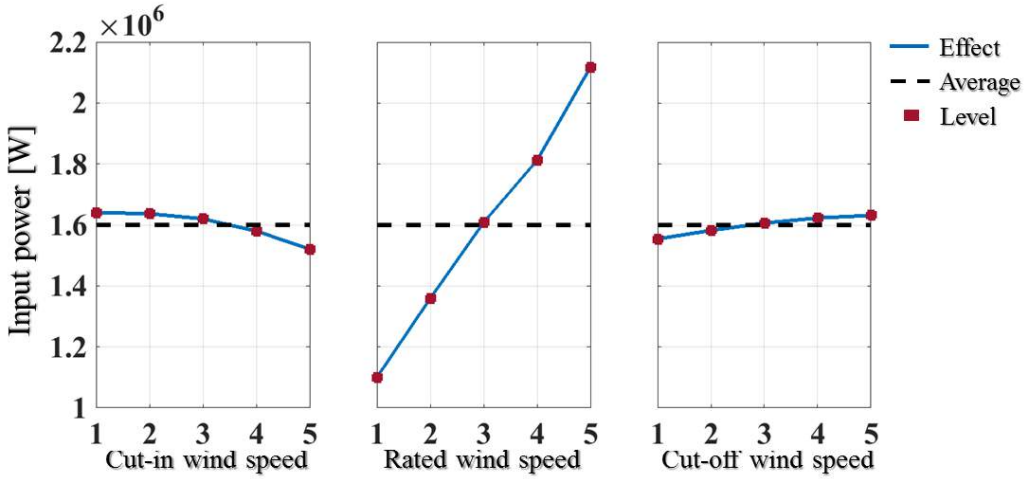

Fig. 3.8 Tendency graph for µWECS total input power

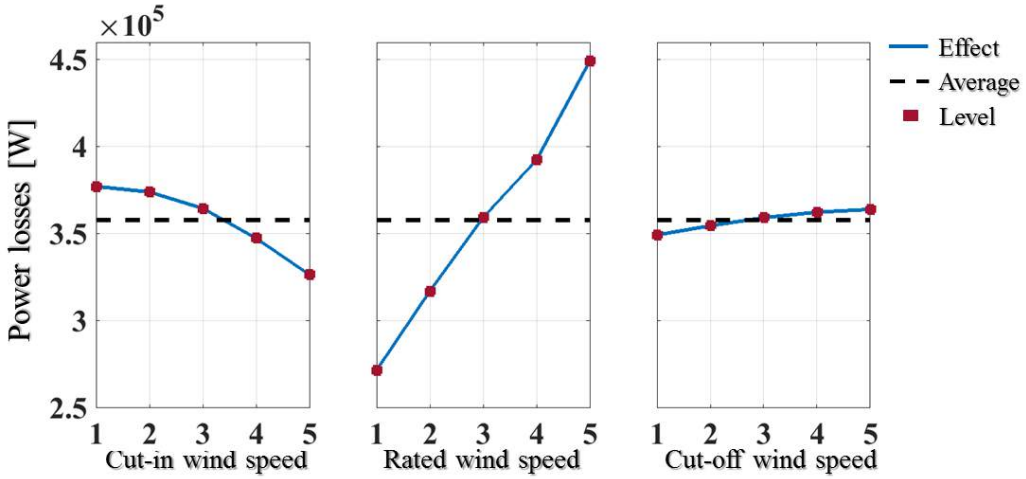

Fig. 3.9 Tendency graph for µWECS total power losses

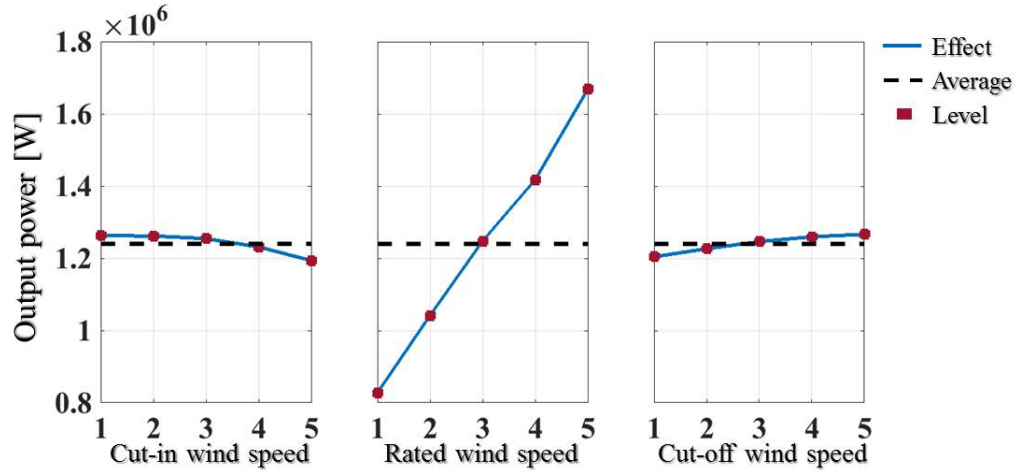

Fig. 3.10 Tendency graph for µWECS total output power

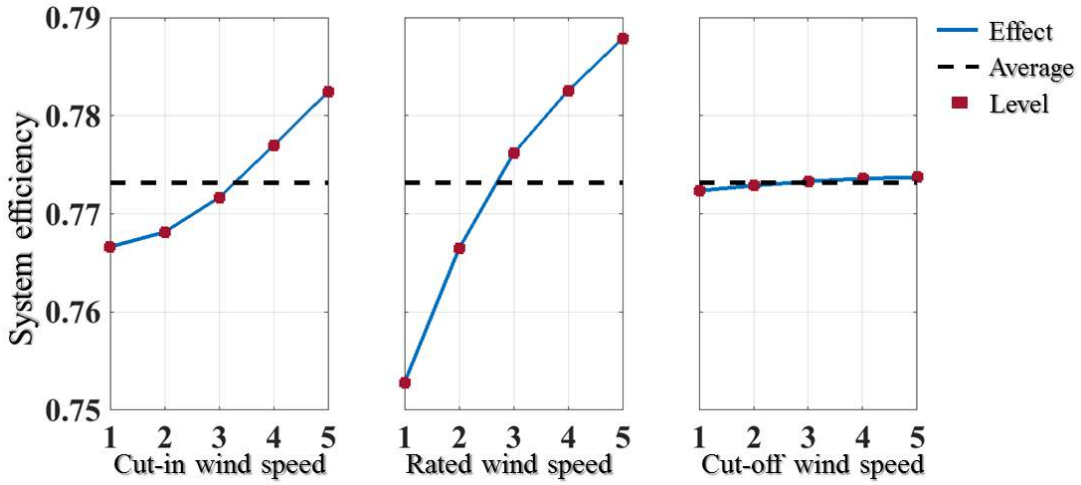

Fig. 3.11 Tendency graph for μWECS global efficiency

Lower value of the rated wind speed results in a decrease of power extraction and losses and also with negative impact upon the system efficiency. As high wind speeds are quite few in the studied wind profile, a lower or an increased value of the cut-off wind speed of the turbine does not affect that much neither one of the responses.

To better observe the efficiency of the different components of the wind energy system the semi-analytical model was simulated for a variety of speed and torque values and their contour maps are represented in the figures below.

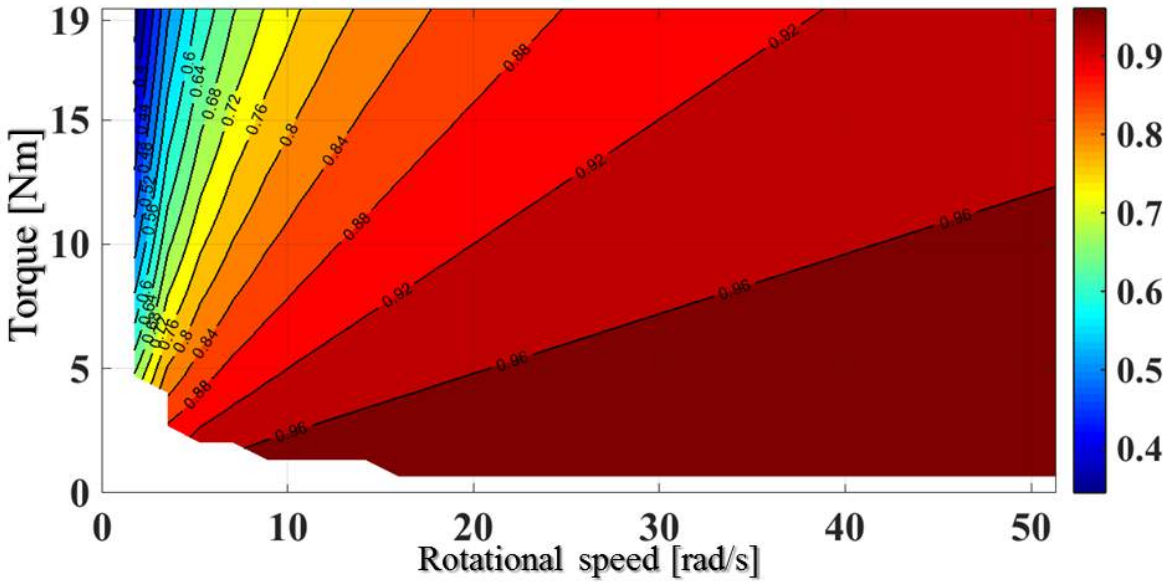

a)

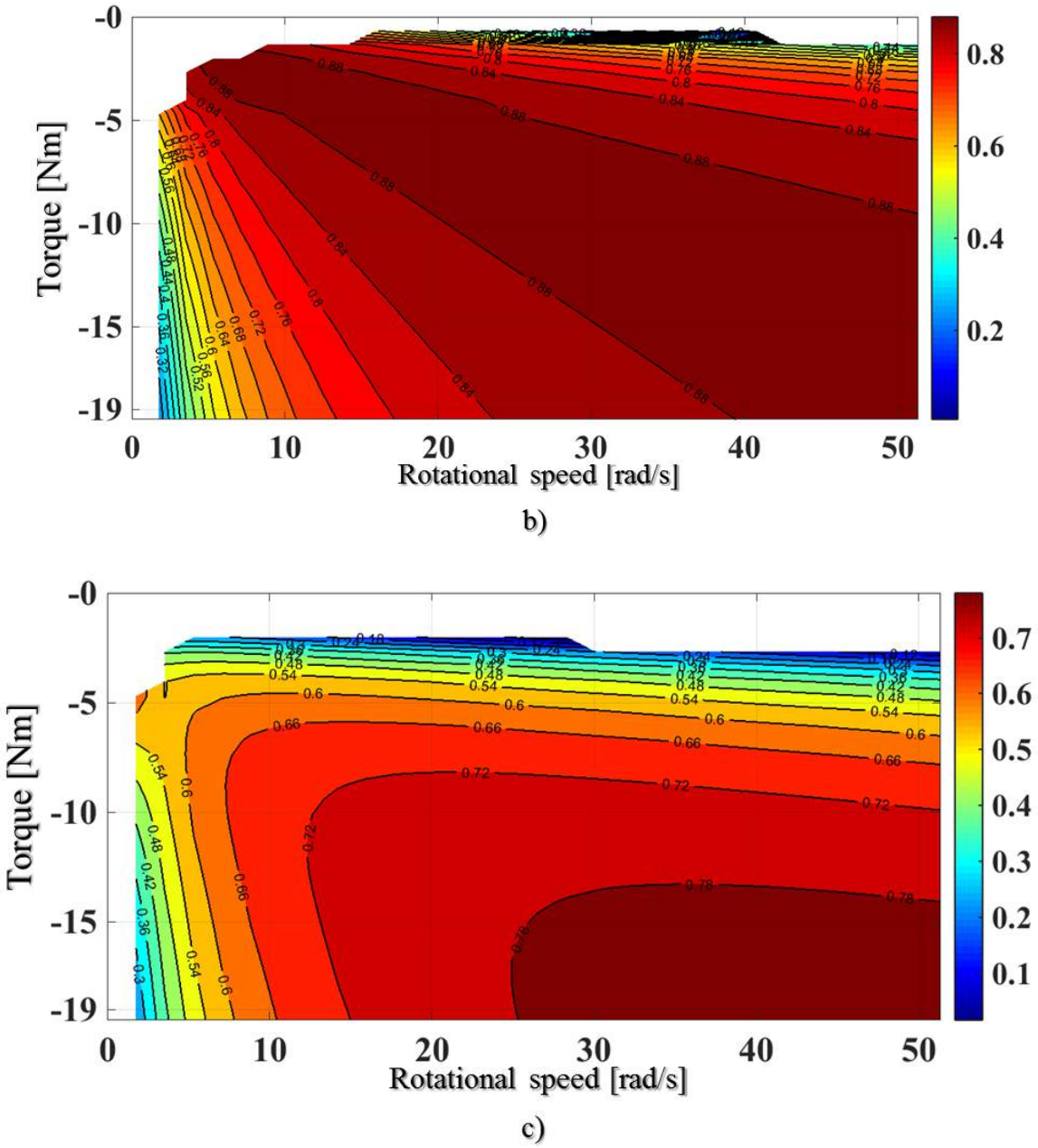

Fig. 3.12 Efficiency contour plots for a) micro-wind turbine, b) BLDCPM generator and c) power electronic converter

The contour plot of the mechanical efficiency is depicted by *fig. 3.12-a*, for which only the friction losses were considered as the main disturbance in the turbine performance.

By convention, the electromagnetic torque developed by the BLDCPM machine is negative (*fig. 3.12-b*,c) as the machine functions in the generator operation mode. When the speed of the wind is too small the losses in the system are exceeding the generated power and the turbine does not even start for operation, which describes the area without efficiency values in the contour maps.

Table 3.2. Comparison table of μWECS simulation models

	Semi-analytical model with complete cycle	***Semi-analytical model with barycenter method***	***Analytical model with complete cycle***
No. of operating points	8,759	6	8,759
Simulation time	≈ 2 h	≈ 14 s	≈ 0.003 s
Total input power $\sum_{i=1}^{N}\langle P_{in\_wt}\rangle_i$ [kW]	1,814.9	1,813.2	1,786.1
Total power losses $\sum_{i=1}^{N}\langle P_{losses}\rangle_i$ [kW]	401.52	401.18	468.19
Total mechanical losses $\sum_{i=1}^{N}\langle P_{mech}\rangle_i$ [kW]	149.44	149.35	151.81
Total joule losses $\sum_{i=1}^{N}\langle P_j\rangle_i$ [kW]	58.665	58.593	63.958
Total iron losses $\sum_{i=1}^{N}\langle P_{Fe}\rangle_i$ [kW]	21.140	21.128	21.541
Total converter losses $\sum_{i=1}^{N}\langle P_{conv}\rangle_i$ [kW]	172.28	172.11	230.88
Total output power $\sum_{i=1}^{N}\langle P_{out\_sys}\rangle_i$ [kW]	1,413.4	1,412.0	1,317.9
System efficiency $\eta_{sys}=\frac{\sum_{i=1}^{N}\langle P_{out\_sys}\rangle_i}{\sum_{i=1}^{N}\langle P_{in\_wt}\rangle_i}$	0.7788	0.7787	0.7379

Further on, other simulations with both models are conducted. These simulation results allow comparing several quantities of the analytical and semi-analytical models over complete and reduced wind cycle operation, which are give in *table 3.2.*, likewise in terms of computation time and operating points. It is worth noting that for the semi-analytical model, each operating point of the wind cycle was simulated at steady state for one electrical period of the BLDCPM generator ($0 \leq t \leq T$) under $\Delta t = 5 \cdot 10^{-6}$ sampling time.

Based on the above comparison, it can be concluded that by using the barycenter method for reduction of the wind-speed cycle a certain gain in the simulation time of the semi-analytical model is achieved with satisfactory accuracy. The analytical model exhibits the smallest simulation time, but with precision penalty. Therefore, the semi-analytical model associated to the barycenter method proves to be well-suited for the design optimization

process. An error graph for some of the quantities from the above table are illustrated in f*ig. 3.13.*

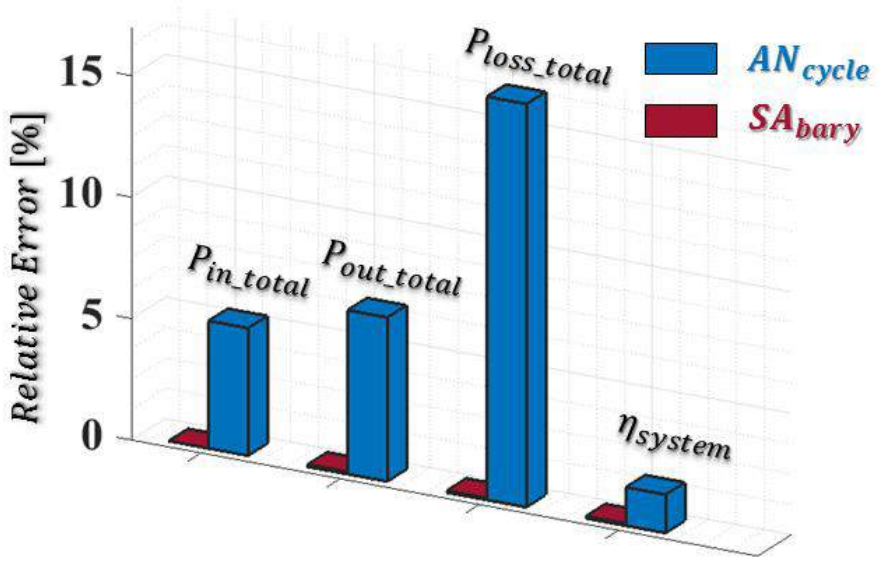

Fig. 3.13. Relative error between the analytical and semi-analytical models

3.3 Conclusions

This chapter was intended to enlighten that long-term wind-speed profile can be employed in simulations of the analytical and semi-analytical models retained for further analysis.

Therefore, in the first part of this chapter three methods were analyzed for reducing the wind cycle:

- The average value method, which reduces the duration of the profile to a single operating point. However, it is found to be an inefficient solution as the majority of speed values are situated above the rated power limit, and therefore not fully exploited through the MPPT strategy.
- The statistical distribution based histogram method appears to be a better alternative, but displays higher relative error when several output quantities of the system were compared to the ones obtained over complete cycle operation.
- The barycenter method demonstrates the most efficient solution to reduce the duration of the wind profile and consequently the simulation time of the system, while revealing small relative errors of the outputs after comparing them against those resulted after complete cycle evaluation.

Further, some simulations have been conducted and the results of the analytical and semi-analytical models over long-term and reduced wind profile operation have been compared. The semi-analytical model with complete cycle denotes an undesirable simulation time for even considering of using it in an optimization process. On the other hand, when coupled to the barycenter method, as mentioned earlier, this time reduces while still providing good precision of the output quantities. However, not the same response yields the analytical model. Even if it performs the fastest, a quite large error is found when compared to the semi-analytical model based complete cycle.

Therefore, the most convenient solution is to employ the semi-analytical model with barycenter method to be used in the design optimization of the wind energy system. Nevertheless, as it will be demonstrated in the up following chapter, if an appropriate optimization strategy is associated to the analytical model this one can likewise offer good results in an even shorter CPU time. As expected, this will be the subject of the following chapter.

Selected references

[1] Sangkla Kreuawan, *Modelling and optimal design in railway applications.*: Engineering Sciences, Ecole Centrale de Lille, 2008.

[2] E. de Cecco, C. Marchand G. Krebs, "Design approach of an axial motor for electrical powertrain vehicle," *Proc. Int. Conf. Electr. Mach.– ICEM 2012*, 2012.

[3] **Andreea Adriana Laczko (Zaharia)**, S. Brisset and M.M. Radulescu, "Modeling approaches to brushless DC permanent-magnet generator for use in micro-wind turbine applications," *International Conference on Electrical Machines ICEM 2016, IEEE,* 2016.

[4] A. Jaafar, B. Sareni, X. Roboam, J. Belhadj M. Belouda, "Design methodologies for sizing a battery bank devoted to a stand-alone and electronically passive wind turbine system," *Renewable and Sustainable Energy Reviews, Elsevier*, vol. 60, pp. 144-154, 2016.

[5] M. Torrent, J.L. Perat, B. Blanque, B., P. Andrada, "Power Losses in Outside-Spin Brushless D.C. Motors," *Rep. Universitat Politecnica de Catalunya, Barcelona, Spain* , 2004.

[6] Texas Instruments, "230-V, 250-W, High Efficiency BLDC Motor Drive With DC-Bus Voltage Ripple Compensation," Application report.

[7] J. Goupy, *Pratiquer les plans d'expériences*. Paris: Dunod., 2005.

[8] M. H. Hassan, *Méthodologies de conception optimale de systèmes de conversion électromécanique*, Université Paris Sud-Paris XI Doctoral dissertation, Ed., 2014.

[9] STMicroelectronics, PowerMESH IGBTs DataSheet, 2007.

Appendix 3.A

Calculation of µWECS power losses based on barycenter method

A.1 Mechanical losses calculation

The mechanical losses caused by the friction phenomena can be estimated based on [4]:

$$P_{mech} = f_{wt}\Omega^2 \tag{A.1}$$

From the tip speed equation results that the rotational angular speed, Ω, can be linked to the wind speed by relation *(A.2)*:

$$\Omega = k_s v_w \tag{A.2}$$

where k_s is a speed coefficient.

In reference to this, *(A.1)* can be reformulated as:

$$P_{mech} = C_{mech} v_w^2 \tag{A.3}$$

with $C_{mech} = k_s^2 f_{wt}$.

Presuming C_{mech} is constant within one region, the sum of mechanical loss for all the points (*p*) in the considered region (*r*) can be expressed:

$$\sum_{p=1}^{N_r} P_{mech,p} = C_{mech,r} \sum_{p=1}^{N_r} v_{w,p}^2 = C_{mech,r} N_r \langle v_w^2 \rangle_r \tag{A.4}$$

As $C_{mech,r}$ is assumed constant, it can be computed for any point of the region, but the barycenter of the considered area is preferred:

$$C_{mech,r} = \frac{P_{mech,b}}{v_{w,b}^2} = \frac{f_{wt}\Omega_b^2}{v_{w,b}^2} = \frac{f_{wt}\Omega_r^2}{v_{w,r}^2} \tag{A.5}$$

with $v_{w,b} = \langle v_w \rangle_r$ and $\Omega_b = \Omega_r$ the rotational speed computed for the wind speed $v_{w,b}$.

In the end the mechanical losses result as:

$$P_{mech,r} = f_{wt}\Omega_r^2 N_r \frac{\langle v_w^2 \rangle_r}{\langle v_w \rangle_r^2} \tag{A.6}$$

requiring Ω_r, $\langle v_w \rangle_r$, $\langle v_w^2 \rangle_r$ for their resolution.

A.2 Copper losses assessment

The copper loss *Pj*, as a time-varying function, can be expressed for the semi-analytical model as:

$$P_j(t) = R[i_a^2(t) + i_b^2(t) + i_c^2(t)] \tag{A.7}$$

From *(A.7)* the average copper loss can be found by determining the RMS value of one period ($0 \leq t \leq T$) of the function through relations *(A.8)-(A.11):*

$$P_j = \langle P_j(t) \rangle_T = \frac{1}{T}\int_0^T P_j(t)dt \tag{A.8}$$

$$P_j = \frac{R}{T}\int_0^T [i_a^2(t) + i_b^2(t) + i_c^2(t)]\, dt \tag{A.9}$$

$$P_j = R\left[\int_0^T i_a^2(t)dt + \int_0^T i_b^2(t)dt + \int_0^T i_c^2(t)dt\right] \tag{A.10}$$

$$P_j = R\left[I_{RMS\_a}^2 + I_{RMS\_b}^2 + I_{RMS\_c}^2\right] \tag{A.11}$$

where $I_{RMS\_ph} = \sqrt{\frac{1}{T}\int_0^T i_{ph}^2(t)dt}$ represents the equation which determines the quadratic mean for each phase current. If assumed that the phase currents have the same RMS value the losses in the stator windings become:

$$P_j = 3RI_{RMS}^2 \tag{A.12}$$

From the turbine power equation it is assumed that the electromagnetic power of the BLDCPM generator is proportional to the cube of the wind speed. Therefore, the torque can be also considered proportional to the square wind speed as in *(A.13)* and linked to the RMS current by *(A.14):*

$$T_{em} = k_w v_w^2 \tag{A.13}$$

$$T_{em} = k_t I_{RMS} \tag{A.14}$$

where k_w , k_t are speed and torque coefficients.

In this context, *(A.12)* becomes:

$$P_j = C_j v_w^4 \tag{A.15}$$

with $C_j = 3R\left(\frac{k_w}{k_t}\right)^2$. Making the same assumption as before, that C_j is constant within one region, then the sum of copper loss for all the points (p) in the considered region (r) can be written as:

$$\sum_{p=1}^{N_r} P_{j,p} = C_{j,r} \sum_{p=1}^{N_r} v_{w,p}^4 = C_{j,r} N_r \langle v_w^4 \rangle_r \tag{A.16}$$

As $C_{j,r}$ is constant, it can be computed for any point of the region, but again, the barycenter of the considered area is preferred:

$$C_{j,r} = \frac{P_{j,b}}{v_{w,b}^4} = \frac{3RI_{RMS,b}^2}{v_{w,b}^4} = \frac{3RI_{RMS,r}^2}{v_{w,r}^4} \tag{A.17}$$

with $v_{w,b} = \langle v_w \rangle_r$ and $I_{RMS,b} = I_{RMS,r}$ its corresponding current, computed for the wind speed $v_{w,b}$.

Finally,

$$P_{j,r} = \sum_{i=1}^{N_r} P_{j,p} = \frac{3RI_{RMS,r}^2}{v_{w,r}^4} N_r \langle v_w^4 \rangle_r \tag{A.18}$$

$$P_{j,r} = 3RI_{RMS,r}^2 N_r \frac{\langle v_w^4 \rangle_r}{\langle v_w \rangle_r^4} \tag{A.19}$$

and it is based on $I_{RMS,r}$, $\langle v_w \rangle_r$, $\langle v_w^4 \rangle_r$ to be computed.

A.3 Iron loss determination

The iron losses in the stator core of the BLDCPM wind generator can be computed in terms of hysteresis and eddy current losses [5] as:

$$P_{Fe\_hys} = k_{hys} f \left(\hat{B}_{th}^{\alpha} + \hat{B}_{sy}^{\alpha}\right) \tag{A.20}$$

$$P_{Fe\_eddy} = \frac{4}{\pi} k_{eddy} f_{ele}^2 \left(\hat{B}_{th}^2 + 2\hat{B}_{sy}^2\right) \tag{A.21}$$

where $\hat{B}_{th}$, $\hat{B}_{sy}$ are the stator tooth and yoke flux densities, and k_{hys} and k_{eddy} represent the hysteresis and eddy current loss coefficients, which can be calculated from manufacturer data, and f_{ele} is the fundamental frequency, which is given by the pole-pairs number and by the rotor angular speed of the machine:

$$\omega_e = N_p \Omega, \qquad w_e = 2\pi f_{ele} \tag{A.22}$$

Thus, *(A.20)* and *(A.21)* become:

$$P_{Fe\_hys} = k_{hys}\frac{N_p}{2\pi}\left(\hat{B}_{th}^{\alpha} + \hat{B}_{sy}^{\alpha}\right)\Omega \tag{A.23}$$

$$P_{Fe\_eddy} = k_{eddy}\frac{N_p^2}{\pi^3}\left(\hat{B}_{th}^{2} + 2\hat{B}_{sy}^{2}\right)\Omega^2 \tag{A.24}$$

Given also the proportionality of the rotor angular speed of the machine to the wind speed:

$$P_{Fe\_hys} = C_{hys}v_w \tag{A.25}$$

$$P_{Fe\_eddy} = C_{eddy}v_w^2 \tag{A.26}$$

where $C_{hys} = k_s k_{hys}\frac{N_p}{2\pi}\left(\hat{B}_{th}^{\alpha} + \hat{B}_{sy}^{\alpha}\right)$ and $C_{eddy} = k_s^2 k_{eddy}\frac{N_p^2}{\pi^3}\left(\hat{B}_{th}^{2} + 2\hat{B}_{sy}^{2}\right)$.

Considering C_{hys} and C_{eddy} constant within one region then the sum of iron loss for all the points (p) in that region (r) can be written as:

$$\sum_{p=1}^{N_r} P_{Fe\_hys,p} = C_{hys,r}\sum_{p=1}^{N_r} v_{w,p} = C_{hys,r}N_r\langle v_w\rangle_r \tag{A.27}$$

$$\sum_{p=1}^{N_r} P_{Fe\_eddy,p} = C_{eddy,r}\sum_{p=1}^{N_r} v_{w,p}^2 = C_{eddy,r}N_r\langle v_w^2\rangle_r \tag{A.28}$$

As C_{hys} and C_{eddy} are constant, they are computed for the barycenter of the area as:

$$C_{hys,r} = \frac{P_{Fe\_hys,b}}{v_{w,b}} = \frac{k_{hys}\frac{N_p}{2\pi}\left(\hat{B}_{th}^{\alpha} + \hat{B}_{sy}^{\alpha}\right)\Omega_b}{v_{w,b}} = \frac{k_{hys}\frac{N_p}{2\pi}\left(\hat{B}_{th}^{\alpha} + \hat{B}_{sy}^{\alpha}\right)\Omega_r}{v_{w,r}} \tag{A.29}$$

$$C_{eddy,r} = \frac{P_{Fe\_eddy,b}}{v_{w,b}^2} = \frac{k_{eddy}\frac{N_p^2}{\pi^3}\left(\hat{B}_{th}^{2} + 2\hat{B}_{sy}^{2}\right)\Omega_b^2}{v_{w,b}^2} = \frac{k_{eddy}\frac{N_p^2}{\pi^3}\left(\hat{B}_{th}^{2} + 2\hat{B}_{sy}^{2}\right)\Omega_r^2}{v_{w,r}^2} \tag{A.30}$$

with $v_{w,b} = \langle v_w\rangle_r$ and $\Omega_b = \Omega_r$ its corresponding rotational speed, computed for the wind speed $v_{w,b}$.

Finally,

$$P_{Fe\_hys,r} = \sum_{p=1}^{N_{pt}} P_{Fe\_hys,p} = \frac{k_{hys}\frac{N_p}{2\pi}\left(\hat{B}_{th}^{\alpha}+\hat{B}_{sy}^{\alpha}\right)\Omega_r}{v_{w,r}} N_r \langle v_w \rangle_r \tag{A.31}$$

$$P_{Fe\_hys,r} = k_{hys}\frac{N_p}{2\pi}\left(\hat{B}_{th}^{\alpha}+\hat{B}_{sy}^{\alpha}\right)\Omega_r N_r \frac{\langle v_w \rangle_r}{\langle v_w \rangle_r} \tag{A.32}$$

$$P_{Fe\_eddy,r} = \sum_{p=1}^{N_{pt}} P_{Fe\_eddy,p} = \frac{k_{eddy}\frac{N_p^2}{\pi^3}\left(\hat{B}_{th}^{2}+2\hat{B}_{sy}^{2}\right)\Omega_r^2}{v_{w,r}^2} N_r \langle v_w^2 \rangle_r \tag{A.33}$$

$$P_{Fe\_eddy,r} = k_{eddy}\frac{N_p^2}{\pi^3}\left(\hat{B}_{th}^{2}+2\hat{B}_{sy}^{2}\right)\Omega_r^2 N_r \frac{\langle v_w^2 \rangle_r}{\langle v_w \rangle_r^2} \tag{A.34}$$

and it is based on Ω_r, $\langle v_w \rangle_r$, $\langle v_w^2 \rangle_r$ to be computed.

A.4 Conduction and switching losses in the generator-side power electronic converter

The losses in the three-phase power converter based IGBT devices with antiparallel diode units can be classified in conduction and commutation or switching losses [6]. Several of the parameters included in the description of the equation can be encountered in the manufacturer's datasheet [9].

- ***Conduction loss in IGBTs***

As the BLDCPM machine has only two phases active for 120° in an electrical cycle (i.e. one third of the electrical cycle), naturally only two switches will be ON, one corresponding to the upper side and the other to the lower side.

The conduction losses in one transistor can be estimated as:

$$P_{CH1\_T} = \frac{1}{3} f_{mod} V_{CE0} I_{C\_RMS} \tag{A.35}$$

$$P_{CH2\_T} = \frac{1}{3} f_{mod} \left(\frac{V_{CE} - V_{CE0}}{I_{n\_IGBT}}\right) I_{C\_RMS}^2 \tag{A.36}$$

$$I_{C\_RMS} = I_{RMS\_ph} \tag{A.37}$$

Based on *(A.13)* and *(A.14)* the above relation can be rewritten as:

$$P_{CH1\_T} = C_{CH1} v_w^2 \tag{A.38}$$

$$P_{CH2\_T} = C_{CH2} v_w^4 \tag{A.39}$$

whit $C_{CH1} = \frac{k_w}{k_t}\frac{1}{3} f_{mod} V_{CE0}$ and $C_{CH2} = \left(\frac{k_w}{k_t}\right)^2 \frac{1}{3} f_{mod} V_{CE0}$.

Like before, C_{CH1} and C_{CH2} are considered constant for one region, then the conduction losses for all the points in the region are deduced as:

$$\sum_{p=1}^{N_r} P_{CH1\_T,p} = C_{CH1,r} \sum_{p=1}^{N_r} v_{w,p}^2 = C_{CH1,r} N_r \langle v_w^2 \rangle_r \tag{A.40}$$

$$\sum_{p=1}^{N_r} P_{CH2\_T,p} = C_{CH2,r} \sum_{p=1}^{N_r} v_{w,p}^4 = C_{CH2,r} N_r \langle v_w^4 \rangle_r \tag{A.41}$$

Further on the barycenter of the area is calculated:

$$C_{CH1,r} = \frac{P_{CH1\_T,b}}{v_{w,b}^2} = \frac{\frac{1}{3} f_{mod} V_{CE0} I_{C\_RMS,b}}{v_{w,b}^2} = \frac{\frac{1}{3} f_{mod} V_{CE0} I_{C\_RMS,r}}{v_{w,r}^2} \tag{A.42}$$

$$C_{CH2,r} = \frac{P_{CH2\_T,b}}{v_{w,b}^4} = \frac{\frac{1}{3} f_{mod} \left(\frac{V_{CE} - V_{CE0}}{I_{n\_IGBT}} \right) I_{C\_RMS,b}^2}{v_{w,b}^4} = \frac{\frac{1}{3} f_{mod} \left(\frac{V_{CE} - V_{CE0}}{I_{n\_IGBT}} \right) I_{C\_RMS,r}^2}{v_{w,r}^4} \tag{A.43}$$

with $v_{w,b} = \langle v_w \rangle_r$ and $I_{C\_RMS,b} = I_{C\_RMS,r}$ its corresponding current, computed for the wind speed $v_{w,b}$.

At last,

$$P_{CH1\_T,r} = \sum_{p=1}^{N_r} P_{CH1\_T,p} = \frac{\frac{1}{3} f_{mod} V_{CE0} I_{C\_RMS,r}}{v_{w,r}^2} N_r \langle v_w^2 \rangle_r \tag{A.44}$$

$$P_{CH1\_T,r} = \frac{1}{3} f_{mod} V_{CE0} I_{C\_RMS,r} \, N_r \frac{\langle v_w^2 \rangle_r}{\langle v_w \rangle_r^2} \tag{A.45}$$

$$P_{CH2\_T,r} = \sum_{p=1}^{N_r} P_{CH2\_T,p} = \frac{\frac{1}{3} f_{mod} \left(\frac{V_{CE} - V_{CE0}}{I_{n\_IGBT}} \right) I_{C\_RMS,r}^2}{v_{w,r}^4} N_r \langle v_w^4 \rangle_r \tag{A.46}$$

$$P_{CH2\_T,r} = \frac{1}{3} f_{mod} \left(\frac{V_{CE} - V_{CE0}}{I_{n\_IGBT}} \right) I_{C\_RMS,r}^2 N_r \frac{\langle v_w^4 \rangle_r}{\langle v_w \rangle_r^4} \tag{A.47}$$

relying on $I_{C\_RMS,r}$, $\langle v_w \rangle_r$, $\langle v_w^2 \rangle_r$, $\langle v_w^4 \rangle_r$ to be computed.

The total conduction losses on all the transistors result:

$$P_{cond\_IGBT,r} = 6\left(P_{CH1\_T,r} + P_{CH2\_T,r}\right) \tag{A.48}$$

- ***Switching loss in the IGBTs***

The switching losses in one transistor can be computed starting from the following expression:

$$P_{sw\_IGBT} = \frac{1}{3}(E_{ON} + E_{OFF})\frac{V_n}{V_{CC(test)}I_{CC(test)}} I_{C\_pk}\, f_{sw} \tag{A.49}$$

where I_{C_pk} is calculated for a 110% overload of the generator winding current.

A simplification of the above mentioned equation is:

$$P_{sw\_IGBT} = C_{sw\_IGBT} v_w^2 \tag{A.50}$$

with $C_{sw\_IGBT} = \frac{k_w}{k_t}\frac{1}{3}(E_{ON} + E_{OFF})\frac{V_n}{V_{CC(test)}I_{CC(test)}} f_{sw}$.

If C_{sw} were to be constant in the considered region, the switching losses of all the points in the region result as:

$$\sum_{p=1}^{N_r} P_{sw\_IGBT,p} = C_{sw\_IGBT,r} \sum_{p=1}^{N_r} v_{w,p}^2 = C_{sw\_IGBT,r} N_r \langle v_w^2 \rangle_r \tag{A.51}$$

The calculation of C_{sw} follows on for the barycenter of the considered area:

$$C_{sw\_IGBT,r} = \frac{P_{sw\_IGBT,b}}{v_{w,b}^2} = \frac{\frac{1}{3}(E_{ON} + E_{OFF})\frac{V_n}{V_{CC(test)}I_{CC(test)}} I_{C\_pk\,,b}\, f_{sw}}{v_{w,b}^2}$$

$$= \frac{\frac{1}{3}(E_{ON} + E_{OFF})\frac{V_n}{V_{CC(test)}I_{CC(test)}} I_{C\_pk\,,r}\, f_{sw}}{v_{w,r}^2} \tag{A.52}$$

with $v_{w,b} = \langle v_w \rangle_r$ and $I_{C\_pk\,,b} = I_{C\_pk\,,r}$ the corresponding current, computed for the wind speed $v_{w,b}$.

Finally,

$$P_{sw\_IGBT,r} = \sum_{p=1}^{N_r} P_{sw\_IGBT,p} = \frac{\frac{1}{3}(E_{ON} + E_{OFF})\frac{V_n}{V_{CC(test)}I_{CC(test)}} I_{C\_pk\,,r}\, f_{sw}}{v_{w,r}^2} N_r \langle v_w^2 \rangle_r \tag{A.53}$$

$$P_{sw\_IGBT,r} = \frac{1}{3}(E_{ON} + E_{OFF})\frac{V_n}{V_{CC(test)}I_{CC(test)}} f_{sw} I_{C\_pk\,,r} N_r \frac{\langle v_w^2 \rangle_r}{\langle v_w \rangle_r^2} \tag{A.54}$$

and they depend on $I_{C\_pk,r}$, $\langle v_w \rangle_r$, $\langle v_w^2 \rangle_r$ to be assessed.

- ***Diode losses due to:***

A) PWM switching of the transistors

Whenever during the 120° conduction interval when the upper IGBT turns off during PWM switching the phase current is channeled through the antiparallel diode of the lower IGBT and vice versa. Therefore, the energy that may be dissipated by a diode during a conduction interval can be formulated as in *(A.54).* To be noted that the recovery switching losses in the diode are excluded.

$$P_{sw\_diode} = \frac{1}{3}(1 - f_{mod})V_F I_{C\_RMS} \tag{A.55}$$

Through reformulation:

$$P_{sw\_diode} = C_{sw\_diode} v_w^2 \tag{A.56}$$

where $C_{sw\_diode} = \frac{k_w}{k_t}\frac{1}{3}(1 - f_{mod})V_F$.

Considering C_{sw_diode} constant within one region, then the sum of switching losses in the diode for all the points in that region are:

$$\sum_{p=1}^{N_r} P_{sw\_diode,p} = C_{sw\_diode,r} \sum_{p=1}^{N_r} v_{w,p}^2 = C_{sw\_diode,r} N_r \langle v_w^2 \rangle_r \tag{A.57}$$

The computation of C_{sw_diode} for the barycenter of one particular region is based on:

$$C_{sw\_diode,r} = \frac{P_{sw\_diode,b}}{v_{w,b}^2} = \frac{\frac{1}{3}(1 - f_{mod})V_F I_{C\_RMS,b}}{v_{w,b}^2} = \frac{\frac{1}{3}(1 - f_{mod})V_F I_{C\_RMS,r}}{v_{w,r}^2} \tag{A.58}$$

with $v_{w,b} = \langle v_w \rangle_r$ and $I_{C\_RMS,b} = I_{C\_RMS,r}$ the corresponding current, computed for the wind speed $v_{w,b}$.

On this basis,

$$P_{sw\_diode,r} = \sum_{p=1}^{N_r} P_{sw\_diode,p} = \frac{\frac{1}{3}(1 - f_{mod})V_F I_{C\_RMS,r}}{v_{w,r}^2} N_r \langle v_w^2 \rangle_r \tag{A.59}$$

$$P_{sw\_diode,r} = \frac{1}{3}(1 - f_{mod})V_F I_{C\_RMS,r} N_r \frac{\langle v_w^2 \rangle_r}{\langle v_w \rangle_r^2} \tag{A.60}$$

and requests $I_{C\_RMS,r}$, $\langle v_w \rangle_r$, $\langle v_w^2 \rangle_r$ for computation.

B) Phase commutation

During the commutation interval, as mentioned in *chapter 2*, a freewheeling path of the phase current appears through the antiparallel diode of the commutating IGBT. As a reminder, this commutation period represents the time required by the current of the commutating phase to disappear. As one electrical cycle exposes six commutations of the phases, the diode loss caused by this phenomena is computed as:

$$P_{comm\_diode} = 6V_F I_{F\_AVG} T_{comm} f_{ele} \tag{A.61}$$

where $I_{F\_AVG} = I_{C\_pk}/2$ is the average forward current of the diode during commutation.

Again, through substitution *(A.61)* can be reformulated as:

$$P_{comm\_diode} = C_{comm\_diode} v_w^2 \tag{A.62}$$

where $C_{comm\_diode} = \frac{k_w}{k_t} 6V_F T_{comm} f_{ele}$ and if assumed constant within one region, it helps to determine for all the points in that region the total diode loss caused by phase commutation:

$$\sum_{p=1}^{N_r} P_{comm\_diode,p} = C_{comm\_diode,r} \sum_{p=1}^{N_r} v_{w,p}^2 = C_{comm\_diode,r} N_r \langle v_w^2 \rangle_r \tag{A.63}$$

For computing C_{comm_diode} for the barycenter of the region, the following equation is employed:

$$C_{comm\_diode,r} = \frac{P_{comm\_diode,b}}{v_{w,b}^2} = \frac{6V_F T_{comm} f_{ele}\, I_{F\_AVG,b}}{v_{w,b}^2} = \frac{6V_F T_{comm} f_{ele}\, I_{F\_AVG,r}}{v_{w,r}^2} \tag{A.64}$$

with $v_{w,b} = \langle v_w \rangle_r$ and $I_{F\_AVG,b} = I_{F\_AVG,r}$ the corresponding current, computed for the wind speed $v_{w,b}$.

Ultimately,

$$P_{comm\_diode,r} = \sum_{p=1}^{N_r} P_{comm\_diode,p} = \frac{6V_F T_{comm} f_{ele}\, I_{F\_AVG,r}}{v_{w,r}^2} N_r \langle v_w^2 \rangle_r \tag{A.65}$$

$$P_{comm\_diode,r} = 6V_F T_{comm} f_{ele}\, I_{F\_AVG,r} N_r \frac{\langle v_w^2 \rangle_r}{\langle v_w \rangle_r^2} \tag{A.66}$$

and requires $I_{F\_AVG,r}$, $\langle v_w \rangle_r$, $\langle v_w^2 \rangle_r$ to be determined.

Chapter 4

Design Optimization of the BLDCPM Generator over Wind-Speed Cycle Operation

4.1 Introduction

The design stage of any component or system lien in determining all its characterizing parameters that best describe the objective requirements. The optimal design of the BLDCPM generator for micro-wind turbine applications in order to solve a specific objective function, which in this case is the total power losses minimization under one year wind-speed cycle operation, depends on the appropriate selection of the multiple design parameters. Due to their non-linearity interdependency, this task becomes highly difficult and complex. Therefore, optimization represents the suitable solution for the determination of an appropriate design. Due to the many operating points within the wind-speed cycle and because the optimization process requires many evaluations of the objective function, adapted models and wind cycle reduction methods have to be considered by using the results obtained in previous chapters.

The next step is to establish the architecture of the design optimization process, by determining the optimization algorithm and strategy that need to be properly accommodated with the μWECS model.

4.1.1 Sources of complexity in the optimal design of a system

The optimization may be used as a tool for better understanding the complexity of the design problem as it provides a global view of the design space and for determining the feasible result from an assembly of possible design solutions. The incorporated algorithm helps to collect information from the models to determine the variation direction of the design variables considered in searching for the optimal system configuration while satisfying several imposed constraints. However, the solution and the final decision relies very much on the designer experience.

The design process as presented in *fig. 4.1*, starts from a set of initial/input specifications which pass through several phases before the final decision is made. The second phase after the analysis of the input specifications is represented by the mathematical formulation of the design and optimization problem.

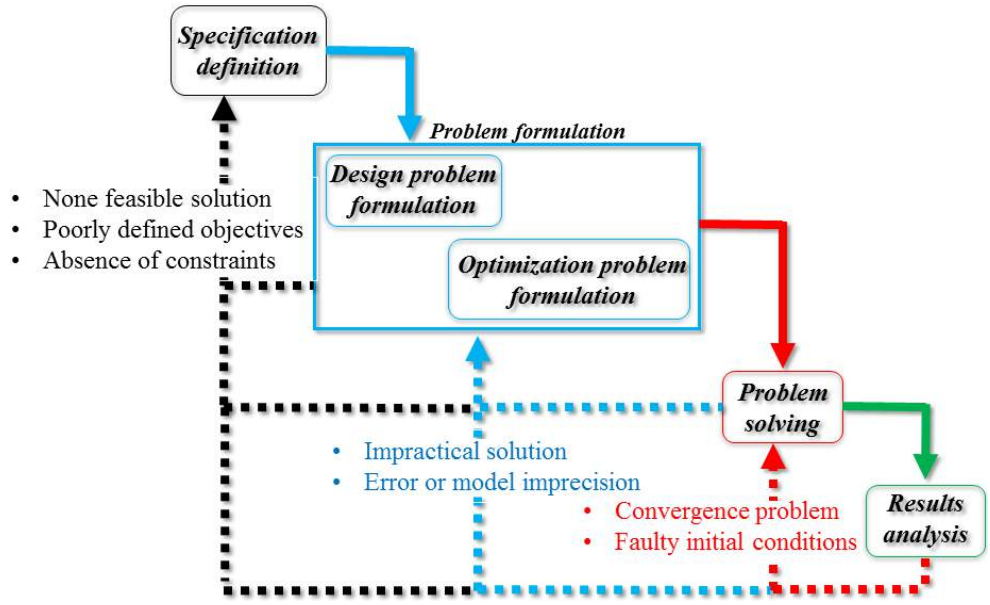

Fig. 4.1. Schematic representation and possible problems of the design optimization process

At this stage, the geometric and physical relations that characterize the behavior of each component in the system are all put together to form the model of the considered system. It is however quite difficult to take into account all the physical phenomena that may appear in each component, therefore, a certain level of hypothesis is a priority in the modeling phase of the design process in order to lower its complexity. This phase represents also the part where the design variables and constraints of the system are selected, which correspond to the geometric, energetic and structural parameters of the system in cause. In the early development phases their number may be fairly high due to the many unknown parameters in the system.

Afterwards the optimization problem can be expressed by designating specific upper and lower limit values to the design variables, by imposing several constraints that have to be analyzed on the input/outputs of the design process of the system and by establishing the desired design objective functions. The aim is to find those optimum parameters that honor those constraints whilst minimizing or maximizing different criteria. The solving of the optimization problem can be done by means of various algorithms (SQP, GA, PSO, etc.) and techniques (Response Surface, Space Mapping, Efficient Global Optimization, etc.). The last step in the design process comprises the analysis of the obtained results and the decision making. Nevertheless, multiple problems [1] can occur in the analysis of design optimization results, which may impose deeper investigations of earlier design phases or even changing the initial design specification parameters (*fig. 4.1*).

Furthermore, the design of electrical systems has become a complex task due to the presence of multiple different elements in interaction within the system to be designed. The difficulties that arise are related to the coexistence of various physical domains of system

components, which, optimized separately, lead to sub-optimal designs. The existence of these couplings in the same system presses the need of considering the system as a whole, meaning that the design of a component has to depend on the others for achieving optimal results. This approach becomes even more relevant as the number of components in the design chain is greater, as represented in *fig. 4.2*.

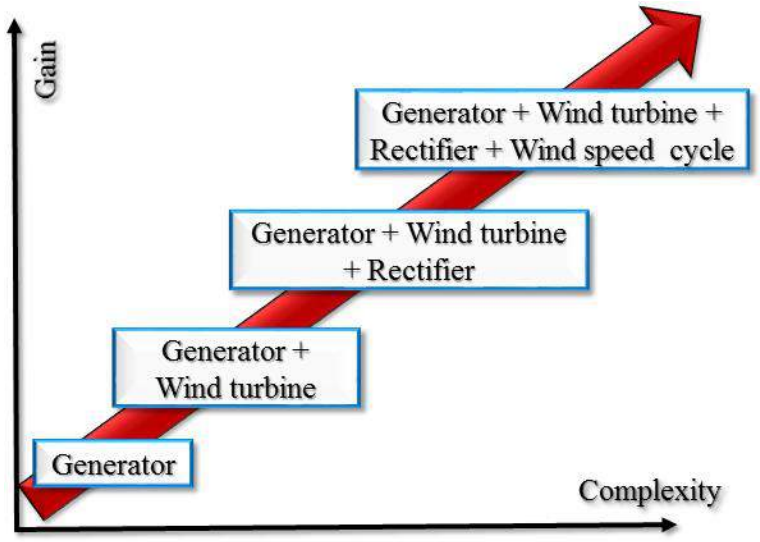

Fig. 4.2. Gain vs. complexity by integration of μWECS components design

4.1.2 Design optimization

As the objective is to find the optimum variables that allow attaining the best technical and/or economical performances, mathematical formulation of the constrained optimization problem with one or multiple objectives represents an important issue of the design optimization process:

$$\begin{aligned} &\min_{X} && f_o(X) && o = 1, \dots, m \\ &subject\ to && g_i(X) \leq 0 && i = 1, \dots, n_g \\ & && h_j(X) = 0 && j = 1, \dots, n_h \end{aligned} \tag{4.1}$$

where $X = [x_1, x_2, \dots, x_{n_v}] \in S$ represents the vector of design variables, that express the physical quantities such as geometric, electric, mechanic, etc. written in a mathematical form and upon which changes can intervene in order to better improve the desired performances of the system. As they can be of several types the design space (S) for each of them can be defined as [1]:

- $S: x_k^L \leq x_k \leq x_k^U, \quad x_k \in \mathcal{R}$ - for continuous design variables (x_k) where each of them has an upper (U) and a lower (L) bound

- $S: x_k \in S_k$ - for discrete design variables where each of them has a finite set of values

The terms $g_i(X)$ and $h_j(X)$ in the above general optimization problem represent the inequality and equality constraints that have to be respected for optimal solution.

4.1.3 Difficulties in design optimization

As stated before, the computation time is of great importance to the optimization process due to the many evaluations of the simulation model involved, by the optimization algorithm. It is possible to highlight some of the factors that may affect the time needed to arrive at the optimum design of the system:

- The number of design variables and constraints
- The nature of the design space : continue, discrete or mixed
- The nature of the optimization problem: constrained, non-constrained
- Number of objectives

Fig. 4.3. Importance of the simulation time for the design optimization process

Moreover, the opportunity of different modeling level becomes also a problem for the design optimization due to multi-physics phenomena of the different components in the system. Three types of models can be exploited with different precision and response time:

- The analytical model expresses the system phenomena through multiple equations, being based on many hypothesis and simplifications which make it fast but in general not very accurate.
- The semi-analytical model allows taking into consideration some electromagnetic nonlinearities in solving nonlinear equations, providing good trade-off among precision and computation time.
- The FE-based numerical model is the most precise among all, as local saturation, among other distributed quantities can be computed. Still, it can be quite time consuming depending on the density of the generated mesh.

In the end, the significance of the computation time for the optimization process is as classified in [2] and depicted in *fig. 4.3*.

4.2. Formulation of the µWECS design optimization problem

Before describing the optimization approaches [3] and the results obtained for the design of the BLDCPM generator, the objectives, variables and imposed constraints of the µWECS model are introduced in the next sections.

4.2.1 Objective function

The objective function proposed for resolution is:

- ***The minimization of the overall power losses in the µWECS over a long-term wind-speed cycle operation***.

These losses consist of mechanical losses in the turbine (P_{mech}), copper (P_j) and iron (P_{fe}) losses in the generator, conduction and switching (P_{conv}) losses in the power converter, the power flow in the system being represented by *fig. 4.4*.

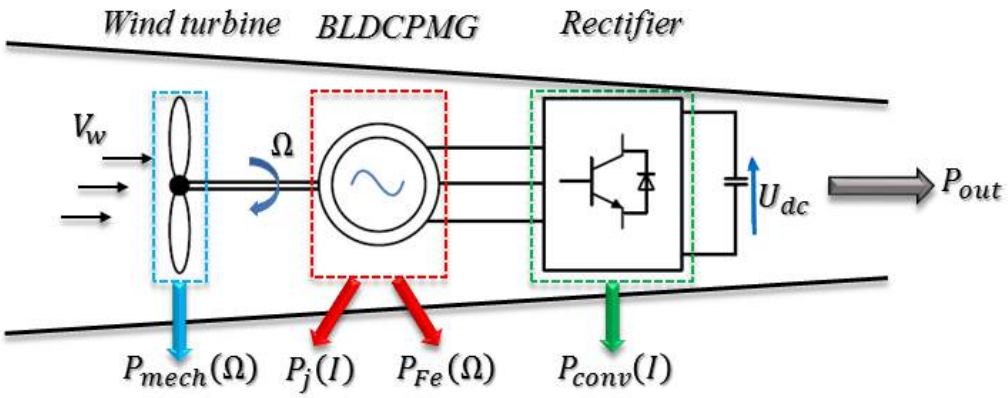

Fig. 4.4. Power flow in the wind energy conversion system

The optimization problem can be therefore formulated as:

$$\boldsymbol{min}\left(\boldsymbol{OF}(\boldsymbol{X}) = \boldsymbol{P_{total\_loss}}\right) = \boldsymbol{min}\left(\boldsymbol{P_{mech\_t}} + \boldsymbol{P_{j\_t}} + \boldsymbol{P_{Fe\_t}} + \boldsymbol{P_{conv\_t}}\right) \quad (4.2)$$

It can be stated that minimizing the total losses in the system implies maximizing the output useful power.

4.2.2 Design variables and constraints

The continuous (c) and discrete (d) type design variables of the wind energy system considered to be optimized, as well as those fixed at a certain value are summarized in *table 4.1*, along with their nature and variation domain.

Table 4.1. List of the μWECS design variables

Component	Variable	Notation	Type	To optimize ?	Definition domain	Unit
Wind turbine	Rotor blade radius	R_{wt}	c	Fixed	1.5	[m]
	Friction coefficient	f_{wt}	c	Fixed	0.025	[Nm/rad]
	Cut-in wind speed	v_{in}	c	Yes	[1÷4]	[m/s]
	Nominal wind speed	v_n	c	Yes	[4÷20]	[m/s]
	Cut-off wind speed	v_{max}	c	Yes	[20÷25]	[m/s]
Generator	Number of pole pairs	p	d	Yes	{2,…,20}	-
	Number of phases	m	c	Fixed	3	-
	Stator bore diameter	D_s	c	Yes	[100÷500]	[mm]
	Magnetic length	L_m	c	Yes	[50÷500]	[mm]
	Air gap thickness	g	c	Yes	[0.5÷5]	[mm]
	Ratio length rotor/stator	r_{rs}	c	Yes	[1÷1.2]	-
	Stator's laminated filling factor	k_{st}	c	Fixed	0.95	-
	Slot copper filling coefficient	k_r	c	Fixed	0.5	-
	Remnant induction of the magnets	B_r	c	Fixed	1	[T]
	Peak magnetic induction in the airgap	$\hat{B}_g$	c	Yes	[0.5÷1]	[T]
	Peak magnetic induction in the rotor yoke	$\hat{B}_{ry}$	c	Yes	[0.6÷1.6]	[T]
	Peak magnetic induction in the stator yoke	$\hat{B}_{sy}$	c	Yes	[0.6÷1.6]	[T]

	Peak magnetic induction in the stator teeth	$\hat{B}_{th}$	c	Yes	[0.6÷1.8]	[T]
	Current density	δ_{dens}	c	Yes	[0.5÷8]	[A/mm^2]
	Ratio DC voltage/EMF	k_v	c	Yes	[0.5÷10]	-
Rectifier	Commutation frequency	f_{sw}	c	Yes	[1÷30]	[kHz]
	DC bus voltage	V_{dc}	c	Yes	[48÷300]	[V]
	Number of IGBTs in parallel	n_{IGBT}	d	Fixed	-	-

- *Micro-wind turbine variables for design optimization*

As a direct coupling between the wind turbine and electrical generator is considered in this work the performance operating points of the wind turbine, i.e. the cut-in, rated and cut-off wind speeds are set as variables to be optimized in order to provide the optimal turbine power curve and consequently the nominal power of the generator. As they strongly influence the length of the wind profile to be considered in the calculation of the wind energy system power losses and due to the nature of the employed optimization algorithm, their range of definition is slightly narrowed so that the turbine to start its operation at a cut-in wind speed less than the average wind of the profile. The cut-off wind speed is chosen to prevent the forces acting on the turbine structure at high wind speeds to damage the rotor. Depending on the design cost of the wind turbine a lower value can be set for this parameter, however in this work its proposed definition domain was favored to assess the large amount of data within the wind speed profile.

- *BLDCPM generator variables for design optimization*

The three-phase stator-winding generator imposes that the number of pole pairs to be set as a discrete variable due to the fact that only the even values can be retained for feasible winding configuration. Another important aspect is that the magnetic induction in the different parts of the generator are also appointed as variables to be optimized to avoid multiplying the constraints on the system model.

- *Generator-side rectifier variables for design optimization*

Regarding the rectifier, as only the power losses are going to be determined, the parameters considered for optimization are the commutation frequency and the DC bus voltage.

The many design variables to be optimized may lead to non-feasible configurations as results of the optimization process. To resolve this difficulty it is important to impose several constraints, which are implemented simply as nonlinear inequality constraints in order to:

- Assure that the output power generated at cut-in wind speed overcomes the power losses in the system:

$$g_1(X): P_{out\_vin} \geq 0 \ [W] \tag{4.3}$$

- Limit the inner diameter of the generator for mechanical reasons:

$$g_2(X): D_{int} \geq 80 \ [mm] \tag{4.4}$$

- Narrow the thickness range of the magnet to avoid a large volume of these parts:

$$g_3(X): h_{pm} \leq 6 \ [mm] \tag{4.5}$$

- Lead to a feasible geometry. To determine the depth of the main stator tooth, a second order equation needs to be resolved, which imposes that its determinant to be considered as constraint by the optimization process [4]:

$$g_4(X): det(D_s, \delta_{dens}, B_{th}, B_g) \geq 0 \tag{4.6}$$

- Ensure that the maximum temperature in the stator windings does not exceed a critical limit:

$$g_5(X): T_{Cu} \leq 130 \ [°C] \tag{4.7}$$

- Guarantee that the magnets can support a current in the phase windings three times the rated current without demagnetization:

$$g_6(X): I_{ph} \leq \frac{I_{max}}{3} \ [A] \tag{4.8}$$

- Achieve a sufficiently small rising time of the phase current:

$$g_7(X): time\_I_{ph} \leq \frac{1}{30 f_{ele}} \ [s] \tag{4.9}$$

where f_{ele} represents the generator frequency.

- Limit the hysteresis band-width of stator current :

$$g_8(X): \frac{\Delta i}{I_{ph}} \leq 0.1 \tag{4.10}$$

- Ensure that the generator mass is less than an imposed value:

$$g_9(X): M_{gen\_t} \leq 20\ [kg] \tag{4.11}$$

- Achieve a good efficiency of the generator over the entire wind cycle, obtained as the ratio between the total output energy $\left(\sum_{i=1}^{N}\langle P_{out\_gen}\rangle_i \cdot \Delta t_i\right)$ of the generator and the total input energy given by the wind turbine $\left(\sum_{i=1}^{N}\langle P_{in\_wt}\rangle_i \cdot \Delta t_i\right)$, with N being the number of wind speeds within the considered wind profile:

$$g_{10}(X): \eta_{gen\_cycle} \geq 0.9 \tag{4.12}$$

4.2.3. Proposed method for design optimization problem resolution

The above problem formulation becomes a constrained mono-objective optimization that appeals to a global algorithm for mixed variables, in particular an evolutionary method based genetic algorithm (GA) [5] from the Matlab® environment to find the geometrical and electrical features that satisfy the problem constraints while performing the minimization of the wind energy system power losses over a long-term wind speed profile.

The reason for choosing an evolutionary method for problem resolution was based on their competence on finding the global optimum of the wind energy system objective function, as they do not require to initialize the design variables at the starting of the process nor the knowledge of the function's gradient for optimal solution, as the deterministic methods do. However, they do oblige that several executions to be performed with the same algorithm parameters in order to take into account their stochastic nature. The considered control parameters of the genetic algorithm are those listed in *table 4.2.*

Table 4.2. Genetic algorithm control parameters used for the optimization process

Population size	500
Number of generations	100*number of design variables
Crossover Probability	0.8
Mutation Rate	1/number of design variables

This genetic algorithm is based on naturel selection, meaning that the individuals from a population that present the best adaptation to their environment demonstrate great survival and reproduction probability, thereby their offspring will also show an even better accommodation feature. The main parameters that control the reproduction ability of the population are the crossover and mutation rate of the chromosomes within the individual's genes. In optimization an individual is considered adapted to the environment if it satisfies the optimization constraints. A general representation of the genetic algorithm is presented in *fig.*

4.5. The beginning of the genetic algorithm corresponds to a random initialization of the population with certain number of individuals. The next step is to evaluate the performances of each individual and the most adapted ones are selected for the creation of the next generation and submitted to crossover and mutation operations.

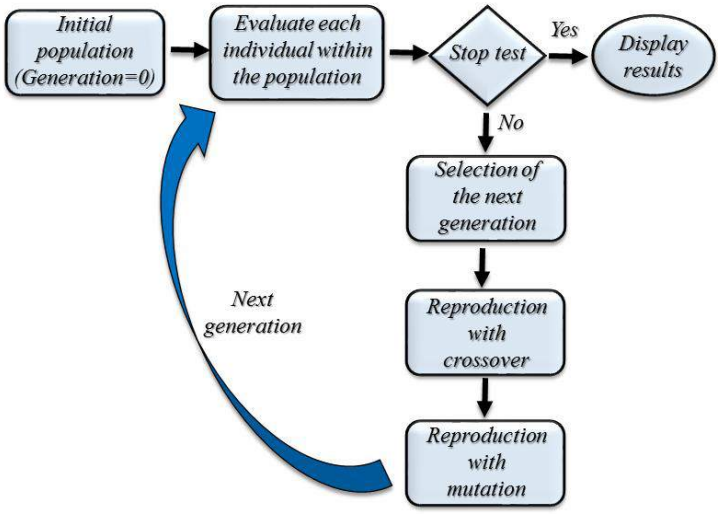

Fig. 4.5. Schematic representation of the standard genetic algorithm principle

To better observe how this algorithm heads towards the global solution the *"wave"* function from Matlab environment was chosen as example for finding the location where the function presents its highest peak (*fig. 4.6*).

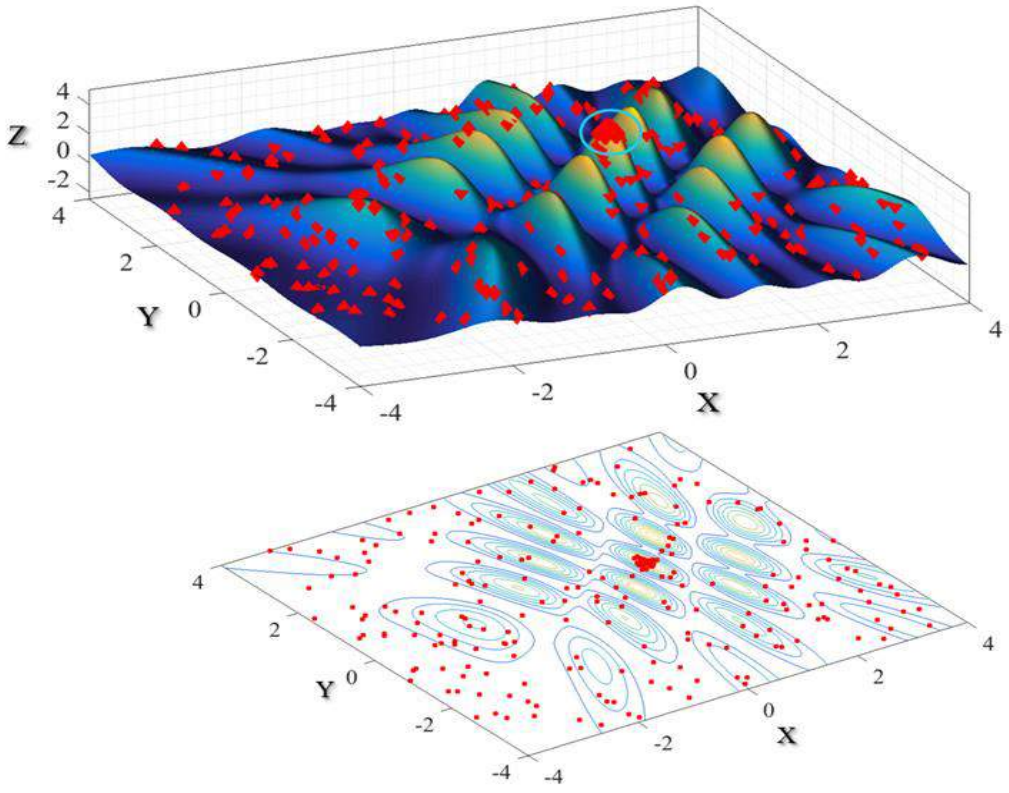

Fig. 4.6 Global maximum searching based on genetic algorithm applied to Matlab *"wave"* function

It finds the best values $x = 1.2608$ and $y = 0.5692$ for the maximum global of the function represented by $z = 4.37$. It is important to add that the optimum results will vary based on the random start points of the solver. Another run of this example with genetic algorithm may give different results for x and y but for the same z.

4.3 Optimization methodology and results of the BLDCPM generator design optimization under wind-speed cycle operation

The results presented throughout this chapter were obtained on MATLAB® R2014b with an Intel® Core ™ i7, 2.40GHz, 4 cores, 8 logical processors and 16GB of RAM. The use of 7 logical processors is employed in parallel by using the command $parpool(7)$ within the parallel computing toolbox of MATLAB.

4.3.1 Single level optimization approach

As expected the first optimization is performed, based on few initial data and specifications, upon the semi-analytical model with barycenter method, as it denotes more precision than the analytical one. Only six regions are chosen to partition the wind cycle and approximate the power losses in the wind energy system, as an acceptable relative error was found in *chapter 3* for this number of barycenters when applied to a reference machine. The workflow of the global optimization process incorporating GA algorithm, as well as the simulation model and the sizing equations of the machine is illustrated by the schematic representation from *fig. 4.7.*

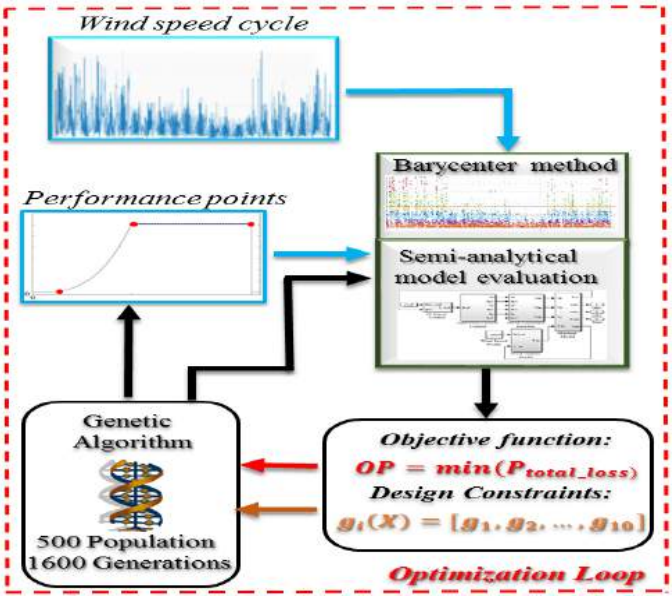

Fig. 4.7. Schematic representation of the optimization process based semi-analytical simulation model with barycenter method

Despite the elevated number of design variables and constraints, the semi-analytical model with barycenter method is able to yield an optimum solution. Once the optimization is finished it is important to verify the results obtained. This can be done at the system level by evaluating the semi-analytical model over complete wind cycle operation with the optimum results, *table 4.3* presenting a comparison for some output quantities of these two models. The proximity between the results can be easily remarked. It is obtained like this a reference (semi-analytical with complete cycle) that allows to compare the other optimization approaches.

Table 4.3. Comparative design output quantities

	Semi-analytical model with complete cycle	***Semi-analytical model with barycenter method***
No. of operating points	8,759	6
Total input power [kW]	≈ 2,866	≈ 2,856
Total power losses [kW]	≈ 501	≈ 500
Total mechanical losses [kW]	101.9	101.8
Total joule losses [kW]	94.7	94.8
Total iron losses [kW]	83.7	83.6
Total converter losses [kW]	221	219.7
Total output power [kW]	≈ 2,365	≈ 2,356
System efficiency	0.8251	0.8249

The second direction in this section is to perform the optimization upon the analytical simulation model based on the same workflow of the optimization process as the one depicted in *fig. 4.7* for the semi-analytical model. The optimization time and number of model evaluations for both optimizations are summarized in *table 4.4*.

Table 4.4 Analytical and semi-analytical models comparison

	Analytic with complete cycle	**Semi-analytic with barycenter method**
No. of operating points	8,759	6
Optimization time	≈ 10 [min]	≈ 13406 [min]
Number of model evaluations	492,501	129,001

Likewise, some of the same output quantities from *table 4.3,* achieved from the optimization process based analytical model were used to make a comparison (*fig. 4.8*) to the previously determined after optimization results of the semi-analytical model with complete wind cycle. However, the feedback of this comparison is not the one aspired as the analytical model presents values for the parameters quite far from those of the semi-analytical model, which is considered as reference given its better accuracy.

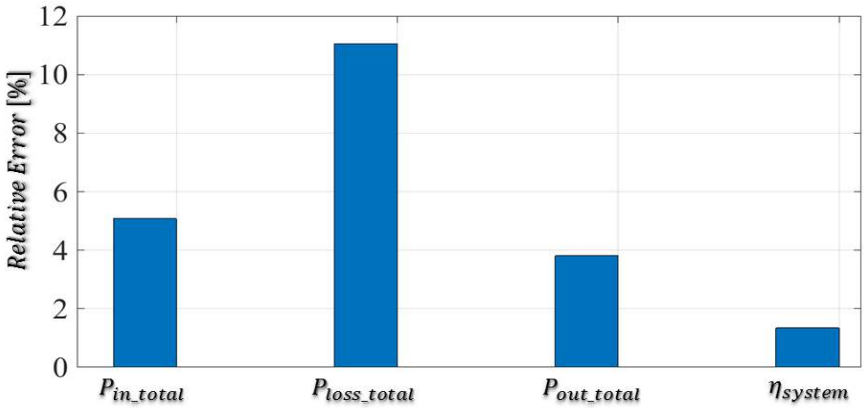

Fig. 4.8 Discrepancy between analytical and semi-analytical optimization results for several output quantities

Nonetheless, as seen above, its optimization time is rather remarkable compared to the one of the semi-analytical model, given the number of model evaluations. The idea that arises is to determine if it is possible to take advantage of this model and affiliate to it an iteratively correction strategy so that get almost the same results as those obtained after realizing the optimization with the semi-analytical model, but in a shorter CPU time.

4.3.2 Two-level optimization approach

For a refining of the optimization results with the analytical model, a correction strategy that uses evaluations of the semi-analytical model associated to the barycenter method is proposed and implemented in the two level optimization approach, as presented in *fig. 4.9.*

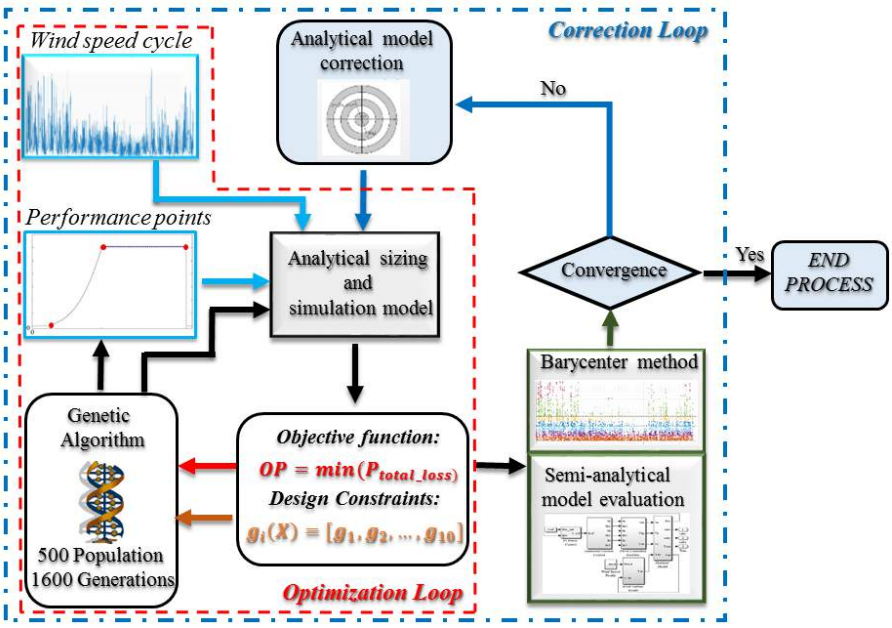

Fig. 4.9 Schematic representation of the correction process of the analytical simulation model

One important aspect should be specified, namely, as a comparison to the optimization approach with semi-analytical model with barycenter method is foreseen in this subchapter and due to the stochastic nature of the GA algorithm, the respective objective function is reformulated as a goal attainment problem and transformed into a distance minimization function by imposing a certain reference value (y) to be reached, which in this case is represented by the value of the total power losses obtained in the single level optimization approach with the semi-analytical model:

$$\min_{X} \quad \| OF(X) - y \|, \qquad with\ y = 500\ [kW] \tag{4.13}$$

As seen in the *section 4.3.1*, some differences arise between the optimization results of the analytical and semi-analytical models under complete cycle operation. This issue is fixed by building a surrogate model that includes the analytical model and a correction on its outputs. This correction is calculated by evaluating the obtained configuration with the semi-analytical model outside the optimization loop, following to apply it to the analytical model at the next iteration. The optimization process is started again until the discrepancy between the surrogate model and the semi-analytical model with barycenter method is small enough.

The stop criterion of the correction loop (*fig. 4.10*) is:

$$\frac{\left| P^{k}_{loss\_total\_SAb} - P^{k}_{loss\_total\_SU} \right|}{\left| P^{k}_{loss\_total\_SAb} \right|} < 10^{-3} \tag{4.14}$$

where the indexes *SAb* and *SU* correspond to the semi-analytical model associated to the barycenter method and surrogate model, respectively, while k denotes the iteration.

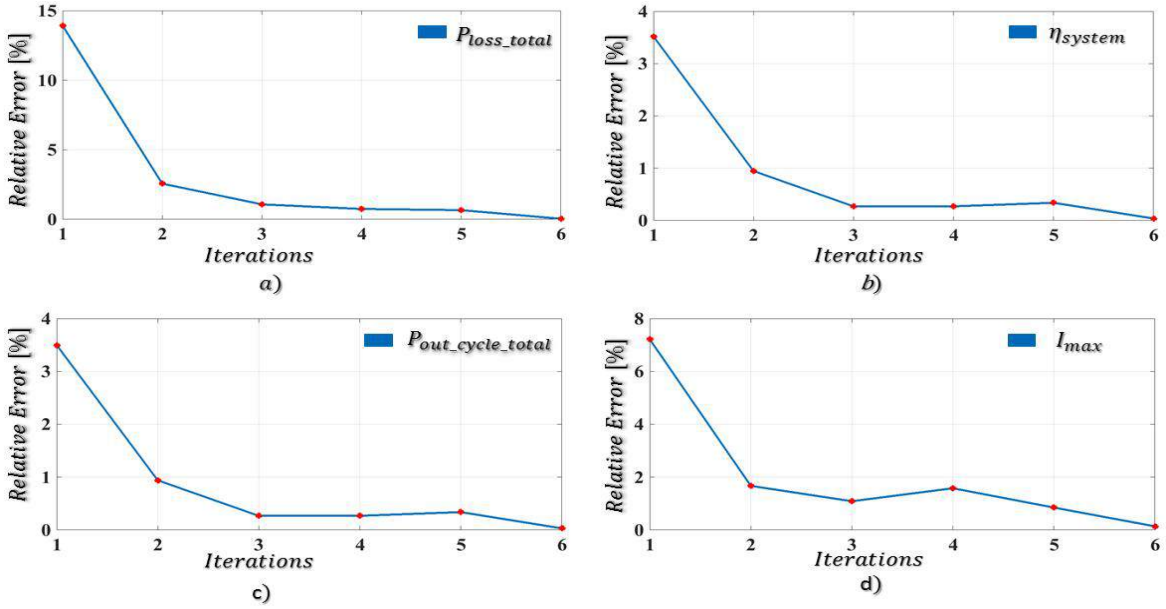

Fig. 4.10 Convergence history for the a) total global losses in the wind turbine system, b) system efficiency, c) total output power over the wind cycle and d) maximum base current

The convergence history for some particular output variables are displayed in *fig. 4.10.*

The optimal results found at the 6th iteration are again confronted to those of the semi-analytical model with complete cycle from *section 4.3.1* in terms of design variables and electromagnetic characteristics, being summarized in *table 4.5*.

Table 4.5. Design optimization results

Parameter	Unit	Surrogate model with complete cycle	Semi-analytical model with complete cycle
Design variables			
$\boldsymbol{v_{in}}$	$[m/s]$	2.9	2.96
$\boldsymbol{v_n}$	$[m/s]$	9.77	9.71
$\boldsymbol{v_{max}}$	$[m/s]$	21.33	21.37
$\boldsymbol{N_p}$		10	12
$\boldsymbol{D_s}$	$[mm]$	216	250
$\boldsymbol{L_m}$	$[mm]$	76	58
$\boldsymbol{g}$	$[mm]$	1.1	1.16
$\boldsymbol{r_{rs}}$		1.128	1.153
$\boldsymbol{\widehat{B}_g}$	$[T]$	0.63	0.64
$\boldsymbol{\widehat{B}_{ry}}$	$[T]$	1.52	1.51
$\boldsymbol{\widehat{B}_{sy}}$	$[T]$	1.22	1.32
$\boldsymbol{\widehat{B}_{th}}$	$[T]$	1.71	1.7
$\boldsymbol{\delta_{dens}}$	$[A/mm^2]$	3.42	2.8
$\boldsymbol{k_v}$		2.55	2.39
$\boldsymbol{f_{sw}}$	$[kHz]$	25.8	24.9
$\boldsymbol{V_{dc}}$	$[V]$	263	234
Optimization function (P_{loss_total})			
$\boldsymbol{OF(X)}$	$[kW]$	500	500
Electromagnetic parameters of the BLDCPM generator			
$\boldsymbol{R_{ph}}$	$[ohm]$	0.14	0.095
$\boldsymbol{L_{ph}}$	$[mH]$	3.7	2.5
$\mathbf{P}_{\boldsymbol{b}}$	$[W]$	1,734	1,716
Geometric parameters of the BLDCPM generator			
$\boldsymbol{D_{int}}$	$[mm]$	155	185
$\boldsymbol{D_{ext}}$	$[mm]$	240	274
$\boldsymbol{l_{th}}$	$[mm]$	12.47	12.43
$\boldsymbol{h_{th}}$	$[mm]$	17.4	20.4
$\boldsymbol{h_c}$	$[mm]$	2.83	2.96
$\boldsymbol{l_{th\_int}}$	$[mm]$	2.5	2.48
$\boldsymbol{h_{c\_int}}$	$[mm]$	2.88	3
$\boldsymbol{h_{pm}}$	$[mm]$	3	3.18
$\boldsymbol{h_{sy}}$	$[mm]$	8.77	8
$\boldsymbol{h_{ry}}$	$[mm]$	7.8	7.54
$\mathbf{n}$		441	470
$\boldsymbol{M_{gen\_t}}$	$[kg]$	14.7	14

Power balance of the wind energy system			
P_{in_total}	$[kW]$	2,775	≈ 2,866
P_{out_total}	$[kW]$	2,339	≈ 2,365
η_{system}		0.8428	0.8251

However, this time by applying the correction strategy of the analytical model, significant improvements of these results can be remarked in an acceptable resolution time of the proposed objective function. As only the total power losses in the system are set for minimization and given the stochastic nature of the genetic algorithm the optimization approaches find slightly different geometries for the same result of the objective function. In addition to this, the dissimilarity that can be noticed among the powers in the system for the two approaches, lies below an acceptable error margin, which is less than 3.5% relative error. It can be concluded that also with the analytical model by applying an adequate methodology, it is capable to provide good results in a much shorter time.

Based on this and given the fact that the semi-analytical model, even associated to the barycenter method does not provide the luxury of performing many exploratory optimizations upon it, this optimization strategy based on the analytical model with a correction strategy was used for performing several other optimizations by iteratively increasing also the number of barycenters. Therefore, the optimizations were realized as follows:

- First the optimization is performed on the analytical model and corrected based on the semi-analytical model with barycenter method, starting from two barycenters.
- When the difference between the two models is small enough, the optimum results are used to evaluate the semi-analytical model with complete cycle in order to make a comparison between the results obtained with complete cycle and with the barycenters.
- This comparison is used to determine if the relative error of these results is situated below an imposed tolerance (< 0.1%). If the stopping criterion is not satisfied, the number of barycenters are increased and the loop is relaunched, otherwise the process stops (*fig. 4.11*).

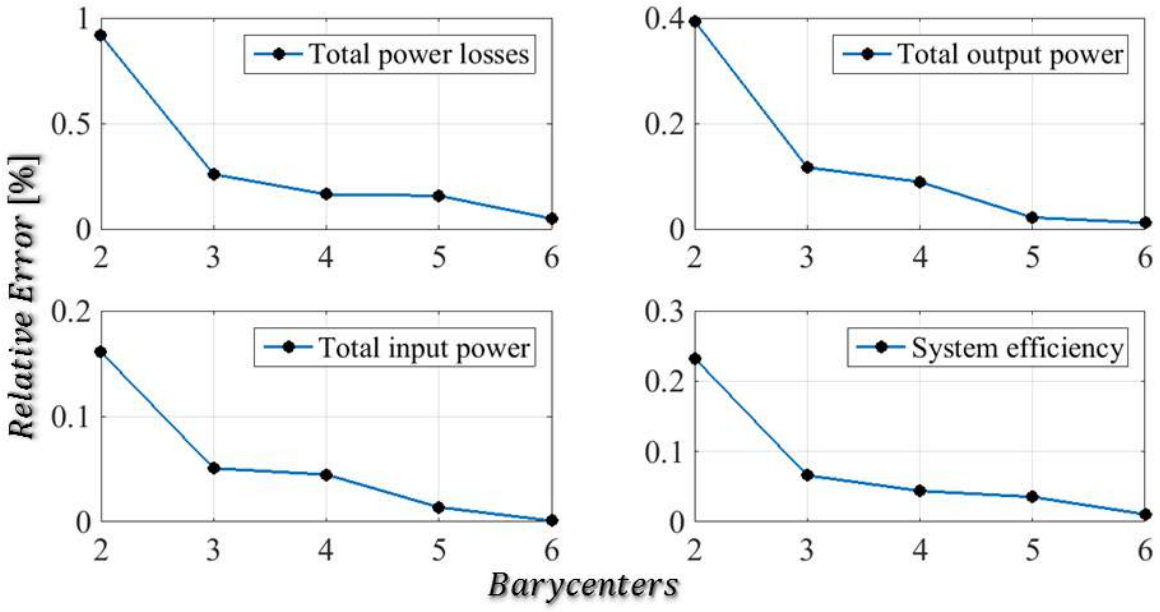

Fig. 4.11 Convergence history for several quantities by iteratively increasing the number of barycenters

4.4 Conclusions

In this chapter the design optimization methodology has been presented and the optimal results found based on these approaches have been analysed. The design optimization process is relies on two simulation models, one more accurate and the other faster but not so precise and relies on the use of an evolutionary optimization algorithm to find the geometrical and electrical parameters that satisfy the problem constraints while performing the minimization of the power losses of the wind energy system over a long-term wind speed profile.

In the first phase, an optimization with the semi-analytical model with the barycenter method has been conducted and several output results were confronted to the semi-analytical model responses under complete wind cycle operation. A good correlation between these results were found, leading to consider them as base or references for the upcoming comparisons.

Next, the design optimization was realized based on the analytical model with complete wind cycle. As expected, the optimum results found with this model are far from the base ones but they are found in a reduced optimization time. The attempt of improving the quality of the optimization compels to implement an iteratively correction strategy that refines the analytical model results by comparison to the semi-analytical one, which is considered as a more precise model. The results of this approach respond well to the optimization problem leading to good results in a very reasonable time, making possible for other optimizations to be relaunched.

Selected references

[1] Stéphane Brisset, *Démarches et Outils pour lq Conception Optimale des Machines Electriques*.: Habilitation à Diriger des Recherches, Université des Sciences et Technologies de Lille, 2007.

[2] F. Gillon, *Methodologies de conception optimale des composants electromagnetiques*, EC Lille - USTL ed., 2009.

[3] **Andreea Laczko (Zaharia)**, Stéphane Brisset,Mircea M. Radulescu, "Design of a brushless DC permanent magnet generator for use in micro-wind turbine applications", *The 14th International Workshop on Optimization and Inverse Problems in Electromagnetism (OIPE)*, September 2016.

[4] S. Brisset, Brochet P., "Analytical model for the optimal design of a brushless DC wheel motor," *COMPEL-The international journal for computation and mathematics in electrical and electronic engineering*, vol. 24, no. 3, pp. 829-848, 2005.

[5] D. E. Goldberg, *Genetic algorithm in search, optimization and machine learning*.: Wesley, 1989.

Chapter 5

Experimental Study of BLDCPM Generator Prototype

5.1 Experimental characterization of the BLDCPM generator prototype

The prototype BLDCPM generator under experimental study is represented by an in-wheel three-phase brushless DC permanent magnet machine, existent in the L2EP laboratory, designed for an electrical bicycle application. Its main features are:

- outer rotor with surface-mounted Nd-Fe-B magnets (*fig. 5.1*)
- inner slotted stator of steel laminations with three-phase star-connected concentrated winding (*fig. 5.2*)
- integrated Hall effect sensors (*fig. 5.2*), mounted on the stator, for rotor position detection, phase commutation and control
- induced stator-phase back-EMFs of quasi-trapezoidal shape.

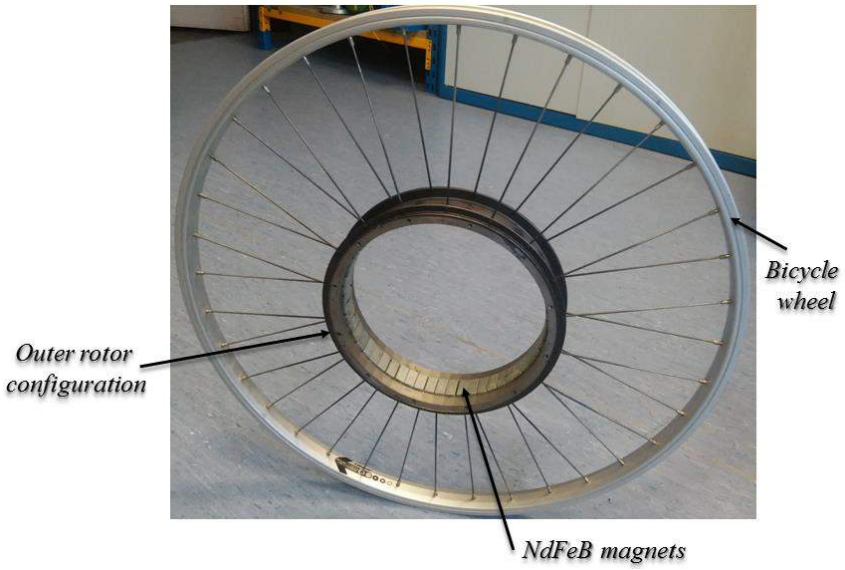

Fig. 5.1. Rotor part configuration of the BLDCPM prototype machine

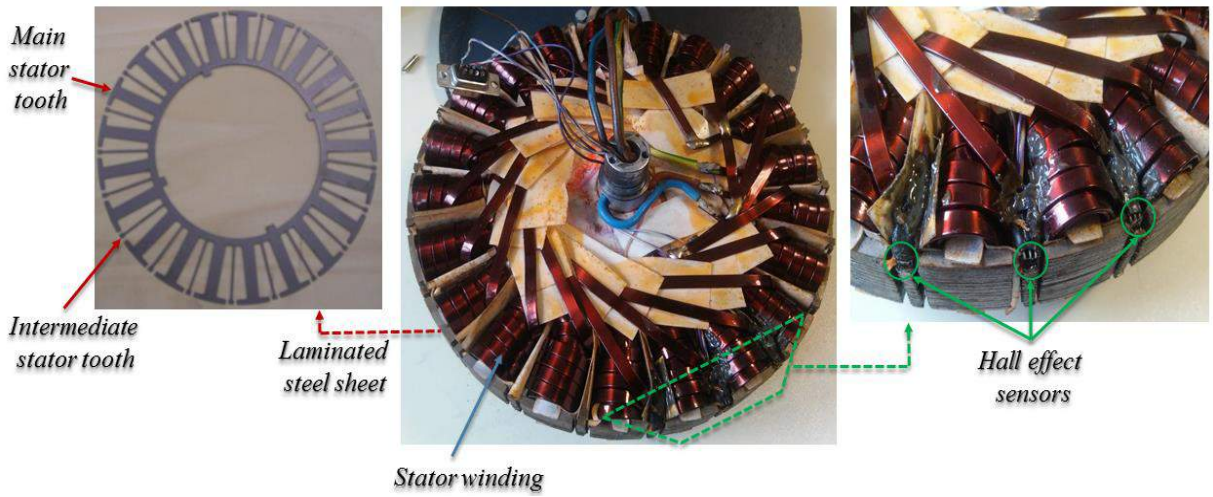

Fig. 5.2. Stator part configuration of the BLDCPM prototype machine

5.1.1 Experimental study of BLDCPM generator no-load operation

Since only few information is provided for the BLDCPM prototype machine, several of its features are found experimentally. As mentioned in *chapter 1*, the electronic commutation of three-phase BLDCPM machine comprises six conduction intervals of 60 electrical degrees per cycle for each stator phase. The stator-phase-current commutation as a function of rotor position is performed using the output signals of three Hall-effect rotor-position sensors mounted in the stator (*fig. 5.2*). The Hall-effect sensors are supplied with constant DC voltage of 5V (±0.5V) and their rotor-position output signals are processed for electronic self-commutation of stator-phase currents by means of PICOLLO converter, shown in *fig. 5.3*, also available in the laboratory.

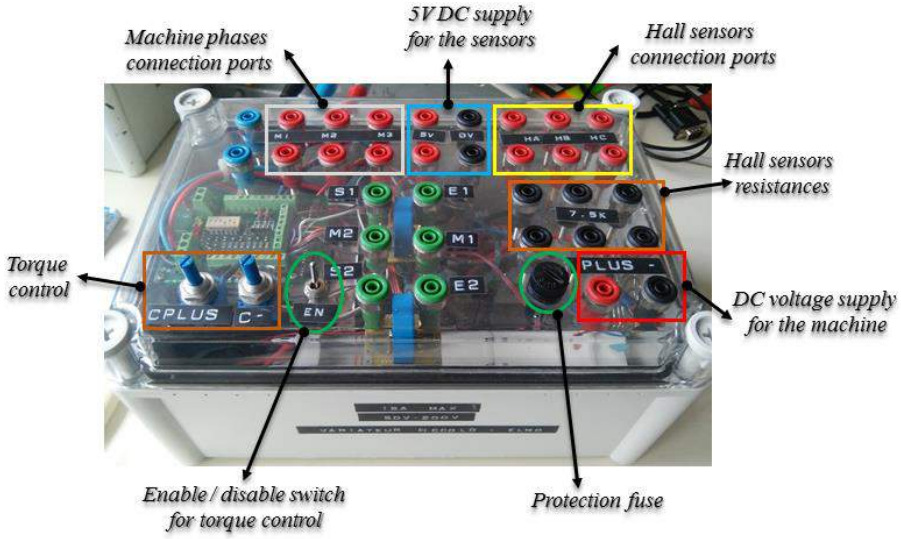

Fig. 5.3. PICCOLO converter used for Hall sensors rotor-position signals processing

The in-wheel BLDCPM machine was set in motion by means of a few adjustments (*fig. 5.4*). Due to the outer rotor topology of the in-wheel motor, it is pulled by a belt connected to the shaft of a rotating motor with speed regulation that emulates the wind turbine, as shown in *fig. 5.4*.

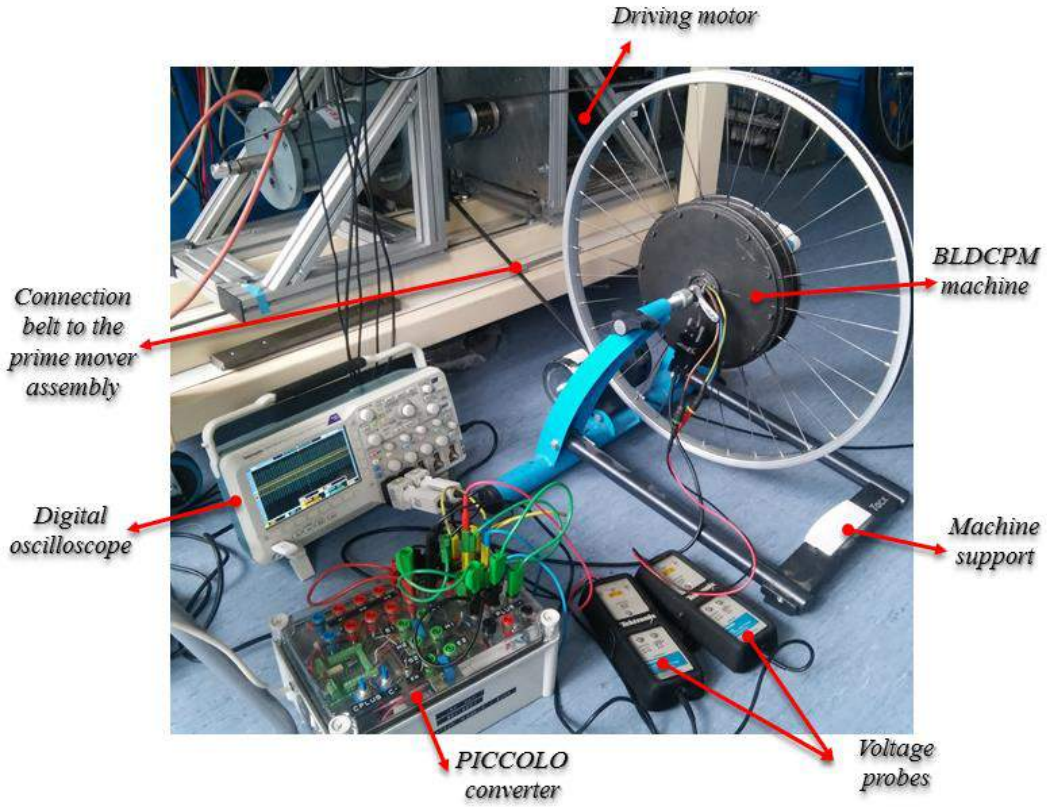

Fig. 5.4. Experimental set-up for no-load operation of the BLDCPM generator prototype

It is noticeable without saying that the exterior diameter of the in-wheel machine is a few times greater than the one of the driving shaft, which leads to different speeds between them. On this basis, the speed of the BLDCPM generator results by dividing the driving motor speed to the ratio of their exterior diameters, which was found to be *7.2*.

No-load (open-circuit stator) experiments for the BLDCPM generator prototype were carried out next, at low speed, which allow determining which sensor corresponds to which phase, by visualizing on the digital oscilloscope with the help of differential voltage probes, the line-to-line back-EMF voltage waveform and the corresponding Hall-effect sensor output signals, as exemplified in *fig. 5.5*.

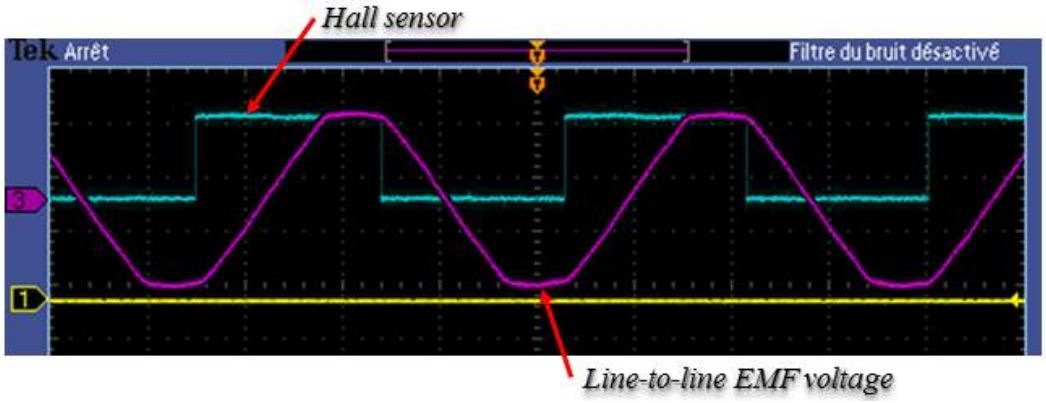

Fig. 5.5. Experimentally-obtained line-to-line back-EMF waveform and Hall-effect sensor output signal under no-load operation of the BLDCPM generator prototype.

As clearly shown by *fig.5.5*, the Hall-effect sensor output signal change its logical state from 0 to 1, when the corresponding back-EMF ascending slope is initiated. The same principle applies to all stator phases of the BLDCPM prototype machine, leading to the stator-phase switching sequence of *table 5.1*.

Table 5.1. Switching sequence of the BLDCPM prototype machine

Hall Sensors			Machine phases		
HA	HB	HC	Phase A	Phase B	Phase C
0	1	0	off	+	-
0	1	1	-	+	off
0	0	1	-	off	+
1	0	1	off	-	+
1	0	0	+	-	off
1	1	0	+	off	-

Other measurements under open-circuit condition were performed to determine the back-EMF coefficient k_{emf}, which directly links the rotational speed of the machine to its RMS stator-phase back-EMF, due to their linear relation, as shown in *fig. 5.6*. Based on repeated no-load experiments at different rotor speeds the value of this coefficient has been obtained $k_{emf} \approx 0.34 \left[\frac{V}{rad/s}\right]$.

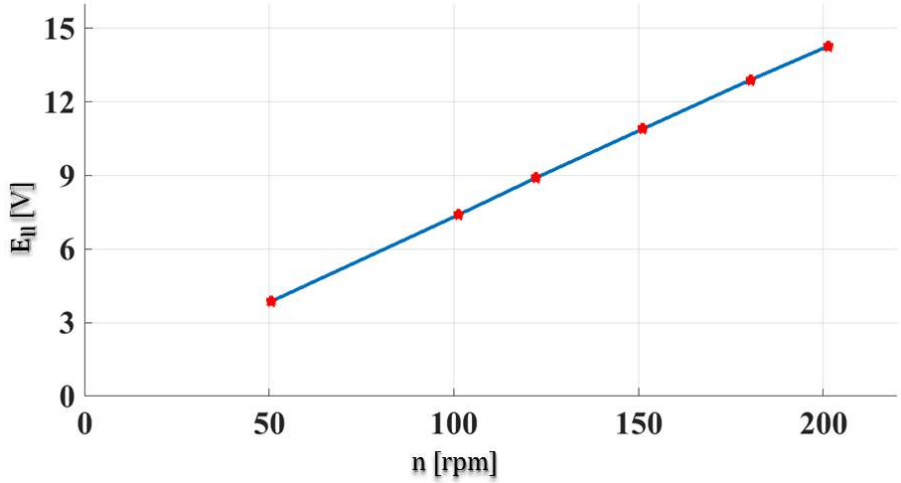

Fig. 5.6. Experimental characteristic of line-to-line back-EMF vs rotor speed of the BLDCPM generator prototype.

5.1.2. Description of the laboratory experimental set-up

For steady-state and dynamic performances analysis of the BLDCPM generator prototype, the laboratory experimental set-up illustrated in *fig. 5.7* was assembled.

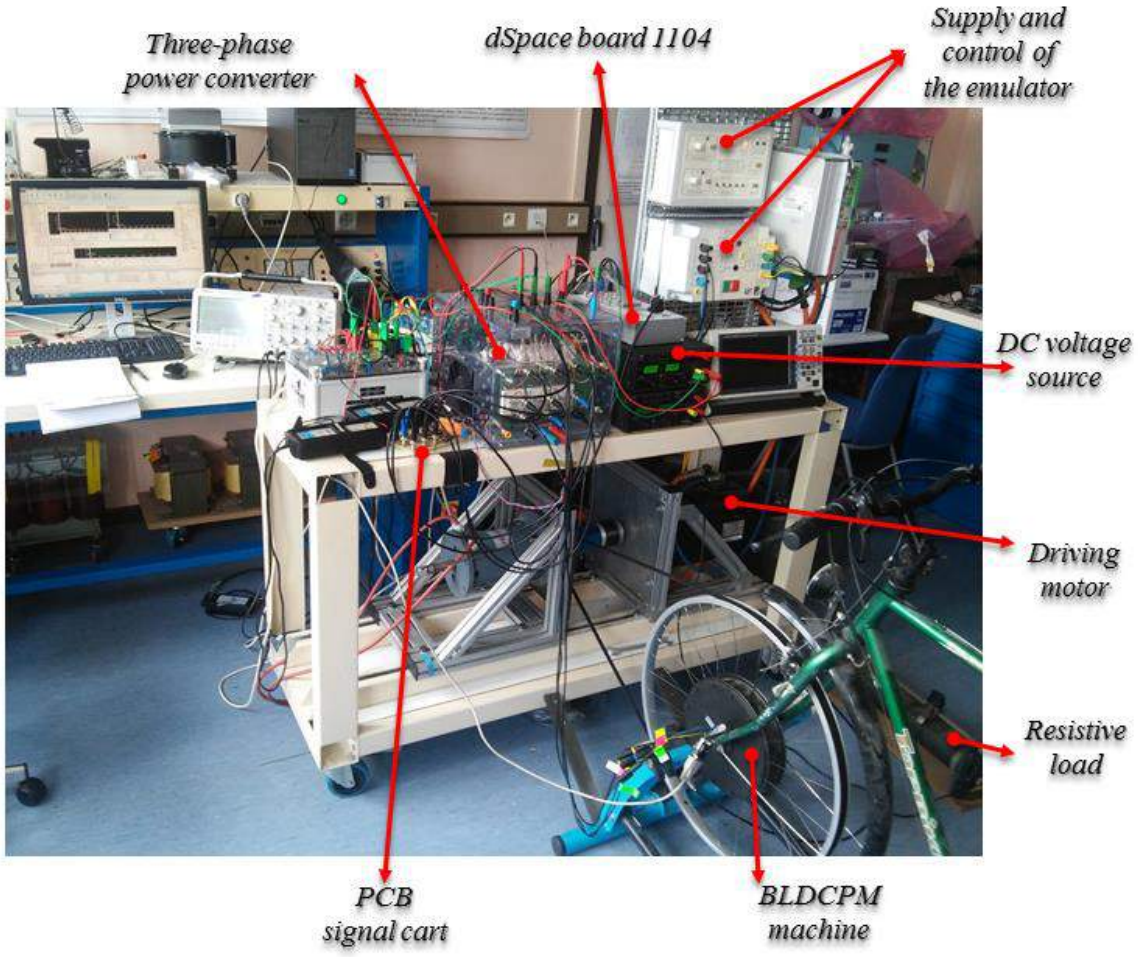

Fig. 5.7. . Experimental laboratory set-up for BLDCPM generator prototype performance analysis

The main components of this set-up are briefly presented below:

- A turbine emulator, which is represented by a driving motor supplied from an industrial converter that allows also a speed control of this motor.
- The brushless DC permanent magnet machine under study.
- A three-phase full bridge power converter, with six commutation devices based IGBT, with anti-parallel diode units and coupled to a DC voltage source. Its primary purpose is to supply and control the reference BLDCPM machine.
- A variable resistive load to replace the storage system or the utility grid.
- The control components represented by a dSPACE board [1] and a PCB signal cart.

The three-phase full-bridge power converter employed for the tests is of Semikron type, characterized by a maximum current supply of 30 [A] for a voltage of 440 [V] (values obtained from its datasheet). It allows the connection of the machine phases in the midpoint of the three arms of the converter and it receives the command signals for the six IBGT devices from a signal conversion card (through six BNC connectors), which represents the liaison between the power converter and the dSPACE board (*fig. 5.9-left*). The latter one, is an interface platform used for the control of the BLDCPM machine. It provides the measurements of the machine phase currents and of the one on the resistive load (*fig. 5.8*) by means of BNC connectors (analog input ports).

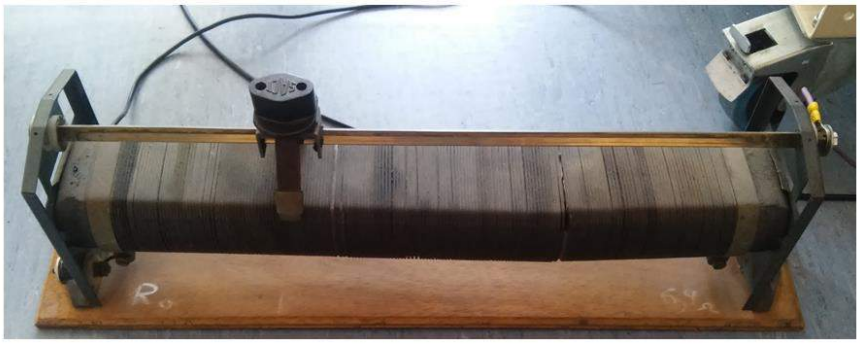

Fig. 5.8. Variable resistor

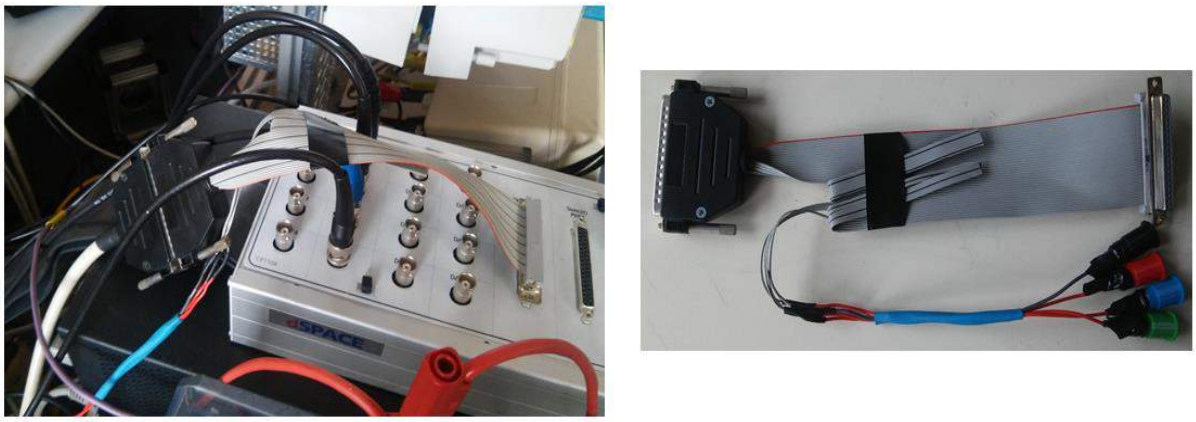

Fig. 5.9. dSpace 1104 controller board (left) and digital input/output ribbon cable for measurements and control (right)

To be able to acquire the position signals of the Hall effect sensors (digital data) and to control the BLDCPM machine based on the 120° electrical degree commutation pattern (six sectors of 60° each) the ribbon cable from *fig. 5.8 (right part)* was created. The communication with the board is done by means of the ControlDesk software and the correspondence with the Matlab/Simulink [2] control blocks is achieved in real-time via the Real Time Interface (RTI), as the compiler generates a C/C++ code of the simulation blocks and loads it into the memory of the dSPACE board.

The general structure of the main program implementation in Matlab/Simulink environment for the real-time tests is depicted in *fig. 5.10.* The first step consists of achieving the real-time measurements of the Hall sensors signals with the rotor position information by means of the input ports from the dSPACE board and of the BLDCPM machine phase currents, respectively, as depicted by the blocks on the left in *fig. 5.11*.

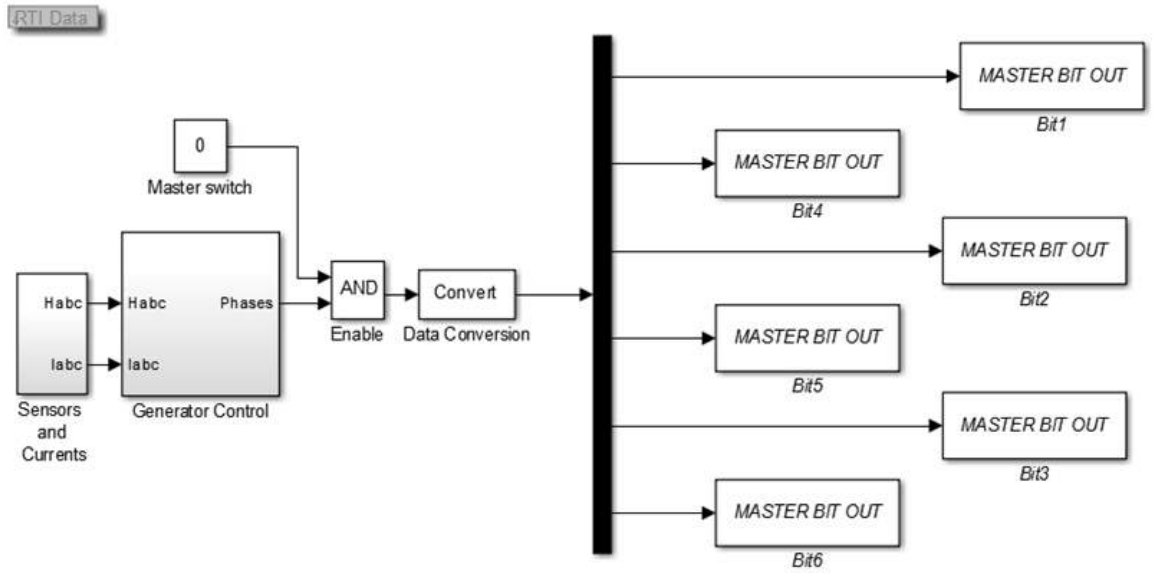

Fig. 5.10. RTI based Matlab/Simulink control model of the BLDCPM machine

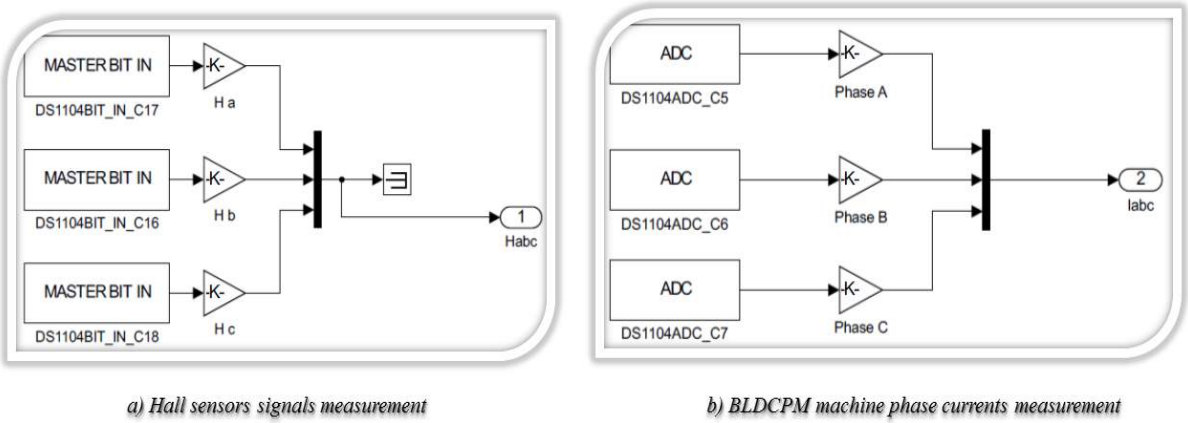

a) Hall sensors signals measurement *b) BLDCPM machine phase currents measurement*

Fig. 5.11. RTI based "Sensors and Currents" block

Therefore, the second step consists of determining the reference currents for each state from 0 to 360° by implementing the commutation sequence from *table 5.1* and based on the previous measurements of the sensors. A representation for the first 60° electrical degree sector is illustrated in *fig. 5.13.*

As a torque control cannot be realized for this set-up, only the phase currents are controlled by means of PI regulators or hysteresis comparators (*fig. 5.12*). The outputs of the current regulation correspond to the signals transmitted to the converter power units (IGBTs) which are controlled by the dSPACE board based on these signal values. The communication with the board is realized by the six "Master Bit Out" RTI blocks from *fig. 5.10.*

The rotational speed of the BLDCPM machine is used as a criterion for cancelling the load if the machine speed exceeds an imposed limit value or if the power converter senses an error. The machine speed is calculated by means of a speed and position sensor attached to the shaft of the driving motor, by multiplying the output response of the motor speed port by 60 and dividing it by 600, which represents the maximum resolution of the encoder and applying a filter to uniform the result (values also provided by the datasheet). At last, the rotational speed of the BLDCPM generator is estimated by dividing the SRM speed to the *7.2*, value previously determined.

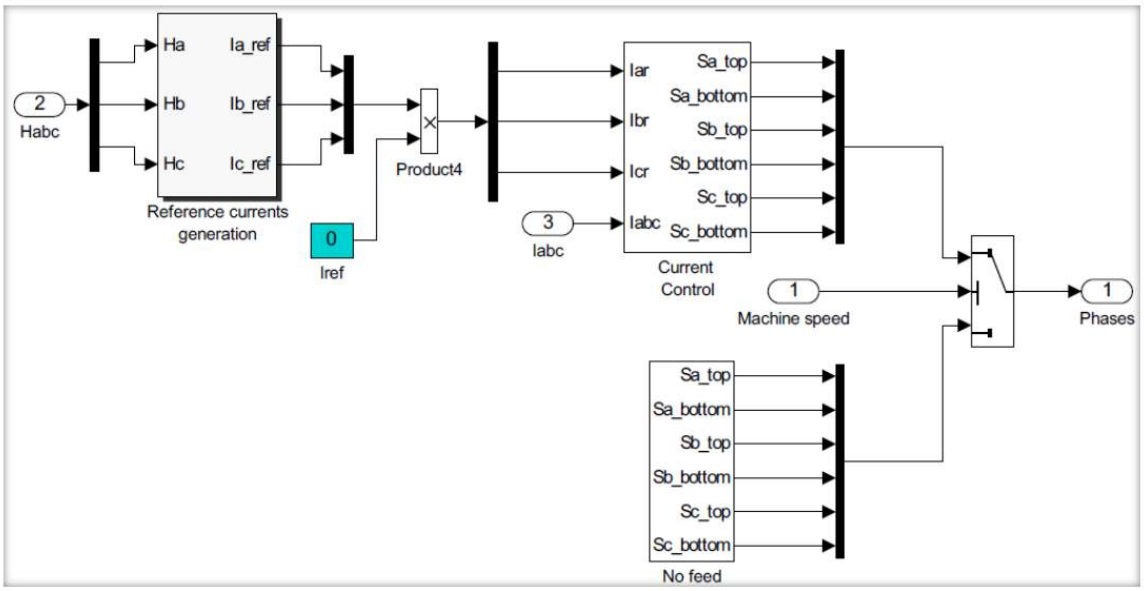

Fig. 5.12. RTI representation of the "Generator Control" block

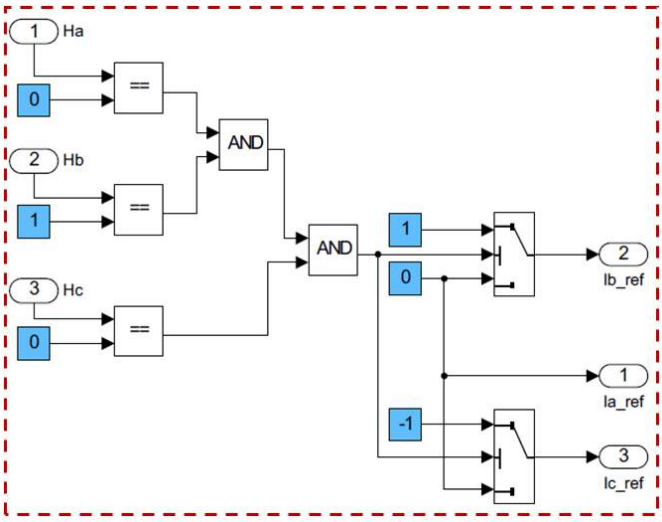

Fig. 5.13. RTI representation for the current control for a 60-electrical-degree sector of an electrical cycle

5.1.3 Experimental results

The ControlDesk interface contains graphical tools for visualizing the measured signals of the real-time experimental investigations and display tools to reveal the instant values for certain quantities. The solver chosen when realizing the tests is the Runge-Kutta with a fixed time step of $\Delta t = 6 \cdot 10^{-5}\ [s]$. The values of two variables are changed during the tests:

- The *"master switch"* which is used to enable *(1)* and disable *(0)* the control strategy
- The *"Iref"* variable which is set to control the peak phase currents of the machine by increasing or decreasing its value

The tests were conducted for various rotational speed, DC voltage source and resistive load values for a regulation of the machine phase currents with PI controllers.

Fig. 5.14 presents the experimental waveforms of the three-phase stator currents of the BLDCPM machine, the DC current on the resistive load as well as the reference current and real current for one phase obtained by engaging the machine in motion at a constant speed of around *30 [rpm]* and setting the current reference value at *1 [A]*, by means of a modifying block, while the resistive load is of *0.8 [ohm]* and the DC voltage is *1.2 [V]*. It should be noted that the lack of the chopper port on the PCB signal card does not allow to control and maintain the DC bus voltage at a constant value. However, at this rotational speed its value does not produce any alteration in the currents waveforms.

Fig. 5.14. Experimental waveforms of the BLDCPM generator through ControlDesk interface

However, a decrease in the DC voltage will have repercussion on the machine phase current, as it will exhibit a peak in its waveform, being noticeable in *figs. 5.15 and 5.16.*

Fig. 5.15. Experimental waveforms of the BLDCPM generator through ControlDesk interface

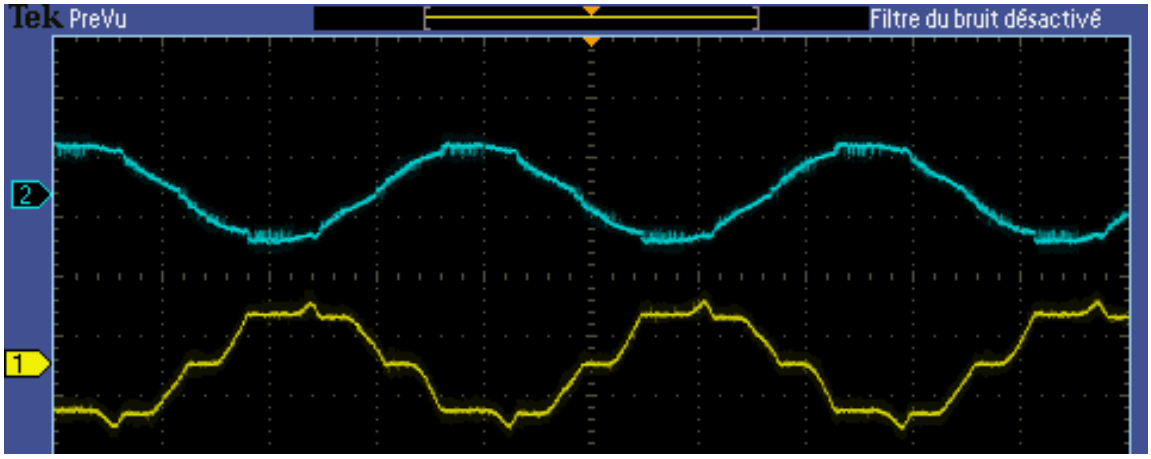

Fig. 5.16. Experimental waveforms of the BLDCPM generator stator-phase current and voltage at a rotational speed of 30 [rpm] measured on the oscilloscope

Other tests were conducted to investigate this phenomena for higher rotational speeds of the BLDCPM machine. At the nominal speed of the machine of *200 [rpm]* the resistive load needed to be increased to a value of *2.2 [ohm]* and the reference current was set to *6 [A]*. For a DC voltage of *13 [V]* the same peak appears in the current's shape (*fig. 5.17*), but it also presents a slightly altered form due to the lack of a control on the DC voltage.

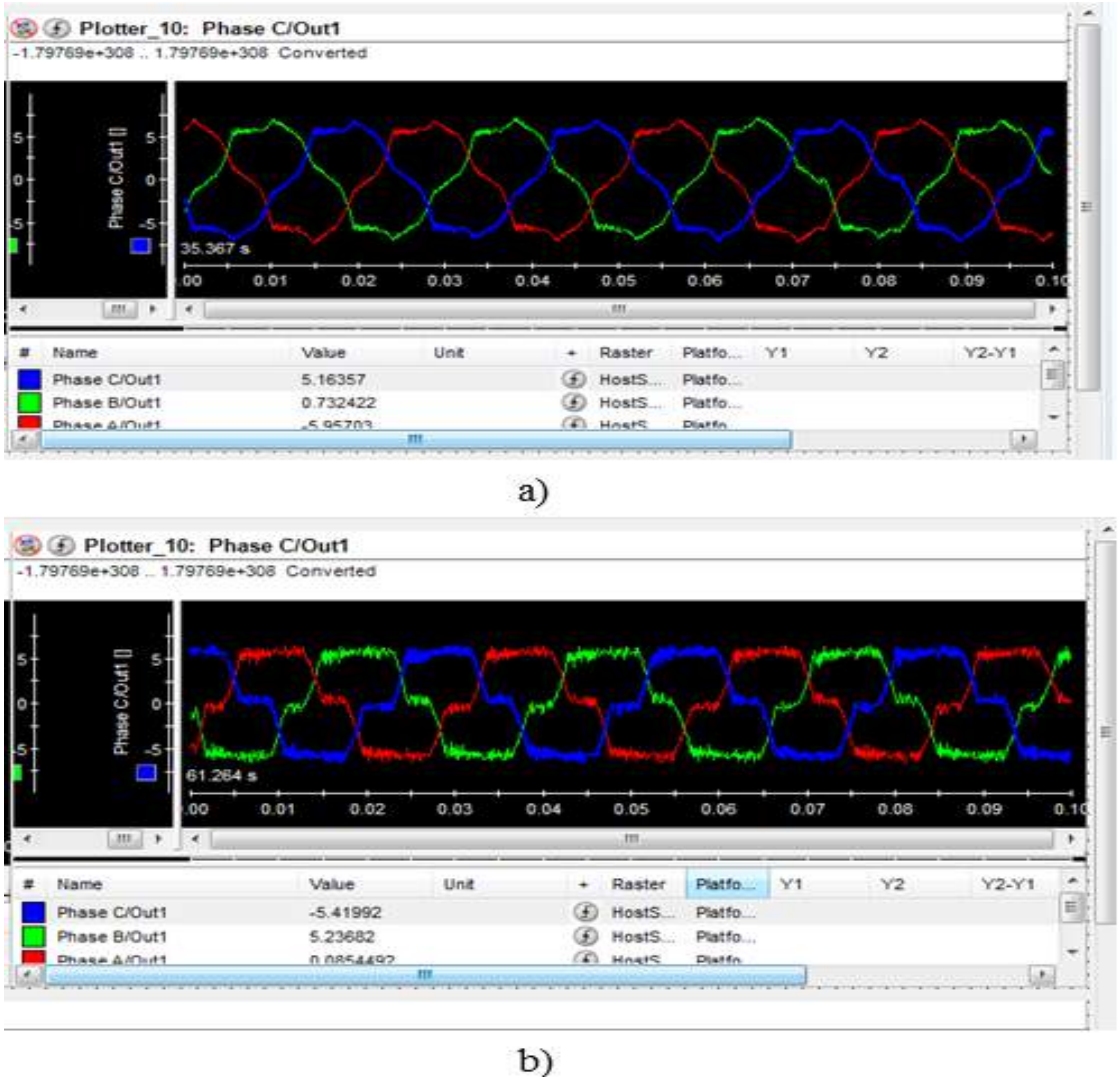

Fig. 5.17. Experimental waveforms of phase currents for a) DC voltage of 13 [V] and b) DC voltage of 18 [V]

5.2 Conclusions

The first part of this chapter has briefly described the BLDCPM generator prototype employed for realizing the experimental assembly and tests, followed by the switching sequence detection for the under study machine based on the information provided by the Hall effect sensors measurements obtained under open-circuit (no-load) conditions.

The hardware and software platform was further on presented along with the main structure of the control model implemented in Matlab/Simulink environment. Several tests at different rotational speed and DC voltage have been performed and visualized through the Control Desk interface. The obtained waveforms for the machine phase currents reinforce the fact that this bus voltage plays a significant role in the quality of the generated electrical energy.

The peak in the current waveform is obtained even for a lack of a chopper control of the DC bus voltage. At last, steady state as well as dynamic experimental tests have also been provided.

Selected references

[1] dSPACE DS1104 user manual. [Online]. https://www.dspace.com/

[2] MathWorks. [Online]. www.mathworks.com/products/matlab/

SEMISTACK - IGBT

SEMITRANS Stack[1)]

Three-phase rectifier + inverter with brake chopper

SEMITEACH - IGBT
SKM 50 GB 123D
SKD 51
P3/250F

Features

- Multi-function IGBT converter
- Transparent enclosure to allow visualization of every part
- IP2x protection to minimize safety hazards
- External banana/BNC type connectors for all devices
- Integrated drive unit offering short-circuit detection/cut-off, power supply failure detection, interlock of IGBTs + galvanic isolation of the user
- Forced-air cooled heatsink

Typical Applications

- Education: One stack can simulate almost all existing industrial applications:
- 3-phase inverter+brake chopper
- Buck or boost converter
- Single phase inverter
- Single or 3-phase rectifier

[1)] Photo non-contractual

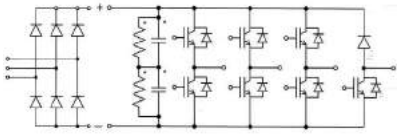

B6U + B6CI + E1CIKF

Circuit	I_{rms} (A)	V_{ac} / V_{dcmax}	Types
B6CI	30	440 / 750	SEMITEACH - IGBT

Symbol	Conditions	Values	Units
I_{rms}	no overload	30	A
	IGBT - 4x SKM 50 GB 123D		
V_{CES}		1200	V
$V_{CE(SAT)}$	I_c= 50A, V_{GE}= 15V, chip level; T_j= 25(125)°C	2,7 (3,5)	V
V_{GES}		±20	V
I_C	T_{case}= 25 (80)°C	50 (40)	A
I_{CM}	T_{case}= 25 (80)°C; t_p= 1ms	100 (80)	A
	Rectifier - 1x SKD 51/14		
$V_{in(max)}$	without filter	3 x 480	V
	with filter	3 x 380	V
	DC Capacitor bank - Electrolytic 2x 2200µF/400V		
C_{eqvl}	total equivalent capacitance	1100 / 800	µF / V
V_{DCmax}	max. DC voltage applied to the capacitor bank	750	V
	Driver - 4x SKHI 22		
Power supply		0 / 15	V
Current consumption	max; per driver	16	mA
Thermal trip	Normally Open type (NO)	71	°C

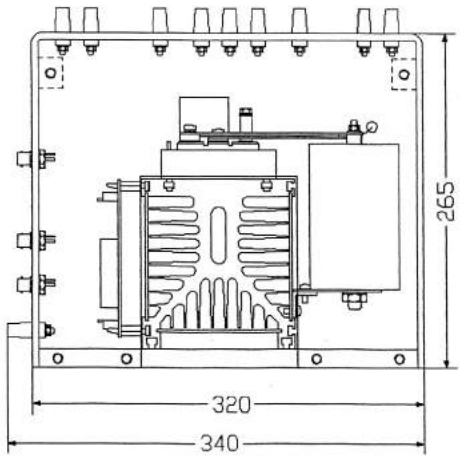

General dimensions

This technical information specifies semiconductor devices but promises no characteristics. No warranty or guarantee expressed or implied is made regarding delivery, performance or suitability.

Incremental encoders

Micro series, with end shaft

Resolution 30...1024 pulses

GI321

GI321 with end shaft

Features

- **Micro encoder with end shaft ø4 mm**
- **Resolution max. 1024 ppr**
- **Housing ø24 mm**
- **High rotation speed max.10000 rpm**
- **Operating temperature range -20...+85°C**
- **Integrated spring washer**
- **Cost-efficient mounting**

Technical data - electrical ratings

Voltage supply	5 VDC ±5 % 8...30 VDC
Reverse polarity protection	Yes (8...30 VDC)
Consumption w/o load	≤25 mA
Resolution (steps/turn)	30...1024
Reference signal	Zero pulse, width 90°
Sensing method	Optical
Output frequency	≤100 kHz
Output signals	A 90° B + N
Output circuit	TTL linedriver final stage Push-pull short-circuit proof
Interference immunity	DIN EN 61000-6-2
Emitted interference	DIN EN 61000-6-4

Technical data - mechanical design

Housing	ø24 mm
Shaft	ø4 mm end shaft
Protection DIN EN 60529	IP 54
Operating speed	≤10000 rpm
Starting torque	≤0.007 Nm
Material	Aluminium, bare
Operating temperature	-20...+85 °C
Relative humidity	90 % non-condensing
Resistance	DIN EN 60068-2-6 Vibration 10 g, 55-2000 Hz DIN EN 60068-2-27 Shock 30 g, 11 ms
Weight approx.	50 g
E-connection	Cable 1 m

Output signals

Clockwise rotating direction when looking at flange.

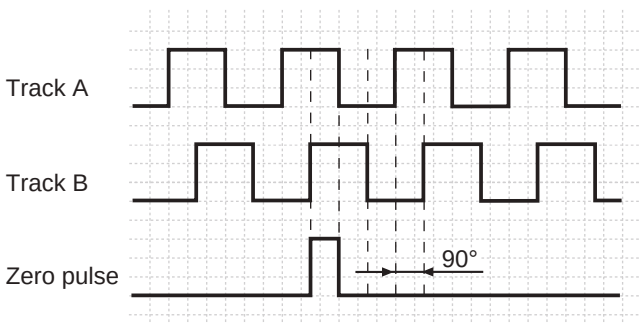

GI321

Part number

GI321. | **0** | | **41** | |

- See part number (pulses)
- E-connection
  - 41 Cable 1 m, radial
- Voltage supply / signals
  - 22 5 VDC / TTL linedriver
  - 60 10…30 VDC / push-pull
- Shaft
  - 0 End shaft ø4 mm IP 54

Part number (pulses)

38 (30)	06 (200)	17 (600)
40 (60)	11 (300)	22 (1000)
41 (100)	13 (360)	23 (1024)

Other pulse numbers upon request.
Example: ordering key 23 = 1024 pulses

Terminal assignment

Core colour	Assignment
green	Track A
yellow	Track B
grey	Track N (zero pulse)
brown	UB
white	GND
transparent	Shield/Housing

Dimensions

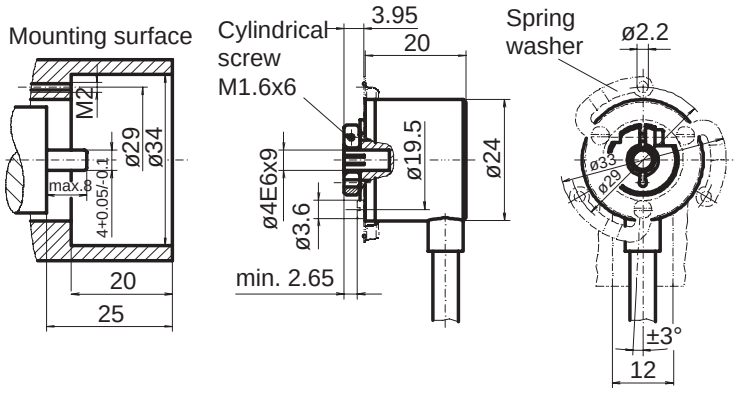

General Conclusions and Perspectives

The subject of this thesis was centered on enquiring into the design of a brushless DC permanent magnet generator for direct-driven micro-wind turbine applications. This investigation was realized for the minimization of the wind energy system power losses over a long-term wind speed cycle operation. However, the wind energy system to be optimized incorporates different subsystems (aerodynamic, mechanic, electric) with strong connection between each other. It is considered that a global optimization of the system is a more adequate solution that would present itself with better results, rather than performing the optimization for each component separately.

The considered architecture of the µWECS is described in the first chapter of the thesis. It is based on a brushless DC permanent magnet generator with direct coupling to the three-bladed horizontal axis wind turbine which delivers energy to a DC bus with constant voltage through a three phase rectifier based IGBTs devices with anti-parallel diode units.

Before passing to the design optimization process several aspects needed to be covered, i.e. the modeling of the complete µWECS. For that reason a long term wind-speed cycle was set as input to the micro-wind turbine model and an analytical model, a semi-analytical model and a FE-based model of the generator-rectifier assembly were developed. Their electrical parameters were determined beforehand based on the implementation of several sizing equations and starting from few geometrical and magnetic parameters. These models were afterwards compared among each other, after simulating them with the values of a reference machine. It was concluded that only the semi-analytical model could be employed in the optimization process as it performs much faster, while still remaining in an acceptable relative error limit in terms of precision and use the FE-based model as a validation model outside of optimization. The best simulation time of the global system with the complete wind profile was given however by the analytical model, but under precision penalty, leading for this model to implement an iterative correction strategy when used in the optimization process.

The following aspect studied in this thesis was the long-term wind-speed profile, as it incorporates a large amount of data. In view of its reduction three methods have been examined, among which a novel developed barycenter method is proposed and described for determining the power losses (mechanical, copper, iron and converter losses) of the micro-wind energy conversion system. This method allows to consider the entire cycle when designing the generator based on its corresponding parameters, being associated with the semi-analytical simulation model. Likewise, a sensitivity analysis upon the performance points of the micro-wind turbine (cut-in, rated and cut-off wind speeds) by means of a full factorial design has been

realized in order to determine how several of the μWECS outputs are affected by the variation of these operating points.

After these analyses, the objective function, design variables and constraints of the optimization problem could be formulated. It is based on minimizing the global power losses in the system over the long-term wind speed profile operation by means of genetic algorithm (GA) in order to find the geometrical and electrical parameters that best satisfy the problem constraints. The use of GA is justified by the fact that it performs well in the optimization of noisy systems, as the semi-analytical simulation model is, due to the hysteresis current regulation. Still, this type of algorithm requires a large number of model evaluations to head towards an optimal solution. This fact is demonstrated by the rather large CPU time required when realizing the optimization with the semi-analytical model associated to the barycenter method. Nevertheless, the results of the single level optimization approach show good agreement when compared to those obtained after simulations of the semi-analytical model over complete wind-speed cycle operation.

In order to also reduce the computation time the analytical model operating under the full wind-speed profile was employed in the optimization process and iteratively corrected by means of a comparison to the outputs of the semi-analytical model with barycenter method. In this case also the obtained results present good agreement to those attained previously with the optimization upon the semi-analytical model only.

Throughout this thesis the contributions brought are considered to be the following:

- The development of an analytical sizing and simulation model in Matlab and a semi-analytical simulation model based PI control of the power and hysteresis regulation of the currents in Matlab/Simulink environment
- 2D modeling and analysis of a BLDCPM generator by means of an automatic link between JMAG Designer and Matlab software through a script file based on Visual Basic language
- The development of a new method adapted to the MPPT region, that reduces a wind-speed profile into several operating points and its adaptation to the calculation of the μWECS power losses (mechanical, copper, iron and converter losses)
- The design optimization of a BLDCPM generator integrated in a complex micro-wind energy conversion system, operating over a long-term wind-speed cycle, by using:

- a developed semi-analytical simulation model in Matlab/Simulink environment associated to an original barycenter method and coupled to a genetic algorithm technique, resulting in a single-level optimization approach
- a two-level optimization approach that consists in inner and outer loops. The inner loop performs an optimization with the developed analytical sizing and simulation model associated to a complete wind-speed cycle operation by using a genetic algorithm. The outer loop adjusts the outputs of the analytical model with the semi-analytical model with barycenter method based on an iteratively correction strategy.

➢ The set-up of a test bench to experimentally characterize a reference three phase BLDCPM machine prototype and the implementation of its commutation and control on the dSPACE platform.

Beyond all of the above, this study opens up a number of perspectives to be proposed:

➢ Vibration and thermal analysis of the generator and thermal model integration for the power converter

➢ To implement a multi-objective design optimization of the µWECS

➢ To extend and perform the optimization of the micro-wind system when considering also a direct coupling to the electrical network or when interconnecting other sources of renewable energy

➢ Topology optimization of the stator, magnets and rotor parts of the BLDCPM generator

europass

Curriculum Vitae

Personal information

First name(s) / Surname(s)	**ZAHARIA, Andreea-Adriana**
Maiden name	**LACZKO**
Address(es)	70-72 Mehedinti Street, 400672,Cluj-Napoca,Romania
Telephone(s)	+40748671065
E-mail	deea87deea@yahoo.com, Andreea.Laczko@mae.utcluj.ro
Nationality	Romanian
Date of birth	4th November 1987
Gender	Female

Work experience

Dates	**19 November 2012 – 30 June 2016**
Occupation or position held	**Research Assistant**
	Research project: '***Innovative wind energy conversion micro-system with direct-driven electric generator for residential uses***'
Name and address of employer	Technical University of Cluj-Napoca
Type of business or sector	Engineering

Education and training

Dates	**2014- 2016**
Occupation or position held	PhD student in co-tutelle under the co-supervision of **MdC HdR Stéphane Brisset**
PhD research activity	**"Brushless DC Permanent Magnet Micro-Wind Generator Modeling and Optimization over Long-Term Wind-Speed Cycle Operation" ("Optimisation du dimensionnement et de la commande sur cycle de fonctionnement d'un générateur à aimants permanents et à auto-commutation pour applications micro-éoliennes")**
Name and type of organisation providing education and training	Ecole Centrale de Lille, France
Dates	**2012- 2016**
Occupation or position held	Full time PhD student under the co-supervision of **Prof. Dr. Ing. Mircea M. Radulescu**
PhD research activity	**"Brushless DC Permanent Magnet Micro-Wind Generator Modeling and Optimization over Long-Term Wind-Speed Cycle Operation** "
Name and type of organisation providing education and training	Technical University of Cluj-Napoca, Faculty of Electrical Engineering, Department of Electrical Machines
Dates	**February 2012 - June 2012**
Occupation or position held	Erasmus student under the co-supervision of Prof. Domenico Casadei
Master thesis research activity	**"Implementation of a control scheme for the doubly-fed induction generator-based wind systems"**
Name and type of organisation providing education and training	Universita Degli Studi Di Bologna, Italy
Dates	**2010-2012**

Title of qualification awarded	Master Engineer Field of study: Energetics Engineering
Name and type of organisation providing education and training	Technical University of Cluj-Napoca, Romania Faculty of Electrical Engineering
Dates	**2006-2010**
Title of qualification awarded	Engineer Field of study: Energy Management
Name and type of organisation providing education and training	Technical University of Cluj-Napoca, Romania Faculty of Electrical Engineering

Publications

2016

Full paper — **Andreea Laczko (Zaharia),** Stéphane Brisset, Mircea M. Radulescu**, "Design of a brushless DC permanent magnet generator for use in micro-wind turbine applications",** *The 14th International Workshop on Optimization and Inverse Problems in Electromagnetism (OIPE)*, September 2016, Rome, Italy.

Full paper — **Andreea Laczko (Zaharia),** S. Brisset and M.M. Radulescu, **"Modeling approaches to brushless DC permanent-magnet generator for use in micro-wind turbine applications",** *International Conference on Electrical Machines (ICEM'2016),*September 2016, Lausanne,Switzerland.

2015

Full paper — **Andreea Laczko (Zaharia),** V. Zaharia, S. Brisset and M.M. Radulescu, **„Modelling and simulation of a brushless DC permanent-magnet generator-based wind energy conversion system"**, *International Conference on Ecological Vehicles and Renewable Energies (EVER 2015),Monaco.*

Full paper — Valentin Zaharia, F. Gillon, **A. Laczko (Zaharia)**, A.A. Pop and M.M. Radulescu, **„Optimal commutation angles of a switched reluctance motor/generator",** *International Conference on Ecological Vehicles and Renewable Energies (EVER 2015),Monaco.*

2014

Full paper — D. L. Irimie, M. M. Radulescu, A.A. Pop, **Andreea Laczko**, **„Loss Analysis of Small Three-Phase Cage-Induction Motors under Sinusoidal and PWM Voltage Supply"** ,*International Conference on Applied and Theoretical Electricity (ICATE 2014),Craiova, Romania*

Languages

Romanian	Native
English	Proficient user (C1)
French	Independent user (B2)

Competences

Computer skills	MS Office, Mathcad, AutoCAD, Matlab, Matlab/Simulink, JMag Designer, dSPACE, Control Desk

Andreea Adriana ZAHARIA

Publications

Journal article (sent for review)

[1] **Andreea Laczko (Zaharia)**, Stéphane Brisset, Mircea M. Radulescu, « Design of a brushless DC permanent magnet generator for use in micro-wind turbine applications », *The International Journal of Applied Electromagnetics and Mechanics (IJAEM).*

International conferences publications

[1] **Andreea Laczko (Zaharia)**, Stéphane Brisset, Mircea M. Radulescu, "Design of a brushless DC permanent magnet generator for use in micro-wind turbine applications", *The 14th International Workshop on Optimization and Inverse Problems in Electromagnetism (OIPE),* Rome, Italy, 13-15 September 2016. **(Poster)**

[2] **Andreea Laczko (Zaharia)**, Stéphane Brisset, Mircea M. Radulescu, "Modeling approaches to brushless DC permanent magnet generator for use in micro-wind turbine applications", *The 22th International Conference on Electrical Machines (ICEM),* Lausanne, Switzerland, 4-7 September 2016. **(Poster)**

[3] **Laczko Andreea Adriana**, Zaharia Mihai Valentin, Mircea M. Radulescu, Stéphane Brisset, "Modeling and simulation of a brushless DC permanent-magnet generator-based wind energy conversion system", *2015 Tenth International Conference on Ecological Vehicles and Renewable Energies (EVER*), IEEE, 2015. **(Oral presentation)**

[4] Zaharia Mihai Valentin, **Laczko Andreea Adriana**, Pop Adrian Augustin, Radulescu M. Mircea, Frédéric Gillon, "Optimal commutation angles of a switched reluctance motor/generator", *2015 Tenth International Conference on Ecological Vehicles and Renewable Energies (EVER),* IEEE,2015.

[5] Irimie Dan Liviu, Radulescu M. Mircea, Pop Adrian Augustin, **Laczko Andreea**, "Loss analysis of small three-phase cage-induction motors under sinusoidal and PWM voltage supply", *2014 International Conference on Applied and Theoretical Electricity (ICATE),* IEEE,2014.

Modeling approaches to brushless DC permanent-magnet generator for use in micro-wind turbine applications

Andreea Adriana Laczko (Zaharia), S. Brisset and M.M. Radulescu

***Abstract* -- This paper reports on the modelling of a direct-driven brushless DC permanent-magnet (BLDCPM) generator to be used in micro-wind turbine applications for long-term wind-speed profiles. Three models are investigated and confronted in precision and computation time. For power loss calculation of BLDCPM generator operating under large time-scale wind-speed fluctuations, an original barycenter method is applied.**

***Index Terms* -- brushless DC permanent-magnet generator, direct drive, finite-element field analysis, long-term wind-speed profile, trapezoidal back-EMF, wind energy conversion system.**

I. INTRODUCTION

BRUSHLESS DC permanent-magnet (BLDCPM) machines operating in generator mode offer several advantages, such as high efficiency over a wide speed range, low maintenance, greater durability, compactness, and higher power density. Moreover, due to the trapezoidal phase back-EMF of the BLDCPM generator, the rectified DC output voltage has reduced pulsations. Such positive features prompt the BLDCPM generator for use in small-scale wind energy conversion systems (WECSs) [1]-[3].

The direct coupling of the BLDCPM generator to the wind turbine compels it to operate under low-speed and high-torque conditions. The downside of the direct-drive technology is reflected in the cost and weight of the wind generator. The purpose is to search for an optimal design solution of the BLDCPM generator in terms of design specifications, that will give as small power losses as possible over a wind-speed cycle with time-span of one year and consequently maximizing the useful power.

This can be achieved through the bias of an optimization process that tries to find the optimal geometrical and electrical parameters of the generator, for further use in micro-wind turbine applications. As the simulation time is of great importance for the optimization process models with high accuracy can evolve it into a time-consuming process, especially when considering optimization over a wind cycle for the minimization or maximization of different quantities. For this purpose, a compromise must be made between the accuracy of the solution and the computation time.

Andreea Adriana Laczko (Zaharia) is with the Technical University of Cluj-Napoca, Cluj-Napoca, Romania and with the Ecole Centrale de Lille, Villeneuve d'Ascq / Lille, France (e-mail: Andreea.Laczko@mae. utcluj.ro)

S. Brisset is with the Ecole Centrale de Lille, Villeneuve d'Ascq / Lille, France (e-mail: stephane.brisset@ec-lille.fr)

M.M. Radulescu is with the Technical University of Cluj-Napoca, Cluj-Napoca, Romania (e-mail: Mircea.Radulescu@emd.utcluj.ro)

Three techniques are investigated in this paper for the modeling of the BLDCPM generator: analytical, semi-analytical and numerical. The finite element (FE)–based numerical model, which is based on transient magnetic field analysis of the generator by taking into account the rotor motion, the electromagnetic nonlinearities and the hysteresis current control, reveals high accuracy but under penalty of lengthy computation time.

On the other hand, the semi-analytical model, faster in computation time than the FE model is still dependent on a basic sampling time for neatness in the simulation results, neglects the electromagnetic properties of the machine and can only compute global quantities. Lastly, the analytical model is a static one that does not compute waveforms but only peak or mean values. This is the fastest but roughest model.

The aim of this paper is to pave the way for the future design optimization process by determining a reduced-order analytical model of the BLDCPM generator that can be used in its design optimization for operation under very large wind-speed profile. Also, a long-term wind-speed profile partition technique based on barycenter method, allowing fast exploitation of the available data from the wind-speed profile, is proposed and discussed in terms of generator power losses. The design characteristics and electrical parameters of the BLDCPM generator considered in this paper are those fully described in references [4] and [5].

II. MODELLING OF BLDCPM MICRO-WIND GENERATOR

A. *Long-term wind-speed profile and turbine model*

Typically, a wind-speed profile consists of a large set of data measurements as shown in Fig.1. The data considered for this paper represent the mean value taken over one hour of wind measurements, every hour for one year, resulting in 8759 of measurements that describe the wind behavior.

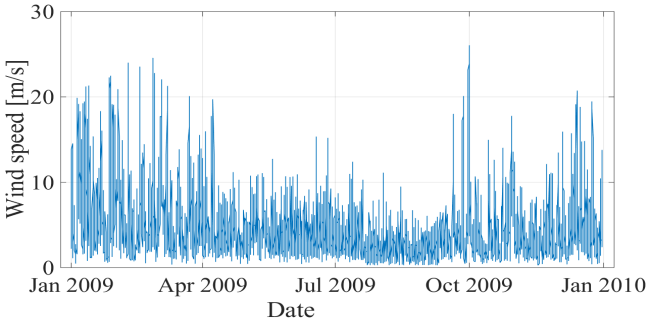

Fig. 1. Long-term wind-speed profile representation

The three-blade wind turbine model, delivers power (Fig. 2) expressed as [9]:

$$P_{wt} = \frac{1}{2}\rho_{air}\,\pi R_{wt}^2\,C_p(\lambda)\,v_w^3 \quad (1)$$

where ρ_{air} is the air density (kg/m^3), R_{wt} is the radius of the turbine-rotor blades (m), v_w, the wind speed (m/s), and $C_p(\lambda)$, the power coefficient of the turbine, which corresponds to the turbine studied in [8] and can be found through interpolation as presented in the appendix.

The cut-in speed of the wind represents the start-up of the turbine and the beginning of the wind power extraction until the wind speed reaches its rated value. For wind speeds outrunning this rated value, the turbine is kept to operate at its nominal power by means of different control techniques. When the cut-off wind speed is finally reached, the turbine ceases power generation through its shut-down, for mechanical damage protection.

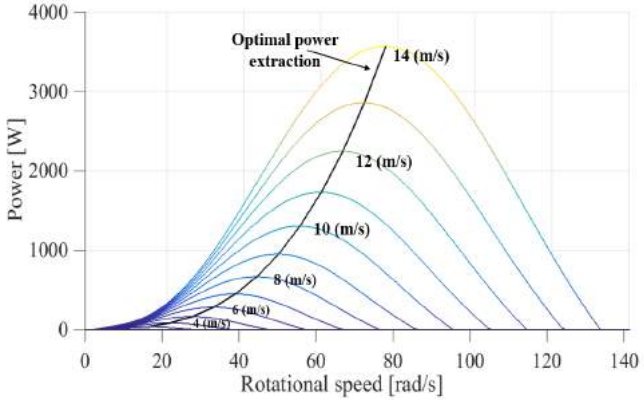

Fig. 2. Power characteristics of the reference micro-wind turbine

B. Semi-analytical model of the BLDCPM generator

The first model to investigate is the time based model. The following phase circuit model for the direct-driven BLDCPM generator having three-phase, star-connected with isolated neutral point stator windings is considered [2], [6]:

$$v - v_n = Ri + (L - M)\frac{di}{dt} + e \quad (2)$$

where R and L are the phase resistance and self-inductance, M is the mutual phase inductance, i and e represent the phase current and back-EMF and v_n is the stator neutral voltage:

$$v_n = \frac{1}{3}(\Sigma v_{abc} - \Sigma e_{abc}) \quad (3)$$

The trapezoidal phase back-EMF waveforms are dependent on the rotational angular speed of the generator, and shifted in all the three stator phases as in Fig. 3.

The electromagnetic torque can be expressed as:

$$T_{em} = \frac{e_a i_a + e_b i_b + e_c i_c}{\Omega} \quad (4)$$

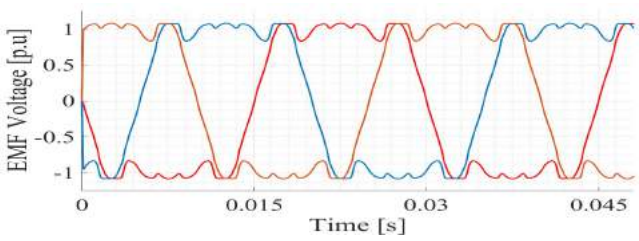

Fig. 3. FE-computed back-EMF waveforms of the considered BLDCPM micro-wind generator

The BLDCPM generator model is implemented in MATLAB/SIMULINK environment for the overall WECS with the schematic representation of Fig.4. The reference power is compared to the power of the system and processed by means of a PI controller. The output of this power-regulation block is used for determining the phase reference currents based on the BLDCPM generator switching pattern dependent on rotor angular position. Hysteresis control of stator phase currents is considered to obtain the driving signals for rectifier power devices and for providing the line-to-neutral stator-phase voltages.

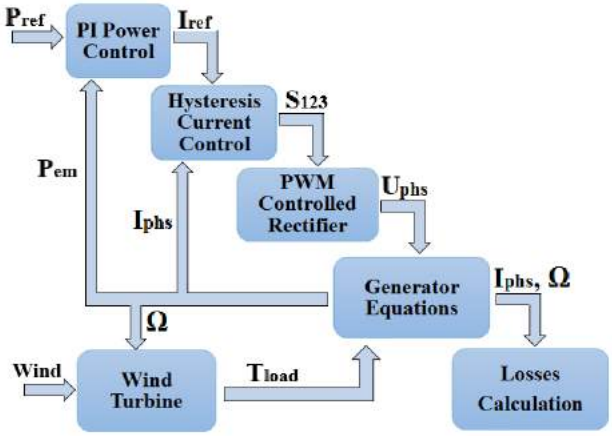

Fig. 4. Simulation model scheme of the direct-driven BLDCPM micro-wind generator under study

Particular quantities, such as the torque ripple and current peak, play a significant part in the design process of the generator. As they are different for each wind speed, in order to see the behavior of the entire system, the wind-speed cycle of 8759 measurements is set as input for the simulation model of the BLDCPM generator and a steady state simulation of one electrical period is carried out for each wind speed in the cycle.

Even before starting the simulation one can presume that it will take a lot of time. That is true, since a fairly large CPU time of 11 hours is needed to perform this type of simulation using MATLAB/SIMULINK software, for basic time-step of 1μs. Hence, considerable time-span is needed in order to use these data together with WECS model in an optimization process that would evaluate them alongside of other design variables for thousands of iterations. Such a strategy is not reasonable, so that the focus should be drifted towards the BLDCPM generator and wind-speed cycle reduced-order models.

C. Long-term wind-speed profile partition by barycenter method

A first attempt in the direction presented above is to maintain the semi-analytical model and find a solution to handle the simulation time over the wind-speed profile. Since through the design optimization of the BLDCPM generator high efficiency is pursued, loss minimization during the wind-speed cycle is required. It should be noted that for this paper, only the copper and the iron losses are taken into discussion.

A first method of determining the power losses of the entire wind cycle is by using each operating point for their calculation. As stated previously, this approach is not adequate due to the large computation time that it requires.

The second method for the losses calculation is based on the barycenter method, which allows to reduce both the simulation time and the wind data that will be considered for the design of the generator. A description of this method was reported in [10], where it was used to reduce the torque and speed driving cycles in the design optimization of an axial-flux traction motor.

This barycenter method is adapted here to the WECS for processing the large amount of wind-speed data. In order to reduce the computation time, the totality of operating points within the wind-speed cycle are replaced with a low number of regions, (Fig.5), whose barycenter are represented by the parameters from (5). These parameters are used for the losses calculation of each region r.

$$Bary_r = \begin{cases} \langle v_w \rangle_r, & \text{mean wind speed} \\ \langle v_w^2 \rangle_r, & \text{mean square wind speed} \\ \langle v_w^4 \rangle_r, & \text{mean wind speed of 4th power} \\ N_{pt} & \text{number of points in the region } r \end{cases} \quad (5)$$

The copper loss P_j, and iron loss P_{Fe_hys} and P_{Fe_eddy} for each barycenter are calculated as:

$$P_{j,r} = 3RI^2_{RMS,r} N_{pt} \frac{\langle v_w^4 \rangle_r}{\langle v_w \rangle_r^4} \quad (6)$$

$$P_{Fe\_hys,r} = k_{hys} \frac{N_p}{2\pi} (B_{th}^{\alpha} + B_{sy}^{\alpha}) \Omega_r N_{pt} \frac{\langle v_w \rangle_r}{\langle v_w \rangle_r} \quad (7)$$

$$P_{Fe\_eddy,r} = k_{eddy} \frac{N_p^2}{\pi^3} (B_{th}^2 + 2B_{sy}^2) \Omega_r^2 N_{pt} \frac{\langle v_w^2 \rangle_r}{\langle v_w \rangle_r^2} \quad (8)$$

A more detailed explanation on the entire process of how these losses equations were determined can be found in the appendix.

To validate the method, at the first step the copper and iron losses of the BLDCPM wind generator were calculated for all points of the wind cycle by using the semi-analytical model and the totality of each loss was obtained through their addition.

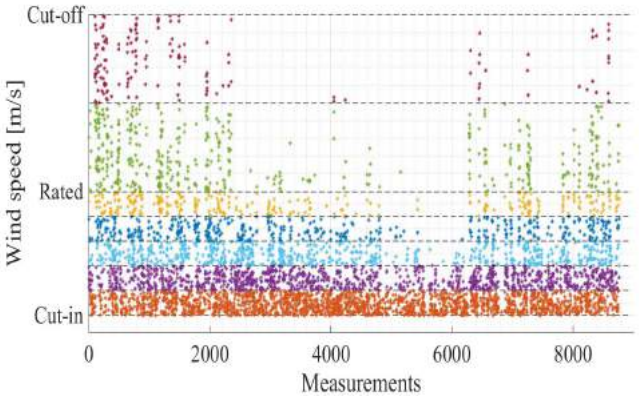

Fig. 5. Division example of a long-term wind-speed profile into a chosen number of regions

The second step was to compute the losses with the help of the same semi-analytical model by applying the barycenter method and the relations (6)-(8), considering a certain number of regions. A relative error was then calculated between the values obtained at the first step and those from the second step and presented in Figs. 6 and 7 with and without taking into account the ratio of the barycenter parameters. The curves in the figures show that the usage of the barycenter ratio allows to achieve a small error faster and with fewer regions.

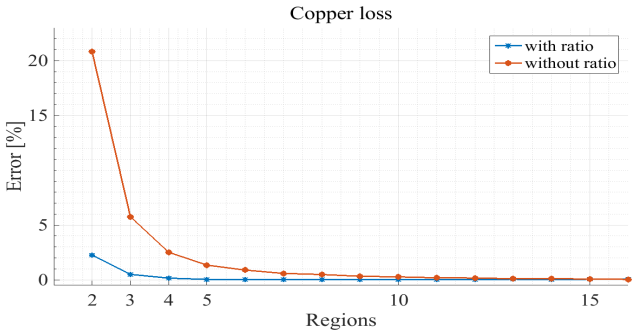

Fig. 6. Percentage errors between calculated copper losses of the considered BLDCPM generator

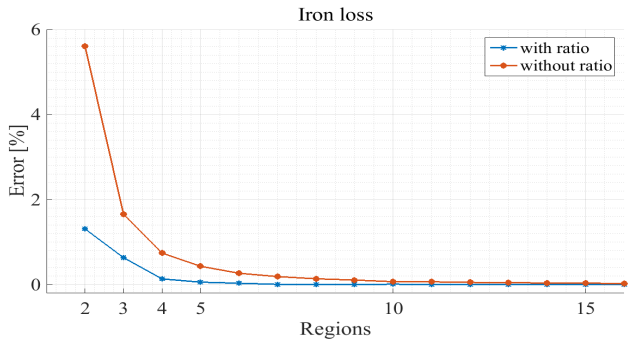

Fig. 7. Percentage errors between calculated iron losses of the considered BLDCPM generator

D. Analytical model of the BLDCPM generator

The second approach is to preserve the wind cycle and instead reduce the semi-analytical model. To develop an analytical model of the BLDCPM wind generator, the time-based characteristics of the above described model have to

be discharged and reshaped for faster usage. This new model is based on the circuit equations written by considering only the amplitude of the involved quantities. The rotational speed of the generator, being a linear function of the wind speed, it can easily be computed based on the tip-speed ratio equation:

$$\lambda = \Omega R_{wt} / v_w \tag{9}$$

The electromagnetic power of the generator (P_{em}) is assumed to result as:

$$P_{em} = \begin{cases} 0, & v_w < v_{in},\ v_w \geq v_{\max} \\ \frac{\pi}{2}\rho_{air} R_{wt}^5 \frac{C_{p\,opt}}{\lambda_{opt}^3}\Omega^3 - P_{mech}, & v_{in} \leq v_w \leq v_b \\ P_r - P_{mech}, & v_b < v_w < v_{\max} \end{cases} \tag{10}$$

where P_r defines the rated power, v_{in}, v_b, v_{max} represent the cut-in, base and cut-off wind speeds and P_{mech} represents the mechanical loss as [8]:

$$P_{mech} = f_{wt}\,\Omega^2 \tag{11}$$

Due to the fact that the back EMF is proportional to the rotational speed, its amplitude is sufficient to be taken into account for the calculation of the generator phase-stator current peak value:

$$E = k_e\,\Omega \tag{12}$$

$$I = \frac{P_{em}}{2E} \tag{13}$$

Furthermore, the developed electromagnetic torque can be computed as:

$$T_{em} = 2\,k_e\,I \tag{14}$$

The main advantage of this model resides in the fast evaluation time, which is less than one second for the 8759 wind speed measurements, whereas its drawbacks consist in its inability to predict the current and torque ripples.

E. FE-based numerical model of the BLDCPM generator

As the non-linearity, the geometry and mechanical movement are not considered by neither one of the previous (the semi-analytical and analytical) models and to ensure a certain accuracy of the system a third model is being investigated and that is the FE-based numerical model.

FE-discretized cross-sectional model of the BLDCPM generator (Fig. 8) was created and subjected to numerical field analysis by means of JMAG Designer software [11].

This model was used only for evaluating the simulation performances in precision and computing time of the previous models of the BLDCPM wind generator.

FE simulations were performed for 2-D time-stepping transient field analysis of the BLDCPM wind generator, operating at rated speed of 490 [rpm] (equivalent to 9 [m/s] wind speed) for supplying an isolated rectifier load. The obtained stator-winding phase-current and electromagnetic torque waveforms are presented in Figs. 9 and 10.

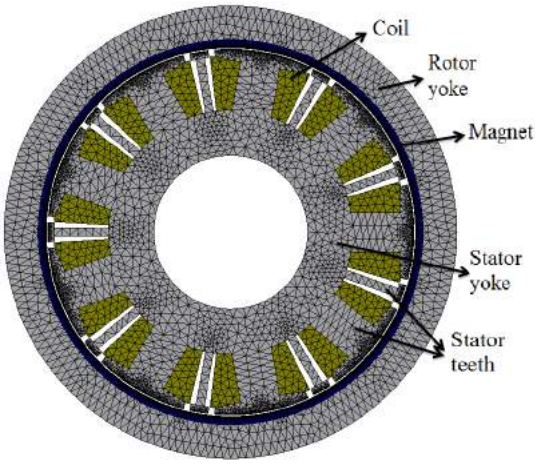

Fig. 8. FE-discretized cross-sectional model of the considered BLDCPM generator

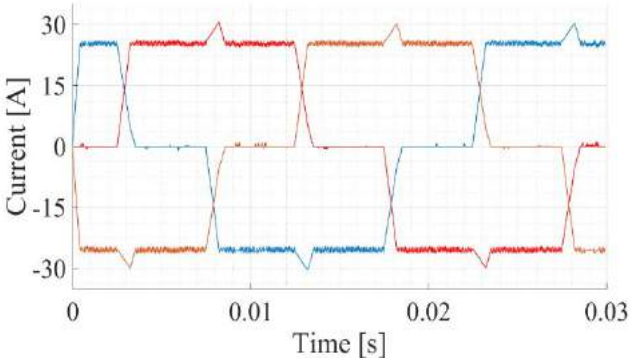

Fig. 9. FE-computed three-phase stator-current waveforms of the considered BLDCPM generator

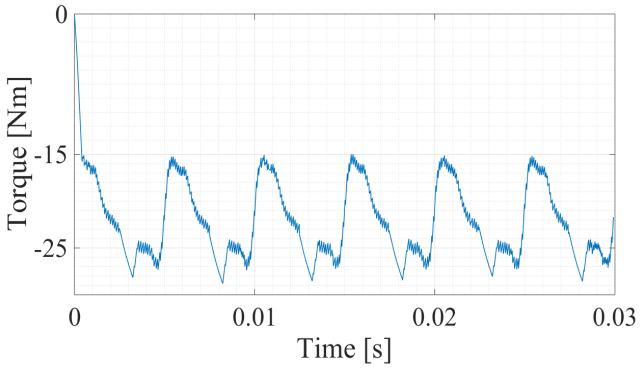

Fig. 10. FE-computed electromagnetic torque waveform of the considered BLDCPM generator

As it can be seen from the above figures a peak in the current waveforms results into an additional ripple in the electromagnetic torque. An average torque error between the (i) numerical and analytical models (orange rhomb) and (ii) numerical and semi-analytical models (red circle), as well as a maximum current error obtained likewise are represented in Fig. 11 alongside the CPU computation time, for the base operating point. Whereas the CPU time necessary for one FE simulation of one operating speed of the wind profile is of 1h and 20 minutes, estimation for the entire long-term wind profile gives one year of simulation time.

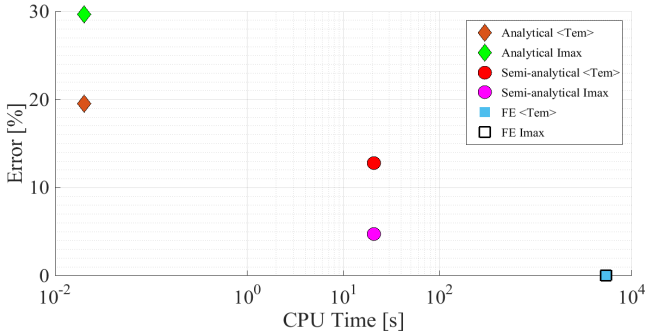

Fig. 11. Errors for average electromagnetic torque and maximum current in FE, semi-analytical, analytical models vs. CPU time in log-scale

A comparative analysis of the FE-computed and analytically-obtained average electromagnetic torque results for different operating points was carried out and reported in Fig.12. The low rotational speed of the turbine at low wind speeds resides in a larger error between the torque quantities of the models. As the wind speed and consequently the rotational speed of the turbine increase the tendency of the error is to decrease and stabilize at a certain value representing the error difference between the analytical and FE models. However, due to the peak in the current waveform, instantly transmitted to the torque curve, the direction of the error changes, as seen in Fig. 12.

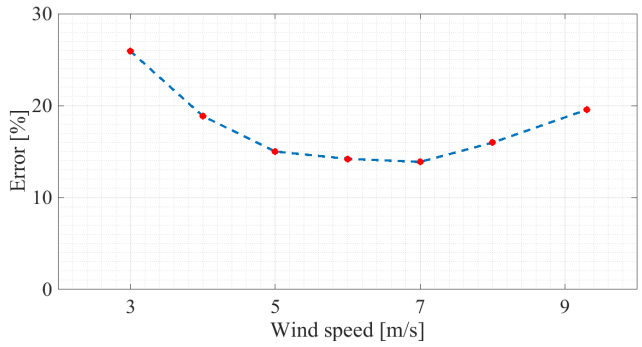

Fig. 12. Error between FE-computed and analytically-obtained electromagnetic torque results vs. wind speed

This rises several constraints to be imposed to the design optimization process in order to achieve the desired performances. Still, regardless of the waveforms of the currents or torque, a significant difference can be observed between the two models, hence, a correction of the analytical model should be effected if considered to be used in design optimization. The same principle is assumed for the semi-analytical model as well.

III. Conclusions

In this paper, a reduced-order analytical model is developed for BLDCPM generator in micro-wind turbine applications under wind-speed cycle constraints. The model can be used in design optimization of the generator operating under very large wind-speed profile. Withal, a wind-speed cycle partition technique based on barycenter method, allowing easy exploitation of large amount of available data from the wind-speed profile, is proposed and discussed in terms of copper and iron losses of the BLDCPM generator. At last, models performances in terms of accuracy and computation time were confronted against finite element-based numerical field model of the considered BLDCPM wind generator.

IV. Appendix

A. *Reference wind turbine parameters*

Radius of the turbine-rotor blades: $R_{wt} = 1.25$ [m]
Friction coefficient: $f_{wt} = 0.02$ [Nm/rad]
Optimal power coefficient: $C_{p\_opt} = 0.441$
Optimal tip speed ratio: $\lambda_{opt} = 6.9$

The Cp (λ) power coefficient of the reference wind turbine is a function of tip speed ratio (λ) and can be found through interpolation:

$$C_p(\lambda) = -3.98\cdot10^{-8}\cdot\lambda 7 - 4.21\cdot10^{-6}\cdot\lambda^6 + 2.1\cdot10^{-4}\cdot\lambda^5 - 3.1\cdot10^{-3}\cdot\lambda^4 + 1.64\cdot10^{-2}\cdot\lambda^3 - 0.0176\cdot\lambda^6 + 0.0174\cdot\lambda - 1.93\cdot10^{-3}$$

where λ depends on the turbine rotational speed, Ω and on the wind speed, v_w as in (9).

B. *Barycenter method*

The copper loss P_j, as a time-varying function, can be expressed for the semi-analytical model as:

$$P_j(t) = R\left[i_a^2(t) + i_b^2(t) + i_c^2(t)\right] \quad (15)$$

From (15) the average copper loss can be found by determining the RMS value of one period ($0 \le t \le T$) of the function through relations (16)-(19):

$$P_j = \left\langle P_j(t)\right\rangle_T = \frac{1}{T}\int_0^T P_j(t)dt \quad (16)$$

$$P_j = \frac{R}{T}\int_0^T \left[i_a^2(t) + i_b^2(t) + i_c^2(t)\right]dt \quad (17)$$

$$P_j = R\left[\frac{1}{T}\int_0^T i_a^2(t)dt + \frac{1}{T}\int_0^T i_b^2(t)dt + \frac{1}{T}\int_0^T i_c^2(t)dt\right] \quad (18)$$

$$P_j = R\left[I_{RMS\_a}^2 + I_{RMS\_b}^2 + I_{RMS\_b}^2\right] \quad (19)$$

where $I_{RMS\_ph} = \sqrt{\frac{1}{T}\int_0^T i_{ph}^2(t)dt}$ represents the equation which determines the quadratic mean for each phase current. Assuming that the phase currents have the same RMS value the losses in the stator windings become:

$$P_j = 3R\,I_{RMS}^2 \quad (20)$$

From the turbine power equation it is assumed that the electromagnetic power of the BLDCPM generator is proportional to the cube of the wind speed, whereas its rotational angular speed, Ω, is linked to the wind speed by relation (21). Therefore, the torque can be also considered

proportional to the square wind speed as in (22) and linked to the RMS current by (23):

$$\Omega = k_S v_W \tag{21}$$

$$T_{em} = k_W v_W^2 \tag{22}$$

$$T_{em} = k_t I_{RMS} \tag{23}$$

where k_s, k_t, k_w are speed and torque coefficients.

In this context, (20) becomes:

$$P_j = k_j v_W^4 \tag{24}$$

where $k_j = 3R\left(k_w / k_t\right)^2$. Assuming k_j is constant within one region, then the sum of copper loss for all the points (p) in the considered region (r) can be written as:

$$\sum_{p=1}^{Npt} P_{j,p} = k_{j,r} \sum_{p=1}^{Npt} v_{w,p}^4 = k_{j,r}\, N_{pt} \left\langle v_w^4 \right\rangle_r \tag{25}$$

As $k_{j,r}$ is constant, it can be computed for any point of the region, but the barycenter of the considered area is preferred:

$$k_{j,r} = \frac{P_{j,b}}{v_{w,b}^4} = \frac{3RI_{RMS,b}^2}{v_{w,b}^4} = \frac{3RI_{RMS,r}^2}{v_{w,r}^4} \tag{26}$$

with $v_{w,b} = \left\langle v_w \right\rangle_r$ and $I_{RMS,b} = I_{RMS,r}$ its corresponding current, computed for the wind speed $v_{w,b}$.

Finally,

$$P_{j,r} = \sum_{p=1}^{Npt} P_{j,p} = \frac{3RI_{RMS,r}^2}{v_{w,r}^4} N_{pt} \left\langle v_w^4 \right\rangle_r \tag{27}$$

$$P_{j,r} = 3RI_{RMS,r}^2 N_{pt} \frac{\left\langle v_w^4 \right\rangle_r}{\left\langle v_w \right\rangle_r^4} \tag{28}$$

and it is based on $I_{RMS,r}$, $\langle v_w \rangle_r$, $\langle v^4_w \rangle_r$ to be computed.

The iron losses in the stator core of the BLDCPM wind generator can be computed in terms of hysteresis and eddy current losses [7] as:

$$\begin{aligned} P_{Fe\_hys} &= k_{hys}\ f\ (B_{th}^{\alpha} + B_{sy}^{\alpha}) \\ P_{Fe\_eddy} &= \frac{4}{\pi} k_{eddy}\ f^2\ (B_{th}^2 + 2B_{sy}^2) \end{aligned} \tag{29}$$

where B_{th}, B_{sy} are the stator tooth and yoke flux densities, and k_{hys} and k_{eddy} represent the hysteresis and eddy current loss coefficients, which can be calculated from manufacturer data, and f is the electrical frequency, which is given by the pole-pairs number and by the rotor angular speed of the machine:

$$\omega_e = N_p\, \Omega, \qquad \omega_e = 2\pi f \tag{30}$$

In this context, (29) becomes:

$$\begin{aligned} P_{Fe\_hys} &= k_{hys}\ \frac{N_p}{2\pi} (B_{th}^{\alpha} + B_{sy}^{\alpha})\ \Omega \\ P_{Fe\_eddy} &= k_{eddy}\ \frac{N_p^2}{\pi^3}\ (B_{th}^2 + 2B_{sy}^2)\ \Omega^2 \end{aligned} \tag{31}$$

Given also the proportionality of the rotor angular speed of the machine to the wind speed:

$$\begin{aligned} P_{Fe\_hys} &= C_{hys}\ v_w \\ P_{Fe\_eddy} &= C_{eddy}\ v_w^2 \end{aligned} \tag{32}$$

where $C_{hys} = k_s k_{hys} \frac{Np}{2\pi} (B_{th}^{\alpha} + B_{sy}^{\alpha})$ and $C_{eddy} = k_s^2 k_{eddy} \frac{Np^2}{\pi^3} (B_{th}^2 + 2B_{sy}^2)$.

Assuming C_{hys} *and* C_{eddy} are constant within one region then the sum of iron loss for all the points (p) in the considered region (r) can be written as:

$$\begin{aligned} \sum_{p=1}^{Npt} P_{Fe\_hys,p} &= C_{hys,r} \sum_{p=1}^{Npt} v_{w,p} = C_{hys,r}\ N_{pt} \left\langle v_w \right\rangle_r \\ \sum_{p=1}^{Npt} P_{Fe\_eddy,p} &= C_{eddy,r} \sum_{p=1}^{Npt} v_{w,p}^2 = C_{hys,r}\ N_{pt} \left\langle v_w^2 \right\rangle_r \end{aligned} \tag{33}$$

As C_{hys} and C_{eddy} are constant, they can be computed for any point of the region, but the barycenter of the considered area is preferred:

$$\begin{aligned} C_{hys,r} &= \frac{P_{Fe\_hys,b}}{v_{w,b}} = \frac{k_{hys}\ \frac{N_p}{2\pi} (B_{th}^{\alpha} + B_{sy}^{\alpha})\ \Omega_b}{v_{w,b}} \\ &= \frac{k_{hys}\ \frac{N_p}{2\pi} (B_{th}^{\alpha} + B_{sy}^{\alpha})\ \Omega_r}{v_{w,r}} \\ C_{eddy,r} &= \frac{P_{Fe\_eddy,b}}{v_{w,b}^2} = \frac{k_{eddy}\ \frac{N_p^2}{\pi^3} (B_{th}^2 + 2B_{sy}^2)\ \Omega_b^2}{v_{w,b}^2} \\ &= \frac{k_{eddy}\ \frac{N_p^2}{\pi^3} (B_{th}^2 + 2B_{sy}^2)\ \Omega_r^2}{v_{w,r}^2} \end{aligned} \tag{34}$$

with $v_{w,b} = \left\langle v_w \right\rangle_r$ and $\Omega_b = \Omega_r$ its corresponding rotational speed, computed for the wind speed $v_{w,b}$.

Finally,

$$P_{Fe\_hys,r} = \sum_{p=1}^{Npt} P_{Fe\_hys,p} = \frac{k_{hys}\ \frac{N_p}{2\pi} (B_{th}^{\alpha} + B_{sy}^{\alpha})\ \Omega_r}{v_{w,r}} N_{pt} \langle v_w \rangle_r \tag{35}$$

$$P_{Fe\_hys,r} = k_{hys}\ \frac{N_p}{2\pi} (B_{th}^{\alpha} + B_{sy}^{\alpha})\ \Omega_r\, N_{pt} \frac{\left\langle v_w \right\rangle_r}{\left\langle v_w \right\rangle_r} \tag{36}$$

$$P_{Fe\_eddy,r} = \sum_{p=1}^{Npt} P_{Fe\_eddy,p} = \frac{k_{eddy}\ \frac{N_p^2}{\pi^3} (B_{th}^2 + 2B_{sy}^2)\ \Omega_r^2}{v_{w,r}^2} N_{pt} \left\langle v_w^2 \right\rangle_r \tag{37}$$

$$P_{Fe\_eddy,r} = k_{eddy}\ \frac{N_p^2}{\pi^3}\ (B_{th}^2 + 2B_{sy}^2)\ \Omega_r^2\, N_{pt} \frac{\left\langle v_w^2 \right\rangle_r}{\left\langle v_w \right\rangle_r^2} \tag{38}$$

and it is based on Ω_r, $\langle v_w \rangle_r$, $\langle v_w^2 \rangle_r$ to be computed.

V. REFERENCES

[1] R. Krishnan, G.-H. Rim, "Modeling, simulation, and analysis of variable-speed constant frequency power conversion scheme with a permanent magnet brushless DC generator", *IEEE Trans. Ind. Electron.*, Vol. 37, No. 4, 1990, pp. 291 – 296.

[2] H.-W. Lee, T.-H. Kim, M. Ehsani, "Practical control for improving power density and efficiency of the BLDC generator", *IEEE Trans. Power Electron.*, Vol. 20, No. 1, 2005, pp. 192-199.

[3] B. Singh, S. Sharma, "PMBLDCG based stand-alone wind energy conversion system for small scale applications", *International Journal of Engineering, Science and Technology*, Vol. 4, No. 1, 2012, pp. 65-73A.

[4] T.J.E. Miller, J.R. Hendershot Jr., "Design of Brushless Permanent-Magnet Motors", *Magna Physics Publishing and Clarendon Press*, Oxford, UK, 1994.

[5] S. Brisset, P. Brochet, "Analytical model for the optimal design of a brushless DC wheel motor", *COMPEL*, Vol. 24, No. 3, 2005, pp. 829-848.

[6] Andreea Laczko, M.V. Zaharia, M.M. Radulescu, S. Brisset, "Modeling and simulation of a brushless DC permanent-magnet generator-based wind energy conversion system", *Proc. Int. Conf. Ecol. Veh. Renew. Energ. – EVER 2015*, 7pp.

[7] P. Andrada, M. Torrent, J.L. Perat, B. Blanque, B., "Power Losses in Outside-Spin Brushless D.C. Motors", *Rep. Universitat Politecnica de Catalunya*, Barcelona, Spain, 2004.

[8] M. Belouda, A. Jaafar, B. Sareni, X. Roboam, J. Belhadj, "Design methodologies for sizing a battery bank devoted to a stand-alone and electronically passive wind turbine system", *Renewable and Sustainable Energy Reviews, Elsevier*, 2016, vol. 60, pp. 144-154.

[9] J.F. Manwell, J.G. McGowan, A.L. Rogers,"Wind Energy Explained: Theory, Design and Application", *John Wiley & Sons Publication*, New York, USA, 2009.

[10] G. Krebs, E. de Cecco, C. Marchand, "Design approach of an axial motor for electrical powertrain vehicle", *Proc. Int. Conf. Electr. Mach. – ICEM 2012*, 6 pp.

[11] www.jmag-international.com.

VI. BIOGRAPHIES

Andreea Adriana Laczko (Zaharia) was born in Romania in 1987. She received the M.Sc. degree from Faculty of Electrical Engineering, Technical University of Cluj-Napoca, Cluj-Napoca, Romania, in 2012. Since October 2012, she pursues a full-time Ph.D. study program in Electrical Engineering at the Technical University of Cluj-Napoca under international co-supervision of Ecole Centrale de Lille, France. Her research interests are in special electric machines for renewable energy applications.

Stephane Brisset is a graduate of Engineer School in 1992 at Ecole Centrale de Lille, France, PhD in Electrical Engineering in 1995 at Université des Sciences et Technologies de Lille. He joined Ecole des Hautes Etudes Industrielles in 1996 and Ecole Centrale de Lille in 2001 where he is now Associate Professor at Laboratoire d'Electrotechnique et d'Electronique de Puissance (L2EP). His main interests are the simulation, design and optimization of electric machines. He is author or co -author of many published scientific papers in refereed technical journals and international conference.

Mircea M. Radulescu received the Dipl.-Ing. degree with honors from the Technical University of Cluj-Napoca, Cluj-Napoca, Romania, in 1978 and the Ph.D. degree from the Polytechnic University of Timisoara, Timisoara, Romania, in 1993, both in electrical engineering. Since 1983, he has been with the Faculty of Electrical Engineering, Technical University of Cluj-Napoca, Romania, where he is currently Full Professor in the Department of Electric Machines and Drives, as well as Head of the Special Electric Machines and Light Electric Traction (SEMLET) Research Laboratory. He is author or co-author of more than 150 published scientific papers in refereed technical journals and international conference and symposium proceedings. His teaching and research activities include classical and special electric machines, computer-aided design of electromechanical devices, design and control of small electronically-commutated motors, actuators and mechatronic drives, light electric traction systems.

2015 Tenth International Conference on Ecological Vehicles and Renewable Energies (EVER)

Modeling and simulation of a brushless DC permanent-magnet generator-based wind energy conversion system

Andreea Adriana Laczko (Zaharia)[1,2], M.V. Zaharia[1,2], M.M. Radulescu[1]

S. Brisset[2]

[1]Technical University of Cluj-Napoca, Cluj-Napoca, Romania
Email: Andreea.Laczko@mae.utcluj.ro
Valentin.Zaharia@mae.utcluj.ro
Mircea.Radulescu@mae.utcluj.ro

[2]L2EP, Ecole Centrale de Lille, Villeneuve d'Ascq, France
Email:stephane.brisset@ec-lille.fr

***Abstract*— This paper deals with a brushless DC (BLDC) generator-based wind energy conversion system (WECS) for distributed electric power generation. Three-phase PWM rectifier and maximum-power-point-tracking algorithm are used for controlling the BLDC generator speed to achieve optimum energy output from the wind turbine. A PWM voltage-source inverter is connected to the DC bus for voltage and frequency regulation of AC supply to consumer loads. The BLDC generator-based WECS is modeled by sub-systems, and its dynamic behavior is simulated in MATLAB/SIMULINK environment for different wind-speed conditions and consumer loads.**

***Keywords*— *brushless DC permanent-magnet generator, wind energy conversion system, simulation model, MPPT control, trapezoidal back-EMF*.**

I. INTRODUCTION

Brushless DC (BLDC) permanent-magnet machines operating in generator mode offer several advantages, such as high efficiency over a wide speed range, low maintenance, greater durability, compactness, and higher power density. Moreover, due to the trapezoidal phase back-EMF of the BLDC generator, the rectified DC output voltage has reduced pulsations. Such positive features prompt the BLDC generator for use in small-scale wind energy conversion systems (WECSs) [1], [2].

Few papers in the literature treat the problem of simulations in the wind energy conversion systems of an entire system consisting of direct driven BLDC-generator with trapezoidal back-EMFs, back-to-back PWM converters with their control, inductive filter and utility grid.

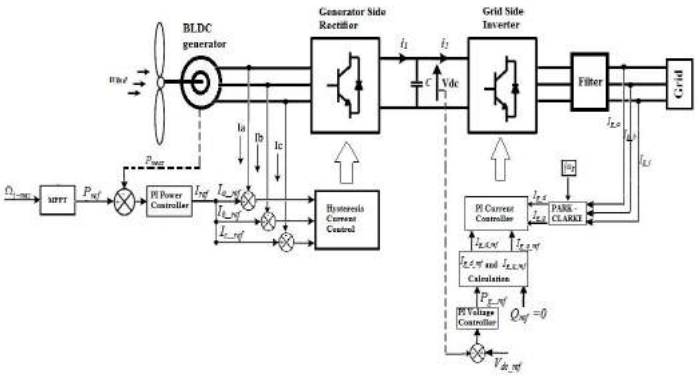

Fig.1. Schematic representation of the direct-driven BLDC generator-based WECS under study.

This paper proposes the modeling and simulation of distributed electric power generation system based on wind-turbine direct-driven three-phase BLDC generator (Fig.1). The output terminals of the BLDC wind generator are connected to a controlled PWM rectifier and the maximum-power-point tracking (MPPT) control is based on determining the maximum available power from the wind turbine. A DC-link capacitor allows the decoupling of the PWM rectifier from the PWM inverter used for grid connection and also for keeping constant the DC-link voltage. The proposed system is simulated using MATLAB/ SIMULINK software.

II. WIND TURBINE MODEL AND MPPT CONTROL

The direct-driven variable-speed wind turbine is modeled by the characteristics of the power coefficient, defined as the ratio of the mechanical power generated by the turbine and the power available in the wind.

978-1-4673-6785-1/15/$31.00 ©2015 European Union

In its turn, the value of the turbine power coefficient varies as a function of the tip-speed ratio, which is dependent on wind speed and angular velocity of turbine blades. Therefore, the mechanical power of the wind turbine extracted from the wind has the following expression [3]:

$$P_t = 0.5 \cdot C_p(\beta, \lambda) \cdot \rho \cdot A \cdot v_w^3 \quad (1)$$

$$C_p(\lambda, \beta) = C1 \cdot \left(\frac{C2}{\lambda_i} - C3 \cdot \beta - C4 \right) \cdot e^{-\frac{C5}{\lambda_i}} + C6 \cdot \lambda \quad (2)$$

where ρ is the air density (kg/m3), A is the area swept by turbine-rotor blades, v_w the wind speed and C_p the power coefficient of the turbine with C1=0.5176, C2=116, C3=0.4, C4=5, C5=-21, C6=0.0068.

The normal start-up of a wind turbine is for a wind speed of 2.5-5 m/s. Until the wind reaches its nominal speed of 9-15 m/s (depending on the generator power) the turbine operates under the MPPT (maximum power point tracking) control, in order to maximize the power extracted from the wind. For speeds exceeding this nominal value, the turbine operates at nominal power, i.e. the wind generator rated power, to prevent the overload of the conversion system. For the proposed system, the start-up wind speed is at 3 m/s, and the generator reaches its rated power of 3 kW at 11.3 m/s. For a wind speed less than 25 m/s, the wind turbine operates at rated power, and, finally, if the speed of the wind is higher than the admissible one, the wind turbine is stopped (Fig.2). The pitch angle for the proposed system is set to zero.

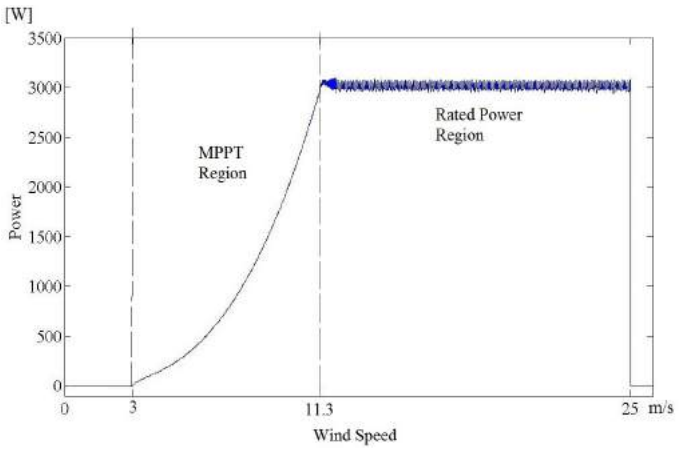

Fig.2. Generated power vs. wind speed for the proposed system

The MPPT control algorithm is based on computing the optimal rotational speed of the wind generator (ω_r) from the wind speed measurements, and further determining the maximum power that can be extracted from the wind. The equations for the optimal rotational speed and maximum power are as follows [4]:

$$\omega_r = \frac{\lambda\_opt}{Rt} \cdot v_w \quad (3)$$

$$P_{\max} = \frac{1}{2} \cdot \pi \cdot R_t^5 \cdot \rho_{air} \cdot \frac{C_{p\_\max}}{\lambda_{\_opt}^3} \cdot \omega_r^3 \quad (4)$$

$$P_{\max} = K_{optim} \cdot \omega_r^3 \quad (5)$$

where R_t is the radius of the turbine-rotor blades and λ_opt is the optimal tip speed ratio.

III. Brushless DC Permanent-Magnet Generator Model and Control

The simulation model of the three-phase star-connected BLDC wind generator is built in MATLAB/ SIMULINK, considering identical resistances and inductances for the three stator-phase windings [5]:

$$v_{ab} = R \cdot (i_a - i_b) + (L - M) \cdot \frac{d(i_a - i_b)}{dt} + e_a - e_b \quad (6)$$

$$v_{bc} = R \cdot (i_b - i_c) + (L - M) \cdot \frac{d(i_b - i_c)}{dt} + e_b - e_c \quad (7)$$

$$i_a + i_b + i_c = 0 \quad (8)$$

where R and L are phase resistance and inductance, M is the mutual inductance, i_k and e_k are the phase currents and the induced back-EMFs, with k being the a, b or c phase .

The motion equation is expressed as:

$$T_e = T_L + J \cdot \frac{d\omega_r}{dt} + B \cdot \omega_r \quad (9)$$

where T_e is the electromagnetic torque developed by the generator, T_L is the load torque given by the wind turbine, J and B represent the rotor inertia and the viscous friction coefficient.

The trapezoidal back-EMF is a function of rotor position, and has the amplitude:

$$E = k_e \cdot \omega_r \quad (10)$$

with k_e being the back-EMF constant.

Considering that back-EMF waveforms are identical in all three stator phases, the back-EMF expression for phase a is [5]:

$$e_a = \begin{cases} (\frac{6 \cdot E}{\pi}) \cdot \theta_r, & 0 < \theta_r < \frac{\pi}{6} \\ E, & \frac{\pi}{6} < \theta_r < \frac{5 \cdot \pi}{6} \\ -(\frac{6 \cdot E}{\pi}) \cdot \theta_r + 6 \cdot E, & \frac{5 \cdot \pi}{6} < \theta_r < \frac{7 \cdot \pi}{6} \\ -E, & \frac{7 \cdot \pi}{6} < \theta_r < \frac{11 \cdot \pi}{6} \\ (\frac{6 \cdot E}{\pi}) \cdot \theta_r - 12 \cdot E, & \frac{11 \cdot \pi}{6} < \theta_r < 2 \cdot \pi \end{cases} \quad (11)$$

The expressions for stator-phases *b* and *c* can be expressed according to (11), knowing that each phase has 120-degree phase shift from the other two phases.

The electromagnetic torque expression results as:

$$T_e = \frac{e_a\, i_a + e_b\, i_b + e_c\, i_c}{\omega_r} \quad (12)$$

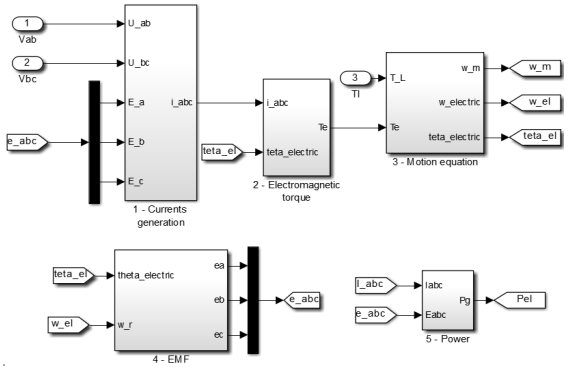

Fig.3 MATLAB/SIMULINK implementation of the BLDC wind-generator model.

The blocks in Fig. 3 represent the implementation of equations (6) to (12) in MATLAB/SIMULINK environment for the BLDC generator model having as main outputs the phase currents, the active power, the back-EMFs, the electromagnetic torque and the speed of the machine. The inputs are represented by the line-to-line stator voltages and the active torque produced by the wind turbine.

The error signal representing the difference between the maximum reference power achieved from the MPPT control and the active power of the generator is processed through PI controller, whose output is then used to obtain the phase reference currents, based on 120°-switching pattern of the generator-side rectifier according to the generator-rotor angular position (Table 1).

TABLE 1: ROTOR ANGULAR POSITION AND CORRESPONDING REFERENCE PHASE CURRENTS

Sector	θ_r	I_{a_ref}	I_{b_ref}	I_{c_ref}
1	330^0-30^0	0	-Ir	Ir
2	30^0-90^0	Ir	-Ir	0
3	90^0-150^0	Ir	0	-Ir
4	150^0-210^0	0	Ir	-Ir
5	210^0-270^0	-Ir	Ir	0
6	270^0-330^0	-Ir	0	Ir

Further, the 'ON/OFF' PWM signals for driving the power devices of the wind generator-side rectifier are achieved from the hysteresis current control after adjusting the generator currents in order to follow the reference ones, as shown in Fig.4. These power electronic devices of the rectifier are considered ideal and without power losses.

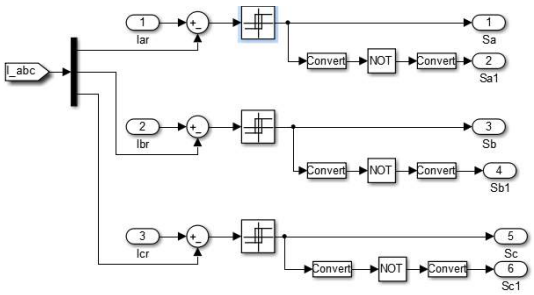

Fig.4. Hysteresis current-control implementation in MATLAB/SIMULINK.

IV. GENERATOR-SIDE PWM RECTIFIER MODEL

The three-phase PWM rectifier connected between the BLDC generator terminals and the DC-link circuit is modeled for six operation states (or sectors), each one (of 60°) consisting of a commutation interval and a conduction interval (Fig.5).

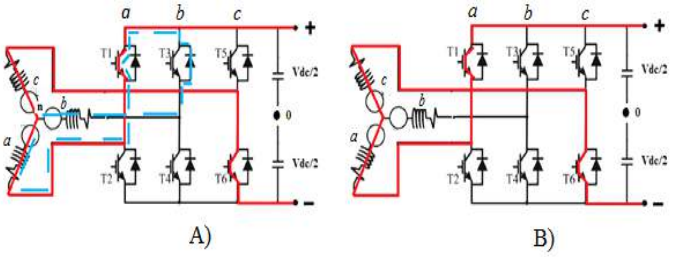

Fig.5. Equivalent circuit and current path corresponding to the commutation interval (A) and conduction interval (B) of one of the six operation states (sectors) of the generator-side three-phase PWM rectifier.

During the commutation interval (Fig.5, *A*) all three phases are active due to the freewheeling current flowing in the phase just switched-off. For example, in Fig. 5, *A*, the main current path is through *a*-phase and *c*-phase windings, allowed by the open upper-side power switch T1 and lower-side power switch T6; the second current path is the freewheeling one through b-phase winding via the upper-side power switch T1 and the upper-side fly-back diode D3. At the end of the commutation interval, the free-wheeling current vanishes and the conduction interval begins (Fig.5,*B*) with only two energized phases, according to the operating states of the PWM rectifier.

TABLE 2: STATOR-PHASE VOLTAGES OF THE BLDC GENERATOR

Sector	θ_r	V_{an}		V_{bn}		V_{cn}	
		Commutation Interval	Conduction Interval	Commutation Interval	Conduction Interval	Commutation Interval	Conduction Interval
1	330^0-30^0	$\frac{1}{3}\cdot Vdc+\frac{e_{sum}}{3}$	e_a	$-\frac{2}{3}\cdot Vdc+\frac{e_{sum}}{3}$	$Vb01+\frac{(e_b+e_c)}{2}$	$\frac{1}{3}\cdot Vdc+\frac{e_{sum}}{3}$	$Vc0+\frac{(e_b+e_c)}{2}$
2	30^0-90^0	$\frac{2}{3}\cdot Vdc+\frac{e_{sum}}{3}$	$Va0+\frac{(e_a+e_b)}{2}$	$-\frac{1}{3}\cdot Vdc+\frac{e_{sum}}{3}$	$Vb01+\frac{(e_a+e_b)}{2}$	$-\frac{1}{3}\cdot Vdc+\frac{e_{sum}}{3}$	e_c
3	90^0-150^0	$\frac{1}{3}\cdot Vdc+\frac{e_{sum}}{3}$	$Va0+\frac{(e_a+e_c)}{2}$	$\frac{1}{3}\cdot Vdc+\frac{e_{sum}}{3}$	e_b	$-\frac{2}{3}\cdot Vdc+\frac{e_{sum}}{3}$	$Vc01+\frac{(e_a+e_c)}{2}$
4	150^0-210^0	$-\frac{1}{3}\cdot Vdc+\frac{e_{sum}}{3}$	e_a	$\frac{2}{3}\cdot Vdc+\frac{e_{sum}}{3}$	$Vb0+\frac{(e_b+e_c)}{2}$	$-\frac{1}{3}\cdot Vdc+\frac{e_{sum}}{3}$	$Vc01+\frac{(e_b+e_c)}{2}$
5	210^0-270^0	$-\frac{2}{3}\cdot Vdc+\frac{e_{sum}}{3}$	$Va01+\frac{(e_a+e_b)}{2}$	$\frac{1}{3}\cdot Vdc+\frac{e_{sum}}{3}$	$Vb0+\frac{(e_a+e_b)}{2}$	$\frac{1}{3}\cdot Vdc+\frac{e_{sum}}{3}$	e_c
6	270^0-330^0	$-\frac{1}{3}\cdot Vdc+\frac{e_{sum}}{3}$	$Va01+\frac{(e_a+e_c)}{2}$	$-\frac{1}{3}\cdot Vdc+\frac{e_{sum}}{3}$	e_b	$\frac{2}{3}\cdot Vdc+\frac{e_{sum}}{3}$	$Vc0+\frac{(e_a+e_c)}{2}$

After calculating the stator-phase voltages for commutation and conduction intervals of each of the six operation states of the PWM rectifier, their expressions have been synthesized in Table 2, where $e_{sum}=e_a+e_b+e_c$.

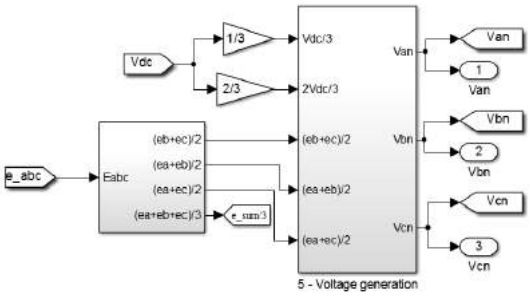

Fig.6. Stator-phase voltage generation block in MATLAB/SIMULINK.

Fig. 6 shows the implementation of Table 2 in MATLAB/SIMULINK environment for the stator-phase voltage determination. This implementation is done for each operation state (sector) of the BLDC generator-side PWM rectifier; detail of one sector is shown in Fig. 7, where V_{ao} and V_{co1} represent the voltages for the upper-side power switch of phase *a* and the lower-side switch of phase *c* and S_{ao} and S_{co1} are the corresponding PWM signals. These voltages are obtained as:

$$V_{ao}=\frac{Vdc}{2}*S_{ao}$$

$$V_{co1}=-\frac{Vdc}{2}*S_{co1} \qquad (13)$$

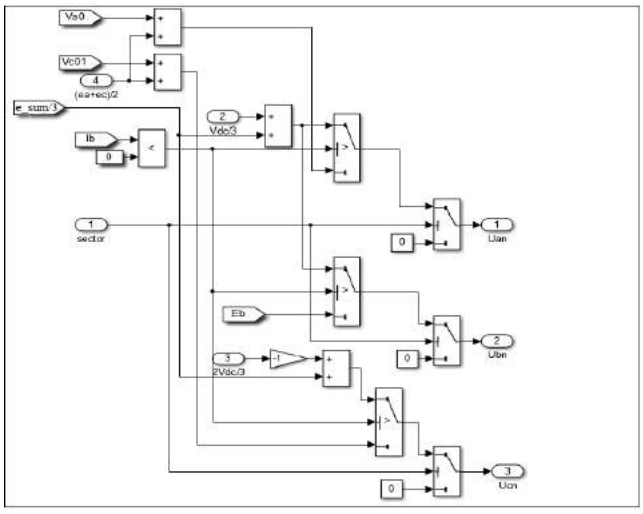

Fig. 7. Scheme of an operation sector of the three-phase PWM rectifier in Matlab/Simulink.

V. CONTROL OF THE GRID-SIDE PWM INVERTER

The electric energy provided by the three-phase BLDC wind generator and transmitted to the DC-link circuit via the PWM rectifier is then applied to a PWM inverter, which is conceived and simulated to keep the DC-link voltage constant at a proper value, and to provide a 50Hz-sinusoidal supply to the consumer loads or utility grid by means of an inductive filter [4] [6].

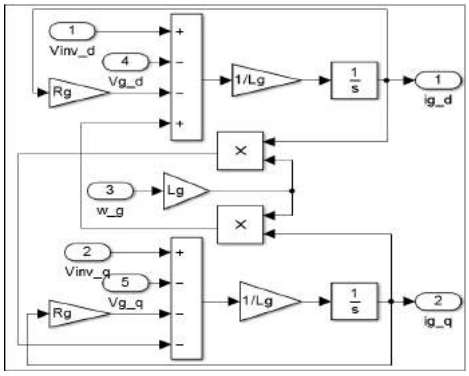

Fig. 8. Grid-connection implementation in MATLAB/SIMULINK.

The dynamic model of the grid connection, developed in the reference frame rotating synchronously with the grid-voltage space vector, is presented in Fig.8.

A. DC-link voltage control

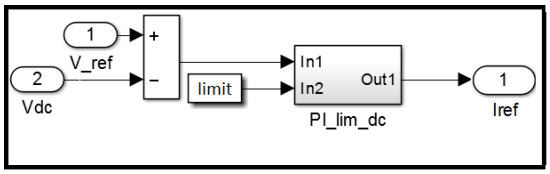

Fig. 9. DC-link voltage control and active reference current value generation.

The measured DC voltage across the capacitor is compared to a reference voltage, as shown in Fig. 9. The DC-link voltage regulation is based on the following equations:

$$\frac{dV_{dc}}{dt} = \frac{1}{C} \cdot (i_1 - i_2) \tag{14}$$

$$i_{dc} = i_1 - i_2 \tag{15}$$

where

$$i_1 = \frac{1}{2} \cdot (S_a \cdot i_a + S_b \cdot i_b + S_c \cdot i_c)$$

$$i_2 = \frac{1}{2} \cdot (S_{ga} \cdot i_{ga} + S_{gb} \cdot i_{gb} + S_{gc} \cdot i_{gc}) \tag{16}$$

with S_i denoting the PWM switching functions for each converter leg of generator-side rectifier and grid-side inverter, respectively.

B. Current control

The currents are controlled using PI controller to provide the reference voltages (Figs. 10 and 11).

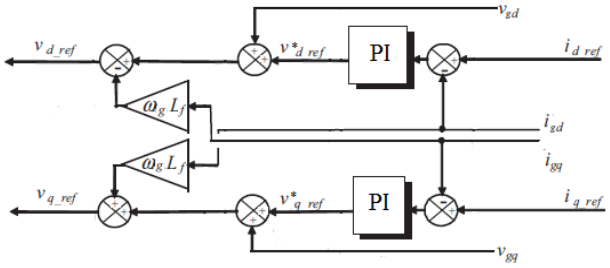

Fig. 10. Block-diagram of the grid-side PWM inverter current control [7].

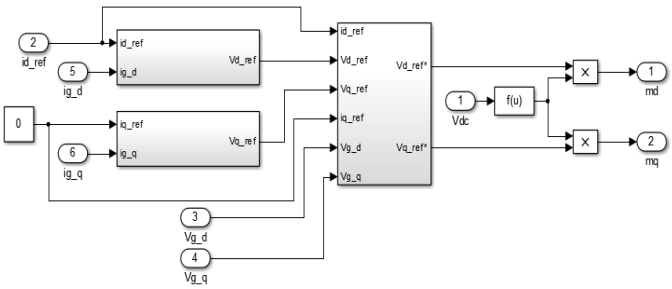

Fig. 11. Grid-side PWM inverter current-control implementation in MATLAB/SIMULINK.

The *d*-current component is used for DC voltage regulation and the *q*-current component is used for the reactive power regulation. A zero value was imposed to the *q*-component of the reference current, in order to maintain a unity power factor.

VI. SIMULATION RESULTS

The overall simulation model of the BLDC generator-based WECS under study is implemented in MATLAB/SIMULINK environment, using a fix-time step solver with a basic time step 10μs.

The active torque on the generator shaft is applied by the wind turbine, and the MPPT control yields the reference power needed to control the BLDC wind generator.

The wind speed profile, shown in Fig. 12, was chosen for simulations in order to analyze the wind turbine performances in MPPT and rated-power regions.

The active power of the BLDC wind generator and the wind turbine power are illustrated in Fig. 13. As it can be seen, starting from 3 m/s wind speed, the turbine is

activated and operates under the MPPT region and then at the rated power, when the nominal wind speed is reached.

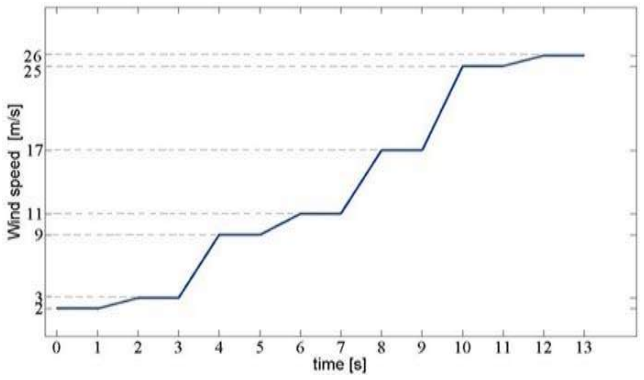

Fig. 12. Wind speed profile.

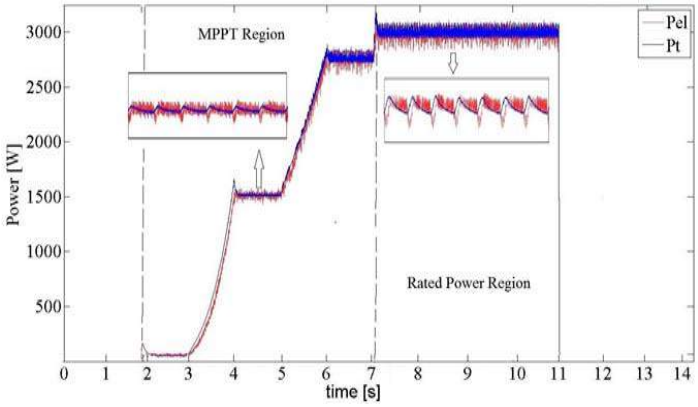

Fig. 13.Wind turbine power and BLDC-generator delivered active power.

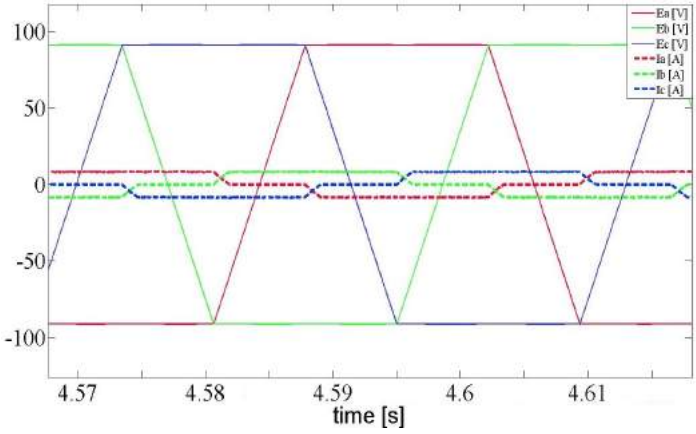

Fig. 14. Three-phase stator currents and back-EMFs of the wind turbine-driven BLDC generator under study.

Fig. 14 shows in detail the waveforms of the BLDC wind-generator stator currents and back-EMFs. Due to the generator operating mode, currents and back-EMFs are time-varying in opposite phase.

The line-to-neutral and line-to-line voltages of the BLDC wind generator, determined by using Table 2, are emphasized in Figs. 15 and 16.

Simulation results for the DC-link voltage regulation are presented in Fig. 17, pointing out rather small variations around the preset value of 530 Vcc for wind speed changes.

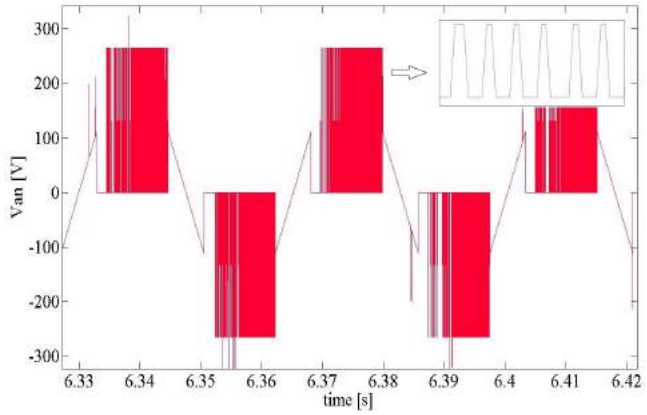

Fig. 15. Line-to-neutral voltage of the wind turbine-driven BLDC generator under study.

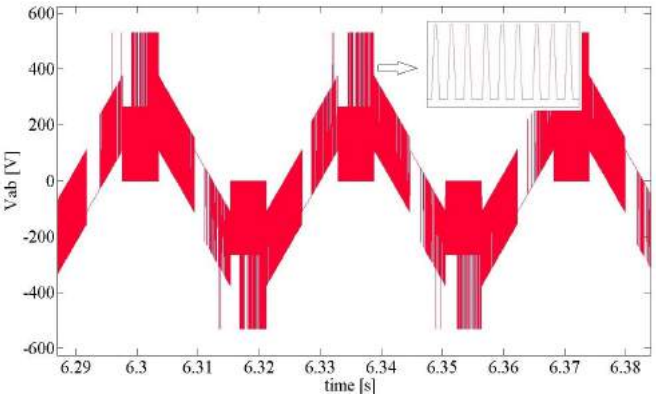

Fig. 16. Line-to-line voltage of the wind turbine-driven BLDC generator under study.

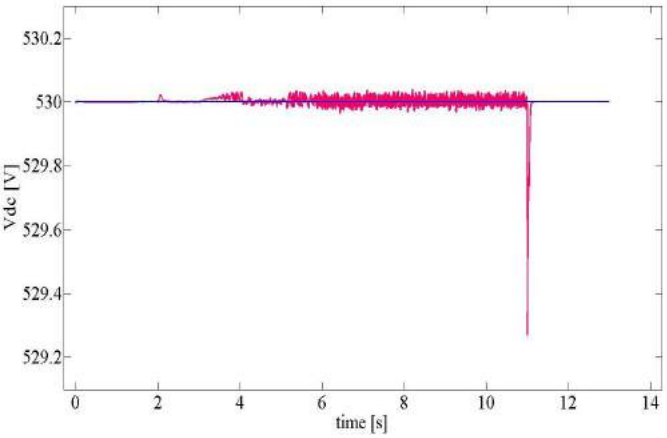

Fig. 17. Simulation results for the DC-link voltage regulation by the grid-side three-phase PWM inverter.

VII. Conclusions

The present paper has proposed and developed in MATLAB/SIMULINK environment a complete

simulation model of a small-scale WECS consisting of wind turbine with MPPT control strategy, BLDC permanent-magnet generator, back-to-back PWM converters with their control, inductive filter and utility grid.

Mathematical models and simulation results for all these WECS sub-systems have been given, providing a simulation tool for performance analysis and control design of direct-driven BLDC generator–based WECSs.

A perspective is to use this model in an optimization process to minimize the torque ripple and maximize the energy sent to the grid.

REFERENCES

[1] R. Krishnan, G.-H. Rim, "Modeling, simulation, and analysis of variable-speed constant frequency power conversion scheme with a permanent magnet brushless DC generator", *IEEE Trans. Ind. Electron.*, Vol. 37, No. 4, 1990, pp. 291 – 296.

[2] H.-W. Lee, T.-H. Kim, M. Ehsani, "Practical control for improving power density and efficiency of the BLDC generator", *IEEE Trans. Power Electron*., Vol. 20, No. 1, 2005, pp. 192-199.

[3] B. Singh, S. Sharma, "PMBLDCG based stand-alone wind energy conversion system for small scale applications", *International Journal of Engineering, Science and Technology*, Vol. 4, No. 1, 2012, pp. 65-73A.

[4] M. Mansour, M.N. Mansouri, M.F. Mmimouni, " Study and control of a variable-speed wind-energy system connected to the grid", *International Journal of Renewable Energy Research*, Vol.1, No.2, pp.96-104 ,2011.

[5] B.-K. Lee, M. Ehsani, "Advanced simulation model for brushless DC motor drives", *Electric Power Components and Systems*, Volume 31, No. 9, 2003.

[6] B. Singh, A.L. Vyas, N. Adhikari, "Design and control of variable-speed wind energy conversion system employing PMBLDC generator", *Proc. 2012 IEEE International Conference on Power Electronics, Drives and Energy Systems – PEDES 2012*, CD-ROM, 7 pp.

[7] T. Ghennam, E.M.Berkouk, B.François, „Modeling and Control of a Doubly Fed Induction Generator (DFIG) Based Wind Conversion System", *POWERENG*, Lisbon, Portugal, March 18-20, 2009.

Résumé étendu

Le travail réalisé pour le développement de cette thèse a été accompli lors d'une cotutelle entre l'Université Technique de Cluj-Napoca en Roumanie et l'Ecole Centrale de Lille en France.

La conception d'un système autonome de conversion de l'énergie micro-éolienne représente le cœur de cette étude. L'attention est portée vers le générateur BLDCPM en étoile à trois phases, ayant un rotor extérieur avec des aimants permanents montés en surface et des enroulements concentrés avec des forces électromotrices trapézoïdales. Une connexion directe entre la turbine à axe horizontal et la machine tournant à vitesse variable est considérée puisque l'application visée est résidentielle et nécessite un fonctionnement à faible vitesse. Le convertisseur électronique de puissance à courant alternatif (redresseur) et à pont complet triphasé du côté générateur est considéré pour contrôler la tension constante du bus continu de sortie. En raison de la vitesse variable du vent, de nombreuses fluctuations se produisent dans la puissance et la fréquence du générateur BLDCPM, ce qui oblige sa conception pour un fonctionnement à une large plage de vitesse. Ainsi, le travail de la thèse vise à déterminer les paramètres optimaux de conception géométriques et électriques du générateur BLDCPM, en assurant des pertes de puissance minimales dans le μWECS. Un fonctionnement sur un cycle long terme d'une année avec une vitesse moyenne du vent mesurée toutes les heures est considéré pour maximiser la puissance éolienne extraite et augmenter l'efficacité du système dans son ensemble. Par conséquent, il est nécessaire de déterminer le niveau de modélisation, ainsi que les variables de conception de chacun des composants du système. Comme l'optimisation fait appel à un algorithme pour le processus de conception, le nombre d'évaluations du modèle peut être assez important. Plus les variables de conception et les contraintes sont nombreuses, plus élevé est le nombre d'évaluations. En conséquence, la réduction du temps de simulation, ainsi que l'intégration et l'exploitation des données provenant du profil de vitesse du vent pour déterminer la totalité des pertes de puissance dans le μWECS considérées sont les principales préoccupations. Ensuite, la méthodologie d'optimisation est présentée, ainsi que les résultats optimaux obtenus et la comparaison de plusieurs paramètres d'entrée et de sortie.

Il est maintenant possible de fournir une vue d'ensemble sur les objectifs fixés pour cette thèse qui consistent à (i) analyser et développer un modèle de simulation d'un système micro-éolien, ainsi que (ii) la détermination et le développement d'une méthode de réduction du profil de vitesse du vent sur la base desquels (iii) les pertes de puissance dans le système peuvent être calculées et (iv) incluses dans les approches d'optimisation en vue de leur minimisation tout en déterminant les paramètres géométriques et électriques optimaux du générateur BLDCPM.

Enfin, des essais expérimentaux sont également effectués sur un prototype de machine BLDCPM de référence afin de vérifier la technique de commutation et de contrôle électronique.

Chapitre 1

Générateur sans balais à aimants permanents et auto-commutation pour applications micro-éoliennes

Après une courte introduction sur le contexte du marché de l'éolien actuel et des capacités installées dans le monde entier, une présentation simple des topologies des systèmes micro-éoliens est faite. Cette classification permet un passage facile à la description de l'architecture retenue du système d'énergie éolienne qui va être étudiée tout au long de la thèse. La configuration est représentée par la micro-éolienne, le générateur électrique, le convertisseur CA / CC côté générateur (redresseur) et le bus continu. Il est supposé que le bus continu est connecté à la banque des batteries et présente une tension constante.

Cette structure peut être considérée comme un bon exemple d'un système de conversion d'énergie éolienne complexe (même si la limite est fixée au niveau du bus continu) car il intègre des sous-systèmes appartenant à différents domaines physiques tels qu'aérodynamique, mécanique, magnétique, thermique et électrique avec de fortes interférences entre eux, imposant de considérer le système dans sa globalité durant le processus de conception, plutôt que de les optimiser séparément. Par conséquent, l'approche basée sur la conception par optimisation, qui représente l'objectif principal de cette thèse, est justifiée et peut-être même nécessaire pour atteindre des performances compétitives. De plus, une justification de la connexion mécanique et du type d'ensemble générateur-redresseur est fournie.

La topologie d'une micro-turbine à l'axe horizontal et vitesse variable est considérée pour une étude plus approfondie. Le choix est justifié par les avantages que cette configuration assure pour le fonctionnement à vitesse variable. Une configuration d'entraînement direct est préférée pour le système de micro-éolienne étudié car il s'agit d'une solution moins coûteuse et moins complexe, plus favorisée pour les petites éoliennes à usage résidentiel, caractérisée par une faible vitesse de rotation et un couple élevé, une maintenance réduite et une fiabilité accrue.

Le générateur triphasé sans balais à rotor externe et à aimants permanents montés en surface avec des forces électromotrices trapézoïdales et des enroulements concentrés est proposé comme solution de générateur électrique pour l'application de micro-éolienne. Le générateur consiste en une construction simple, basée sur des enroulements d'induit sur le stator et des aimants permanents sur le rotor. Le principe de fonctionnement de cette machine est également détaillé dans cette partie de la thèse. L'absence de balais dans sa configuration donne plusieurs

avantages pour cette topologie comme l'amélioration de l'efficacité énergétique, une meilleure fiabilité, une durée de vie plus longue avec moins d'entretien, une densité de puissance plus élevée et un rapport couple / poids plus élevé. Le convertisseur statique associé au générateur est représenté par un redresseur triphasé avec six interrupteurs IGBT et des diodes en antiparallèle. Une brève description des états de commutation du redresseur est aussi donnée.

Chapitre 2

Modélisation en vue de son optimisation du système de conversion de l'énergie d'une micro-éolienne comportant un générateur sans balais

Établir le bon niveau de la modélisation qui permet de résoudre le problème de conception au moyen d'une optimisation d'une manière assez rapide représente un défi. Par conséquent, la première partie de ce chapitre commence par la modélisation des composants associés au système de conversion de l'énergie de la micro-éolienne.

Le premier composant à étudier est représenté par la micro-turbine, en introduisant les équations pour le calcul de la puissance mécanique et la détermination du coefficient de puissance. La modélisation de l'ensemble générateur-redresseur est discutée après. Pour cela, trois niveaux de modélisation du générateur sont analysés afin d'établir le modèle approprié qui peut être utilisé dans le processus de conception par optimisation du système de conversion d'énergie micro-éolienne. Chaque modèle de simulation inclut les caractéristiques de dimensionnement du générateur qui seront déterminées au préalable par un modèle de dimensionnement unique au cours de l'optimisation. Les équations géométriques examinées pour la conception du générateur sont détaillées dans l'annexe 2.A portant sur le modèle de dimensionnement.

Le premier modèle développé est le modèle analytique de simulation qui peut être caractérisée comme un modèle statique basé sur les équations de dimensionnement et de circuit de la machine écrites en ne considérant que l'amplitude des quantités impliquées. Comme il ne calcule que les valeurs moyennes ou maximales, son meilleur avantage réside dans le court temps de simulation alors que son incapacité à prédire certains phénomènes dans les formes d'onde des courants et du couple représente son principal inconvénient. Plusieurs hypothèses sont faites pour ce modèle afin de simplifier sa construction. Tout d'abord, sachant que pour une connexion en étoile deux phases sont activées simultanément et que la force électromotrice est proportionnelle à la vitesse de rotation du générateur, ainsi son amplitude est suffisante pour le calcul du courant de phase et du couple électromagnétique du générateur. Deuxièmement, comme le générateur est à entraînement direct, on suppose que sa vitesse de rotation peut être

déterminée à partir du coefficient de vitesse réduite (tip speed ratio) alors que sa puissance électromagnétique développée est supposée dériver de l'équation de puissance mécanique d'éolienne en considérant une extraction maximale de la puissance du vent. La mise en œuvre des équations sur lesquelles ce modèle repose se fait dans l'environnement de programmation Matlab et aucun contrôle n'est mis en œuvre pour ce modèle car la commutation des phases n'est pas explicitement prise en compte.

Afin d'évaluer les propriétés dynamiques du générateur, qui ont un impact important sur la qualité de l'énergie électrique générée, un deuxième modèle de simulation est étudié, c'est-à-dire le modèle semi-analytique en fonction du temps, dont la mise en œuvre se fait dans l'environnement Matlab / Simulink. Sa description repose sur trois parties: la première présente les équations électriques sur lesquelles la modélisation du générateur est réalisée, tandis que la deuxième et la troisième partie révèlent le contrôle et le modèle de convertisseur de puissance associé.

L'analyse du générateur triphasé est basée sur un couple d'hypothèses telles que: (i) l'effet de saturation des matériaux n'est pas pris en compte, (ii) les résistances et inductances des enroulements de phase sont considérées comme identiques et constantes et (ii) la force électromotrice est présumée trapézoïdale et identique dans toutes les phases. Les équations électriques pour les tensions de phase et les forces électromotrices sont détaillées ainsi que les équations d'énergie électromagnétique et de couple. En ce qui concerne la section de commande du générateur, une boucle externe de puissance et un contrôle du courant par hystérésis sont mis en œuvre pour assurer que le générateur soit capable de développer une puissance égale à celle récoltée par la turbine du vent.

La sortie de la régulation de puissance basée sur le régulateur PI permet de déterminer les courants de référence des phases sur la base d’une technique de commutation du générateur à 120 degrés qui dépend de la position angulaire du rotor. Le schéma de commande de courant par hystérésis, établi sur le réglage des courants d'enroulement d'induit pour suivre celles de référence, est utilisé ensuite pour obtenir les signaux MLI de commande des interrupteurs du redresseur. Ce contrôleur d'hystérésis maintient les courants de phase dans un intervalle imposé, en transmettant, par des signaux ON (1) et OFF (0), aux dispositifs de puissance quand s’ouvrir et quand se fermer. La stratégie de commutation à 120 degrés permet de diviser un cycle électrique de 360 degrés en six secteurs de fonctionnement de 60 degrés. Chacun de ces secteurs est constitué à son tour par des intervalles de commutation (changement des phases alimentées du générateur) et de conduction (écoulement normal du courant à travers deux phases du stator) dont les caractéristiques opérationnelles sont soulignées dans ce chapitre par une illustration uniquement sur un secteur car le même principe s'applique pour les autres.

Comme ni le modèle analytique ni le semi-analytique ne prend en considération les caractéristiques non linéaires des matériaux et la géométrie complexe de la machine, un troisième modèle est étudié et c'est le modèle numérique à base d'éléments finis. L'avantage d'utiliser ce modèle est sa grande précision mais malheureusement il est bien connu pour son gros temps d'évaluation, ce qui en fait une stratégie déplaisante à considérer dans l'optimisation. Le modèle en coupe transversale discrétisé en éléments finis du générateur a été créé sur la base des paramètres dimensionnels d'une machine de référence et soumis à une analyse numérique du champ magnétique au moyen du logiciel JMAG Designer. Plusieurs étapes ont été suivies pour créer le modèle avec JMAG.

Ainsi, un lien a été créé entre JMAG Designer et Matlab via un fichier de script basé sur le langage Visual Basic. Il facilite la configuration automatique de la conception du générateur et du circuit électrique associé dans un temps court, permettant également de modifier les spécifications d'entrée, de mettre en œuvre les conditions aux limites, d'effectuer une analyse transitoire sur le modèle, et d'enregistrer les résultats qui peut être facilement visualisés ensuite dans Matlab.

Pour faire un choix sur le modèle à utiliser, des simulations sont effectuées au niveau du point de fonctionnement de base avec les valeurs d'une machine de référence, ce qui permet de déterminer la précision et le temps de simulation requis pour chacun des modèles. Le modèle numérique révèle une grande précision, mais son temps d'évaluation énorme en fait une solution non viable pour l'optimisation. D'autre part, le modèle semi-analytique, plus rapide en temps de calcul, démontre sa capacité à détecter les phénomènes qui apparaissent dans les formes d'onde de plusieurs grandeurs au cours des périodes de commutation et de conduction du redresseur. Enfin, le modèle analytique a l'avantage d'être le plus rapide et pourtant le moins précis des modèles. Ces deux derniers modèles semblent être la solution appropriée pour le processus d'optimisation avec une précision tout à fait acceptable, bien qu'une différence significative peut être observée entre eux et le modèle numérique à base d'éléments finis, par conséquent, une correction doit être calculé et appliqué aux sorties de ces modèles.

Chapitre 3

Modélisation et simulation du cycle du vent à long terme pour le système de conversion de l'énergie micro-éolienne

Comme la puissance de la micro-éolienne varie avec le cube de la vitesse du vent, son expression souligne l'impact important que la vitesse du vent ait sur le système de conversion de l'énergie micro-éolienne. Le profil du vent considéré pour cette thèse représente la valeur

moyenne prise sur une heure de mesures de vent, toutes les heures pendant un an, résultant en 8759 mesures qui décrivent le comportement du vent. Pour évaluer l'efficacité de l'ensemble du système, des simulations sur ce cycle long sont nécessaires. Cette approche n'est toutefois pas souhaitable dans le cadre de l'optimisation de la conception du fait que la simulation du système se répète à chaque fois que l'algorithme d'optimisation évalue une nouvelle solution.

Ainsi, le temps nécessaire pour trouver la solution de dimensionnement optimale du système est influencé par la durée du profil du vent. En ce qui concerne cela, on pourrait conclure qu'un profil de vent plus court, mais toujours pertinent pour l'objectif du processus de conception, représenterait une bonne alternative. Aussi, des analyses sont menées dans ce chapitre ainsi que la présentation des méthodes qui peuvent être utilisées pour la réduction de la complexité du profil du vent dans le but de réduire le temps de simulation du système micro-éolien sur un profil long terme de la vitesse du vent couvrant une année.

Trois méthodes sont étudiées pour simplifier le profil de vitesse du vent. La première approche consiste à réduire le profil à un seul point de fonctionnement égal à la vitesse moyenne du vent dans le profil. Cependant, cette méthode se révèle être une solution inefficace puisque la majorité des valeurs de vitesse sont situées au-dessus de la limite de puissance nominale et donc pas pleinement exploitées par la stratégie MPPT.

La deuxième méthode, représentée par la distribution statistique basée sur l'approche de l'histogramme, peut aider à caractériser en termes d'occurrences le profil de vitesse du vent à long terme et à le réduire en un nombre réduit de points de fonctionnement. Sur cette base, la distribution des données du vent peut être discrétisée en N intervalles, distribués uniformément. Cette méthode semble être une meilleure alternative mais conduit à une erreur relative plus élevée lorsque plusieurs grandeurs de sortie du système sont comparées à celles obtenues lors de la simulation sur cycle complet.

Enfin, la troisième méthode explorée pour simplifier le cycle du vent est basée sur la méthode du barycentre qui permet de réduire à la fois le temps de simulation et la quantité de données de vent qui seront prises en compte pour la conception du générateur. Cette méthode de barycentre est adaptée au système d'énergie éolienne pour lequel il y a une relation directe entre la vitesse du vent et la puissance extraite. Afin de réduire le cycle et par conséquent le temps de calcul, la totalité des points de fonctionnement dans le cycle de du vent sont remplacés par un faible nombre de régions. Chaque région est représentée par un barycentre et ses paramètres correspondants, qui sont en outre utilisés pour le calcul des pertes de chaque région.

Les expressions pour les pertes de puissance reformulées en relation avec la méthode du barycentre sont présentées pour les pertes mécaniques, cuivre, fer et convertisseur, tandis que l'explication détaillée de l'ensemble du processus de détermination de ces équations de pertes est

fournie en Annexe 3.A. Cette méthode révèle de faibles erreurs relatives sur les sorties après les avoir comparées à celles obtenues par une évaluation sur le cycle complet, ce qui se confirme cette solution comme la plus efficace.

Pour voir comment les points de performances de la micro-éolienne affectent les sorties du système éolien, plusieurs simulations sont réalisées avec le modèle semi-analytique pour un fonctionnement sur cycle complet. On remarque que toutes les réponses retenues pour la présentation sont affectées par la variation de ces facteurs, certaines plus que d'autres. La puissance d'entrée du système éolien et donc les pertes et la puissance de sortie diminuent lorsque la vitesse de mise en rotation « cut-in » de la turbine augmente. Une valeur inférieure de la vitesse nominale du vent entraîne une diminution de l'extraction et des pertes de puissance ainsi qu'un impact négatif sur l'efficacité du système. Comme les vitesses de vent élevées sont très rares dans le profil étudié, une valeur inférieure ou une valeur augmentée de la vitesse de vent de coupure de la turbine n'affecte pas significativement les réponses.

En outre, certaines simulations ont été menées et les résultats des modèles analytique et semi-analytique sur le fonctionnement à long terme et à profil du vent réduit ont été comparés. Le modèle semi-analytique avec cycle complet indique un temps de simulation indésirable pour envisager de l'utiliser dans un processus d'optimisation. D'autre part, lorsqu'il est couplé à la méthode du barycentre, comme mentionné précédemment, ce temps se réduit tout en fournissant encore une bonne précision pour les grandeurs de sortie. Cependant, on n'obtient pas la même réponse avec le modèle analytique. Même s'il est le plus rapide, une erreur assez grande est trouvée par rapport au modèle semi-analytique basée sur le cycle complet. Par conséquent, il est conclu que la solution la plus commode est d'utiliser le modèle semi-analytique avec la méthode du barycentre dans la conception par optimisation du système micro-éolien.

Chapitre 4

Optimisation de la conception du générateur sans balais à aimants permanents et auto-commutation sur cycle de fonctionnement de la vitesse du vent

La phase de conception d'un composant ou système consiste à déterminer tous ses paramètres caractéristiques qui correspondent le mieux aux exigences spécifiées. La conception optimale du générateur pour les applications micro-éoliennes afin de minimiser un critère spécifique repose sur la sélection appropriée des multiples paramètres de conception.

L'objectif proposé est la minimisation des pertes de puissance globales dans le système sur un cycle long terme de la vitesse du vent. Les variables continues (c) et discrètes (d) du système éolien considéré à optimiser ainsi que celles fixées à une certaine valeur sont également

décrites. Des contraintes sont imposées sur le diamètre intérieur du générateur, l'épaisseur de l'aimant, la température maximale dans les enroulements du stator, le courant de démagnétisation, la largeur de bande d'hystérésis relative au courant de stator, la masse du générateur, l'efficacité du générateur pendant tout le cycle du vent, etc. La conception du système conduit à une optimisation mono-objectif sous contraintes qui fait appel à une méthode stochastique, en particulier une méthode évolutionniste basée sur l'algorithme génétique (GA) de l'environnement Matlab® pour trouver les caractéristiques géométriques et électriques qui satisfont aux contraintes tout en minimisant les pertes de puissance du système éolien sur un profil de vitesse du vent à long terme.

Comme on pouvait s'y attendre, la première optimisation est réalisée, sur la base de quelques données et spécifications initiales, avec le modèle semi-analytique et la méthode du barycentre car il est plus précis que le modèle analytique. Seules six régions sont choisies pour partitionner le cycle du vent et approximer les pertes de puissance dans le système d'énergie éolienne. En effet, une erreur relative acceptable a été trouvée dans le chapitre 3 pour ce nombre de barycentres avec la machine de référence. Malgré le nombre élevé des variables de conception et des contraintes, le modèle semi-analytique avec la méthode barycentrique est capable de donner une solution optimale. Une fois que l'optimisation est terminée, les résultats obtenus ont été vérifiés au moyen du modèle semi-analytique sur le cycle complet du vent et une comparaison pour certaines grandeurs de sortie de ces deux modèles a été présentée. La proximité entre les résultats a permis de considérer celui-ci comme une référence qui permettra de comparer les autres approches d'optimisation.

La deuxième direction était d'effectuer une optimisation avec le modèle de simulation analytique par le même processus que celui représenté pour le modèle semi-analytique. Ensuite, les grandeurs de sortie d'intérêt résultant de l'optimisation avec le modèle analytique sont comparées avec celles obtenues par une évaluation du modèle semi-analytique lorsque les entrées sont prises égales à celles en fin du processus d'optimisation avec le modèle analytique. Il est observé que le modèle analytique présente des valeurs pour les grandeurs de sortie d'intérêt assez éloignées de celles du modèle semi-analytique qui est considéré comme une référence compte tenu de sa meilleure précision. Néanmoins, le temps d'optimisation avec le modèle analytique est très faible par rapport à celui du modèle semi-analytique.

Par conséquent, pour un raffinage des résultats d'optimisation avec le modèle analytique, une stratégie de correction qui utilise des évaluations du modèle semi-analytique associé à la méthode du barycentre est proposée et mise en œuvre dans l'approche d'optimisation à deux niveaux. Pour être en mesure de faire une comparaison, le problème d'optimisation est reformulé comme un problème d'atteinte d'une valeur cible. La fonction objectif est transformée en une

distance entre la fonction objectif initiale et une valeur cible dont on cherche à minimiser la norme euclidienne. Les différences qui apparaissent entre les grandeurs de sortie des modèles analytique et semi-analytique en cycle complet sont localement annulées par la construction d'un modèle de substitution qui inclut le modèle analytique et une correction sur ses sorties.

Cette correction est appliquée en évaluant la configuration obtenue avec le modèle semi-analytique en dehors de la boucle d'optimisation puis en l'appliquant au modèle analytique à la prochaine itération. Le processus d'optimisation est démarré à nouveau jusqu'à ce que l'écart entre le modèle substitutif et le modèle semi-analytique avec la méthode du barycentre soit suffisamment petit. Ainsi, en appliquant la stratégie de correction du modèle analytique, des améliorations significatives de ces résultats sont remarquées dans un temps de résolution acceptable. Sur cette base et compte tenu du fait que le modèle semi-analytique, même associé à la méthode du barycentre, n'offre pas le luxe d'effectuer de nombreuses optimisations d'exploration sur lui, cette stratégie d'optimisation basée sur le modèle analytique avec une stratégie de correction a été utilisée pour effectuer d'autres optimisations en augmentant progressivement le nombre de régions utilisées dans la méthode des barycentres.

Chapitre 5

Etude expérimentale du prototype du générateur sans balais à aimant permanent et auto-commutation

La première partie de ce chapitre a brièvement décrit le prototype utilisé pour réaliser l'assemblage expérimental et les essais. Le générateur de référence étudié pour la caractérisation expérimentale est représenté par une machine à aimants permanents à courant continu sans balais de type « in-wheel », existant dans le laboratoire L2EP, conçu pour une application de vélo électrique. En outre, la détection de la séquence de commutation pour la machine d'étude sur la base des informations fournies par les mesures des capteurs à effet Hall a été obtenue à vide en entrainant le rotor.

La plateforme matérielle et logicielle a ensuite été présentée avec la structure principale du modèle de contrôle mis en œuvre dans l'environnement Matlab / Simulink. Les principales composantes de ce montage sont :

- Un émulateur de turbine qui est représenté par un moteur d'entraînement alimenté par un convertisseur industriel qui permet un contrôle de vitesse de ce moteur.
- La machine à aimant permanent sans balais à l'étude.

- Un convertisseur de puissance en pont triphasé, avec six interrupteurs IGBT et six diodes en antiparallèle couplé à une source de tension continue. Sa fonction principale est d'alimenter et de contrôler la machine de référence.
- Une charge résistive variable pour remplacer le système de stockage ou le réseau de distribution.
- Les composants de contrôle représentés par une carte dSPACE et une carte électronique pour générer les signaux.

La première étape consiste à réaliser les mesures en temps réel des signaux des capteurs Hall avec les informations de position du rotor au moyen des ports d'entrée de la carte dSPACE et des courants de phase de la machine. La carte dSPACE est une plateforme d'interface utilisée pour le contrôle de la machine, en fournissant également les mesures de certains de ses paramètres électromagnétiques. La deuxième étape consiste à déterminer les courants de référence pour chaque état de 0 à 360° en mettant en œuvre la séquence de commutation et en fonction des précédentes mesures des capteurs. Les courants de phase sont commandés au moyen de régulateurs PI. Les sorties de la régulation de courant correspondent aux signaux transmis aux unités de puissance de convertisseur (IGBT) qui sont commandés par la carte dSPACE sur la base de ces valeurs de signal.

Plusieurs tests à vitesse de rotation et tension du bus continu différentes ont été réalisés et visualisés via l'interface Control Desk. Les formes d'onde obtenues pour les courants de phase de la machine renforcent le fait que cette tension de bus joue un rôle significatif dans la qualité de l'énergie électrique générée. Le pic dans la forme d'onde de courant est obtenu même en l'absence d'une commande de la tension du bus par le hacheur. Enfin, des tests expérimentaux dynamiques et stables ont été réalisés.

Conclusion Générale et Perspectives

Le sujet de cette thèse a été centré sur la conception d'un générateur à aimants permanents sans balais pour des applications micro-éoliennes. Cette enquête a été réalisée pour minimiser les pertes de puissance du système micro-éolien sur le fonctionnement à long terme du profil du vent. Cependant, le système d'énergie micro-éolienne à optimiser intègre différents sous-systèmes (aérodynamique, mécanique, électrique) avec forte connexion entre eux. On considère qu'une optimisation du système dans sa globalité est une solution plus adéquate qui se présenterait avec de meilleurs résultats, plutôt que d'effectuer l'optimisation pour chaque composant séparément.

Tout au long de cette thèse, les contributions apportées sont considérées les suivantes:

- Le développement d'un modèle analytique de dimensionnement et de simulation dans Matlab et d'un modèle de simulation semi-analytique basée sur le contrôle PI de la puissance et régulation du courant par hystérésis dans l'environnement Matlab / Simulink
- Modélisation 2D et analyse d'un générateur à aimants permanents sans balais au moyen d'un lien automatique entre JMAG Designer et le logiciel Matlab via un fichier script basé sur le langage Visual Basic
- Le développement d'une nouvelle méthode adaptée à la région de MPPT, qui réduit le profil de vitesse du vent en quelques points de fonctionnement et son adaptation au calcul des pertes de puissance du système micro-éolienne (pertes mécaniques, cuivre, fer et convertisseur).
- L'optimisation du générateur intégré dans le système de conversion d'énergie micro-éolienne complexe, opérant sur un cycle de vitesse du vent à long terme, en utilisant:
  - un modèle de simulation semi-analytique développé dans l'environnement Matlab / Simulink associé à une méthode barycentrique originale et couplé à une technique d'algorithme génétique, résultant à une approche d'optimisation à un seul niveau
  - une approche d'optimisation à deux niveaux qui consiste à boucles interne et externe. La boucle interne effectue une optimisation avec le modèle analytique développé et associé à une opération de cycle complète de vitesse du vent en utilisant un algorithme génétique. La boucle externe ajuste les sorties du modèle analytique avec le modèle semi-analytique avec la méthode du barycentre sur la base d'une stratégie de correction itérative.
- La mise en place d'un banc d'essais pour caractériser expérimentalement un prototype de générateur a aimants permanents et auto-commutation et la mise en œuvre de sa commutation et de son contrôle sur la plate-forme dSPACE.

Cette étude ouvre un certain nombre de perspectives à proposer qui sont brièvement décrites à la fin de la section.

Optimisation du dimensionnement et de la commande sur cycle de fonctionnement d'un générateur à aimants permanents et auto-commutation pour applications micro-éoliennes

Résumé

La conception d'un microsystème autonome de conversion de l'énergie éolienne représente le cœur de cette étude. L'attention est portée vers le générateur BLDCPM en étoile à trois phases, ayant un rotor extérieur avec des aimants permanents montés en surface et des enroulements concentrés avec des forces électromotrices trapézoïdales. Une connexion directe entre la turbine à axe horizontal et la machine tournant à vitesse variable est considérée puisque l'application visée est résidentielle et nécessite un fonctionnement à faible vitesse. Le convertisseur électronique de puissance à courant alternatif (redresseur) et à pont complet triphasé du côté générateur est considéré pour contrôler la tension constante du bus continu de sortie. En raison de la vitesse variable du vent, de nombreuses fluctuations se produisent dans la puissance et la fréquence du générateur BLDCPM, ce qui oblige sa conception pour un fonctionnement à une large plage de vitesse. Ainsi, le travail de la thèse vise à déterminer les paramètres optimaux de conception géométriques et électriques du générateur BLDCPM, en assurant des pertes de puissance minimales dans le μWECS. Un fonctionnement sur un cycle long terme d'une année avec une vitesse moyenne du vent mesurée toutes les heures est considéré pour maximiser la puissance éolienne extraite et augmenter l'efficacité du système dans son ensemble. Par conséquent, il est nécessaire de déterminer le niveau de modélisation, ainsi que les variables de conception de chacun des composants du système. Comme l'optimisation fait appel à un algorithme pour le processus de conception, le nombre d'évaluations du modèle peut être assez important. Plus les variables de conception et les contraintes sont nombreuses, plus élevé est le nombre d'évaluations. En conséquence, la réduction du temps de simulation, ainsi que l'intégration et l'exploitation des données provenant du profil de vitesse du vent pour déterminer la totalité des pertes de puissance dans le μWECS considérées sont les principales préoccupations. Ensuite, la méthodologie d'optimisation est présentée, ainsi que les résultats optimaux obtenus et la comparaison de plusieurs paramètres d'entrée et de sortie. Enfin, des essais expérimentaux sont également effectués sur un prototype de machine BLDCPM de référence afin de vérifier la technique de commutation et de contrôle électronique.

Mots clefs : générateur sans balais à aimant permanent et auto-commutation, méthode de barycentre, modélisation, multi-physique, optimisation de conception, microsystème autonome de conversion de l'énergie éolienne, cycle long terme du vent

---

Brushless DC permanent magnet micro-wind generator modeling and optimization over long-term wind-speed cycle operation

Abstract

The design of a stand-alone micro-wind energy conversion system represents the core of this study. The attention is derived towards the three-phase star-connected BLDCPM generator, having outer rotor with Nd-Fe-B surface-mounted PMs, and concentrated stator-armature windings with quasi-trapezoidal stator-phase back-EMF voltages. A direct connection to the variable speed horizontal axis wind turbine is considered as the residential use application for which is desired requires low-speed operation. Generator-side three-phase full-bridge AC/DC power electronic converter (rectifier) is considered for controlling the output DC-bus constant voltage. Due to the variable wind speed, many fluctuations occur in the power and frequency of the BLDCPM generator, compelling its design for large speed-range operation. Hence, the thesis work aims at determining the optimal design parameters of the BLDCPM generator ensuring minimum power losses of μWECS over long-term wind-speed cycle operation, and thereby maximizing the extracted wind power and increasing the efficiency of the overall system. Therefore, it is necessary to determine the modeling level, as well as the design variables of each component of the system. As the optimization appeals to an algorithm for the design process, the number of model evaluations can be fairly important. The more design variables and constraints, the higher the model evaluation count. As a result, reduction of the simulation time, as well as integration and exploitation of the available data from the wind-speed profile for determining the total power losses of considered μWECS are of main concern. Afterwards, the optimization methodology is presented along with the optimum results obtained, as well as comparison of several input/output parameters. Finally, experimental tests are also carried out on a reference BLDCPM machine prototype in order to verify its electronic commutation and control technique.

Keywords: barycenter method**,** brushless DC permanent magnet generator**,** design optimization, modeling, multi-physics, stand-alone micro-wind energy conversion system, long-term wind speed cycle.

Modelarea și optimizarea micro-generatorului cu magneți permanenți și auto-comutație electronică cu operare sub un profil al vântului de lungă durată

Rezumat :

Designul unui micro-sistem autonom de conversie a energiei provenită de la o micro-turbină eoliană reprezintă nucleul acestui studiu. Atenția este îndreptată asupra generatorului trifazic cu configurație de rotor exterior cu magneți permanenți montați pe suprafața acestuia și cu înfășurări concentrate pe stator. O legătură directă între turbina cu ax orizontal și generatorul de viteză variabilă este considerată, deoarece aplicația avută în vedere este rezidențială și necesită funcționare la viteză mică. Convertorul electronic de curent alternativ (redresor) cu trei faze asociat generatorului este considerat pentru a menține tensiunea de ieșire pe bus cc la o valoare constantă. Din cauza vitezei variabile a vântului, multe fluctuații apar în puterea și frecvența generatorului, forțând designul acestuia la o funcționare într-o gamă largă de viteză. Astfel, activitatea tezei este de a determina parametri geometrici și electrici optimi ai generatorului, asigurând pierderi minime de putere în micro-sistemul de conversie al energiei considerat. O operațiune pe un ciclu de vânt cu durata unui an, cu o viteză medie a vântului, măsurată la fiecare oră este considerat pentru a maximiza puterea extrasă din vânt și de a crește eficiența globală a micro-sistemului. Prin urmare, este necesar să se determine nivelul de modelare, precum și variabilele de proiectare pentru fiecare dintre componentele sistemului. Datorită faptului că optimizarea apelează la un algoritm pentru procesul de proiectare, numărul de evaluări ale modelului poate fi destul de important. Cu cât există mai multe variabile de proiectare și constrângeri, cu atât numărul de evaluări este mai mare. În consecință, reducerea timpului de simulare, precum și integrarea și exploatarea datelor provenite de la profilul de viteză al vântului pentru a determinarea pierderile totale de energie din micro-sistem, sunt principalele preocupări. În următoarea etapă este prezentată metodologia de optimizare, precum și rezultatele optime obținute și compararea mai multor parametri de intrare și de ieșire. În final, teste experimentale sunt, de asemenea, efectuate pe un prototip de mașină cu magneți permanenți și auto-comutație electronică de referință pentru a verifica tehnica de comutare și de control electronic.

Cuvinte cheie : generator cu magneți permanenți și auto-comutație electronică, metoda baricentrului, proiectare prin optimizare, micro-sistem autonom de conversie al energiei, ciclu de vânt de lungă durată